VU VRIJE UNIVERSITEIT AMSTERDAM

UNIVERSITEIT VAN AMSTERDAM

Complete Analytic Calculation of Drell-Yan Angular Coefficients at $\mathcal{O}(\alpha_s^2)$

MSc Thesis

written by

Daria Trotsenko

under the supervision of **Dr Wouter Waalewijn** and **Dr Johannes Michel**, and submitted in partial fulfillment of the requirements for the degree of

MSc in Physics and Astronomy

at the *Universiteit van Amsterdam*

Date of the submission:
August 1, 2025

Members of the Thesis Committee:
Supervisor Dr Wouter Waalewijn
Daily supervisor Dr Johannes Michel
Examiner Prof Dr Eric Laenen

Abstract

The Drell-Yan process is a key tool for testing the Standard Model at hadron colliders. Angular coefficients, which characterize the angular distribution of leptons in the Drell-Yan process, provide direct access to the polarization structure of the intermediate boson and are especially useful for extracting detailed information from experimental data. To make precise comparisons with measurements, we need accurate theoretical predictions that include higher-order QCD corrections. Having fully analytic expressions for these corrections helps improve both the efficiency of calculations and interpretability of the underlying physics.

In this project, we compute the angular coefficients for Drell-Yan at finite transverse momentum, including radiative corrections up to $(\mathcal{O}(\alpha_s^2))$ for both real-real and real-virtual contribution. The final result is a complete analytic prediction for helicity-resolved Drell-Yan at NNLO.

Acknowledgements

This thesis would not have been possible without the support and encouragement of many people at both Nikhef and DESY. First and foremost, I want to thank Johannes Michel for his guidance, support, and for always being available for a good discussion. This project simply wouldn't have happened without it, and I feel I have learned a lot in the last year. I also want to thank Wouter Waalewijn for being my primary supervisor, for keeping us grounded, and for supporting me even beyond this project.
I'm very grateful to Alessandro Gavardi and Bahman Dehnadi for supervising me during the DESY Summer School 2024, which became the starting point of this project. I am thankful for all the helpful and enjoyable discussions during that time and in the months that followed. I also want to especially thank Frank Tackmann for the opportunity to work with the DESY theory group.
My sincere thanks also go to the Nikhef theory group for their warm and welcoming atmosphere – within just a year, it came to feel like a second home. Lastly, I would like to thank the entire group of Nikhef theory master's students for their moral support, and for making this year not only intellectually stimulating but also genuinely fun and enjoyable.

Contents

1 Introduction **4**

2 General theory **6**
2.1 Quantum Chromodynamics . . . 6
2.2 Hadron-hadron collision factorization . . . 8
2.2.1 Projectors . . . 9
2.2.2 Helicity Projections . . . 10
2.3 Amplitude and Squared Amplitude Classification . . . 13
2.3.1 Color structure . . . 16
2.3.2 Charge configuration . . . 17
2.4 Poles and renormalization . . . 18
2.4.1 Pole structure . . . 18
2.4.2 PDF renormalization . . . 19
2.5 Introduction to Soft-Collinear Effective Theory . . . 21
2.5.1 Degrees of Freedom in SCET . . . 21
2.5.2 Leading-Power SCET Operators and SCET Lagrangian . . . 22
2.6 Using V + jet threshold factorization as an analytic subtraction . . . 25
2.6.1 Parametrizing the PDF convolution integral . . . 25
2.6.2 Structure of soft and final-state collinear singularities . . . 26
2.6.3 Factorized singular cross section from the V + jet threshold limit . . . 27
2.6.4 Final result . . . 31

3 Flavor decomposition of partonic cross-sections **32**
3.1 Introduction to the approach . . . 32
3.2 $gg \to VX$ . . . 33
3.3 $qg \to VX$ . . . 35
3.4 $q\bar{q} \to VX$ . . . 36
3.5 $qq \to VX$ . . . 37

4 Helicity decomposition of real-virtual contributions at amplitude level **38**
4.1 Spinor-Helicity Method . . . 38
4.1.1 Introduction and main idea . . . 38
4.1.2 Projected lepton current . . . 40
4.1.3 $\mathcal{A}_{\text{full}}$ . . . 42
4.1.4 Lepton Configurations and Solving the System . . . 49
4.2 Power Scaling of Helicity Amplitudes . . . 54
4.2.1 Soft Scaling of Z-helicity Amplitudes in the $q_T/Q \to 0$ Limit . . . 54
4.3 Treatment of γ_5 . . . 57
4.4 Final results for LO_1 and NLO_1 . . . 58
4.5 Rewriting $2 \to 2$ phase space . . . 66

5 Computation of double-real remainder terms **68**
5.1 Calculating and squaring matrix elements . . . 68
5.2 Integrating over k-particle phase space . . . 69
5.2.1 Phase space of decay into N particles . . . 69
5.2.2 Final cross section . . . 72
5.2.3 Master integrals . . . 72

5.2.4 Partial fraction decomposition . . . 79
5.3 PDF renormalization for double-real term . . . 81
5.4 γ_5 scheme for double-real terms . . . 83
5.5 Obtaining the non-singular remainder terms . . . 86

6 Comparison with previous results in the literature **88**
6.1 Cross-checks and Comparing with literature . . . 88

Conclusions **91**

A Feynman Rules **93**

B Spinor Identities **95**

C Functions and Distributions **97**
C.1 Plus Distribution . . . 97
C.2 Distributional expansion . . . 98

D PDF Renormalization **99**

E Helicity Configurations **101**
E.1 F.1 LO_1 (and NLO_1) . . . 101
E.2 F.2 LO_2 . . . 102
E.2.1 $q\bar{q} \to q\bar{q}\ell\bar{\ell}$ . . . 102
E.2.2 $qq \to qq\ell\bar{\ell}$ . . . 102
E.2.3 $gg \to q\bar{q}\ell\bar{\ell}$ . . . 103
E.2.4 $qg \to qg\ell\bar{\ell}$ . . . 103
E.2.5 $q\bar{q} \to gg\ell\bar{\ell}$ . . . 103

Chapter 1

Introduction

Physics, at its heart, is a search for the hidden simplicity that lies beneath the complex and often chaotic behavior of the natural world. Over centuries, seemingly unrelated phenomena have been merged together under unified frameworks. The same field that explains the motion of electric charges also describes the nature of light, the same quantum rules that govern radioactive decay apply to the structure of matter around us.

At the center of our current understanding stands the Standard Model: a compact and elegant mathematical structure that unifies the electromagnetic, weak, and strong interactions into a single self-consistent theory. It is built on the gauge symmetry group $\mathrm{SU}(3)_C \times \mathrm{SU}(2)_L \times \mathrm{U}(1)_Y$, and its field content and dynamics have been confirmed time and time again by experiment. The discovery of the Higgs boson in 2012 at CERN's Large Hadron Collider [1, 2] marked a major milestone. And importantly, rather than being a surprise, it was a confirmation – the final predicted piece of the puzzle, completing a framework that had already withstood decades of tests.

However beyond the Standard Model lies a landscape of open questions: it does not incorporate gravity, nor does it account for dark matter or the nonzero masses of neutrinos, and it offers no explanation for the observed matter-antimatter asymmetry. Additionally, many of its parameters, such as masses, mixing angles or couplings, are inputs, not predictions.

In the absence of new particles or interactions appearing directly at accessible energies, the search for physics beyond the Standard Model has turned to indirect strategies. One of the most promising paths is plainly increasing the precision: measuring known processes with higher accuracy, and comparing them against equally precise theoretical predictions, hoping that tiny, subtle deviations between data and theory can hint at new physics. To do this well, one needs both sides of the equation to be sharp: experiments must deliver clean, high-resolution data and theory has to be able to keep up with rising precision. This has pushed collider physics into a new era, where full control over multi-differential observables and higher-order corrections is no longer optional, but essential for both experimental and theoretical sides.

Among the most important of these high-precision observables is the Drell-Yan process, where a lepton pair is produced in hadron-hadron collisions via the exchange of a vector boson, such as a virtual photon γ^*, Z boson or a $W^\pm$ boson (refer to Figure 1.1 for an illustration of the Drell-Yan process), and the dilepton transverse momentum spectrum, which is one of the cleanest and most precisely measured observables at the LHC [3] that has been recently used to both obtain the W boson mass [4] and the strong coupling constant [5, 6]. The true power of it lies not just in the total cross section, but also in the shape of the final state, in the angular correlations that access the spin and polarization state of the intermediate boson, which in turn is easily influenced by both strong (QCD) and electroweak (QED) corrections. These angular distributions are typically decomposed into a set of coefficients A_i, which carry all the dependence on the polarization structure of the boson and, most importantly, the QCD dynamics of the initial state. Their precise prediction and measurement allow us to test QCD factorization, study parton distributions, and even extract fundamental parameters.

However, producing high-precision theoretical predictions for these coefficients at the next-to-next-to-leading order (NNLO) in QCD remains quite computationally expensive. There is a multitude of state-of-the-art tools used in collider phenomenology - numerical codes such as `DYTurbo` [7] and `FEWZ` [8], but generally generating differential cross sections with sufficient statistics and precision can require

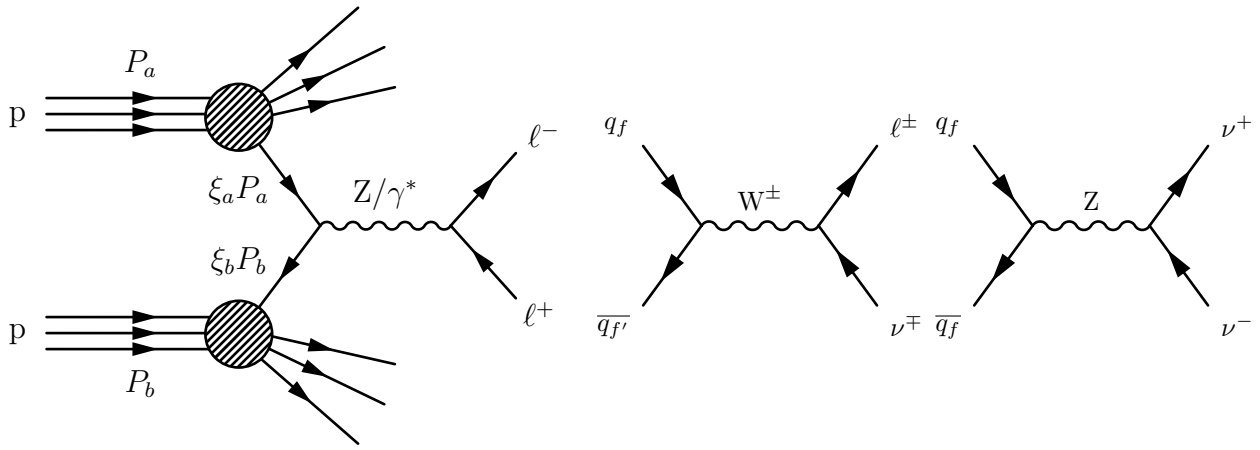


Figure 1.1: An illustration of the Drell-Yan process involving various partons and intermediate vector bosons. In the leftmost diagram, two protons collide, producing partons $\xi_a P_a$ and $\xi_b P_b$, which in turn leads to the formation of an intermediate virtual photon or Z boson and some final hadronic state (radiation) X. The boson decays into a lepton-antilepton pair ($\ell^+\ell^-$). The other two diagrams depict the production of different lepton pairs via a $W^\pm$ and Z boson. Each diagram represents different possible channels of the Drell-Yan process which leads to the production of neutral or charged vector bosons.

thousands of CPU hours[1]. Every scale variation, observable bin or cut configuration must be recomputed multiple times, which is incredibly computationally expensive, especially when computing a set of multiple angular components.

Analytic results offer a clean solution to this problem. Once derived, they can be evaluated orders of magnitude faster, are reusable and modifiable, are fully transparent in their structure, which might give us physical insights into the origin of various terms, such as soft or collinear logarithms, and allow one to identify and isolate the key physics contributions in a way that numerical output cannot.

Therefore, **the purpose of this thesis is to provide a complete analytic calculation of the Drell-Yan angular coefficients at $\mathcal{O}(\alpha_s^2)$**, in the regime of finite boson transverse momentum and at leading order in the electroweak coupling.

This thesis is organized as follows:

In Chapter 2, we introduce the theoretical framework and outline our overall strategy. We begin with a brief overview of QCD, followed by a discussion of factorization in hadron-hadron collisions. We define helicity cross sections and their connection to angular coefficients. We also classify the contributing Feynman diagrams at $\mathcal{O}(\alpha_s^2)$, and describe the expected infrared pole structure of the bare cross section. To handle these divergences, we will be working in the framework of Soft-Collinear Effective Theory (SCET), using which we introduce an analytic subtraction method based on the $V+$jet threshold factorization, which cleanly separates singular terms in the invariant mass of the hadronic final state from the regular part of the cross section. In Chapter 3 we describe the flavor decomposition procedure used to organize the electroweak couplings. In Chapter 4, we compute the loop real-virtual (RV) contributions to the singular helicity cross section. These terms are obtained by helicity decomposing the RV amplitudes using an exptension of the spinor-helicity formalism. In Chapter 5, we evaluate the remainder of the double-real (RR) tree-level contributions using conventional Feynman rules combined with the helicity projection formalism introduced in Chapter 2. Here we also perform analytically the phase space integration over the hadronic radiation and we derive a dedicated set of master integrals to do so. In this chapter we assemble the various contributions into the full helicity-resolved cross section. In Chapter 6 we compare our analytic results with known partial results from the literature. Finally, in Chapter 7 (Conclusions), we conclude and reflect on the outcome of the project, outlining possible directions for future work.

[1]For example, computing the fully integrated Drell-Yan cross section at NNLO using purely Monte Carlo methods (as in illustrated in `DYTurbo` [7]) can require around 8 hours per bin over 100 bins, even when parallelized over 20 threads - totaling approximately 16 000 CPU-hours. In contrast, by implementing partial analytic results in the calculation, the same result can be obtained in roughly 68 CPU-hours. This illustrates the substantial computational advantage of analytic methods.

Chapter 2

General theory

This chapter establishes the main theoretic frameworks required for the research conducted in the thesis, as well as introduces our project pipeline.

2.1 Quantum Chromodynamics

Quantum Chromodynamics (QCD) is the quantum field theory describing the dynamics of the strong interaction, one of the fundamental forces in the Standard Model. It is a non-Abelian gauge theory based on the symmetry group $SU(N_c)$, with $N_c = 3$ in nature. The elementary degrees of freedom in QCD are the **quark** and **gluon** fields. Quark fields $q_f^i(x)$ are in general massive spin-1/2 Dirac fermions, where f labels the flavor and $i = 1, \ldots, N_c$ indexes the color degrees of freedom, which transform in the fundamental representation of $SU(N_c)$. Gluon fields $A_\mu^a(x)$ are massless spin-1 gauge bosons, where $a = 1, \ldots, N_c^2 - 1$ runs over the adjoint representation. The gluons mediate the strong force and carry color charge themselves, leading to self-interactions.

Under a local $SU(N_c)$ gauge transformation, these fields transform as

$$q(x) \to U(x)q(x), \tag{2.1}$$

$$A_\mu(x) \to U(x)A_\mu(x)U^\dagger(x) + \frac{i}{g_s}U(x)\partial_\mu U^\dagger(x), \tag{2.2}$$

where $U(x) = \exp[i\alpha^a(x)T^a]$ is a position-dependent element of $SU(N_c)$, and T^a are the group generators in the fundamental representation, satisfying

$$[T^a, T^b] = if^{abc}T^c, \quad \mathrm{Tr}(T^aT^b) = T_F\delta^{ab} = \frac{1}{2}\delta^{ab},$$

where f^{abc} are the structure constants of the color group $SU(3)$. More identities for the T^a are used in Section 2.3.1.

The full QCD Lagrangian in four-dimensional Minkowski space is given by

$$\mathcal{L}_{\mathrm{QCD}} = \sum_f \bar{q}_f \left(i\gamma^\mu D_\mu - m_f\right) q_f - \frac{1}{4}G^a_{\mu\nu}G^{a\,\mu\nu} + \theta_{\mathrm{QCD}}\frac{g_s^2}{32\pi^2}\epsilon_{\mu\nu\rho\sigma}G^{a,\rho\sigma}G^{a,\mu\nu}, \tag{2.3}$$

where: $G^a_{\mu\nu} = \partial_\mu A^a_\nu - \partial_\nu A^a_\mu + g_s f^{abc}A^b_\mu A^c_\nu$ is the non-Abelian field strength tensor, $D_\mu = \partial_\mu - ig_s A^a_\mu T^a$ is the gauge-covariant derivative acting on quark fields, m_f is the mass of quark flavor f, and g_s is the strong coupling constant.

The Lagrangian contains these key terms:

1. The **gluon kinetic term**, $-\frac{1}{4}G^a_{\mu\nu}G^{a\,\mu\nu}$, which includes gluon self-interactions due to its non-Abelian structure.
2. The **quark kinetic** and **mass terms**, describing free quark propagation.
3. The **quark-gluon interaction**, arising from the covariant derivative term $\bar{q}\gamma^\mu A^a_\mu T^a q$, which couples quark color and spin to the gluon field.

4. The **θ-term**, which is proportional to a total derivative, and therefore does not contribute to perturbative calculations, where the field is assumed to vanish at infinity asymptotically. In this project we assume $\theta_{\text{QCD}} = 0$.

At this moment we can modify our (classical) QCD Lagrangian and add a few extra terms tackling the fixing of the gauge. To quantize the theory in a consistent way, one must fix the gauge redundancy introduced by the local $SU(N_c)$ invariance. In the path integral formalism this is done via the Faddeev-Popov method [9], which fixes the gauge at the cost of introducing auxiliary fields known as **ghosts**. The ghost term and the gauge fixing term in the Lagrangian take the form:

$$\mathcal{L}_{\text{ghost}} = \bar{c}^a(-\partial^\mu D_\mu^{ab})c^b, \quad \mathcal{L}_{g.f.} = -\frac{1}{2\xi}(\partial^\mu A_\mu^a), \tag{2.4}$$

where c^a, $\bar{c}^a$ are Grassmann-valued scalar fields, $D_\mu^{ab} = \delta^{ab}\partial_\mu + g_s f^{acb} A_\mu^c$ is the adjoint covariant derivative and ξ is a continuous parameter, value of which sets the gauge.

Although ghost fields do not correspond to physical particles (they cannot appear as external states in any observable) they play an important role in ensuring gauge invariance and unitarity in covariant quantization schemes. In particular, in covariant gauges such as Feynman ($\xi = 1$) or Landau ($\xi \to 0$) gauge, ghost contributions must be included in loop diagrams to cancel unphysical degrees of freedom associated with longitudinal gluon polarizations.

In this project we encounter situations where the inclusion of ghost diagrams is necessary when working in Feynman gauge, specifically in contractions involving external gluon fields (see Section 5.1 for further discussion). Alternatively, it is possible to avoid ghost contributions altogether by choosing a gauge that restricts gluons to their physical polarizations, such as the lightcone or axial gauge. These gauges eliminate the unphysical modes by construction at the cost of introducing more complex propagators. For completeness, we summarize the Feynman rules relevant for both covariant and lightcone gauges, and in general Feynman rules for both QCD and QED in Appendix A.

Like all quantum field theories with ultraviolet divergences, QCD requires renormalization. In this process, the strong coupling constant

$$\alpha_s = \frac{g_s^2}{4\pi}$$

becomes scale-dependent, and its evolution is described by the renormalization group equation:

$$\mu\frac{\mathrm{d}\alpha_s(\mu)}{\mathrm{d}\mu} = \beta(\alpha_s) = -2\beta_0\frac{\alpha_s^2(\mu)}{4\pi} + \mathcal{O}(\alpha_s^3), \tag{2.5}$$

where μ is the renormalization scale, $\alpha_s(\mu)$ is the renormalized strong coupling at the scale μ and the one-loop coefficient of the QCD beta function is

$$\beta_0 = \frac{11}{3}C_A - \frac{4}{3}T_F n_f, \tag{2.6}$$

where for QCD with gauge group $SU(3)$, we have $C_A = 3$, $T_F = \frac{1}{2}$, and n_f denotes the number of active (effectively massless) quark flavors at the renormalization scale μ.

At typical LHC energies (e.g., $m_W, m_Z, m_H \sim 100\,\text{GeV}$), the up, down, strange, charm, and bottom quarks can be treated as massless to a good approximation. Therefore, the perturbative QCD calculations in this thesis are performed in a theory with $n_f = 5$ massless flavors. The only parameter of the theory is the renormalized gauge coupling $\alpha_s(\mu)$.

The important point is the sign of β_0: for $n_f < 17$, we have $\beta_0 > 0$, which implies a decreasing coupling at high energies. This phenomenon is known as **asymptotic freedom** [10, 11], and it allows the use of perturbative techniques in QCD at short distances. On the other hand, as $\mu \to \Lambda_{\text{QCD}}$, the coupling becomes large, marking the breakdown of perturbation theory and the appearance of non-perturbative dynamics such as confinement and hadronization. The scale dependence of α_s is thus central to the structure of QCD.

In the $\overline{\text{MS}}$ scheme, which is used throughout this thesis, the bare (g_s) and renormalized couplings ($\alpha_s(\mu)$) are related by

$$\frac{g_s^2}{4\pi} = \mu^{2\epsilon}\alpha_s(\mu)\, Z_{\alpha_s}(\epsilon, \mu), \tag{2.7}$$

with the renormalization factor given by

$$Z_{\alpha_s}(\epsilon,\mu) = \frac{e^{\epsilon\gamma_E}}{(4\pi)^\epsilon}\left[1 + \frac{\alpha_s(\mu)}{4\pi}\left(-\frac{\beta_0}{\epsilon}\right) + \mathcal{O}(\alpha_s^2)\right]. \tag{2.8}$$

where γ_E is the Euler-Mascheroni constant.

2.2 Hadron-hadron collision factorization

The **Drell-Yan** (DY) process, predicted by S. Drell and T. M. Yan in the early 1970s [12], describes the production of a lepton pair through an intermediate vector boson in unpolarized proton-proton (pp) collisions. It is one of the most important processes for studying QCD and electroweak interactions at hadron colliders. In this section, we introduce the general formalism used to describe vector boson production in hadronic collisions, focusing on the decomposition of the cross section into helicity structure functions and the subsequent derivation of the angular distribution of the final-state leptons. The theory in this section is primarily based on the second chapter of the ref. [13] and the material of this section is a short overview of it.

We are interested in the production of a single (either neutral or charged) vector boson V from an unpolarized proton-proton collision, followed by its decay into a colorless leptonic final state L. The process can be represented as

$$p(P_a)\, p(P_b) \to V(q)\, X, \tag{2.9}$$

where $V = Z, \gamma^*, W^\pm$ is a (potentially offshell) electroweak boson with invariant mass $q^2 = Q^2$, which decays as

$$\begin{aligned} Z/\gamma^*(q) &\to \ell^-(q_1)\,\ell^+(q_2)\,, & Z(q) &\to \nu(q_1)\,\bar{\nu}(q_2)\,, \\ W^+(q) &\to \nu_\ell(q_1)\,\ell^+(q_2)\,, & W^-(q) &\to \ell^-(q_1)\,\bar{\nu}_\ell(q_2)\,, \end{aligned} \tag{2.10}$$

and X denotes any additional final-state hadronic radiation.

The differential cross section for this process, measured in the laboratory frame (which we assume coincides with the hadronic rest frame), can be factorized into a contraction of the **leptonic tensor $L_{\mu\nu}$** and the **hadronic tensor $W^{\mu\nu}$**, as follows:

$$\frac{\mathrm{d}\sigma(\Theta)}{\mathrm{d}^4q\, d\mathcal{O}} = \frac{1}{2E_{\mathrm{cm}}^2}\sum_{VV'} L_{\mu\nu,VV'}(q,\mathcal{O},\Theta) W^{\mu\nu}_{VV'}(q,P_a,P_b), \tag{2.11}$$

where q^μ is the momentum of the vector boson V, which corresponds to the total momentum carried by the final-state leptons L, P_a and P_b represent the momenta of the incoming protons, $E_{\mathrm{cm}}^2 = (P_a + P_b)^2$ is the square of the center-of-mass energy of the hadronic system, Θ represents potential fiducial cuts applied to the leptonic final state, which are determined by the detector's acceptance and the signal region, $\mathcal{O}$ is a set of differential observables associated with the final-state leptons. Note that the incoming protons are taken to be massless. This expression also contains an explicit sum over possible vector bosons V and V' that could be produced in the collision.

The Hadronic Tensor $W^{\mu\nu}$

The hadronic tensor $W^{\mu\nu}$ encodes the QCD dynamics of the proton-proton collision and is independent of the specific cuts and measurements applied to the leptonic final state. It sums over all possible hadronic radiation states X and integrates over their phase space, as follows:

$$W^{\mu\nu}_{VV'}(q,P_a,P_b) = \sum\!\!\!\!\!\!\int_X \langle pp|J_V^{\dagger\mu}|X\rangle\langle X|J^\nu_{V'}|pp\rangle (2\pi)^4\delta^4(P_a + P_b - q - k_X), \tag{2.12}$$

where we have kept the intermediate boson indices VV' explicit, J_V^μ represents the hadronic current associated with the production of the vector boson V, and k_X is the four-momentum of the final-state hadronic radiation. The delta function enforces momentum conservation, ensuring that the total momentum of the incoming protons is equal to the sum of the vector boson momentum q and the hadronic radiation momentum k_X.

The Leptonic Tensor $L_{\mu\nu}$

The leptonic tensor $L_{\mu\nu}$ describes the decay of the vector boson V into the final-state leptons L. It encodes the kinematics of the leptonic final state and depends on the polarization and nature of the vector boson. The general form of the leptonic tensor is given by:

$$L^{\mu\nu}_{VV'}(q, \mathcal{O}(,)\Theta) = \int \mathrm{d}\phi_L(q) \mathcal{M}^{*\mu}_{V\to L}(\phi_L) \mathcal{M}^{\nu}_{V'\to L}(\phi_L) \delta(\mathcal{O} - \hat{\mathcal{O}}(q, \phi_L)) \hat{\Theta}(q, \phi_L), \tag{2.13}$$

where ϕ_L represents the phase space measure of the leptonic final state, $\mathcal{M}^{\mu}_{V\to L}(\phi_L)$ is the amplitude for the vector boson V decaying into the leptonic state L, $\hat{\mathcal{O}}(q, \phi_L)$ is the set of measured observables determined by the kinematics of the final leptons, $\hat{\Theta}(q, \phi_L)$ applies the fiducial cuts on the leptonic final state. The delta function enforces the correspondence between the measured observables $\mathcal{O}$ and the actual values determined by the kinematics of the leptons.

In the subsequent calculations, we will simplify expressions by working in four dimensions, following the conventions of ref. [13]. While dimensional regularization can be implemented for rigor, it is useful only in the calculation of the hadronic tensor and terms derived from it, since the leptonic tensor is divergence-free. The poles that emerge solely in the hadronic tensor will be treated in dimensional regularization in $D = 4 - 2\epsilon$ before inserting the results into the final cross section formula.

Fully Inclusive Cross Section

When we sum over all possible final states of the leptons (i.e., fully inclusive over the leptonic decay products), the cross section simplifies to:

$$\frac{\mathrm{d}\sigma}{\mathrm{d}^4 q} = \frac{1}{2E^2_{\mathrm{cm}}} \sum_{VV'} L_{VV'}(q^2) \left(\frac{q_\mu q_\nu}{q^2} - g_{\mu\nu} \right) W^{\mu\nu}_{VV'}(q, P_a, P_b), \tag{2.14}$$

where we have used the fact that the leptonic tensor can be expressed in terms of the vector boson momentum q^μ and metric tensor $g^{\mu\nu}$.
This further reduces to:

$$\frac{\mathrm{d}\sigma}{\mathrm{d}^4 q} = \frac{1}{2E^2_{\mathrm{cm}}} \sum_{VV'} L_{VV'}(q^2) W_{\mathrm{incl},VV'}(q, P_a, P_b), \tag{2.15}$$

where $W_{\mathrm{incl}}(q, P_a, P_b)$ represents the inclusive hadronic contribution to the cross section, integrated over all possible final hadronic states.

2.2.1 Projectors

To express the non-inclusive hadronic tensor in a form that is suitable for further calculations and to have an even clearer separation between the hadronic and leptonic tensors, we decompose $W^{\mu\nu}$ into a set of Lorentz-scalar projections with respect to four orthogonal vectors. These vectors are constructed from the external momenta P_a, P_b, and the momentum of the vector boson q.

In the massless limit ($P_a^2 = P_b^2 = 0$), which is relevant for our calculations, the so-called **projectors** are defined as follows:

$$t^\mu = \frac{q^\mu}{\sqrt{Q^2}}, \tag{2.16a}$$

$$z^\mu = \frac{s_{bq} P_a^\mu - s_{aq} P_b^\mu}{\sqrt{s_{ab} s_{aq} s_{bq}}}, \tag{2.16b}$$

$$x^\mu = \frac{s_{aq} s_{bq} q^\mu - s_{bq} q^2 P_a^\mu - s_{aq} q^2 P_b^\mu}{\sqrt{s_{aq} s_{bq} q^2 (s_{aq} s_{bq} - s_{ab} q^2)}}, \tag{2.16c}$$

$$y^\mu = \epsilon^{\mu\nu\rho\sigma} t_\nu x_\rho z_\sigma, \tag{2.16d}$$

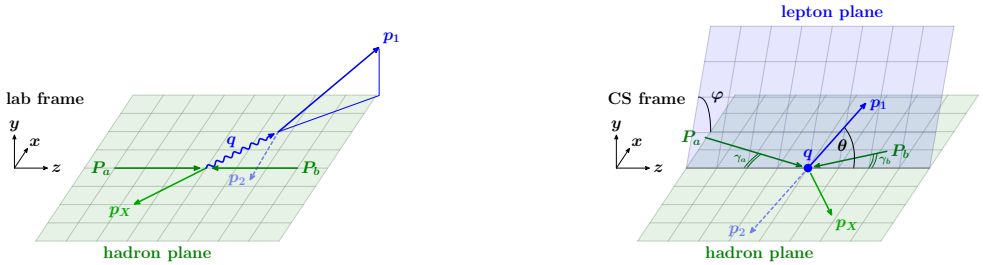
where the four-dimensional Levi-Civita convention is $\epsilon^{0123} = 1$.
In the previous expressions we defined the following scalar parameters:

$$q^\mu q_\mu = Q^2, \quad s_{ab} \equiv 2P_a \cdot P_b, \quad s_{aq} \equiv 2P_a \cdot q, \quad s_{bq} \equiv 2P_b \cdot q. \tag{2.17}$$

It is important to note that the projectors t^μ, z^μ, x^μ, and y^μ are orthogonal to each other, and their squared magnitudes in D-dimensions are: $t^2 = 1$, $x^2 = -1$, $z^2 = -1$, and $y^2 = 3 - D$. Thus, in the neighborhood of four dimensions, the projector t^μ is time-like, while x^μ, z^μ, and y^μ are space-like.

Another vital point is that these projectors, when contracted with the hadronic tensor, do not introduce any new denominators dependent on the momenta of hadronic radiation. This is particularly useful for future calculations of processes involving two partons in the final state, as it ensures that the projectors do not add extra dependence on the external momentum of the hadronic radiation. Consequently, there should be no significant increase in complexity when moving from inclusive cross section to the projections of hadronic tensor, particularly with regard to the structure of the denominators, which is important for phase space integration over hadronic radiation.

Finally, in four dimensions, these vectors define a reference frame known as the Collins-Soper (CS) frame [14], in which the vector boson remains at rest, see Figure 2.1b.



(a) Lab frame **(b)** Collin-Soper frame

Figure 2.1: Kinematics of the Drell-Yan process in two reference frames. (a) In the lab frame, the head-on collision of incoming hadrons with momenta P_a and P_b and their decay into the intermediate boson with momentum q define the hadron plane. (b) In the Collins-Soper frame the vector boson is at rest and the leptons are produced back-to-back. In general, the orientation of hadrons in the CS frame is not symmetric, but the angles γ_a, γ_b become equal in the massless-hadron limit. The lepton plane defines the angular variables θ and φ, which are used to parameterize the lepton angular distribution. Figure taken from ref. [13]

2.2.2 Helicity Projections

We define the polarization vectors of the vector boson in the Collins-Soper frame as follows[1]:

$$\epsilon^\mu_\pm = \frac{1}{\sqrt{2}}(x^\mu \pm iy^\mu), \qquad \epsilon^\mu_0 = z^\mu. \tag{2.18}$$

Using these polarization vectors, we project the helicities of the hadronic tensor $W^{\mu\nu}$ onto the components of the helicity density matrix $W_{\lambda\lambda'}$ [16]:

$$W_{\lambda\lambda'}(q, P_a, P_b) = \epsilon^\mu_\lambda \epsilon^{*\nu}_{\lambda'} W_{\mu\nu}(q, P_a, P_b), \tag{2.19}$$

where the helicity indices λ, λ' take values $\{+, -, 0\}$.

These components can be further combined into nine Lorentz-invariant **structure functions**:

$$\begin{aligned}
W_{-1} &= W_{++} + W_{--} && = (x^\mu x^\nu + y^\mu y^\nu) W_{\mu\nu}, \\
W_0 &= 2W_{00} && = 2z^\mu z^\nu W_{\mu\nu}, \\
W_1 &= -\frac{1}{\sqrt{2}}(W_{+0} + W_{0+} + W_{-0} + W_{0-}) && = -(x^\mu z^\nu + z^\mu x^\nu) W_{\mu\nu}, \\
W_2 &= -2(W_{+-} + W_{-+}) && = -2(x^\mu x^\nu - y^\mu y^\nu) W_{\mu\nu}, \\
W_3 &= -\sqrt{2}(W_{+0} + W_{0+} - W_{-0} - W_{0-}) && = 2i(y^\mu z^\nu - z^\mu y^\nu) W_{\mu\nu}, \\
W_4 &= 2(W_{++} - W_{--}) && = 2i(x^\mu y^\nu - y^\mu x^\nu) W_{\mu\nu}, \\
W_5 &= -i(W_{+-} - W_{-+}) && = -(x^\mu y^\nu + y^\mu x^\nu) W_{\mu\nu}, \\
W_6 &= -\frac{i}{\sqrt{2}}(W_{+0} - W_{0+} - W_{-0} + W_{0-}) && = -(y^\mu z^\nu + z^\mu y^\nu) W_{\mu\nu}, \\
W_7 &= -\sqrt{2}i(W_{+0} - W_{0+} + W_{-0} - W_{0-}) && = -2i(x^\mu z^\nu - z^\mu x^\nu) W_{\mu\nu}.
\end{aligned} \tag{2.20}$$

[1] Note that we adopt a slightly different definition of the polarization vectors than what is used in [13]. This choice becomes important only later in the calculation, where the explicit form of the polarization vectors enters (in Section 4.1.2). The results that depend on this definition are computed separately from those that use coordinate-based projectors, so there is no inconsistency. Our choice follows the convention in [15] and was made to ensure compatibility with angular momentum conservation in the Born process. A more detailed explanation is given in Section 4.2.1.

The inclusive structure function from Eq.(2.15) can now be written as:

$$W_{\rm incl} = W_{++} + W_{--} + W_{00} = W_{-1} + \frac{W_0}{2}. \tag{2.21}$$

More generally, the second column in Eq.(2.20) defines combinations of x_μ, y_μ, z_μ – projectors $\tilde{P}_i^{\mu\nu}$ – using which the structure functions are defined through:

$$W_i(q, P_a, P_b) = \tilde{P}_i^{\mu\nu}(q, P_a, P_b)\, W^{\mu\nu}(q, P_a, P_b). \tag{2.22}$$

Note that $\tilde{P}_i^{\mu\nu}(q, P_a, P_b)$ are invariant under the rescaling of the momenta:

$$\tilde{P}_i^{\mu\nu}(\alpha\, q, \beta\, P_a, \gamma\, P_b) = \tilde{P}_i^{\mu\nu}(q, P_a, P_b), \quad \text{for any real numbers } \ \alpha, \beta, \gamma > 0. \tag{2.23}$$

Since the projections W_i are orthogonal, which is the consequence of the orthogonality of the CS frame axes, we can invert them to reconstruct the original hadronic tensor:

$$W^{\mu\nu} = \sum_{i=-1}^{7} P_i^{\mu\nu} W_i, \tag{2.24}$$

where $P_i^{\mu\nu}$ are the inverted projectors.
With this, the differential cross section is given by:

$$\begin{aligned}\frac{\mathrm{d}\sigma(\Theta)}{\mathrm{d}^4 q\, d\mathcal{O}} &= \frac{1}{2E_{\rm cm}^2} \sum_{VV'} L_{\mu\nu,VV'}(q, \mathcal{O}, \Theta) W_{VV'}^{\mu\nu}(q, P_a, P_b) \\ &= \frac{1}{2E_{\rm cm}^2} \sum_{VV'} \sum_{i=-1}^{7} L_{i,VV'}(q, \mathcal{O}, \Theta) W_{i,VV'}(q, P_a, P_b),\end{aligned} \tag{2.25}$$

where we absorb the projectors into the scalar lepton coefficients $L_i(q, \mathcal{O}, \Theta) = L_{\mu\nu} P_i^{\mu\nu}$.

By parameterizing the 1-to-2 leptonic decay phase space $\mathrm{d}\phi_L \equiv \mathrm{d}\phi_{q\to q_1 q_2}$ using CS angles (θ, ϕ), we can rewrite the leptonic tensor contracted with the inverted projectors, achieving the following expression for L_i as a product of a leptonic factor $L_{\pm(i)}$ and real combinations of spherical harmonics:

$$\begin{aligned}L_i(q, \mathcal{O}, \Theta) &= \int_{-1}^{1} d\cos\theta \int_0^{2\pi} \frac{\mathrm{d}\phi}{32\pi^2} L_i(q^2, \theta, \phi) \delta(\mathcal{O} - \hat{\mathcal{O}}(q, \theta, \phi)) \hat{\Theta}(q, \phi_L), \\ L_i(q^2, \theta, \phi) &= \frac{3}{16\pi} L_{\pm(i)}(q^2) g_i(\theta, \phi), \quad \text{with} \quad \pm(i) = \begin{cases} +, & i \in \{-1, 0, 1, 2, 5, 6\}, \\ -, & i \in \{3, 4, 7\} \end{cases}\end{aligned}$$

where the explicit forms of the spherical harmonics $g_i(\theta, \phi)$ are:

$$\begin{aligned} g_{-1}(\theta,\phi) &= 1 + \cos^2\theta, & g_2(\theta,\phi) &= \tfrac{1}{2}\sin^2\theta\cos(2\phi), & g_5(\theta,\phi) &= \sin^2\theta\sin(2\phi), \\ g_0(\theta,\phi) &= 1 - \cos^2\theta, & g_3(\theta,\phi) &= \sin\theta\cos\phi, & g_6(\theta,\phi) &= \sin(2\theta)\sin\phi, \\ g_1(\theta,\phi) &= \sin(2\theta)\cos\phi, & g_4(\theta,\phi) &= \cos\theta, & g_7(\theta,\phi) &= \sin\theta\sin\phi, \end{aligned}$$

and the leptonic prefactors $L_{(\pm),i}$ are derived in full in ref. [13].

Finally, the differential cross section becomes:

$$\begin{aligned}\frac{\mathrm{d}\sigma(\Theta)}{\mathrm{d}^4 q \mathrm{d}\mathcal{O}} = \int_{-1}^{1} d\cos\theta \int_0^{2\pi} d\phi \frac{1}{2E_{\rm cm}^2} \frac{3}{16\pi} \sum_{VV'} \sum_{i=-1}^{7} L_{\pm(i),VV'}(q^2, \theta, \phi) W_{i,VV'}(q, P_a, P_b) g_i(\theta, \phi) \\ \times \delta(\mathcal{O} - \hat{\mathcal{O}}(q, \theta, \phi)) \hat{\Theta}(q, \phi_L),\end{aligned} \tag{2.26}$$

with the reduced form:

$$\frac{\mathrm{d}\sigma}{\mathrm{d}^4 q \mathrm{d}\cos\theta \mathrm{d}\phi} = \frac{1}{2E_{\rm cm}^2} \frac{3}{16\pi} \sum_{VV'} \sum_{i=-1}^{7} L_{\pm(i),VV'}(q^2, \theta, \phi) W_{i,VV'}(q, P_a, P_b) g_i(\theta, \phi) \tag{2.27}$$

$$= \frac{3}{16\pi} \frac{\mathrm{d}\sigma}{\mathrm{d}^4 q} \Big(1 + \cos^2\theta + \frac{1}{2} A_0 (1 - 3\cos^2\theta) + \sum_{i=1}^{7} A_i g_i(\theta, \phi)\Big), \tag{2.28}$$

where in the final line the sum over the intermediate bosons is assumed. We define the cross sections with definite vector boson helicities – **helicity cross sections**:

$$\frac{\mathrm{d}\sigma_i}{\mathrm{d}^4q} = \frac{1}{2E_{\mathrm{cm}}^2} L_{\pm(i)}(q^2,\theta,\phi) W_i(q,P_a,P_b),$$
$$\frac{\mathrm{d}\sigma}{\mathrm{d}^4q} = \frac{\mathrm{d}\sigma_{-1}}{\mathrm{d}^4q} + \frac{1}{2}\frac{\mathrm{d}\sigma_0}{\mathrm{d}^4q}.$$

The **angular coefficients A_i** are then defined as the normalized helicity cross sections as:

$$A_i = \frac{\mathrm{d}\sigma_i}{\mathrm{d}\sigma_{-1} + 1/2 d\sigma_0}.$$

The angular coefficients describe not only the angular distribution of the final-state leptons but also carry information about the helicity structure of the intermediate vector boson. These coefficients depend on QCD radiation in a nontrivial way: when the transverse momentum q_T of the boson becomes small, some coefficients are suppressed, while others (A_0, A_4) stay finite. Because of this, the angular coefficients are sensitive to soft and collinear QCD effects.

Several of these coefficients have been measured experimentally with growing precision in recent years [17, 18, 19, 20, 21], and they are now important observables for testing the Standard Model. On the theory side, analytic predictions at NNLO currently exist only for the inclusive (see [22, 23] at $q_T > 0$, total results can be restored through the q_T subtraction [24, 25]) and partially for other (see [16] for the $W_{-1,0,1,2}$ and [16, 26, 27] for the $W_{5,6,7}$) helicity cross sections. Fully differential results for *all* (i.e. including the $A_{3,4}$) individual angular coefficients at NNLO are not yet available.

The goal of this project is to compute all the NNLO contributions to helicity cross sections analytically in the finite-q_T region. What we ultimately want are the angular coefficients A_i, which are built from the $\sigma_{i,ab}$. These, in turn, are given by known lepton-side prefactors $L_{(\pm)i}$ times the hadronic structure functions W_i. The prefactors are already known, so the main task is to compute the structure functions W_i from scratch. These are the core objects we need – once we have them, we can assemble the full helicity cross sections and extract the angular coefficients.

Collinear factorization

Finally, it is important to note that in the context of the Drell-Yan process, the differential cross section $d\sigma_i/d^4q$ satisfies the collinear factorization theorem and therefore can be factorized using parton distribution functions (PDFs). This factorization separates the long-distance non-perturbative effects, described by the PDFs, from the short-distance perturbative effects described by the perturbatively calculable hard (partonic, i.e. quarks and gluons) scattering cross section. The differential cross section is thus expressed as a convolution of the PDFs $f_a^{[h_a]}(\xi_a,\mu)$ and $f_b^{[h_b]}(\xi_b,\mu)$, which describe the probability densities for finding partons a and b within the hadrons (in our case, protons) h_a and h_b at momentum fractions ξ_a and ξ_b, with the partonic scattering cross section, summed over all possible initial partons:

$$\frac{\mathrm{d}\sigma_i}{\mathrm{d}^4q} = \sum_{a,b} \int \frac{\mathrm{d}\xi_a}{\xi_a}\frac{\mathrm{d}\xi_b}{\xi_b} f_a^{[h_a]}(\xi_a,\mu) f_b^{[h_b]}(\xi_b,\mu) \hat{\sigma}_{i,ab}(\xi_a P_a, \xi_b P_b, q), \tag{2.29}$$

where μ is the factorization scale and $\hat{\sigma}_{i,ab}(\xi_a P_a, \xi_b P_b, q)$ is the partonic cross section for the process for partons going into the vector boson and hadronic radiation. Perturbative calculations are usually done at the level of partonic observables, which later are combined with PDFs or equivalent non-perturbative objects to obtain the hadronic observables. In our project we will use the information that the CS frame defined in terms of the *partonic* momenta $\xi_a P_a$ and $\xi_b P_b$ is identical to the one that is experimentally reconstructed in terms of the proton *hadronic* momenta P_a and P_b thanks to Eq.(2.23), where in particular the V boson momentum is also held fixed between the two. This means it is not necessary to switch to another, intermediate basis of projectors in order to perform the partonic calculation. Rather, one can directly organize the calculation in terms of the physical observables of interest, without the need for a basis change. Therefore we can simply perform the projections at the level of the *partonic helicity cross sections* $\hat{\sigma}_{i,ab}(\xi_a P_a, \xi_b P_b, q)$ and in the end convolve the result with appropriate PDFs to obtain the hadronic cross sections.

2.3 Amplitude and Squared Amplitude Classification

In high-energy processes like Drell-Yan amplitudes and their squares can be organized according to their scaling with the strong coupling constant α_s. This classification helps to keep track of the different contributions appearing at various orders in perturbation theory and is especially useful when combining results from different types of diagrams.

Amplitude Classification

In perturbative calculations the amplitudes are expanded as power series in α_s, where each term corresponds to a different set of Feynman diagrams. For the Drell-Yan the leading contribution comes from the Born-level amplitude, which is purely electroweak and scales as $\mathcal{O}(\alpha_s^0)$. This corresponds to the basic Drell-Yan process $q\bar{q} \to V \to \ell^+\ell^-$, without any QCD corrections, see Figure 1.1 for an example. Unfortunately, at this level in perturbation theory the vector boson is emitted with null transverse momentum, which corresponds to most of the angular coefficients being zero. We are interested in the limit $q_T > 0$ therefore we focus our calculation on processes with at least one extra final state particle.

The first finite-q_T amplitude appears at order $\mathcal{O}(\alpha_s^{1/2})$. These are known as **$\mathbf{LO_1}$ amplitudes** and describe tree-level processes involving a single absorbed/emitted gluon, such as:

$$q\bar{q} \to Vg, \quad qg \to Vq,$$

with other configurations obtained by crossing. These diagrams play a key role in the cancellation of divergences, as could be seen in the Section 2.4.1. The full set of LO_1 diagrams can be seen in Figure 2.2 We have already established that in our convention our incoming partons have the momenta $p_a \equiv \xi_a P_a$ and $p_b \equiv \xi_b P_b$, and overall the structure of the momenta for the $2 \to 2$ process is shown in Figure 2.2, where

$$q(p_a)\bar{q}(p_b) \to V(q)g(k), \quad q(p_a)g(p_b) \to V(q)q(k).$$

At higher orders, we encounter virtual corrections to the LO_1 amplitudes, referred to as **$\mathbf{NLO_1}$ amplitudes**, which appear at $\mathcal{O}(\alpha_s^{3/2})$. These involve one-loop diagrams and do not change the number or type of external partons, meaning the initial and final states remain the same as in the LO_1 processes:

$$q\bar{q} \to Vg, \quad qg \to Vq.$$

Overall there are 13 possible one-loop diagrams for each of the channels, all of them are shown in Figures 2.3 and 2.4. The external momenta convention is the same as for the LO_1 process.

At a higher perturbative order, we also include a new class of tree-level diagrams, referred to as **$\mathbf{LO_2}$**, which involve two real partons in the final state. Examples of such processes are shown in Figures 2.6 and 2.5. The corresponding partonic channels include:

$$q\bar{q} \to Vq\bar{q}, \quad q\bar{q} \to Vgg, \quad qg \to Vqg, \quad qq \to Vqq, \quad gg \to Vq\bar{q}.$$

The momentum convention is

$$\begin{gathered} q(p_a)\bar{q}(p_b) \to V(q)q(k_1)\bar{q}(k_2), \quad q(p_a)\bar{q}(p_b) \to V(q)g(k_1)g(k_2), \\ q(p_a)g(p_b) \to V(q)q(k_1)g(k_2), \quad q(p_a)q(p_b) \to V(q)q(k_1)q(k_2), \\ g(p_a)g(p_b) \to V(q)q(k_1)\bar{q}(k_2). \end{gathered}$$

In general, the label LO_n, NLO_n, etc., indicates both the perturbative order and the number of final-state partons (i.e., hadronic radiation) in the process. For example:

- LO_1: Tree-level with one emitted parton ($\mathcal{O}(\alpha_s^{1/2})$ in amplitude),
- NLO_1: One-loop corrections to the LO_1 process ($\mathcal{O}(\alpha_s^{3/2})$ in amplitude),
- LO_2: Tree-level with two emitted partons ($\mathcal{O}(\alpha_s^1)$ in amplitude).

The complete classification of amplitudes relevant for our calculations is summarized in Table 2.1.

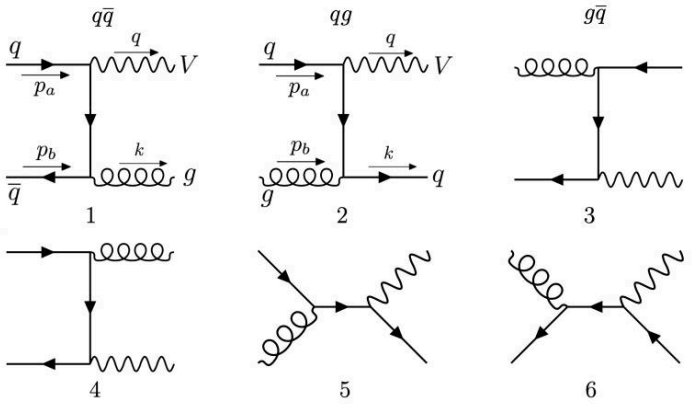


Figure 2.2: Quark-antiquark annihilation with production of a vector boson and hard gluon ($q\bar{q}$ and $\bar{q}q$) and quark-gluon Compton scattering (gq, qg, $g\bar{q}$ and $\bar{q}g$). $\bar{q}q$, gq and $\bar{q}g$ diagrams can be achieved from reversing the direction of the fermion line (from $q\bar{q}$ to $\bar{q}q$, qg to $\bar{q}g$ and $g\bar{q}$ to gq)

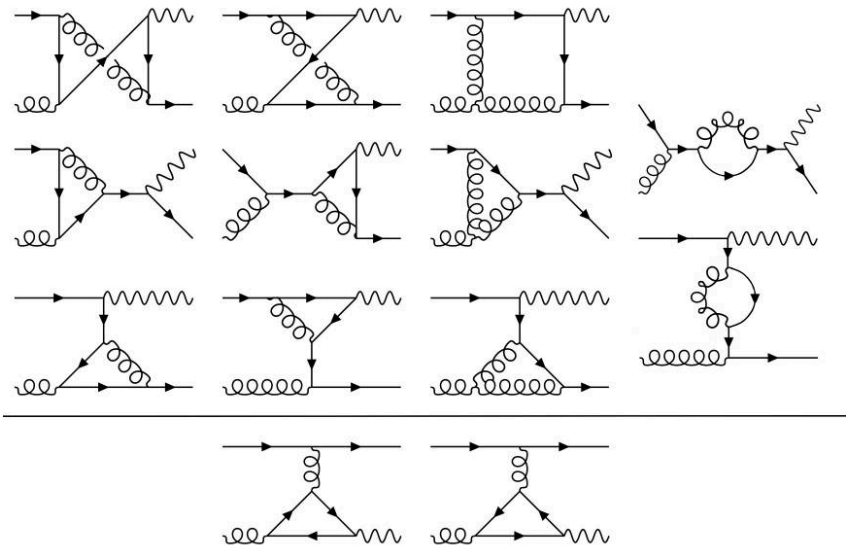


Figure 2.3: NLO_1 diagrams for $qg \to Vq$ process.

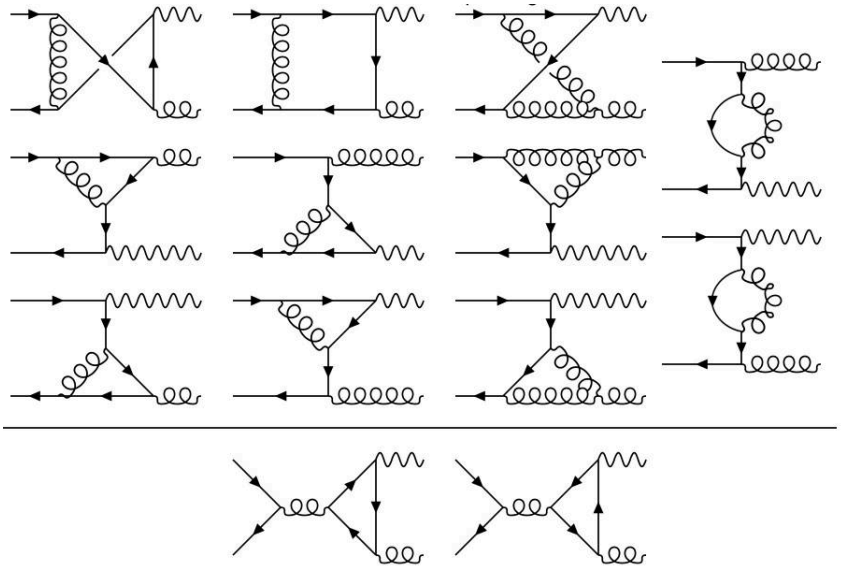


Figure 2.4: NLO_1 diagrams for $q\bar{q} \to Vg$ process.

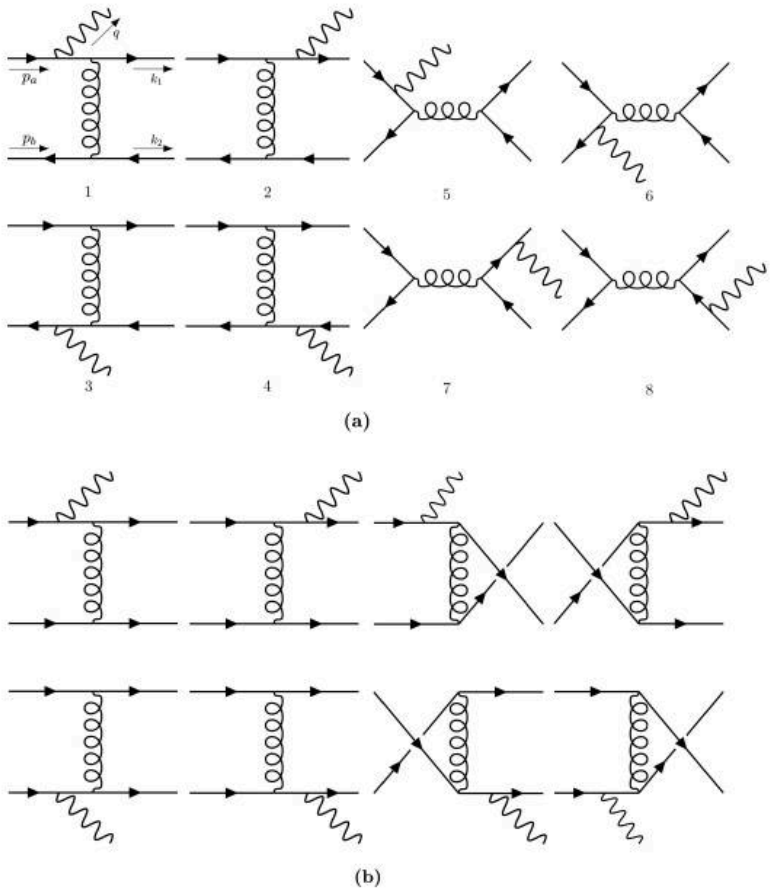


Figure 2.5:
(a) All possible diagrams for the $q\bar{q} \to Vq\bar{q}$ channel: T-channel (1, 2, 3, 4) and S-channel (5, 6, 7, 8)
(b) All possible diagrams for the $qq \to Vqq$ channel: T-channel (1, 2, 3, 4) and U-channel (5, 6, 7, 8)

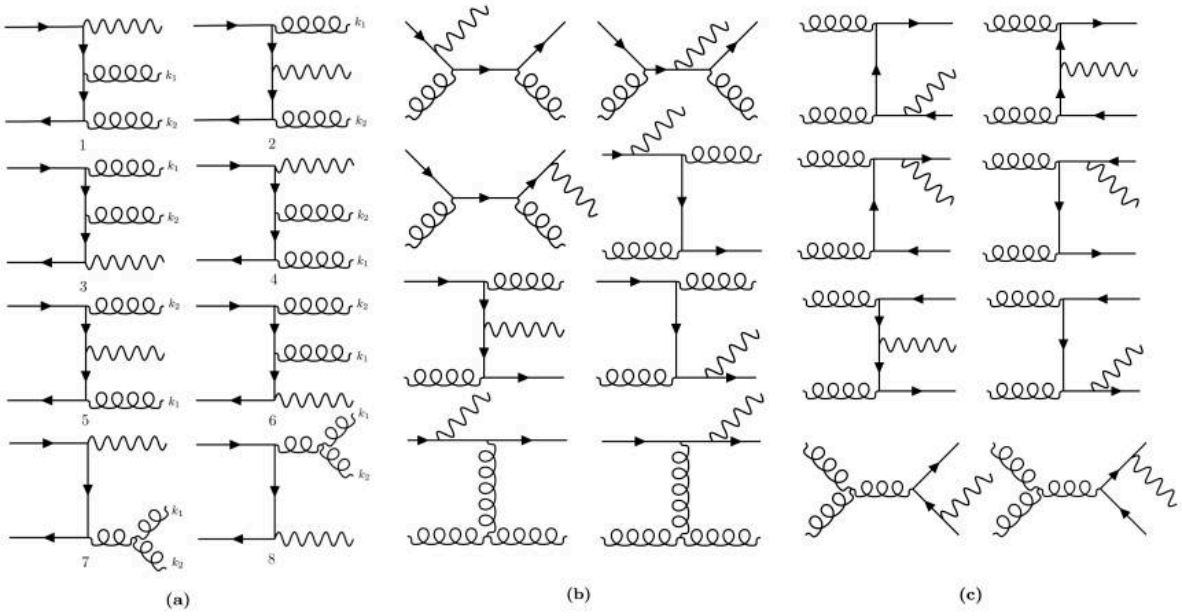


Figure 2.6: All possible diagrams for the (a) $q\bar{q} \to Vgg$, (b) $qg \to Vqg$, (c) $gg \to Vq\bar{q}$ channels

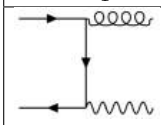
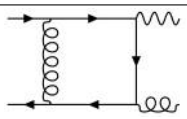
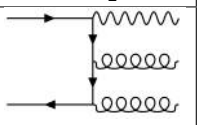
Amplitudes classification $q_T > 0$		
$\mathcal{O}(\alpha_s^{1/2})$	$\mathcal{O}(\alpha_s^{3/2})$	$\mathcal{O}(\alpha_s^1)$
LO_1	NLO_1	LO_2
		
Figure 2.2	Figure 2.4	Figure 2.6

Table 2.1: Classification of Feynman diagrams according to the order of the strong coupling constant α_s at finite vector boson transverse momentum. The table presents different amplitude contributions: leading-order (LO_1) ($\mathcal{O}(\alpha_s^{1/2})$), next-to-leading order (NLO_1) ($\mathcal{O}(\alpha_s^{3/2})$), and higher-order LO_2 ($\mathcal{O}(\alpha_s^1)$). Each column corresponds to a specific order, with associated example Feynman diagrams for $q\bar{q} \to VX$ processes and references to figures with all relevant diagrams.

Squared Amplitude Classification

To compute cross sections, one must square the amplitudes and sum over all relevant partonic channels. These squared amplitudes also follow a classification by their order in α_s. At leading order, the cross section is given by squaring the Born-like amplitude, which contributes at $\mathcal{O}(\alpha_s^0)$. As mentioned above, we are not interested in the null transverse momentum limit, therefore any combination of Born diagrams are beyond this project.

At next-to-leading order (NLO) in finite-q_T, we have the square of the LO_1 amplitude, which contributes at $\mathcal{O}(\alpha_s^1)$. We will refer to this contribution as the **single-real (R)**.

At next-to-next-to-leading order (NNLO, $\mathcal{O}(\alpha_s^2)$), we encounter two types of contributions: the interference between the LO_1 and NLO_1 amplitudes (called **real-virtual or RV**, as the NLO_1 has both real and virtual contributions), and the square of the LO_2 tree-level amplitude (called **double real or RR**, as LO_2 has two real final state emissions). The structure of these contributions is shown in Table 2.2.

Amplitudes squared classification $q_T > 0$	
$\mathcal{O}(\alpha_s^1)$	$\mathcal{O}(\alpha_s^2)$
NLO = $LO_1 \times LO_1$=R	NNLO = $LO_1 \times NLO_1$+ $LO_2 \times LO_2$=RV+RR
	
Figure 2.2 × Figure 2.2	Figure 2.2 × Figure 2.4, Figure 2.6 × Figure 2.6

Table 2.2: Classification of squared amplitudes based on the order of the strong coupling constant α_s at finite-q_T. The table presents different contributions: next-to-leading order (NLO) and next-to-next-to-leading order (NNLO). Each term is constructed by squaring or cross-multiplying amplitudes from different orders, as illustrated by the corresponding example Feynman diagrams for $q\bar{q} \to VX$ and references to figures with all relevant diagrams.

2.3.1 Color structure

Furthermore, it is possible to divide the combinations of diagrams into types based on their color structure, which is defined through the overall **color factor** that appears after summing over (but not yet averaging!) the internal color degrees of freedom in the Feynman diagrams. This classification allows to identify different contributions from different processes and helps isolate terms based on specific color factors or their combinations. These factors represent the Casimir of the fundamental representation (C_F) and the adjoint representation (C_A) of the $SU(3)$ color group, while T_F is the trace normalization factor for the fundamental representation, defined by

$$\mathrm{Tr}[T^a T^b] = T_F \delta^{ab}, \text{ with } T_F = \frac{1}{2} \text{ in } SU(3).$$

This classification simplifies the process of organizing and computing the contributions from various color channels, as the terms with different color structures do not interfere with each other and contribute independently to the final cross-sections.

The main $SU(3)$ relations useful for calculating color structures include:

- $\mathrm{Tr}[T^a T^b] = T_F \delta^{ab}$, where T^a are the generators in the fundamental representation.
- $T^{ai}_j T^{aj}_k = C_F \delta^i_k$, where the Casimir operator for quarks is $C_F = \frac{N_c^2 - 1}{2N_c} = \frac{4}{3}$
- $f^{abc} f^{abd} = C_A \delta^{cd}$, where the Casimir operator for gluons is $C_A = N_c = 3$.

NLO channels can have only one possible color structure $C_F C_A$, therefore all the single-real and real-virtual terms will be proportional to it.

Tables 2.3 and 2.4 display the color factors for the combinations of diagrams corresponding to the real-real processes $q\bar{q} \to Vgg$ and $q\bar{q} \to Vq\bar{q}$, respectively. Other partonic channels can be obtained by crossing from $q\bar{q} \to Vgg$ and $q\bar{q} \to Vq\bar{q}$, and thus inherit the same color factors. In particular, $q\bar{q} \to Vq\bar{q}$ and $qq \to Vqq$ have identical color factors. Similarly, $q\bar{q} \to Vgg$, $qg \to Vqg$, and $gg \to Vq\bar{q}$ share the same color structure.

<table>
<tr><th></th><th>1</th><th>2</th><th>3</th><th>4</th><th>5</th><th>6</th><th>7</th><th>8</th></tr>
<tr><td>1</td><td colspan="3" rowspan="3">$C_F^2 C_A$</td><td colspan="3" rowspan="3">$C_F^2 C_A - \frac{1}{2} C_F C_A^2 \sim C_F$</td><td colspan="2" rowspan="4">$C_F C_A^2$</td></tr>
<tr><td>2</td></tr>
<tr><td>3</td></tr>
<tr><td>4</td><td colspan="3" rowspan="3">$C_F^2 C_A - \frac{1}{2} C_F C_A^2 \sim C_F$</td><td colspan="3" rowspan="3">$C_F^2 C_A$</td></tr>
<tr><td>5</td></tr>
<tr><td>6</td></tr>
<tr><td>7</td><td colspan="6">$C_F C_A^2$</td><td colspan="2">$C_F C_A^2$</td></tr>
<tr><td>8</td></tr>
</table>

Table 2.3: Color structure for diagrams for process $q\bar{q} \to Vgg$ as illustrated in Fig.2.6. Note that the blue ($\sim C_F$ section) is a linear combination of the $C_F^2 C_A$ and $C_F C_A^2$ color structures.

<table>
<tr><th></th><th>1</th><th>2</th><th>3</th><th>4</th><th>5</th><th>6</th><th>7</th><th>8</th></tr>
<tr><td>1</td><td colspan="4" rowspan="4">$T_F C_F C_A$</td><td colspan="4" rowspan="4">$C_F^2 C_A - \frac{1}{2} C_F C_A^2 \sim C_F$</td></tr>
<tr><td>2</td></tr>
<tr><td>3</td></tr>
<tr><td>4</td></tr>
<tr><td>5</td><td colspan="4" rowspan="4">$C_F^2 C_A - \frac{1}{2} C_F C_A^2 \sim C_F$</td><td colspan="4" rowspan="4">$T_F C_F C_A$</td></tr>
<tr><td>6</td></tr>
<tr><td>7</td></tr>
<tr><td>8</td></tr>
</table>

<table>
<tr><th></th><th>1</th><th>2</th><th>3</th><th>4</th><th>5</th><th>6</th><th>7</th><th>8</th></tr>
<tr><td>1</td><td>Q_u^2</td><td colspan="2">$Q_u Q_d$</td><td colspan="4" rowspan="2">Q_u^2
final state the same
in both diagrams</td></tr>
<tr><td>2</td></tr>
<tr><td>3</td><td colspan="2">$Q_u Q_d$</td><td>Q_d^2</td></tr>
<tr><td>4</td></tr>
<tr><td>5</td><td colspan="3" rowspan="4">Q_u^2
final state the same
in both diagrams</td><td colspan="2">Q_u^2</td><td colspan="2">$Q_u Q_d$</td></tr>
<tr><td>6</td></tr>
<tr><td>7</td><td colspan="2">$Q_u Q_d$</td><td colspan="2">Q_d^2</td></tr>
<tr><td>8</td></tr>
</table>

Table 2.4: Color structures (left) and charge configurations (right) for the combinations of diagrams for the process $q\bar{q} \to Vq\bar{q}$, as illustrated in Fig. 2.5. The left side displays the color factors. The right side shows the charge factors, where for diagrams 1, 2, 3 and 4 we have assumed that antiquark is $\bar{u}$ and quark is d. For diagrams 5, 6, 7 and 8 incoming states are $u\bar{u}$ and outgoing states are $d\bar{d}$. Q_u and Q_d represent the charges of up-type and down-type quarks, respectively. Upper left corner of the tables corresponding to combinations of 1, 2, 3 and 4 diagrams is referred as T-channel and lower right corner with 5, 6, 7 and 8 as S-channel.

2.3.2 Charge configuration

Additionally, diagrams can be categorized based on their **charge factors**, as the coupling of the vector boson depends on the flavor and charge of the particles involved. Diagrams may have different charge factors depending on which line (incoming or outgoing) the boson couples to. Since only the flavor of the incoming partons is specified in the partonic cross section, the flavor of the outgoing particles can vary, leading to different charge factors. Similar to the color factors, diagrams with different charge factors are independent and can be treated separately in calculations. The right table in Table 2.4 lists the charge factors for the process $q\bar{q} \to Vq\bar{q}$. Charge factors for $q\bar{q} \to Vgg$ would all be identical, since there is only one quark line participating in the interaction.

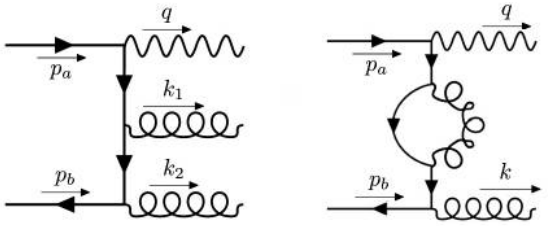


Figure 2.7: Example pole structures in double-real (left) and real-virtual (right) diagrams.

2.4 Poles and renormalization

2.4.1 Pole structure

Throughout this section and in all related computations, we use *dimensional regularization*, which is essential due to the potential appearance of divergences. These divergences manifest as poles in the regulator $\epsilon = (4 - D)/2$ when working in D spacetime dimensions. In general, two kinds of divergences may appear: **ultraviolet (UV)** divergences, which arise from the high-momentum (short-distance) behavior of loop integrals, and **infrared (IR)** divergences, which are associated with soft and collinear limits of massless particles.

Double-real emission diagrams exhibit IR divergences in configurations where the final-state partons become soft or collinear. As a concrete example, consider the left diagram in Fig. 2.7, where the internal quark propagator scales as $(p_b - k_2)^{-2}$. Assuming massless external partons, this becomes $(p_b \cdot k_2)^{-1}$, which further reduces to $(E_{p_b} E_{k_2}(1 - \cos\theta_{p_b k_2}))^{-1}$, where E_{p_b} and E_{k_2} are the energies of the particles p_a and k_1 respectively and the $\theta_{p_b k_2}$ is the angle between these two particles. This expression diverges either when the emitted gluon becomes soft, $k_2^\mu \to 0$, which is defined as the k_2 soft limit, or when it becomes collinear with the incoming quark, $\cos\theta_{p_b k_2} \to 1$, which is referred to as the initial-final collinear limit. Additional IR singularities appear when the two final-state particles themselves become collinear (final-final collinear limit). These various configurations can contribute overlapping divergences, and the generic structure of the resulting poles takes the form

$$-\frac{1}{\epsilon_{\rm IR}^2} + \frac{a}{\epsilon_{\rm IR}}\,, \tag{2.30}$$

where the double pole arises from the overlapping soft and collinear regions of the phase space.

Real-virtual terms, on the other hand, contain both loop and real emission components and are therefore sensitive to both IR and UV regions. An example is shown in the right diagram of Fig. 2.7, where a gluon loop leads to an integral of the form $\int \mathrm{d}^D\ell/\ell^3$, which diverges in the ultraviolet limit $\ell \to \infty$. The structure of poles in such diagrams is typically

$$\frac{1}{\epsilon_{\rm UV}} + \frac{1}{\epsilon_{\rm IR}^2} + \frac{b}{\epsilon_{\rm IR}}\,. \tag{2.31}$$

The infrared double-divergences in the RV processes must cancel with those arising from the RR diagrams, because these are the only places at our order in the strong coupling where the $1/\epsilon^2$ could arise, therefore for physical consistency they have to cancel at the end. The single IR poles in the RV and RR are not necessarily identical, as the mechanism and structure of how the divergence shows up can differ.

The leftover divergences in RV and RR processes are canceled by renormalization. Specifically, the renormalization of the strong coupling constant in the single real processes compensates for the UV divergences in RV diagrams. As mentioned in the Section 2.4.1, during renormalization of the strong coupling constant α_s, the bare coupling g_s takes the form as in Eq.(2.7) in dimensional regularization. This renormalization procedure in the single-real diagrams introduces an ultraviolet pole in ϵ : $-1/\epsilon_{\rm UV}$. When higher-order corrections are included, this pole cancels against corresponding UV divergences from the real-virtual processes.

Therefore at this moment we are only left with the IR poles. For inclusive observables such as the total cross section, the cancellation of soft and collinear divergences can be proven to all orders in perturbation theory. This is a consequence of the Kinoshita-Lee-Nauenberg (KLN) theorem [28, 29], which ensures infrared finiteness in any unitary theory provided that all degenerate final states within a given energy resolution are summed over. Most known example of the infrared safe observable is the

total cross section with initial states as hadrons (in our case, protons) and final state other hadrons and a pair of leptons $\sigma(P_aP_b \to X\ell\bar{\ell})$.
An important example of an observable that is not infrared safe is the *partonic* cross section $\hat{\sigma}(p_ap_b \to X\ell\bar{\ell})$, which is the one we are calculating. Even though the initial particles in hadronic collisions are hadrons, the actual interaction takes place between their constituent quarks and gluons, which do not exist as physical asymptotic states. Because of confinement, partons cannot be observed directly, and their hadronization into physical states is inherently non-perturbative. This means that the assumptions behind the KLN theorem no longer hold. As a result, infrared divergences in the partonic cross section do not cancel, and instead have to be absorbed into the parton distribution functions. This process is referred to as **PDF renormalization**, and it effectively moves the IR poles into the renormalized PDFs, which are the non-perturbative objects extracted from experimental data. The renormalization of parton distribution functions addresses the remaining $(a+b)/\epsilon_{\rm IR}$ IR divergences.
PDFs renormalization is discussed in the section below and a full derivation of the bare PDFs is presented in the Appendix D.

In our final result in order to further simplify the pole subtraction across RV and RR channels we will resort to using the V + jet threshold factorization as an analytic subtraction, as described in the Section 2.6.

2.4.2 PDF renormalization

For some of the IR divergences the poles in the RR and RV will be canceled by renormalizing the PDFs in front of the cross sections of the single real NLO processes. In this section we will derive the master formula for these renormalized cross sections.

So far we have the bare general setup of the collinear factorization theorem from Eq.(2.29):

$$\frac{\mathrm{d}\sigma_i}{\mathrm{d}^4q} = \sum_{a,b} \int \frac{\mathrm{d}\xi_a}{\xi_a}\frac{\mathrm{d}\xi_b}{\xi_b} f_a^{[h_a],\,\mathrm{bare}}(\xi_a) f_b^{[h_b],\,\mathrm{bare}}(\xi_b) \hat{\sigma}_{i,ab}^{\mathrm{bare}}(\xi_aP_a, \xi_bP_b, q, \mu), \tag{2.32}$$

where the UV poles in $\hat{\sigma}_{i,ab}^{\mathrm{bare}}$ have already been renomalized by the strong coupling renormalization.

Our goal is to find the renormalized partonic cross section $\hat{\sigma}_{i,ab}$ in terms of the bare one $\hat{\sigma}_{i,ab}^{\mathrm{bare}}$ by using the expression for the bare PDFs from Eq.(D.7) up to $\mathcal{O}(\alpha_s^2)$. Inserting the expressions for the bare PDFs we obtain:

$$\begin{aligned}\frac{\mathrm{d}\sigma_i}{\mathrm{d}^4q} &= \sum_{a',b'} \int \frac{\mathrm{d}\xi_a'}{\xi_a'}\frac{\mathrm{d}\xi_b'}{\xi_b'} \sum_a \int_{\xi_a'}^1 \frac{\mathrm{d}z_a}{z_a}\Gamma_{a'a}(z_a) f_a^{[h_a]}\Big(\frac{\xi_a'}{z_a},\mu\Big) \sum_b \int_{\xi_b'}^1 \frac{\mathrm{d}z_b}{z_b}\Gamma_{b'b}(z_b) f_b^{[h_b]}\Big(\frac{\xi_b'}{z_b},\mu\Big) \hat{\sigma}_{i,ab}^{\mathrm{bare}}(\xi_a'P_a, \xi_b'P_b, q, \mu) \\ &\equiv \sum_{a,b} \int \frac{\mathrm{d}\xi_a}{\xi_a}\frac{\mathrm{d}\xi_b}{\xi_b} f_a^{[h_a]}(\xi_a,\mu) f_b^{[h_b]}(\xi_b,\mu) \hat{\sigma}_{i,ab}(\xi_aP_a, \xi_bP_b, q, \mu),\end{aligned}$$

where

$$\Gamma_{ij}(z) = \delta_{ij}\delta(1-z) + \frac{\alpha_s(\mu)}{4\pi}\frac{P_{ij}^{(0)}(z)}{\epsilon} + \mathcal{O}(\alpha_s^2), \tag{2.33}$$

and the DGLAP splitting functions [30, 31, 32] $P_{ij}(z)$ – the probabilities that a parton of type j emits a (collinear) parton of type i, with a fraction z – are defined in the Appendix D.
After rearranging the sums, identifying the $\xi_{a,b}'/z_{a,b} \equiv \xi_{a,b}$ and rewriting in terms of partonic momenta one achieves the following expression for the renormalized partonic cross section:

$$\hat{\sigma}_{i,ab}(p_a,p_b,q,\mu) = \lim_{\epsilon\to 0} \sum_{a',b'} \int_{z_a\xi_a}^1 \frac{\mathrm{d}z_a}{z_a}\Gamma_{a'a}(z_a) \int_{z_b\xi_b}^1 \frac{\mathrm{d}z_b}{z_b}\Gamma_{b'b}(z_b) \hat{\sigma}_{i,a'b'}^{\mathrm{bare}}(z_ap_a, z_bp_b, q, \mu), \tag{2.34}$$

where we have already switched to the partonic momenta p_a, p_b.
Now one can expand both renormalized and bare cross sections in powers of the strong coupling:

$$\hat{\sigma}_{i,ab}^{\mathrm{bare}}(p_a,p_b,q,\mu) = \sum_n \left[\frac{\alpha_s(\mu)}{4\pi}\right]^n \hat{\sigma}_{i\,ab}^{\mathrm{bare}\,(n)}(p_a,p_b,q,\mu) \tag{2.35}$$

$$\hat{\sigma}_{i,ab}(p_a,p_b,q,\mu) = \sum_n \left[\frac{\alpha_s(\mu)}{4\pi}\right]^n \hat{\sigma}_{i\,ab}^{(n)}(p_a,p_b,q,\mu), \tag{2.36}$$

and solve for the renormalized cross section order-by-order.
A quick check for NLO ($\mathcal{O}(\alpha_s^1)$) gives $\hat{\sigma}^{(1)}_{i,ab}(p_a,p_b,q,\mu) = \hat{\sigma}^{\text{bare }(1)}_{i,ab}(p_a,p_b,q,\mu)$ for $\epsilon \to 0$ and $q_T > 0$.
For NNLO ($\mathcal{O}(\alpha_s^2)$) one gets:

$$\hat{\sigma}^{(2)}_{i,ab}(p_a,p_b,q,\mu) = \hat{\sigma}^{\text{bare }(2)}_{i,ab}(p_a,p_b,q,\mu) + \sum_{a'} \int \frac{\mathrm{d}z_a}{z_a} \frac{P^{(0)}_{a'a}(z_a)}{\epsilon} \hat{\sigma}^{\text{bare }(1)}_{i,a'b}(z_a p_a, p_b, q, \mu) + \sum_{b'} \int \frac{\mathrm{d}z_b}{z_b} \frac{P^{(0)}_{b'b}(z_b)}{\epsilon} \hat{\sigma}^{\text{bare }(1)}_{i,ab'}(p_a, z_b p_b, q, \mu).$$

The integrals over the momentum fractions z_a/z_b can be written in the following way:

$$\int \frac{\mathrm{d}z_a}{z_a} P^{(0)(z_a)}_{a'a} \hat{\sigma}^{\text{bare }(1)}_{i,a'b}(z_a p_a, p_b, q, \mu) = \int \frac{\mathrm{d}z_a}{z_a} P^{(0)}_{a'a}(z_a) \bar{\sigma}_{i,a'b}(z_a p_a, p_b, q, \mu) \delta(k^2)\Big|_{k=z_a p_a + p_b - q} \equiv \frac{1}{\Delta_a^*} P^{(0)}_{a'a}(z_a^*) \bar{\sigma}_{i,a'b}(z_a^* p_a, p_b, q, \mu), \tag{2.37}$$

where the barred cross section is

$$\hat{\sigma}^{\text{bare }(1)}_{i,a'b}(z_a p_a, p_b, q, \mu) = \bar{\sigma}^{\text{bare }(1)}_{i,a'b}(z_a p_a, p_b, q, \mu) \delta(k^2)\Big|_{k=z_a p_a + p_b - q}.$$

Here we have used the fact that the first-order cross section, single real one, within the assumption of the massless external states has a $\delta(k^2)$ enforcing the final state k parton to be massless. We have separated out the k parton zero-mass delta function $\delta(k^2) = \delta((z_a p_a + p_b - q)^2)$ and denoted the rest of the cross section as $\bar{\sigma}_{i,a'b}$. The z_a^* is the solution to the $(z_a p_a + p_b - q)^2 = 0$ and Δ_a^* is the derivative of the $(z_a p_a + p_b - q)^2$ with respect to z_a at point z_a^*.

In order to give explicit expressions for these variables we will go to the lightcone coordinates, which in 4 dimensions for a 4-momentum $k = (E, k_x, k_y, k_z)$ are defined as follows:

$$\begin{cases} k^- = E + k_z \\ k^+ = E - k_z \\ k_T = \sqrt{k_x^2 + k_y^2} \\ \phi = \arctan \dfrac{k_y}{k_x} \end{cases} \tag{2.38a}$$

$$\begin{cases} E = \dfrac{k^- + k^+}{2} \\ k_x = k_T \cos\phi \\ k_y = k_T \sin\phi \\ p_z = \dfrac{k^- - k^+}{2} \end{cases} \tag{2.38b}$$

In terms of light cone coordinates these starred momentum fractions and Jacobians for both a and b hadrons are:

$$z_a^* = \frac{k^+ q^- + q_T^2}{k^+(k^- + q^-)}, \tag{2.39a}$$

$$\Delta_a^* = k^+(k^- + q^-), \tag{2.39b}$$

$$z_b^* = \frac{k^- q^+ + q_T^2}{k^-(k^+ + q^+)}, \tag{2.39c}$$

$$\Delta_b^* = k^-(k^+ + q^+). \tag{2.39d}$$

Finally, the master formula for the renormalized NNLO cross section reads:

$$\hat{\sigma}^{(2)}_{i,ab}(\xi_a P_a, \xi_b P_b, q, \mu) = \hat{\sigma}^{\text{bare }(2)}_{i,ab}(\xi_a P_a, \xi_b P_b, q, \mu) + \frac{1}{\epsilon} \sum_{a'} \frac{P^{(0)}_{a'a}(z_a^*)}{\Delta_a^*} \bar{\sigma}^{\text{bare }(1)}_{i,a'b}(z_a^* p_a, p_b, q, \mu) + \frac{1}{\epsilon} \sum_{b'} \frac{P^{(0)}_{b'b}(z_b^*)}{\Delta_b^*} \bar{\sigma}^{\text{bare }(1)}_{i,ab'}(p_a, z_b^* p_b, q, \mu). \tag{2.40}$$

2.5 Introduction to Soft-Collinear Effective Theory

The great complexity of the pole structure expected in the final result motivates the use of a more systematic and efficient method for handling renormalization. To this end, we use threshold factorization as a subtraction scheme in the limit $k_X^2 \to 0$. This approach naturally leads to the framework of Soft-Collinear Effective Theory, which provides the tools to implement the factorization.

Soft-Collinear Effective Theory (SCET)[33, 34, 35, 36, 37] is a top-down effective field theory developed to describe the dynamics of QCD in specific kinematic regimes. Unlike other EFTs, such as the Fermi effective theory of weak interactions [38, 39], where entire particles are integrated out, SCET integrates out only the off-shell modes of the fields.

In this way, SCET provides a framework for describing QCD in regions where radiation is either soft (low energy) or collinear (small angle). In the section on the pole structure 2.4.1 we have already used this terminology when referring to the various behavior limits of the final state particles. Here these regions are defined more strictly. These kinematic configurations are everywhere in high-energy processes at hadron colliders, where the associated soft and collinear singularities dominate the structure of the cross section in many observables.

SCET is formulated as a systematic expansion in a small power-counting parameter $\lambda \ll 1$, which encodes the hierarchy between the soft/collinear and hard momentum scales. Therefore this theory has a wide range of applications, ranging from the derivation of factorization theorems to the resummation of Sudakov logarithms.

In this thesis SCET is used for formulation of the factorization formula at the V + jet threshold in Section 2.6. The following sections on SCET introduction are based on ref. [40] and ref. [41]

2.5.1 Degrees of Freedom in SCET

To set up SCET, one first identifies the relevant degrees of freedom (modes) based on the scaling of their momenta with λ.

In SCET, the relevant degrees of freedom correspond to highly energetic, nearly massless particles propagating close to the light cone, making lightcone coordinates a natural choice for describing their momenta. Therefore, the lightcone decomposition is used, introducing lightlike reference vectors $n_i^\mu = (1, \vec{n}_i)$ and $\bar{n}_i^\mu = (1, -\vec{n}_i)$ satisfying $n_i^2 = \bar{n}_i^2 = 0$, $n_i \cdot \bar{n}_i = 2$. These vectors can either correspond to the incoming hadron directions or the outgoing hadron or jet directions. Any four-momentum p^μ can be then decomposed in lightcone coordinates with respect to each of the reference vectors, as

$$p^\mu = \frac{n_i \cdot p}{2} \bar{n}_i^\mu + \frac{\bar{n}_i \cdot p}{2} n_i^\mu + p_\perp^\mu \equiv (p^+, p^-, \vec{p}_\perp),$$

where the p^+, p^- correspond to the components along the reference vectors $n_i, \bar{n}_i$ and the last two-dimensional entry $\vec{p}_\perp$ corresponds to the transverse plane to the reference vectors:

$$p^+ \equiv n_i \cdot p, \quad p^- \equiv \bar{n}_i \cdot p. \tag{2.41}$$

The four-momentum squared is thus:

$$p^2 = p^+ p^- + p_\perp^2 = p^+ p^- - \vec{p}_\perp^2, \tag{2.42}$$

where we have highlighted the difference between the Minkowski $p_\perp^\mu$ and Euclidean $\vec{p}_\perp$. In the following we will denote the magnitude of the Minkowski vector as $p_T^2 = -p_\perp^2 > 0$. In the proton-proton collision with reference vectors aligning with the direction of the two protons, both of which travel along the z axis, p_T would be equivalent to the transverse momentum of the particle with momentum p^μ. For the simplicity in the future we will drop the subscript i in the reference vector n_i, assuming that there is a whole set of possible collinear directions.

In SCET we are aiming to integrate out particles with $p^2 \sim \lambda Q^2, Q^2$, but keep the degrees of freedom that have weaker scaling with λ. That means that hard modes such as whose that scale as

$$p_h^\mu \sim Q(1, 1, 1),$$

and their effects will be encoded in Wilson coefficients of local SCET operators which are obtained via matching from QCD.

The key momentum modes with $p^2 \lesssim \lambda^2 Q^2$ in SCET (ignoring the Glauber modes[2]) are:

- **(Anti-)Collinear modes:** These describe energetic particles traveling along the reference directions $(\bar{n}_i^\mu)$ n_i^μ. Their momenta scale as

$$p_n^\mu \sim Q(\lambda^2, 1, \lambda), \tag{2.43}$$
$$p_{\bar{n}}^\mu \sim Q(1, \lambda^2, \lambda), \tag{2.44}$$

  where the components refer to scaling in the $(n \cdot p, \bar{n} \cdot p, p_\perp) = (p^+, p^-, p_\perp)$ directions. Note that the power counting parameter λ is not unique, as its definition depends on the process.

- **Soft modes:** These are the isotropic (i.e. scaling homogeneously with λ) low energy modes with scaling

$$p_{\rm s}^\mu \sim Q(\lambda, \lambda, \lambda).$$

  Since the lightcone components of the soft modes are larger that the ones for the collinear modes, the interaction between them will take the collinear particle off the mass shell. Essentially, since the interaction of the soft modes with collinear ones would be scaling as λQ:

$$p_n \cdot p_s \sim \frac{1}{2} Q^2 (p_n^+ p_s^- + p_n^- p_s^+ - 2\vec{p}_{n,\perp} \vec{p}_{s,\perp}) = \frac{1}{2} Q^2 (\lambda^3 + \lambda - \lambda^2) \sim \lambda Q^2,$$

  interactions between soft and collinear modes has to be integrated out and incorporated into the EFT matching coefficient.

- **Ultrasoft (or usoft) modes:** These correspond to isotropic lowest-energy radiation and scale homogeneously as

$$p_{\rm us}^\mu \sim Q(\lambda^2, \lambda^2, \lambda^2).$$

  The interactions of these modes with collinear one is included into the SCET Lagrangian.

In many cases, the description of a given observable involves only collinear modes and either ultra-soft or soft modes, depending on what is relevant to the measurement. These two regimes are categorized as $\mathrm{SCET_I}$, when the dominant soft radiation is usoft, and $\mathrm{SCET_{II}}$, when soft modes $\sim (\lambda, \lambda, \lambda)$ are relevant instead. For our case we will be using the Lagrangian with $\mathrm{SCET_I}$ fields and refer to the ultrasoft field as just soft for the simplicity.

2.5.2 Leading-Power SCET Operators and SCET Lagrangian

The objective of this section is to describe SCET operators and write down the full form of the leading-power SCET Lagrangian.
At leading power $\mathcal{O}(\lambda^0)$, operators in the SCET Lagrangian are constructed from gauge-invariant combinations of collinear and soft fields that scale homogeneously with λ, obey the symmetries of the theory (including gauge and reparameterization invariance, which are not covered in this thesis, for detailed explanation see e.g. chapter 5 in ref. [41]), and respect the power-counting rules. The allowed operator structures are determined by these scaling and symmetry constraints, and subleading corrections are systematically organized as higher-order terms in the λ-expansion.
The relevant degrees of freedom describing quarks and gluons are:

$$\psi(x) = \psi_n(x) + \psi_{\bar{n}}(x) + \psi_s(x); \tag{2.45}$$
$$A^\mu(x) = A_n^\mu(x) + A_{\bar{n}}^\mu(x) + A_s^\mu(x), \tag{2.46}$$

where we have separated out the fields into the (anti-)collinear $(\psi_{\bar{n}}, A_{\bar{n}}^\mu)$ ψ_n, A_n^μ and soft ψ_s, A_s^μ terms. It is not necessary to introduce explicit fields for other momentum regions, such as the hard region, since their effects are integrated out and encoded in the Wilson coefficients multiplying operators constructed

[2]Glauber modes ($p_{\rm G}^\mu \sim Q(\lambda^2, \lambda^2, \lambda)$) are spacelike momentum modes that can mediate long-range interactions between different collinear sectors. They can, in some cases, obstruct factorization by introducing non-local effects. However, for many standard observables, their contributions cancel or are power suppressed. Since we are not deriving factorization from first principles and focus only on the leading-power operator structure in $\mathrm{SCET_I}$, we will neglect Glauber modes in this discussion. For a detailed treatment, see [42].

from soft and collinear fields.
The fermionic field in each collinear sector is further decomposed into two components:

$$\psi_n(x) = \xi_n(x) + \varphi_n(x), \tag{2.47}$$

where

$$\xi_n(x) = \frac{\not{n}\bar{\not{n}}}{4}\psi_n(x), \quad \varphi_n(x) = \frac{\bar{\not{n}}\not{n}}{4}\psi_n(x) \tag{2.48}$$

We make this decomposition because the two components of the fermion field scale differently with λ, since collinear momenta scale differently along different lightcone directions. Also, one of the component, φ, drops out of the SCET Lagrangian at leading power due to its equation of motion being $\bar{\not{n}}\varphi_n = 0$. Following the prescription in ref. [40] we would arrive at the power scaling for the fields:

$$\begin{aligned}
&\text{collinear quark fields:} && \xi_n(x) \sim \lambda, \quad \varphi_n(x) \sim \lambda^2, \\
&\text{soft quark field:} && \psi_s \sim \lambda^3, \\
&\text{collinear gluon fields:} && A_n(x) \sim (\lambda^2, 1, \lambda), \\
&\text{soft gluon field:} && A_s(x) \sim (\lambda^2, \lambda^2, \lambda^2),
\end{aligned} \tag{2.49}$$

where, as noted above, the φ_n field is suppressed in comparison with the ξ_n.

The general SCET Lagrangian is given as a sum of the hard operators $\mathcal{L}_{\text{hard}}$ and a dynamical Lagrangian encoding the low energy interactions $\mathcal{L}_{\text{dyn}}$:

$$\mathcal{L}_{\text{SCET}} = \mathcal{L}_{\text{hard}} + \mathcal{L}_{\text{dyn}}, \tag{2.50}$$

which can be expanded in the λ:

$$\mathcal{L}_{\text{SCET}} = \sum_{i=1}^{\infty} \mathcal{L}_{\text{hard}}^{(i)} + \sum_{i=1}^{\infty} \mathcal{L}_{\text{dyn}}^{(i)}. \tag{2.51}$$

Since we are interested in using the SCET for derive (or at least explain) threshold factorization theorem, we will be focusing on the dynamical Lagrangian. The rest of the leading-power $\mathcal{L}_{\text{dyn}}$ can be written as

$$\mathcal{L}_{\text{dyn}}^{(0)} = \sum_{n_i} \mathcal{L}_{n_i}^{(0)} + \mathcal{L}_s^{(0)}. \tag{2.52}$$

Here, $\mathcal{L}_{n_i}^{(0)}$ describes the leading-power interactions of particles within a given collinear sector $n_i = n, \bar{n}$ (where again, n refers to a possible set of collinear directions, not just one), including their interactions with soft gluons, while $\mathcal{L}_s^{(0)}$ describes the self-interactions of soft particles.

To get the explicit leading order expressions for the SCET Lagrangian, one first defines the covariant derivative:

$$iD_\mu \equiv i\partial_\mu + g_s A_\mu = i\partial_\mu + g_s(A_{n,\mu} + A_{\bar{n},\mu} + A_{s,\mu}). \tag{2.53}$$

The n collinear Lagrangian is thus:

$$\begin{aligned}
\mathcal{L}_{n\xi}^{(0)} = \bar{\psi}_n i\not{D}\psi_n &= \bar{\xi}_n \frac{\bar{\not{n}}}{2} in\cdot D\xi_n + \bar{\xi}_n i\not{D}_\perp \frac{1}{i\bar{n}\cdot D} i\not{D}_\perp \frac{\bar{\not{n}}}{2}\xi_n \\
&= \bar{\xi}_n \frac{\bar{\not{n}}}{2} in\cdot D\xi_n + \bar{\xi}_n i\not{D}_{n,\perp} \frac{1}{i\bar{n}\cdot D_n} i\not{D}_{n,\perp} \frac{\bar{\not{n}}}{2}\xi_n,
\end{aligned} \tag{2.54}$$

where we have both applied the relations $\not{n}\xi_n = 0$, $\bar{\not{n}}\varphi_n = 0$ $\bar{\xi}_n \not{D}_\perp \xi_n = 0$, $\bar{\varphi}_n \not{D}_\perp \varphi_n = 0$ as well as integrated out the φ_n field from the Lagrangian as explained in Section 4.2 in [40]. Note that this Lagrangian now also includes the interaction between soft and collinear fields though the covariant derivative in the first term. Additionally, since at leading power only the $n \cdot A$ component of the gluon field has the same scaling in both the collinear and soft sectors (see. Eq.(2.49)), while all other components of the soft gluon field are power suppressed, the second term in the expression – which involves only contractions with $\bar{n} \cdot A$ and $A_\perp$ – describes exclusively interactions between particles in the collinear sector, and thus contains only the collinear covariant derivative:

$$iD_{n,\mu} \equiv i\partial_\mu + g_s A_{n,\mu}.$$

For the same reason it is possible to expand the covariant derivative in the light cone basis exchanging the $-$ and $\perp$ components for the ones only including collinear fields:

$$D^\mu = n \cdot D \frac{\bar{n}^\mu}{2} + \bar{n} \cdot D_n \frac{n^\mu}{2} + D^\mu_{n,\perp}. \tag{2.55}$$

Since the $n \cdot A_s(x)$ is the only component of the soft gluon field that is not power suppressed with respect to the $n \cdot A_n(x)$ component of the collinear gluon field, it would be the only term entering the interaction of the soft and collinear fields:

$$in \cdot D = in \cdot \partial + g_s \, n \cdot A_n(x) + g_s \, n \cdot A_s(x_-), \tag{2.56}$$

where $n \cdot A_s(x_-)$ is the above mentioned leading power expansion term of the soft gluon field around the point $x_-^\mu = (x \cdot \bar{n}) n^\mu / 2$.

As for the gluon fields, collinear terms in the Lagrangian would have the same form as the QCD Lagrangian with gluon field A^μ exchanged for the collinear gluon field A_c^μ:

$$\mathcal{L}^{(0)}_{ng} = -\frac{1}{4} (F^a_n)_{\mu\nu} (F^a_n)^{\mu\nu}. \tag{2.57}$$

The Lagrangian with soft fields has the exact form as the QCD Lagrangian, but with the fields replaced by their soft equivalents and the covariant derivative including only the soft part:

$$\mathcal{L}^{(0)}_s = \bar{\psi}_s i \not{D}_s \psi_s - \frac{1}{4} (F^a_s)_{\mu\nu} (F^a_s)^{\mu\nu}, \tag{2.58}$$

where, unlike the collinear Lagrangian, which includes covariant derivatives containing both collinear and soft gauge fields, the soft Lagrangian involves only the soft covariant derivative. This asymmetry arises because soft gluons can interact with collinear particles at leading power, due to their long wavelength relative to collinear modes. In contrast, from the perspective of soft fields, collinear fluctuations are highly off-shell and their effects are power-suppressed. As a result, collinear fields do not appear in the soft Lagrangian at leading order but contribute instead through higher-order operators. The soft covariant derivative and field strength are given as:

$$\begin{aligned} iD^\mu_s &= i\partial^\mu + g_s A^\mu_s = i\partial^\mu + g_s (A^a_s)^\mu T^a \,, \\ ig_s (F^a_s)^{\mu\nu} t^a &= [iD^\mu_s, iD^\nu_s] = ig_s \left\{ \partial^\mu A^\nu_s - \partial^\nu A^\mu_s - ig_s [A^\mu_s, A^\nu_s] \right\} \end{aligned}$$

Thus full leading-order SCET dynamical Lagrangian is:

$$\mathcal{L}^{(0)}_{\text{dyn}} = \bar{\psi}_s i \not{D}_s \psi_s - \frac{1}{4} (F^{s,a}_{\mu\nu})^2 + \bar{\xi}_n \frac{\not{\bar{n}}}{2} \left[in \cdot D + i \not{D}_{n,\perp} \frac{1}{i\bar{n} \cdot D_n} i \not{D}_{n,\perp} \right] \xi_n - \frac{1}{4} (F^{n,a}_{\mu\nu})^2 + (n \leftrightarrow \bar{n}), \tag{2.59}$$

where we have kept the color coding from [40] with soft terms being colored in brown and collinear ones colored in blue. In the last term it is assumed replacement of n^μ by $\bar{n}^\mu$ and vice versa only in the collinear sector in order to achieve the anti-collinear term.

At leading power in the λ-expansion, the interaction between collinear quark fields and soft gluons in the SCET Lagrangian appears only through the $n \cdot A_s$ component of the soft gauge field. This coupling has an eikonal form and can be removed via a field redefinition, known as the *decoupling transformation*, which effectively factorizes the Lagrangian into independent soft and collinear parts.
For the collinear quark field and the collinear gluon field in the n-direction, the transformation takes the form respectively:

$$\begin{aligned} \xi_n(x) &\to Y_n(x_-) \, \xi^{(0)}_n(x), \\ A^\mu_n(x) &\to Y_n(x_-) A^{(0)\mu}_n(x) Y^\dagger_n(x_-), \end{aligned} \tag{2.60}$$

where $\xi^{(0)}_n$ and $A^{(0)\mu}_n(x)$ are the decoupled collinear quark and gluon fields, and $Y_n(x)$ is a **soft Wilson line**:

$$Y_n(x) = \mathbf{P} \exp \left(i g_s \int_{-\infty}^0 \mathrm{d}s \, n \cdot A^a_s(x + sn) T^a \right). \tag{2.61}$$

In the last line the symbol $\mathbf{P}$ refers to the path ordering of the color matrices. The conjugate Wilson line $Y^\dagger_n$ is defined with the opposite ordering prescription.

In general, a **Wilson line** $W(x,y)$ is a gauge-invariant, non-local operator defined as the path-ordered exponential of the gauge field along a chosen spacetime path with endpoints x and y. It is customary in SCET to use Wilson lines that go to the infinity $W(x) \equiv W(x, -\infty\bar{n})$. In more broad terms, in QCD Wilson line represents the parallel transport of a color charge through a gauge field and captures the accumulated phase associated with traversing a gauge connection, therefore encoding how gauge-dependent fields transform along that path.
Analogously, the anti-collinear fields $\xi_{\bar{n}}$ are redefined with Wilson lines $Y_{\bar{n}}$ along the $\bar{n}$-direction.

After performing this transformation, the leading-power SCET Lagrangian becomes fully decoupled:

$$\mathcal{L}^{(0)}_{\text{dyn}} = \sum_{n_i=n,\bar{n}} \mathcal{L}^{(0)}_{n_i}(\xi^{(0)}_{n_i}, A^{(0)}_{n_i}) + \mathcal{L}^{(0)}_{s}(\psi_s, A_s), \tag{2.62}$$

in which the interaction term now reads:

$$\bar{\xi}_n \frac{\bar{n}\!\!\!/}{2} in\cdot D \xi_n(x) \to \bar{\xi}^{(0)}_n \frac{\bar{n}\!\!\!/}{2} in\cdot D^{(0)}_n \xi^{(0)}_n(x) = \bar{\xi}^{(0)}_n \frac{\bar{n}\!\!\!/}{2} (in\cdot\partial + g_s n\cdot A^{(0)}_n(x)) \xi^{(0)}_n(x) \tag{2.63}$$

This structure reflects that, at leading power, collinear and soft sectors evolve independently. It is important to emphasize that this decoupling holds only at leading order in the power-counting expansion. At subleading power ($\mathcal{O}(\lambda)$ and beyond), the decoupling breaks down, and subleading Lagrangian terms include nontrivial soft-collinear interactions.

The SCET Lagrangian does more than just identify the relevant degrees of freedom and their scaling with λ, as it also makes clear how the different sectors of the theory interact and organize at leading power. After performing the decoupling transformation, the soft and collinear sectors no longer interact directly in the Lagrangian, which allows us to separate their contributions in physical observables, such as cross sections. This separation forms the basis for writing a factorization theorem, which will be introduced and applied in the following sections.

2.6 Using V + jet threshold factorization as an analytic subtraction

In this section, we go back to the pole structure described in Section 2.4.1 and describe our approach to organizing and handling the infrared and ultraviolet poles that appear in our process. We begin by separating the cross section according to its behavior in the limit there the invariant mass of the final-state hadronic system $k_X^2 \to 0$, which is called **partonic threshold limit**. This limit corresponds to the ***V* + jet configuration**, where the vector boson must recoil against a jet, and the available phase space restricts this jet to be nearly massless. We can apply the threshold factorization theorem derived from SCET, which significantly simplifies the structure of infrared singularities in this limit. This approach allows us to make use of known results for the soft and jet functions, and reduces the remaining task to computing the infrared-finite part of the real-virtual corrections.

2.6.1 Parametrizing the PDF convolution integral

First things first we define the parametrization used in this section.
The partonic cross section depends on p_a^μ, p_b^μ, q^μ, which together fix the total momentum $k_X^\mu \equiv k^\mu$ of the hadronic final state with $k_\perp^\mu = -q_\perp^\mu$. To organize the PDF convolution integral, it is convenient to change integration variables to the rapidity and invariant mass of the hadronic final state,

$$y_k = \frac{1}{2}\ln\frac{k^-}{k^+}\,, \qquad k^2 = k^+k^- - k_T^2 = k^+k^- - q_T^2\,. \tag{2.64}$$

Accounting for the simple Jacobian of $\mathrm{d}\xi_a\,\mathrm{d}\xi_b = \mathrm{d}y_k\,\mathrm{d}k^2/(P_a^- P_b^+)$, this results in

$$\frac{\mathrm{d}\sigma_i}{\mathrm{d}^4 q} = \sum_{a,b}\int \frac{\mathrm{d}\xi_a}{\xi_a}\frac{\mathrm{d}\xi_b}{\xi_b} f_a^{[h_a]}(\xi_a) f_b^{[h_b]}(\xi_b)\hat{\sigma}_{i,ab}(\xi_a P_a, \xi_b P_b, q, \mu) \tag{2.65}$$

$$= \sum_{a,b}\int \frac{\mathrm{d}y_k\,\mathrm{d}k^2}{p_a^- p_b^+} f_a^{[h_a]}\Big(\frac{p_a^-}{P_a^-},\mu\Big) f_b^{[h_b]}\Big(\frac{p_b^+}{P_b^+},\mu\Big)\,\hat{\sigma}_{i\,ab}(p_a,p_b,q,\mu)\,, \tag{2.66}$$

where now $p_{a,b}$ are dependent functions of y_k and k^2 under the integral,

$$p_a^\mu = \frac{n^\mu}{2}\Big(q^- + \sqrt{q_T^2+k^2}\,e^{+y_k}\Big)\,, \qquad p_b^\mu = \frac{\bar{n}^\mu}{2}\Big(q^+ + \sqrt{q_T^2+k^2}\,e^{-y_k}\Big)\,. \tag{2.67}$$

And the $\hat{\sigma}_{i,ab}$ in general would then include terms which arise from the distributional expansion of terms with $1/k^{2+2\epsilon}$, and the finite remainder $\mathcal{O}[(k^2)^0]$. We stress that going from Eq.(2.65) to Eq.(2.66) involves no approximation. In Eq.(2.66), we have kept the integration limits implicit in the physical support of the partonic cross section and the PDFs,

$$f_i(x,\mu) \propto \theta(x)\,\theta(1-x)\,, \qquad \hat{\sigma}_{i\,ab}(p_a,p_b,q,\mu) \propto \theta(k^2)\,, \tag{2.68}$$

where $\theta(k^2)$ is the Heaviside function.

Performing the inner k^2 integral first, the explicit integration range for k^2 at fixed y_k reads

$$0 \le k^2 \le \Big[\min\Big\{(P_a^- - q^-)e^{-y_k}, (P_b^+ - q^+)e^{+y_k}\Big\}\Big]^2 - q_T^2\,. \tag{2.69}$$

The outer integration bounds on y_k are then

$$-\ln\frac{P_b^+ - q^+}{q_T} \le y_k \le \ln + \frac{P_a^- - q^-}{q_T}\,. \tag{2.70}$$

2.6.2 Structure of soft and final-state collinear singularities

The advantage of having k^2 as one of the integration variables in Eq.(2.66) is that at $q_T > 0$ singularities that require a plus distribution prescription in the renormalized partonic cross section uniquely arise as $k^2 \to 0$. This is the limit of small invariant mass of the final-state partonic system, where either (a) all final-state partons except for one become soft or (b) all final-state partons become collinear to each other. By contrast, other singularities that for $q_T \ge 0$ can still manifest as plus distributions within the renormalized partonic cross section, such as the limit of *all* partons becoming soft, are cut off by $q_T > 0$.

Essentially, using this parametrization the partonic cross section divides into two contributions: **singular** and the **non-singular** with respect to the behavior as $k^2 \to 0$,

$$\hat{\sigma}_{i,ab}(p_a,p_b,q,\mu) = \hat{\sigma}_{i,ab}^{\text{sing}}(p_a,p_b,q,\mu) + \underbrace{\Big[\hat{\sigma}_{i,ab}(p_a,p_b,q,\mu) - \hat{\sigma}_{i,ab}^{\text{sing}}(p_a,p_b,q,\mu)\Big]_{k^2>0}}_{\hat{\sigma}_{i,ab}^{\text{non-sing}}(p_a,p_b,q,\mu)}\,. \tag{2.71}$$

In other words, the leading singular behavior of the renormalized partonic cross section takes the following form as $k^2 \to 0$,

$$\hat{\sigma}_{i\,ab}(p_a,p_b,q,\mu) = \hat{\sigma}_{i\,ab}^{\text{sing}}(\tilde{p}_a,\tilde{p}_b,q,k^2,\mu)\Big[1+\mathcal{O}\Big(\frac{k^2}{q^+q^-}\Big)\Big], \tag{2.72}$$

where the all-order structure of the singular cross section is

$$\begin{aligned}\hat{\sigma}_{i\,ab}^{\text{sing}}(\tilde{p}_a,\tilde{p}_b,q,k^2,\mu) = \sum_n \left[\frac{\alpha_s(\mu)}{4\pi}\right]^n \Bigg\{ & c_{i\,ab}^{(n,-1)}(\tilde{p}_a,\tilde{p}_b,q,\mu,\nu)\,\delta(k^2) \\ & + \sum_{m=0}^{2n-1} c_{i\,ab}^{(n,m)}(\tilde{p}_a,\tilde{p}_b,q,\mu,\nu)\left[\theta(k^2)\,\frac{\ln(k^2/\nu^2)}{k^2}\right]_+^{\nu^2}\Bigg\}\,.\end{aligned} \tag{2.73}$$

Here $\big[\theta(k^2)\,q(k^2)\big]_+^{\nu^2}$, denotes a *plus distribution* in the dimensionful variable k^2. Its action on a regular test function $f(k^2)$ is given by

$$\int \mathrm{d}k^2\,\big[\theta(k^2)\,q(k^2)\big]_+^{\nu^2}\,f(k^2) \equiv \int_0^{\nu^2}\mathrm{d}k^2\,q(k^2)\big[f(k^2)-f(0)\big] + \int_{\nu^2}^{\infty}\mathrm{d}k^2\,q(k^2)\,f(k^2)\,. \tag{2.74}$$

More information on plus distributions is given in Appendix C.

The dependence on the (arbitrary) boundary condition ν of the plus distributions exactly cancels at each individual perturbative order in Eq.(2.73) between the plus distributions and logarithmic terms in the various coefficients in Eq.(2.73).

The single-real and real-virtual contributions, as well as higher-loop corrections to subprocesses with a single on-shell parton with $k^2 = 0$ in the final state ($\mathrm{N}^n\mathrm{LO}_1$), are entirely localized at $k^2 \to 0$ and appear as terms proportional to $\delta(k^2)$. Their infrared singularities cancel against those arising from the integration over soft or final-state collinear radiation. The remaining finite pieces at $k^2 = 0$ contribute to the singular part of the cross section, $\hat{\sigma}^{\text{sing}}_{i,ab}$.
The real-real contributions on the other hand can have terms local to $k^2 = 0$, but can also include k^2-finite terms $\mathcal{O}(1)$ or $\mathcal{O}(k^2)$, these will enter in the regular piece of the full cross section $\hat{\sigma}^{\text{non-sing}}_{i,ab}$.

This analytic separation into singular and nonsingular parts also allows for an efficient convolution with PDFs. The singular terms, involving distributions like $\delta(k^2)$ and $[1/k^2]_+$, require careful treatment near the $k^2 \to 0$ limit. Meanwhile, the nonsingular part is fully finite and can be integrated numerically using a parametrization like the one in Eq.(2.66) as a standard two-dimensional integral over y_k and k^2 .

In the remainder of this section we describe how the coefficients $c^{(n,m)}_{i\,ab}$ are obtained from the all-order threshold factorization for V + jet production, and then discuss how the desired total cross section can be assembled by performing a separate, simpler calculation of the renormalized partonic cross section at $k^2 > 0$. The specific implementation of these two steps for the case of the Drell-Yan angular coefficients at $\mathcal{O}(\alpha_s^2)$ is then described in Chapter 4 and Chapter 5, respectively, in turn covering the real-virtual and real-real contributions to the cross section.

Choice of Born projection

Before we proceed, we have yet to comment on the notation $\tilde{p}_{a,b}$ that we introduced in Eq.(2.73) for the arguments of the singular cross section. Here the tildes indicate that the arguments p_a, p_b, and q of the partonic cross section, which in general correspond to a phase space point $p_a + p_b = q + k$ with a massive hadronic final state $k^2 \geq 0$, are projected onto the underlying Born phase space of a $2 \to 2$ scattering process $\tilde{p}_a + \tilde{p}_b = \tilde{q} + \tilde{k}$ with $\tilde{p}_a^2 = \tilde{p}_b^2 = 0$ as before, but with a single massless final-state momentum $\tilde{k}^2 = 0$. There are some choices involved in how this Born projection is performed, and in the following we motivate the choices we make and give the explicit expressions for the Born projection.

We are aiming for an analytic calculation of the cross section fully differential in q, so we are required to keep $q = \tilde{q}$ fixed in this projection. This means that the change from k to $\tilde{k}$ must be absorbed by adjusting the initial-state parton momenta from $p_{a,b}$ to $\tilde{p}_{a,b}$. Furthermore, we would like to ensure that the CS frame is held fixed under the projection to avoid having to account for mixing between structure functions. Thanks to Eq.(2.23), this is easily implemented by taking $\tilde{p}_{a,b}$ to still be along the z axis and be proportional to the unity vectors along it, n and $\bar{n}$ respectively, and not pick up any transverse momentum. This implies $\tilde{k}^\mu_\perp = k^\mu_\perp$, but still leaves a choice in which other properties of k to hold fixed in the projection. A projection that plays particularly nicely with our integral parametrization in Eq.(2.66) is to hold the rapidity fixed,

$$y_{\tilde{k}} = \frac{1}{2}\ln\frac{\tilde{k}^-}{\tilde{k}^+} \stackrel{!}{=} y_k = \frac{1}{2}\ln\frac{k^-}{k^+}\,. \tag{2.75}$$

Overall, this results in the following Born projection:

$$\begin{aligned}
\tilde{k}^\mu &= \frac{n^\mu}{2}\,q_T\,e^{+y_k} + \frac{\bar{n}^\mu}{2}\,q_T\,e^{-y_k} - q^\mu_\perp \equiv w_J\frac{n^\mu_J}{2}\,,\\
\tilde{p}^\mu_a &= \frac{n^\mu}{2}\,(q^- + \tilde{k}^-) \equiv w_a\frac{n^\mu_a}{2}\,, \qquad \tilde{p}^\mu_b = \frac{\bar{n}^\mu}{2}\,(q^+ + \tilde{k}^+) \equiv w_b\frac{n^\mu_b}{2}\,,
\end{aligned} \tag{2.76}$$

where we have already defined the momenta of the Born projection to be along three principal collinear directions: n^μ_J is the *jet* direction and n^μ_a, n^μ_b are the *beam* directions.

2.6.3 Factorized singular cross section from the V + jet threshold limit

As mentioned above, the $k^2 \to 0$ corresponds to the partonic threshold limit, there the physical configuration corresponds to the vector boson recoiling against a nearly massless jet – "V + jet". The singular terms in Eq.(2.71) are localized in this limit, therefore this section will deal only with them. An efficient way to organize the cancellation of the IR and UV singularities for these terms in this limit is to make use of the known factorization theorem of V + jet production at threshold [43, 44, 45], in the limit where the invariant mass of the V + jet system approaches the available hadronic center-of-mass energy ($k^2 \to 0$ at $Q \sim q_T \sim E_{\text{cm}}$).

Thus the renormalized singular $k^2 \to 0$ partonic cross section is obtained by stripping off the renormalized PDFs from the V + jet threshold factorization theorem, which in our notation results in

$$\hat{\sigma}^{\text{sing}}_{i\,ab}(\tilde{p}_a, \tilde{p}_b, q, k^2, \mu) = \frac{1}{2\tilde{p}_a^- \tilde{p}_b^+} \sum_{VV'} L_{\pm(i)\,VV'}(q^2)\, H_{i\,VV'\,ab}(\tilde{p}_a, \tilde{p}_b, q, \mu) \tag{2.77}$$
$$\times \int \mathrm{d}(\tilde{k}\cdot k_s)\, S_{ab}(\tilde{k}\cdot k_s, y_k, \mu) \int \mathrm{d}s\, J_{j(ab)}(s,\mu)\, \delta\big(k^2 - s - 2\tilde{k}\cdot k_s\big)\,.$$

On the first line, $\tilde{p}_a^- \tilde{p}_b^+ = 2\tilde{p}_a \cdot \tilde{p}_b = \xi_a \xi_b E_{\text{cm}}^2$ is the partonic center-of-mass energy squared, $L_{\pm\,VV'}$ are the leptonic prefactors from Eq.(2.27) and $H_{i\,VV'\,ab}$ is the **hard function**, which encodes the effect of hard virtual corrections to the underlying Born process. The hard function is given by the square of the IR-finite part of the Born and virtual amplitudes for the process $a(\tilde{p}_a)\, b(\tilde{p}_b) \to V(q)\, j(\tilde{k})$, projected onto the vector-boson helicity channel i. At example of the NLO contribution to the hard function is shown in Figure 2.8

On the second line, S_{ab} is the V + jet threshold **soft function**, which describes the effect of isotropic soft radiation in the event. It is given by a vacuum matrix element of fundamental and adjoint soft Wilson lines $(Y_{n_i}, Y_{n_i}^\dagger)$ along the directions $\tilde{p}_{a,b}^\mu$ of the incoming partons and the direction of the outgoing jet $\tilde{k}^\mu$ $(n_i = n_a, n_b, n_J)$:

$$\langle 0|\,\mathrm{Tr}\,\overline{\mathbf{T}}\left[\left(Y_a^\dagger Y_k T^a Y_k^\dagger Y_b\right)(x_-)\right]\mathbf{T}\left[\left(Y_b^\dagger Y_k T^a Y_k^\dagger Y_a\right)(0)\right]|0\rangle = C_F N_c \int_0^\infty \mathrm{d}(\omega_J k_s^+)\, e^{-ik_s^+ x^-/2}\, S_{q\bar{q}}(\omega_J k_s^+),$$
$$\langle 0|\,\mathrm{Tr}\,\overline{\mathbf{T}}\left[\left(Y_a^\dagger Y_b T^a Y_b^\dagger Y_k\right)(x_-)\right]\mathbf{T}\left[\left(Y_k^\dagger Y_b T^a Y_b^\dagger Y_a\right)(0)\right]|0\rangle = C_F N_c \int_0^\infty \mathrm{d}(\omega_J k_s^+)\, e^{-ik_s^+ x^-/2}\, S_{qg}(\omega_J k_s^+),$$

where $x_- = \bar{n}_J \cdot x$ and $k_s^+ = n_J \cdot k_s$, such that $\omega_J k_s^+ = \tilde{k}\cdot k_s$. T^a are the fundamental color generators. $\mathbf{T}$ denoted time ordering, while $\overline{\mathbf{T}}$ denotes anti-time ordering – it orders operators from left to right in increasing time (later to earlier). As could be seen from the definition above the soft function only depends on the color charges of the particles in the Born process (i.e., whether the process is $q\bar{q} \to Vg$ or $qg \to Vq$), and the conformal cross ratio of their dot products – the polar angle of the jet as encoded in y_k. In addition, it depends on the quantity that is measured on the soft radiation, which is the projection $\tilde{k}\cdot k_s$ of the total soft partonic momentum k_s^μ onto $\tilde{k}^\mu$.

Finally, the **jet function** J_j encodes the effect of collimated final-state collinear radiation and depends on the total invariant mass s of the jet system, which ends up contributing to the total partonic invariant mass k^2 as $k^2 = s + 2\tilde{k}\cdot k_s$. The jet function depends on the parton type of j (on whether j is a quark/antiquark or a gluon), and is defined as a vacuum matrix element of collinear quark or gluon fields, respectively:

$$\langle 0|\bar{\chi}_J^i(x)\, \tfrac{\bar{\not{n}}_J}{2}\chi_J^j(0)|0\rangle = \delta^{ij} \int \frac{\mathrm{d}^4p}{(2\pi)^3}\, \theta(p^0)\, \delta(\bar{n}_J\cdot p)\, J_q(p^2)\, e^{-ix\cdot p},$$
$$\langle 0|\mathcal{A}_{J,\perp}^{a\,\mu}(x)\, \mathcal{A}_{J,\perp}^{b\,\nu}(0)|0\rangle = \delta^{ab}\,(-g_\perp^{\mu\nu})\, g_s^2 \int \frac{\mathrm{d}^4p}{(2\pi)^3}\, \theta(p^0)\, \delta(p^2)\, J_g(p^2)\, e^{-ix\cdot p},$$

where $p^2 = (k - k_s)^2$, which in Eq.(2.77) is shifted to s by the $\delta(k^2 - s - 2\tilde{k}\cdot k_s)$. In the definition $\mathcal{A}_{j,\perp}^{a\,\mu}(x)$ is the perpendicular component of the gauge-invariant $n_i = n_J$-collinear gluon field with color index a and $\chi_J^j(x)$ is the gauge-invariant quark n_J-collinear field with color index i. These gauge-invariant fields are defined as:

$$\chi_i(x) = W_i^\dagger(x)\, \frac{\bar{\not{n}}_i \not{n}_i}{4}\, \psi_i(x), \qquad \mathcal{A}_{n,\perp}^\mu(x) = W_i^\dagger(x)\, [iD_{n,\perp}^\mu W_i(x)], \tag{2.78}$$

where $\psi_i(x)$ is the previously defined collinear quark field, and $D_{n,\perp}^\mu$ is the perpendicular component of the collinear covariant derivative. $W_i(x)$ is the **collinear Wilson line**:

$$W_i(x) = \mathbf{P}\exp\left(ig\int_{-\infty}^0 ds\, \bar{n}_i \cdot A_i(x + s\bar{n}_i)\right). \tag{2.79}$$

Both above-mentioned soft and jet function are normalized to

$$S_{ab}(\tilde{k}\cdot k_s, y_k, \mu) = \delta(\tilde{k}\cdot k_s) + \mathcal{O}(\alpha_s)\,, \qquad J_j(s,\mu) = \delta(s) + \mathcal{O}(\alpha_s) \tag{2.80}$$

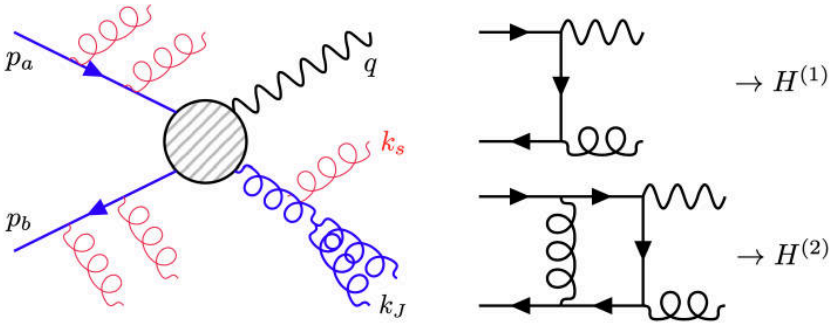


Figure 2.8: Left: V + jet threshold factorization of the scattering amplitude, p_a, p_b are the incoming partons, q is the outgoing vector boson and $k = k_J + k_s$ is the hadronic radiation. Blue lines correspond to the particles collinear to the outgoing jet and red thin lines denote soft emissions. Right: Virtual corrections to the hard function H. The first-order term $H^{(1)}$ corresponds to the squared tree-level single-emission (LO_1) amplitude. The second-order term $H^{(2)}$ comes from the one-loop correction to this amplitude, which correspond to the finite part of the real-virtual cross section. Figure adapted from ref.[48]

at tree level and – rather impressively, in the case of the soft function – are fully known to $\mathcal{O}(\alpha_s^3)$ [43, 44, 45, 46], sufficient for the overall $\mathcal{O}(\alpha_s^4)$ ($\mathrm{N^3LO_1}$) at cross-section level [47] .

The most useful for the IR and UV renormalization fact about the all-order factorization theorem in Eq.(2.77) is that it involves *renormalized* matrix elements and Wilson coefficients (i.e., the IR-finite parts of hard amplitudes) that are individually finite in $D = 4$. Therefore for the singular cross section *it is not required to perform the strong coupling and PDF renormalizations*, as they have been handled internally within each part of the factorization theorem.

About the PDF renormalization in the Eq.(2.77) it is relevant to point out that the factorization theorem in Eq.(2.77) can be written down at the level of *either* the renormalized *or* the bare partonic cross section due to the fact that taking the threshold limit commutes with the PDF renormalization when the DGLAP kernels P_{ij} are also consistently expanded to their leading $\mathcal{O}[(1-z)^{-1}]$ ($z \to 1$, as $k^2 \to 0$) terms. In particular, $k^2 \to 0$ at the level of the renormalized cross section retains the leading $\mathcal{O}[(1-z)^{-1}]$ terms from the splitting functions in the PDF counterterms, which are absorbed into the renormalized threshold-factorized cross section. By contrast, convolutions of the finite $\mathcal{O}[((1-z)^0]$ remainders of the splitting functions with the bare cross section at lower orders (either leading or subleading in k^2) result in a term that is overall power suppressed in k^2. Therefore for our convenience we choose to use the already renormalized threshold-factorized cross section in our singular calculation, in order to not to have to deal with the IR and UV poles for the RV loop terms.

While the PDF renormalization is thus still required to obtain the complete finite remainder at $k^2 > 0$, and will also contribute nontrivial finite terms to it, including it is made significantly simpler since at $\mathcal{O}(\alpha_s^2)$ we only need to account for the PDF counterterm at $z < 1$ ($k^2 > 0$), which greatly simplifies the functions of the splitting kernels P_{ij} and therefore the master formula in Section 2.4.2.

Here we will provide more explicit expressions for the right-hand part of the Eq.(2.77) using the expressions for the renormalized NLO soft and jet functions from ref. [43].
All of the QCD-dependent terms in the Eq.(2.77) can be expanded as perturbative series in strong coupling:

$$H_{i\,VV'\,ab}(\tilde{p}_a, \tilde{p}_b, q, \mu) = \sum_{n=1} \left(\frac{\alpha_s(\mu)}{4\pi}\right)^n H^{(n)}_{i\,VV'\,ab}(\tilde{p}_a, \tilde{p}_b, q, \mu),$$

$$S_{ab}(\tilde{k}\cdot k_s, y_k, \mu) = \sum_{n=1} \left(\frac{\alpha_s(\mu)}{4\pi}\right)^n S^{(n)}_{ab}(\tilde{k}\cdot k_s, y_k, \mu),$$

$$J_{j(ab)}(s, \mu) = \sum_{n=1} \left(\frac{\alpha_s(\mu)}{4\pi}\right)^n J^{(n)}_{j(ab)}(s, \mu).$$

Combining them and expressing the term $\mathcal{O}(\alpha_s^2)$:

$$
\begin{aligned}
&H_{i\,VV'\,ab}(\tilde{p}_a,\tilde{p}_b,q,\mu)\int \mathrm{d}(\tilde{k}\cdot k_s)\,S_{ab}(\tilde{k}\cdot k_s,y_k,\mu)\int \mathrm{d}s\,J_{j(ab)}(s,\mu)\,\delta\big(k^2-s-2\tilde{k}\cdot k_s\big)\\
&=\left(\frac{\alpha_s^2}{4\pi}\right)^2\left[H^{(2)}_{i\,VV'\,ab}(\tilde{p}_a,\tilde{p}_b,q,\mu)\delta(k^2)+H^{(1)}_{i\,VV'\,ab}(\tilde{p}_a,\tilde{p}_b,q,\mu)\big(S^{(1)}_{ab}(k^2,y_k,\mu)+J^{(1)}_{j(ab)}(k^2,\mu)\big)\right],
\end{aligned}
$$

where the factors multiplying $H^{(n)}_{i\,VV'\,ab}$ are derived through taking the combinations of different $(\alpha_s^n,\ n<2)$ orders of soft and jet functions. Here again, $H^{(2)}_{i\,VV'\,ab}(\tilde{p}_a,\tilde{p}_b,q)$ is the second order hard function, which encodes the RV corrections to the Born process. $H^{(1)}_{i\,VV'\,ab}(\tilde{p}_a,\tilde{p}_b,q)$ is the first order hard function, which is just proportional to the single real cross section without any loop corrections.
At the leading order, α_s^0, the S and J are proportional to δ-functions of their variables, therefore the convolution of them reads:

$$
\begin{aligned}
&S^{(0)}_{ab}(\tilde{k}\cdot k_s,y_k,\mu)=\delta(\tilde{k}\cdot k_s)\,,\qquad J^{(0)}_{j},(s,\mu)=\delta(s)\\
&\int \mathrm{d}(\tilde{k}\cdot k_s)\,S^{(0)}_{ab}(\tilde{k}\cdot k_s,y_k,\mu)\int \mathrm{d}s\,J^{(0)}_{j(ab)}(s,\mu)\,\delta\big(k^2-s-2\tilde{k}\cdot k_s\big)=\delta(k^2).
\end{aligned}
\tag{2.81}
$$

The cross term of the first order soft function with a tree-level jet function is:

$$
\begin{aligned}
&S^{(1)}_{ab}(\tilde{k}\cdot k_s,y_k,\mu)=C_i\left\{\left[2\ln^2\left(\frac{2n_a\cdot n_b}{n_a\cdot n_J\;n_b\cdot n_J}\right)-\frac{\pi^2}{3}\right]\delta(\tilde{k}\cdot k_s)+\left[\frac{16\ln\left(\frac{\tilde{k}\cdot k_s}{\mu}\sqrt{\frac{2n_a\cdot n_b}{n_a\cdot n_J\;n_b\cdot n_J}}\right)}{\tilde{k}\cdot k_s}\right]_+^{[\tilde{k}\cdot k_s,\mu]}\right\},\\
&J^{(0)}_{j}(s,\mu)=\delta(s),
\end{aligned}
$$

$$
\begin{aligned}
&\int \mathrm{d}(\tilde{k}\cdot k_s)\,S^{(1)}_{ab}(\tilde{k}\cdot k_s,y_k,\mu)\int \mathrm{d}s\,J^{(0)}_{j(ab)}(s,\mu)\,\delta\big(k^2-s-2\tilde{k}\cdot k_s\big)=S^{(1)}_{ab}(k^2,y_k,\mu)\\
&=C_1\Bigg[\left(2\ln^2\left(\frac{4}{n_a\cdot n_J\;n_b\cdot n_J}\right)-\frac{\pi^2}{3}\right)\delta(k^2)\\
&\qquad+16\Bigg(\mathcal{L}_1(k^2,\nu^2)+\mathcal{L}_0(k^2,\nu^2)\ln\left(\frac{\nu^2}{w_J\,\mu}\right)+\frac{1}{2}\delta(k^2)\ln^2\left(\frac{\nu^2}{w_J\,\mu}\right)\\
&\qquad-\frac{1}{2}\ln\left(\frac{n_a\cdot n_J\;n_b\cdot n_J}{4}\right)\left(\mathcal{L}_0(k^2,\nu^2)+\delta(k^2)\ln\left(\frac{\nu^2}{w_J\,\mu}\right)\right)\Bigg)\Bigg],
\end{aligned}
\tag{2.82}
$$

where $C_1=C_F-\frac{1}{2}C_A$ for a gluon, so process $ab=q\bar{q}$ $(q\bar{q}\to Vg)$ and $C_1=\frac{1}{2}C_A$ for $ab=qg$ $(qg\to Vq)$. Here we have also introduced the notation

$$
\mathcal{L}_n(x,\mu)\equiv\frac{1}{\mu}\mathcal{L}_n(x/\mu),\quad \mathcal{L}_n(x)=\left[\frac{\theta(x)\ln^n x}{x}\right]_+^{[x,1]},
$$

where the so-called boundary condition μ can be shifted by applying:

$$
\begin{aligned}
\mathcal{L}_1(x,\mu)&=\mathcal{L}_1(x,\mu')+\ln\frac{\mu'}{\mu}\mathcal{L}_0(x,\mu')+\frac{1}{2}\ln^2\frac{\mu'}{\mu}\delta(x),\\
\mathcal{L}_0(x,\mu)&=\mathcal{L}_0(x,\mu')+\ln\frac{\mu'}{\mu}\delta(x).
\end{aligned}
$$

As mentioned above, all dependence on the arbitrary boundary condition ν drops out in the full result. The terms with first-order jet functions are as follows:

a) quark jet for $ab = qg$

$$S^{(0)}_{ab}(\tilde{k}\cdot k_s, y_k, \mu) = \delta(\tilde{k}\cdot k_s)\,, \qquad J^{(1)}_{q}(s,\mu) = C_F\left[\left(7-\pi^2\right)\delta(s) + 4\left[\frac{\ln(s/\mu^2)}{s}\right]_+^{[s,\mu^2]} - 3\left[\frac{1}{s}\right]_+^{[s,\mu^2]}\right]$$

$$\begin{aligned}\int \mathrm{d}(\tilde{k}\cdot k_s)\, S^{(0)}_{qg}(\tilde{k}\cdot k_s, y_k, \mu)\int \mathrm{d}s\, J^{(1)}_{q(qg)}(s,\mu)\,\delta\big(k^2 - s - 2\tilde{k}\cdot k_s\big) &= J^{(1)}_{q(qg)}(k^2,\mu)\\ = C_F\Bigg[\left(7-\pi^2\right)\delta(k^2) + 4\left(\mathcal{L}_1(k^2,\nu^2) + \mathcal{L}_0(k^2,\nu^2)\ln\left(\frac{\nu^2}{\mu^2}\right) + \frac{1}{2}\delta(k^2)\ln^2\left(\frac{\nu^2}{\mu^2}\right)\right)&\\ -3\left(\mathcal{L}_0(k^2,\nu^2) + \delta(k^2)\ln\left(\frac{\nu^2}{\mu^2}\right)\right)\Bigg],&\end{aligned} \tag{2.83}$$

b) gluon jet for $ab = q\bar{q}$

$$\begin{aligned}S^{(0)}_{ab}(\tilde{k}\cdot k_s, y_k, \mu) = \delta(\tilde{k}\cdot k_s)\,, \qquad J^{(1)}_{g}(s,\mu) &= \left(C_A\left(\frac{67}{9}-\pi^2\right) - \frac{20}{9}T_F n_f\right)\delta(s)\\ &\quad + 4C_A\left[\frac{\ln(s/\mu^2)}{s}\right]_+^{[s,\mu^2]} - \beta_0\left[\frac{1}{s}\right]_+^{[s,\mu^2]}\\ \int \mathrm{d}(\tilde{k}\cdot k_s)\, S^{(0)}_{q\bar{q}}(\tilde{k}\cdot k_s, y_k, \mu)\int \mathrm{d}s\, J^{(1)}_{g(q\bar{q})}(s,\mu)\,\delta\big(k^2 - s - 2\tilde{k}\cdot k_s\big) &= J^{(1)}_{g(q\bar{q})}(k^2,\mu)\\ = \left(C_A\left(\frac{67}{9}-\pi^2\right) - \frac{20}{9}T_F n_f\right)\delta(k^2) + 4C_A\left(\mathcal{L}_1(k^2,\nu^2) + \mathcal{L}_0(k^2,\nu^2)\ln\left(\frac{\nu^2}{\mu^2}\right) + \frac{1}{2}\delta(k^2)\ln^2\left(\frac{\nu^2}{\mu^2}\right)\right)&\\ - \beta_0\left(\mathcal{L}_0(k^2,\nu^2) + \delta(k^2)\ln\left(\frac{\nu^2}{\mu^2}\right)\right).&\end{aligned} \tag{2.84}$$

2.6.4 Final result

Here we recap that the fully renormalized partonic cross section is given by:

$$\hat{\sigma}_{i,ab}(p_a,p_b,q,\mu) = \hat{\sigma}^{\text{sing}}_{i,ab}(\tilde{p}_a,\tilde{p}_b,q,k^2,\mu) + \hat{\sigma}^{\text{non-sing}}_{i,ab}(p_a,p_b,q,k^2,\mu), \tag{2.85}$$

where the fully IR- and UV- finite singular term captures all threshold-localized contributions as $k^2 \to 0$, and is written as:

$$\begin{aligned}\hat{\sigma}^{\text{sing}}_{i\,ab}(\tilde{p}_a,\tilde{p}_b,q,\mu) = \frac{1}{2\tilde{p}_a^-\tilde{p}_b^+}\sum_{VV'} L_{(\pm)i,VV'}\Big(&H^{(2)}_{i\,VV'\,ab}(\tilde{p}_a,\tilde{p}_b,q,\mu)\delta(k^2)\\ &+ \frac{\alpha_s(\mu)}{4\pi}H^{(1)}_{i\,VV'\,ab}(\tilde{p}_a,\tilde{p}_b,q,\mu)\big(S^{(1)}_{ab}(k^2,y_k,\mu) + J^{(1)}_{j(ab)}(k^2,\mu)\big)\Big).\end{aligned} \tag{2.86}$$

Here the dependence on the strong coupling α_s has been absorbed into the definition of the hard functions. The structure of factors in the second line – the soft and jet functions, as well as the first-order hard functions, that consist of the finite single-real contributions – are fully known in the literature [43]. However, the full set of helicity-projected *second-order* hard functions $H^{(2)}_{i\,VV'\,ab}$, which receive their contributions from the RV terms, is not known analytically. In Chapter 4 we describe how to efficiently perform the helicity projection of the RV contributions directly at the level of the amplitude, using the well-known spinor-helicity amplitudes for $a(\tilde{p}_a)\,b(\tilde{p}_b) \to \ell^-(p_1)\,\ell^+(p_2)\,j(\tilde{k})$ as input data.

Since all of the real-virtual contributions (and a portion of the real-real ones in the form of $H^{(1)}(S^{(1)} + J^{(1)})$) are included in $\hat{\sigma}^{\text{sing}}_{i,ab}$, the remaining part of the RR contributions must enter the regular component of the cross section. The latter one is obtained by subtracting the singular term from the full (PDF renormalized) RR result:

$$\hat{\sigma}^{\text{non-sing}}_{i,ab}(p_a,p_b,q,k^2,\mu) = \hat{\sigma}^{\text{full, }RR}_{i,ab}(p_a,p_b,q,k^2,\mu) - \hat{\sigma}^{\text{sing}}_{i\,ab}(\tilde{p}_a,\tilde{p}_b,q,k^2,\mu)\Big|_{k^2>0}. \tag{2.87}$$

The condition $k^2 > 0$ ensures that only the part of the singular cross section relevant to RR is subtracted, since the entire RV contribution is proportional to $\delta(k^2)$. In Chapter 5 we describe how we compute these RR remainder terms through the conventional Feynman rules. Subtracting the singular part from the full renormalized RR cross section yields the non-singular remainder that completes the full result.

Chapter 3

Flavor decomposition of partonic cross-sections

In this Chapter we move on from the more ideological concepts of our calculation and talk about the organization of the weak couplings in our final result.

3.1 Introduction to the approach

In our calculation we consider only identical quark flavors and included the $VV' = ZZ$ boson as the intermediate vector boson. Therefore we temporarily drop the indexes VV' in our results, assuming that both the vector boson of both sides of the amplitude and conjugated amplitude are Z bosons. In reality, multiple quark flavors and other neutral or charged bosons (such as γ and $W^{\pm}$) can contribute. However, the most complicated parts of the squared matrix element are structurally independent of the specific quark flavor or boson type – only the electroweak couplings vary. This allows us to take the complete result, remove the specific electroweak coupling factors used, and later reinsert a more general set of couplings to account for the full flavor and boson content.

Each diagram may carry a distinct electroweak coupling structure, for example, some couple to a single quark line, while others connect different quark flavors on the amplitude and conjugated amplitude sides (i.e., "across the cut"). To systematically organize this complexity, we developed a diagrammatic approach based on flavor topologies - the so-called **"Pysanka"** or **"Easter egg diagrams"** - which allow us to track how each flavor flow pattern corresponds to a particular structure of electroweak couplings in the Drell-Yan-type processes. The key idea is to represent the amplitude and its complex conjugate within a single topological diagram, shaped like an Pysanka (a Ukrainian decorated Easter egg).
Figure 3.1 shows how this representation arises from a rearrangement of the standard cut diagram. The partons $1, 2$, which couple to the vector boson, are reflected across the vertical axis, while the incoming partons a, a' and b, b' are grouped at the top and bottom of the diagram. This arrangement ensures that identical incoming parton flavors appear on both sides of the cut, as required for a consistent cross section. Therefore, the external legs represent the initial state partons (a, a' and b, b') and the quarks participating in the weak interaction ($1, 1'$ and $2, 2'$), while the internal structure keeps track of flavor flow between the amplitude and its conjugate.

We assign flavor indices f_1, f_2 to the quarks coupling to the vector boson in the amplitude, and f_1', f_2' to those in the conjugate. The weak couplings are expressed as generic coefficients $c_{f_1 f_2}$, which could be used for both charged and neutral vector bosons, therefore the order of the flavor indexes and the conjugation matter in these couplings:

$$c_{f_1 f_2} = \begin{cases} -iQ_f e, \text{ where } f = f_1 = f_2, \text{ for } \gamma^*, \\ \pm \frac{g_W}{2\sqrt{2}} V_{f_2 f_1}, \text{ where } f_1 \neq f_2, \text{ for } W^{\pm}, \\ \pm i \frac{g_Z}{2} v_f \text{ or } \pm i \frac{g_Z}{2} a_f, \text{ where } f = f_1 = f_2, \text{ for } Z. \end{cases}$$

Each diagram then yields a term of the form

$$\prod_{\text{flavor } i,j} \delta_{ij} \times c_{f_1 f_2} \, c^*_{f_1' f_2'},$$

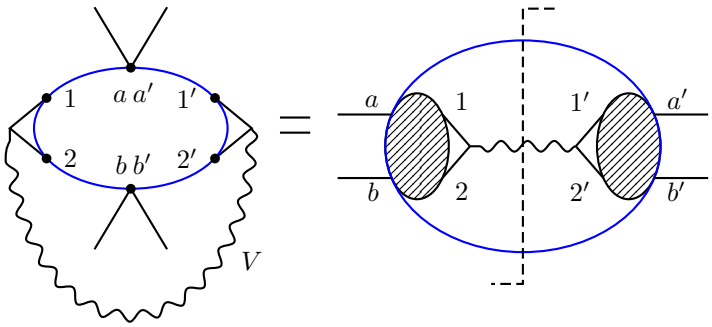


Figure 3.1: Topological representation of the flavor structure in a Drell-Yan-type process involving a neutral vector boson V. The diagram on the right shows the standard cut diagram, with incoming partons a, b and their conjugates a', b', and vector boson couplings to partons $1, 2$ (and $1', 2'$). This can be transformed into the Pysanka diagram on the left by inverting the positions of 1 and 2, and grouping a, a' at the top and b, b' at the bottom of the ellipse.

where the combination of Kroneker-delta's depends on how the flavors are connected: for each line connecting points i and j there would be one δ_{ij} enforcing the same flavor for both partons. We always assume that the incoming particles on both sides of the cut are the same partons and have the same flavor, therefore this assumption can be written down as two additional Kroneker-delta's $\delta_{f_a f'_a}\ \delta_{f_b f'_b}$ in front of all the terms in the cross section.

Since these diagrams inherently represent the flavor flow inside the combination of amplitudes, each of them would represent a unique flavor contraction and therefore a unique EW coupling. There is a roughly[1] one-to-one correspondence between possible EW couplings and the Pysanka diagrams, the problem of finding all of the relevant couplings comes down to purely combinatorial one – drawing all the Pysanka diagrams and then computing the EW couplings from them.

One major advantage of this method is that it keeps the analysis completely agnostic to the color flow. Since gluons are flavor-blind, they can be ignored when identifying weak interaction couplings: we only care about which quark flavors are involved and how they couple to the boson. Therefore one Pysanka diagram would describe a whole set of squared amplitudes. This makes the diagrams very general and useful for organizing all possible weak couplings in a process. It also means the method can be extended to cases at higher orders of strong-coupling. Additionally, we are agnostic to internal quark loops that do not couple to the vector boson or the external states, as their coupling would not be present in the final result.

To count the number of distinct Pysanka diagrams, observe that for j incoming gluons (with $j = 0, 1, 2$ for processes with two incoming partons), there remain $8 - 2j$ flavor-carrying legs that can participate in flavor contractions. This follows from the fact that gluons do not carry flavor/charge and thus do not contribute to the flavor structure inside the diagram. Among these $8-2j$ points, exactly half correspond to incoming flavor currents and half to outgoing ones. The combinatorial problem then reduces to counting all possible pairings between the $4 - j$ incoming and $4 - j$ outgoing points. Denoting the outgoing points as $O_1, \ldots, O_{4-j}$ and the incoming ones as $I_1, \ldots, I_{4-j}$, each diagram corresponds to a bijection $O_i \mapsto I_{\sigma(i)}$ for some permutation $\sigma \in S_{4-j}$. Since there are no constraints on the matching, as the crossings and nonlocal connections are allowed, the total number of such diagrams is simply the number of permutations of $4 - j$ elements, that is, $(4 - j)!$.

Below we describe the possible Pysanka topologies, their couplings and the possible diagrams they represent. Please note that as relevant examples of the physical processes we would refer mostly to either the lowest order diagrams for said topology, and/or to the diagrams that are relevant at our order and are discussed in the sections above: Born, LO_1, NLO_1 and LO_2.

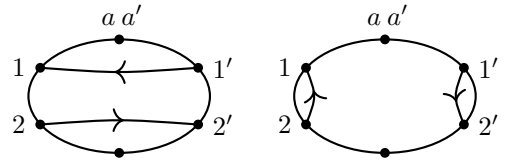
3.2 $gg \to VX$

For two incoming gluons, there are exactly $(4 - 2)! = 2$ possible flavor contraction diagrams, labeled A1 and A2 in Fig.3.2.

The A1 topology corresponds to a quark loop stretching across the cut and contributes starting at order α_s^2. This Pysanka represents all the diagrams for LO_2 $gg \to Vq\bar{q}$.

[1] As could be seen from the explicit results below, it is possible to have two or more unique Pysanka diagrams for one EW coupling, since the diagrams carry a bit more internal information about the process than the coupling.

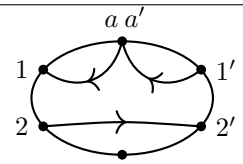
$X\Lambda \to gg$



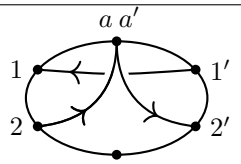
A1

A2

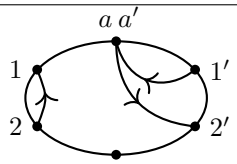
$X\Lambda \to gb$



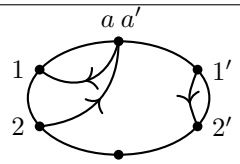
B1



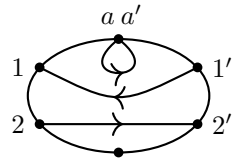
B2



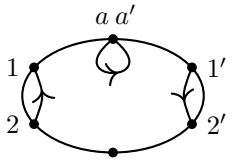
B3



B4

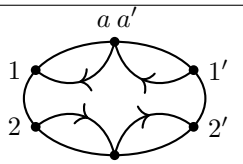


B5

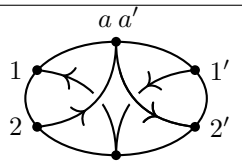


B6

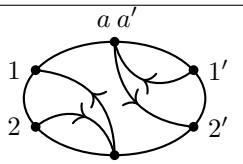
$X\Lambda \to \bar{b}\bar{b}$



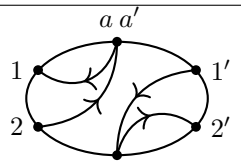
C1



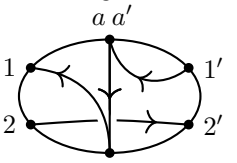
C2



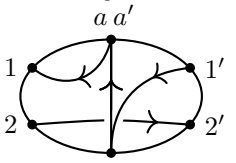
C3



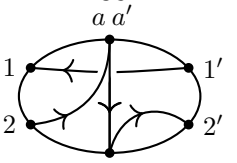
C4



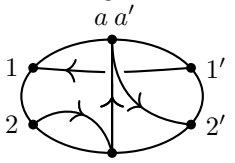
C5



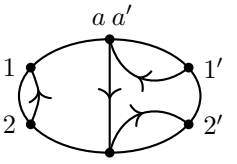
C6



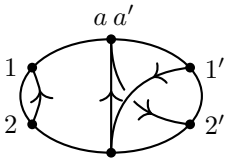
C7



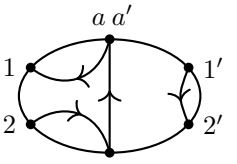
C8



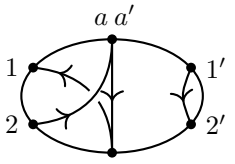
C9



C10

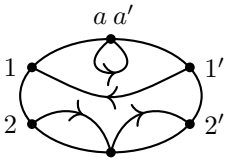


C11

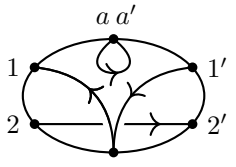


C12

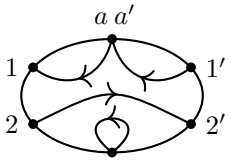
$X\Lambda \to \bar{b}b$



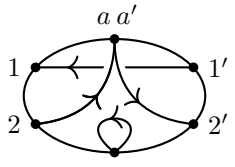
C13



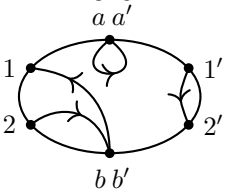
C14



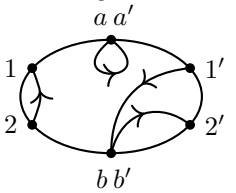
C15



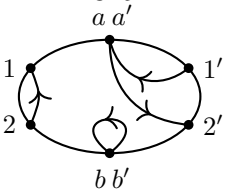
C16



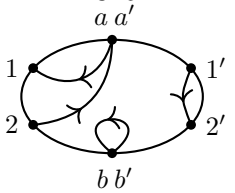
C17



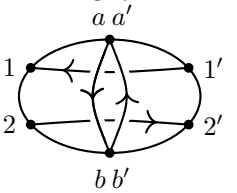
C18



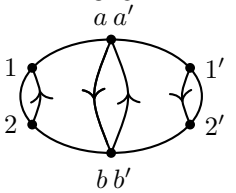
C19



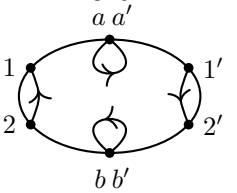
C20



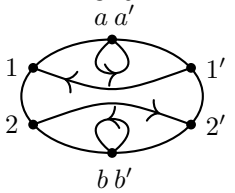
C21



C22



C23



C24

Figure 3.2: Flavor contraction diagrams grouped by partonic channel.

The A2 diagram involves two separate quark triangles, one on each side of the cut, with the vector boson coupling to both. This configuration corresponds to the process $gg \to V$, which vanishes at all orders due to the Landau-Yang theorem [49, 50]: a massive spin-1 boson cannot couple to two identical massless spin-1 bosons in a symmetric state. However, once an additional gluon is radiated, as in $gg \to Vg$, the process becomes allowed, and A2 begins to contribute at α_s^3.

The flavor structure for this channel is

$$\begin{aligned} W_{i,gg}^{VV'} &= \delta_{f_1}^{f_1'}\,\delta_{f_2}^{f_2'}\,c_{f_1 f_2}c_{f_1' f_2'}'^{*} \times \mathrm{A1} + \delta_{f_1}^{f_2}\,\delta_{f_1'}^{f_2'}\,c_{f_1 f_2}c_{f_1' f_2'}'^{*} \times \mathrm{A2} \\ &= \sum_{f_1,f_2} c_{f_1 f_2}c_{f_1 f_2}'^{*} \times \mathrm{A1}(\mathcal{O}(\alpha_s^2)) + \sum_{f_1,f_1'} c_{f_1 f_1}c_{f_1' f_1'}'^{*} \times \mathrm{A2}(\mathcal{O}(\alpha_s^3)), \end{aligned} \tag{3.1}$$

where the sums are over quark flavors, and in the last line the expressions in parentheses indicate the lowest order at which each diagram contributes. As mentioned previously, $c_{f_1 f_2}c_{f_1' f_2'}'^{*}$ are couplings from the diagrams on both sides of the cut: $c_{f_1 f_2}$ on the left (amplitude) side of the cut, $c_{f_1' f_2'}'^{*}$ – on the right (conjugate amplitude) side of the cut.

Importantly, since gluons do not carry flavor, the only way they can couple to a vector boson is via closed quark loops. Consequently, both A1 and A2 necessarily involve internal fermion loops: for A1 it is a quark $f_1 = f_1'$ and $f_2 = f_2'$ stretching across the cut, for A2 it is two quark loops $f_1 = f_2$ and $f_1' = f_2'$ on two sides of the cut. This imposes a strict constraint on the types of vector bosons that can appear in such diagrams: *only neutral bosons* like the Z and γ^*, which couple to flavor-diagonal quark currents, can contribute to A2, while charged currents mediated by $W^{\pm}$, which require flavor-changing interactions, are excluded in A2, but are allowed in A1.

In general, if a diagram contains a direct connection between f_1 and f_2 (and/or f_1' and f_2') – that is, if it involves a factor like $\delta_{f_1}^{f_2}$ (and/or $\delta_{f_1'}^{f_2'}$), or equivalently a coupling of the form $c_{f_1 f_1}$ – then only neutral vector bosons such as the Z or γ^* can mediate the interaction. Any other flavor topology, with nontrivial flavor flow, allows the possibility of charged boson exchange.

3.3 $qg \to VX$

For one incoming gluon, there is $(4-1)! = 6$ possible Pysanka diagrams, labeled as B1-B6 in Fig. 3.2. The full flavor structure for this channel is thus:

$$\begin{aligned} W_{i,q_{f_a}g}^{VV'} =& \sum_{f_2} c_{f_a f_2}c_{f_a f_2}'^{*} \times \mathrm{B1}(\mathcal{O}(\alpha_s)) + \sum_{f_1} c_{f_1 f_a}c_{f_1 f_a}'^{*} \times \mathrm{B2}(\mathcal{O}(\alpha_s^3)) \\ &+ \sum_{f_1} c_{f_1 f_1}c_{f_a f_a}'^{*} \times \mathrm{B3}(\mathcal{O}(\alpha_s^2)) + \sum_{f_1'} c_{f_a f_a}c_{f_1' f_1'}'^{*} \times \mathrm{B4}(\mathcal{O}(\alpha_s^2)) \\ &+ \sum_{f_1,f_2} c_{f_1 f_2}c_{f_1 f_2}'^{*} \times \mathrm{B5}(\mathcal{O}(\alpha_s^3)) + \sum_{f_1,f_1'} c_{f_1 f_1'}c_{f_1 f_1'}'^{*} \times \mathrm{B6}(\mathcal{O}(\alpha_s^3)) \end{aligned} \tag{3.2}$$

In diagram B1, the incoming quark directly couples to the vector boson, while the real gluon connects to a closed quark loop across the cut at flavor f_2. The structure effectively resembles a Born-like diagram in its upper half, where the quark line connects uninterrupted to the boson. All of the LO_2 $qg \to Vqg$ and most of the NLO_1 $qg \to Vq$ (except for the top-loop) diagrams fall into this category. Diagram B2 is the crossed counterpart of B1, where the loop now forms on the f_1 side. Since we assume the lower legs b and b' to be gluons, this crossed configuration contributes only at higher orders in the strong coupling.

Diagrams B3 and B4 represent the topologies with a single quark loop on the $f_1 = f_2$ and $f_1' = f_2'$ sides, respectively. The top-loop diagrams from NLO_1 $qg \to Vq$ crossed with the LO_1 $qg \to Vq$ fall into these categories.

Diagrams B5 and B6 appear at $\mathcal{O}(\alpha_s^3)$ and beyond, as they correspond to the A1 and A2 topologies in the $gg \to VX$ process, with the upper gluon a now coupling to a quark line.

Among these, only B3, B4, and B5 necessarily require mediation by a neutral vector boson, due to the presence of closed quark loops on one or both sides of the cut.
Overall the topologies that contribute at up to $\mathcal{O}(\alpha_s^2)$ are

$$W_{i,q_{f_a}g}^{VV'} = \sum_{f_2} c_{f_a f_2}c_{f_a f_2}'^{*} \times \mathrm{B1} + \sum_{f_1} c_{f_1 f_1}c_{f_a f_a}'^{*} \times (\mathrm{B3} + \mathrm{B4}), \tag{3.3}$$

where we have used the fact that B3 and B4 are mediated by either Z or γ^* bosons, therefore their couplings are hermitian $c_{ij}^* = c_{ij}$ and thus both B3 and B4 have the same type of coupling.

3.4 $q\bar{q} \to VX$

For no incoming gluons, there is $(4-0)! = 24$ possible Pysanka diagrams, labeled as C1-C24 in Fig. 3.2. The full flavor structure for this channel is

$$
\begin{aligned}
W^{VV'}_{i,q_{f_a}\bar{q}_{f_b}} =& c_{f_a f_b} c'^{*}_{f_a f_b} \times \mathrm{C1}(\mathcal{O}(\alpha_s^0)) + c_{f_b f_a} c'^{*}_{f_b f_a} \times \mathrm{C2}(\mathcal{O}(\alpha_s^4)) \\
&+ c_{f_b f_b} c'^{*}_{f_a f_a} \times \mathrm{C3}(\mathcal{O}(\alpha_s^2)) + c_{f_a f_a} c'^{*}_{f_b f_b} \times \mathrm{C4}(\mathcal{O}(\alpha_s^2)) \\
&+ \delta_{f_a f_b} \Bigg[\sum_{f_2} c_{f_b f_2} c'^{*}_{f_a f_2} \times \mathrm{C5}(\mathcal{O}(\alpha_s^2)) + \sum_{f_2} c_{f_a f_2} c'^{*}_{f_b f_2} \times \mathrm{C6}(\mathcal{O}(\alpha_s^2)) \\
&\quad + \sum_{f_1} c_{f_1 f_a} c'^{*}_{f_1 f_b} \times \mathrm{C7}(\mathcal{O}(\alpha_s^2)) + \sum_{f_1} c_{f_1 f_b} c'^{*}_{f_1 f_a} \times \mathrm{C8}(\mathcal{O}(\alpha_s^2)) \Bigg] \\
&+ \delta_{f_a f_b} \Bigg[\sum_{f_1} c_{f_1 f_1} c'^{*}_{f_a f_b} \times \mathrm{C9}(\mathcal{O}(\alpha_s^2)) + \sum_{f_1} c_{f_1 f_1} c'^{*}_{f_b f_a} \times \mathrm{C10}(\mathcal{O}(\alpha_s^4)) \\
&\quad + \sum_{f'_1} c_{f_a f_b} c'^{*}_{f'_1 f'_1} \times \mathrm{C11}(\mathcal{O}(\alpha_s^2)) + \sum_{f'_1} c_{f_b f_a} c'^{*}_{f'_1 f'_1} \times \mathrm{C12}(\mathcal{O}(\alpha_s^4)) \Bigg] \\
&+ \sum_{f_1} c_{f_1 f_b} c'^{*}_{f_1 f_b} \times \mathrm{C13}(\mathcal{O}(\alpha_s^2)) + \sum_{f_2} c_{f_b f_2} c'^{*}_{f_b f_2} \times \mathrm{C14}(\mathcal{O}(\alpha_s^4)) \\
&+ \sum_{f_2} c_{f_a f_2} c'^{*}_{f_a f_2} \times \mathrm{C15}(\mathcal{O}(\alpha_s^2)) + \sum_{f_1} c_{f_1 f_a} c'^{*}_{f_1 f_a} \times \mathrm{C16}(\mathcal{O}(\alpha_s^4)) \\
&+ \sum_{f'_1} c_{f_b f_b} c'^{*}_{f'_1 f'_1} \times \mathrm{C17}(\mathcal{O}(\alpha_s^3)) + \sum_{f_1} c_{f_1 f_1} c'^{*}_{f_b f_b} \times \mathrm{C18}(\mathcal{O}(\alpha_s^3)) \\
&+ \sum_{f_1} c_{f_1 f_1} c'^{*}_{f_a f_a} \times \mathrm{C19}(\mathcal{O}(\alpha_s^3)) + \sum_{f'_1} c_{f_a f_a} c'^{*}_{f'_1 f'_1} \times \mathrm{C20}(\mathcal{O}(\alpha_s^3)) \\
&+ \delta_{f_a f_b} \Bigg[\sum_{f_1, f_2} c_{f_1 f_2} c'^{*}_{f_1 f_2} \times \mathrm{C21}(\mathcal{O}(\alpha_s^2)) + \sum_{f_1, f'_1} c_{f_1 f_1} c'^{*}_{f'_1 f'_1} \times \mathrm{C22}(\mathcal{O}(\alpha_s^4)) \Bigg] \\
&+ \sum_{f_1, f'_1} c_{f_1 f_1} c'^{*}_{f'_1 f'_1} \times \mathrm{C23}(\mathcal{O}(\alpha_s^4)) + \sum_{f_1, f_2} c_{f_1 f_2} c'^{*}_{f_1 f_2} \times \mathrm{C24}(\mathcal{O}(\alpha_s^4))
\end{aligned}
\tag{3.4}
$$

Diagram C1 corresponds to the Born-like topology, where the incoming quarks a and b couple directly to the quark lines f_1 and f_2, respectively. This configuration appears at the lowest order in perturbation theory. All of the contractions of LO_1 $q\bar{q} \to Vg$ with most of the NLO_1 $q\bar{q} \to Vg$ diagrams (except those involving top-quark loops) share this Born topology, since both incoming quarks couple directly to the vector boson. Likewise, all combinations of LO_2 $q\bar{q} \to Vgg$ diagrams fall into this category.

Diagram C2 is the crossed version of the Born configuration: here, quark a couples to f'_2, and quark b to f'_1, rather than to f_1 and f_2 directly. This topology is more suppressed and arises only at higher orders in the strong coupling expansion.

Diagrams C3 and C4 describe the same basic process but appear as conjugate configurations. Each represents an interference of two LO_2 T-channel diagrams with the vector boson emitted from a different external leg (which corresponds to the $Q_u Q_d$ charge factor). As an example, the cut diagram where on one side of the cut the boson is radiated from the upper quark line (1 or 2 in Figure 2.5 (a)), while on the other side it comes from the lower one (3 or 4 in Figure 2.5 (a)) contributes to the C4 cross section.

Diagrams C5 through C12 all feature a direct line connecting the incoming quarks a and b, which imposes the condition that they must be of the same flavor. C5-C8 correspond to various interferences between LO_2 S-channel and T-channel diagrams. In contrast, C9-C12 involve an NLO_1 quark loop on either the f_1 side (C9, C10) or the f_2 side (C11, C12), interfering with a LO_1 Born-like diagram on the opposite side of the cut. Among these, C10 and C12 exhibit strongly crossed topologies and thus appear

only at higher orders in α_s.

Diagrams C13 through C16 depict loop topologies stretching across the cut, corresponding to various combinations of T-channel diagrams where the vector boson is emitted from the same line on both sides (Q_u^2 charge factor). Diagrams C17-C20 represent quark-loop diagrams interfering with T-channel LO_2 topologies, and as such contribute at $\mathcal{O}(\alpha_s^3)$.

Finally, diagram C21 is the interference of two LO_2 S-channel diagrams, while C22 involves the interference of two quark-loop diagrams with identical incoming quark flavors. Diagrams C23 and C24 are analogous to A1 and A2 in the $gg \to VX$ channel, now with gluons coupling to external quark lines instead of forming closed loops.
Therefore at the $\mathcal{O}(\alpha_s^2)$ relevant Pysanka diagrams are:

$$\begin{aligned}
W^{VV'}_{i,q_{f_a}\bar{q}_{f_b}} =& c_{f_a f_b} c'^{*}_{f_a f_b} \times \mathrm{C1} + c_{f_b f_b} c'^{*}_{f_a f_a} \times \mathrm{C3} + c_{f_a f_a} c'^{*}_{f_b f_b} \times \mathrm{C4} \\
&+\delta_{f_a f_b}\Bigg[\sum_{f_2} c_{f_b f_2} c'^{*}_{f_a f_2} \times \mathrm{C5} + \sum_{f_2} c_{f_a f_2} c'^{*}_{f_b f_2} \times \mathrm{C6} \\
&\quad + \sum_{f_1} c_{f_1 f_a} c'^{*}_{f_1 f_b} \times \mathrm{C7} + \sum_{f_1} c_{f_1 f_b} c'^{*}_{f_1 f_a} \times \mathrm{C8}\Bigg] \\
&+\delta_{f_a f_b} \sum_{f_1} c_{f_1 f_1} c'^{*}_{f_a f_b} \Big[\mathrm{C9} + \mathrm{C11}\Big] \\
&\quad + \sum_{f_1} c_{f_1 f_b} c'^{*}_{f_1 f_b} \times \mathrm{C13} + \sum_{f_2} c_{f_a f_2} c'^{*}_{f_a f_2} \times \mathrm{C15} \\
&+\delta_{f_a f_b}\Bigg[\sum_{f_1, f_2} c_{f_1 f_2} c'^{*}_{f_1 f_2} \times \mathrm{C21}\Bigg],
\end{aligned} \tag{3.5}$$

where in some cases we let the $\delta_{f_a f_b}$ to be explicit, since it is a part of important information for the PDF's that will be multiplying the structure function.

3.5 $qq \to VX$

For the $qq \to VX$ channel, the set of Pysanka diagrams remains unchanged, but their physical interpretation and the perturbative order at which they contribute differ. Since the diagrams themselves are the same, the associated set of electroweak couplings is identical to that in the $q\bar{q} \to VX$ case, and we will not repeat it here. However, it is important to note that although the coupling structures are shared, the strong coupling order at which each diagram contributes is not. As such, care must be taken to include only the appropriate electroweak structures corresponding to the desired order in α_s.
The complete list of Pysanka contributions to the $qq \to VX$ channel at $\mathcal{O}(\alpha_s^2)$ is as follows:

$$\begin{aligned}
W^{VV'}_{i,q_{f_a} q_{f_b}} =& c_{f_a f_b} c'^{*}_{f_a f_b} \times \mathrm{C1} + c_{f_b f_a} c'^{*}_{f_b f_a} \times \mathrm{C2} \\
&+ c_{f_b f_b} c'^{*}_{f_a f_a} \times \mathrm{C3} + c_{f_a f_a} c'^{*}_{f_b f_b} \times \mathrm{C4} \\
&+\delta_{f_a f_b}\Bigg[\sum_{f_2} c_{f_b f_2} c'^{*}_{f_a f_2} \times \mathrm{C5} + \sum_{f_2} c_{f_a f_2} c'^{*}_{f_b f_2} \times \mathrm{C6}\Bigg] \\
&+ \sum_{f_1} c_{f_1 f_b} c'^{*}_{f_1 f_b} \times \mathrm{C13} + \sum_{f_2} c_{f_a f_2} c'^{*}_{f_a f_2} \times \mathrm{C15}
\end{aligned} \tag{3.6}$$

Since the process $qq \to VX$ has no Born-level contribution, all corresponding Pysanka diagrams represent flavor contractions that first appear at order α_s^2 or higher.

Diagrams C1 and C2 correspond to the interference between U-channel and T-channel LO_2 $qq \to Vqq$ topologies, where the vector boson is emitted from opposite quark lines on either side of the cut. Diagrams C3 and C4 represent the contraction of two T-channel or two U-channel diagrams, respectively, in which the vector boson is emitted from different fermion lines. Diagrams C5 and C6 correspond to T-U contractions where the boson is emitted from the same quark line on both sides of the cut. Diagrams C13 and C15 describe contractions of two T-channel diagrams with the vector boson emitted and absorbed across the cut on the same leg.

The remaining diagrams either represent crossed versions of those listed above, contributing only at higher orders in α_s, or involve contractions between NLO_2 diagrams (e.g., those with internal quark loops) and LO_2 T- or U-channel diagrams, which themselves begin at $\mathcal{O}(\alpha_s^3)$. Others require additional gluons to support their topology and thus do not contribute at the order considered here.

Chapter 4

Helicity decomposition of real-virtual contributions at amplitude level

4.1 Spinor-Helicity Method

In this chapter, we describe the computation of the hard function $H_{i,VV'\,ab}(\tilde{p}_a, \tilde{p}_b, q, \mu)$ used in the expression for the singular cross section in Eq.(2.77), which is defined as the squared, infrared-finite part of the Born and virtual amplitudes for the partonic process $a(\tilde{p}_a)\, b(\tilde{p}_b) \to V(q)\, j(\tilde{k})$, projected onto a specific vector-boson helicity channel i.

As mentioned previously in Section 3, we will focus mostly on the process with $VV' = ZZ$ and later introduce the appropriate EW couplings. Additionally, since we will be deriving the hard function from the $\mathrm{N}^n\mathrm{LO}_1$ amplitudes, we will drop the tildes in the notation of the Born projection, as it is clear that for these processes the final hadronic state (i.e. the one parton left after the interaction) is apriori massless $k^2 = 0$.

Here in this chapter we outline how this helicity projection can be carried out efficiently at the amplitude level by making use of known spinor-helicity results for the full process $a(p_a)\, b(p_b) \to \ell^-(p_1)\, \ell^+(p_2)\, j(k)$. These relevant amplitudes are fully known up to one-loop $\mathcal{O}(g_s\, \alpha_s^2)$ [51, 22, 52, 53], with partial results available at two loops $\mathcal{O}(g_s\, \alpha_s^3)$ [54, 55].

This method applies to both the LO_1 and LO_2 amplitudes and in this project has been used as a consistency check for these cases. As such, this section presents the spinor-helicity approach for both the real-virtual and double-real contributions. For the RV (NLO_1 amplitudes) case, it is used as the main source of the results, while for the RR (LO_2 amplitudes) case, it serves primarily as a four-dimensional cross-check against analytic results obtained through other means (for that see Chapter 5).

4.1.1 Introduction and main idea

The spinor-helicity formalism is a powerful tool for computing scattering amplitudes in gauge theories, especially in the high-energy limit where particles can often be approximated as massless [56, 57, 58, 59, 60]. Rather than working with conventional four-momenta and polarization vectors, the formalism encodes the momentum and helicity of massless particles using two-component Weyl spinors [61]. Any massless momentum p^μ can be expressed in bispinor form as

$$p^\mu \sigma_\mu = |p\rangle[p|, \qquad p^\mu \bar{\sigma}_\mu = |p]\langle p|, \tag{4.1}$$

where $|p\rangle$ and $|p]$ are commuting spinors associated with the momentum p, and σ^μ, $\bar{\sigma}^\mu$ are the four-dimensional Pauli matrices. These spinors can be contracted to form Lorentz-invariant quantities – the so-called spinor brackets:

$$\langle ij\rangle = \bar{u}_-(p_i) u_+(p_j), \qquad [ij] = \bar{u}_+(p_i) u_-(p_j), \tag{4.2}$$

which serve as the building blocks of massless amplitudes [62].

One of the central advantages of the formalism is that it naturally organizes the computation: instead of performing a sum over all external spin states at the outset, the spinor-helicity formalism isolates and

computes amplitudes for specific helicity configurations. This decomposition and usage of bispinors leads to much simpler expressions, particularly for processes involving many external gauge bosons. The physical cross section can be recovered by squaring and summing over the relevant helicities at the end. Furthermore, the formalism removes the gauge redundancies of conventional polarization vectors, making it ideally suited for QCD and electroweak calculations [63, 60, 57].

Despite its strengths, the spinor-helicity formalism in its standard form is limited to four dimensions, therefore one might worry about its compatibility with dimensional regularization. However, this does not present a problem in our case: as discussed in the previous Section 2.6.3, the singular part of the cross section, for which we are using the spinor-helicity formalism, is described by a fully finite factorization formula, so all ingredients can be computed in exactly four dimensions. This justifies the use of spinor-helicity formalism in our calculation of the real-virtual contributions to the hard function.

Another constraint of the conventional massless spinor-helicity formalism is that it applies directly only to massless external legs with spin (however, massive external legs can still appear in the process as long as they are scalars, since they carry no spinor degrees of freedom). It is important to emphasize that we want to have our calculations performed using this massless spinor-helicity formalism, as it yields significantly more compact and manageable expressions for the amplitudes (although extensions of the method to include massive particles have been developed in the literature, see e.g. ref. [64]). Since we are interested in a process with a massive spin-1 vector boson V in the final state, we cannot directly apply the spinor-helicity approach to our calculation. Therefore, instead of treating V as an external leg, we compute (or more precisely reuse) the full spinor-helicity amplitude for the process where the vector boson decays into the lepton pair and solve for the partonic helicity amplitude.
The key idea is to factorize the full amplitude for the process

$$p_1 p_2 \to \{p_i\}_{i=3}^{n-1}\, \ell(p_n)\bar{\ell}(p_{n+1})$$

into a sum over the helicities $\lambda \in \{+,-,0\}$ of the intermediate vector boson V. The amplitude is decomposed as

$$\mathcal{A}_{\text{full}}(1,2,\ldots,n,n+1) = \sum_{\lambda} \mathcal{A}_{\lambda}(1,2,\ldots,n-1)\,\mathcal{A}_{\ell\lambda}(n,n+1), \tag{4.3}$$

where $1,2,\ldots,n,n+1$ are the shorthand notation for particles $p_1,p_2,\ldots,p_n,p_{n+1}$ taking part in the interaction. The amplitude $\mathcal{A}_{\lambda}$ describes the production of a vector boson with helicity λ, and the leptonic amplitude $\mathcal{A}_{\ell\lambda}$ encodes its decay. For example, in the $\mathrm{N^nLO_1}$ process $p_1p_2 \to p_3(V \to p_4p_5)$, the factorization reads

$$\mathcal{A}_{\text{full}}(1^{\lambda_g},2_{\bar{q}}^{\lambda_q},3_{q}^{-\lambda_q},4_{\ell}^{\lambda_\ell},5_{\bar{\ell}}^{-\lambda_\ell}) = \sum_{\lambda} \mathcal{A}_{\lambda}(1^{\lambda_g},2_{\bar{q}}^{\lambda_q},3_{q}^{-\lambda_q})\mathcal{A}_{\ell\lambda}(1^{\lambda_g},2_{\bar{q}}^{\lambda_q},3_{q}^{-\lambda_q},4_{\ell}^{\lambda_\ell},5_{\bar{\ell}}^{-\lambda_\ell}), \tag{4.4}$$

where λ_g, λ_q and λ_ℓ are the gluon, quark and lepton helicities respectively. The **projected leptonic current** is:

$$\mathcal{A}_{\ell\lambda}(1^{\lambda_g},2_{\bar{q}}^{\lambda_q},3_{q}^{-\lambda_q},4_{\ell}^{\lambda_\ell},5_{\bar{\ell}}^{-\lambda_\ell}) = \epsilon_{\lambda}^{\mu}(1^{\lambda_g},2_{\bar{q}}^{\lambda_q},3_{q}^{-\lambda_q})L_{\lambda_\ell,\mu}(4_{\ell}^{\lambda_\ell},5_{\bar{\ell}}^{-\lambda_\ell}) \tag{4.5}$$

where ϵ_{λ}^{μ} are the polarization vectors of the vector boson in the Collins-Soper frame from Eq.(2.18), and the leptonic current is given by

$$L_{\lambda_\ell,\mu}(4_{\ell}^{\lambda_\ell},5_{\bar{\ell}}^{-\lambda_\ell}) \sim \begin{cases} [4|\gamma_\mu(v_\ell - a_\ell\gamma^5)|5\rangle & \lambda_\ell = +\frac{1}{2}, \\ \langle 4|\gamma_\mu(v_\ell - a_\ell\gamma^5)|5] & \lambda_\ell = -\frac{1}{2}. \end{cases} \tag{4.6}$$

The goal of this decomposition is to solve the system in Eq.(4.4) for lepton-less helicity amplitudes with the final state being the vector boson with the helicity λ. These helicity amplitude we occasionally call **partonic amplitudes** or later when we establish our approach to only Z boson as the final state, **Z-helicity amplitudes**:

$$\mathcal{A}_{\lambda}(1^{\lambda_g},2_{\bar{q}}^{\lambda_q},3_{q}^{-\lambda_q}) = \Big\{\mathcal{A}_0,\mathcal{A}_+,\mathcal{A}_-\Big\}.$$

To extract these helicity amplitudes, we need several ingredients:

$$\begin{cases} \mathcal{A}_{\text{full}} = \mathcal{A}_0 \mathcal{A}_{\ell 0} + \mathcal{A}_+ \mathcal{A}_{\ell +} + \mathcal{A}_- \mathcal{A}_{\ell -}, \\ \mathcal{A}_{\text{full}} = \dots, \\ \mathcal{A}_{\text{full}} = \dots. \end{cases} \tag{4.7}$$

1. Projected leptonic current: The first step is to obtain analytic expressions for the projected leptonic current $\mathcal{A}_{\ell\lambda}$, defined in Eq.(4.5). The derivation is presented in Section 4.1.2.

2. Full amplitude input: Next, we need the full QCD amplitude $\mathcal{A}_{\text{full}}$ that appears on the left-hand side of Eq.(4.4). These amplitudes can be either computed directly or taken from the literature. In our case, we rely on the expressions from ref. [65], which we review in Section 4.1.3. That section also explains how to obtain different external helicity configurations, allowing us to reconstruct the full set of Z-helicity amplitudes for different helicities of the external particles.

3. Generating independent equations: Since the system in Eq.(4.4) involves three unknowns but initially provides only one equation, we need a way to increase the number of independent equation. For this we notice that the Z-helicity amplitudes are independent of the specific lepton momenta. We can therefore choose three linearly independent lepton configurations, which affect the spinor products with the leptons and therefore both $\mathcal{A}_{\ell\lambda}$ and $\mathcal{A}_{\text{full}}$, but not $\mathcal{A}_\lambda$, and obtain three independent equations. This procedure is discussed in detail for both analytic and numerical implementation in Section 4.1.4.

Once these Z-helicity amplitudes are determined, the helicity density matrix can be reconstructed as

$$W_{\lambda\lambda'} \sim \langle P| J_\mu |X\rangle \langle X| J_\nu |P\rangle \epsilon^\mu_\lambda \epsilon^{*\nu}_{\lambda'} = \mathcal{A}^*_{\lambda'} \mathcal{A}_\lambda, \tag{4.8}$$

where $\mathcal{A}_{\lambda'} = \langle X| J_\nu |P\rangle \epsilon^{*\nu}_{\lambda'}$, such that in the decomposition

$$\mathcal{A}_{\text{full}}(1,2,\dots,n,n+1) = \sum_\lambda \mathcal{A}_\lambda(1,2,\dots,n-1)\, \mathcal{A}_{\ell\lambda}(n,n+1) = \sum_\lambda \langle X| J_\mu |P\rangle \epsilon^{*\mu}_\lambda \epsilon^\nu_\lambda L_\nu.$$

However, the correct helicity density matrix has to account for the sum over the internal possible helicities in the system:

$$W_{\lambda\lambda'} \sim \sum_{\text{helicities in the system}} \mathcal{A}^*_{\lambda'} \mathcal{A}_\lambda, \tag{4.9}$$

which is directly comparable to the hadronic tensor projected using the standard Lorentz basis in Eq.(2.19) and later with structure functions.

This method offers several advantages as a strong comparison with the results from conventional Feynman rules. First, it avoids the need for dimensional regularization at the amplitude level since the spinor algebra is performed strictly in four dimensions. Second, it isolates helicity structures explicitly on the amplitude level, allowing flexibility in the calculation. Third, the compactness and literature accessibility of spinor expressions drastically reduces algebraic overhead in multi-leg computations. Most importantly for our purposes, this decomposition provides an independent and robust cross-check of the structure functions derived through projection methods in Chapter 5. Any discrepancy in the helicity density matrix would signal an inconsistency in the projection procedure or in the derivation of the amplitudes through Feynman rules.

4.1.2 Projected lepton current

First we turn towards expressing lepton-dependent terms $\mathcal{A}_{\ell\lambda}$ on the right-hand side of the system in Eq.(4.4).
We have used the following rule for the replacement between physical 4-momenta (p_a, p_b as incoming partons, k_i, $i = 1$ for LO_1 and $i = 1, 2$ for LO_2 as outgoing partons and q_1, q_2 as outgoing leptons) and

all-outgoing momenta in spinor-helicity formalism $(p_1, p_2, p_3, \ldots, p_n, p_{n+1})$:

$$\begin{array}{ll} \text{LO}_1/\text{NLO}_1 & \text{LO}_2 \\ p_a^\mu = -p_1^\mu, & p_a^\mu = -p_1^\mu, \\ p_b^\mu = -p_2^\mu, & p_b^\mu = -p_2^\mu, \\ k^\mu = p_3^\mu, & k_1^\mu = p_3^\mu, \\ & k_2^\mu = p_4^\mu, \\ q_1^\mu = p_4^\mu, & q_1^\mu = p_5^\mu, \\ q_2^\mu = p_5^\mu, & q_2^\mu = p_6^\mu. \end{array} \tag{4.10}$$

Using the definitions of the projectors from Eq.(2.16a) we can calculate the projected currents:

$$\begin{aligned} \lambda_\ell > 0: \quad z^\mu [4|\gamma_\mu(v_\ell - a_\ell\gamma^5)|5\rangle &= \frac{s_{2q}p_1^\mu - s_{1q}p_2^\mu}{\sqrt{s_{12}s_{1q}s_{2q}}}[4|\gamma_\mu(v_\ell - a_\ell\gamma^5)|5\rangle \\ = \frac{s_{2q}(v_\ell[4|\not{p}_1|5\rangle - a_\ell[4|\not{p}_1\gamma^5|5\rangle) - s_{1q}(v_\ell[4|\not{p}_2|5\rangle - a_\ell[4|\not{p}_2\gamma^5|5\rangle)}{\sqrt{s_{12}s_{1q}s_{2q}}} \\ &= (v_\ell - a_\ell)\frac{s_{1q}[24]\langle 25\rangle - s_{2q}[14]\langle 15\rangle}{\sqrt{s_{12}s_{1q}s_{2q}}}. \end{aligned}$$

$$\begin{aligned} \lambda_\ell < 0: \quad z^\mu \langle 4|\gamma_\mu(v_\ell - a_\ell\gamma^5)|5] &= \frac{s_{2q}p_1^\mu - s_{1q}p_2^\mu}{\sqrt{s_{12}s_{1q}s_{2q}}}\langle 4|\gamma_\mu(v_\ell - a_\ell\gamma^5)|5] \\ &= (v_\ell + a_\ell)\frac{s_{1q}\langle 24\rangle[25] - s_{2q}\langle 14\rangle[15]}{\sqrt{s_{12}s_{1q}s_{2q}}}, \end{aligned}$$

where we have kept notation $s_{ab} = 2p_ap_b$, such that $s_{1q} = 2p_1q$. In the final line we have used the completeness relation from Eq.(B.7).
In a similar manner we derived the contraction of the lepton tensor with x^μ projector:

$$\begin{aligned} \lambda_\ell > 0: \quad x^\mu [4|\gamma_\mu(v_\ell - a_\ell\gamma^5)|5\rangle &= \frac{s_{1q}s_{2q}q^\mu - s_{2q}q^2p_1^\mu - s_{1q}q^2p_2^\mu}{\sqrt{s_{1q}s_{2q}q^2(s_{1q}s_{2q} - s_{12}q^2)}}[4|\gamma_\mu(v_\ell - a_\ell\gamma^5)|5\rangle \\ &= (v_\ell - a_\ell)\frac{q^2s_{1q}[24]\langle 25\rangle + q^2s_{2q}[14]\langle 15\rangle}{\sqrt{s_{1q}s_{2q}q^2(s_{1q}s_{2q} - s_{12}q^2)}}. \\ \lambda_\ell < 0: \quad x^\mu \langle 4|\gamma_\mu(v_\ell - a_\ell\gamma^5)|5] &= \frac{s_{1q}s_{2q}q^\mu - s_{2q}q^2p_1^\mu - s_{1q}q^2p_2^\mu}{\sqrt{s_{1q}s_{2q}q^2(s_{1q}s_{2q} - s_{12}q^2)}}\langle 4|\gamma_\mu(v_\ell - a_\ell\gamma^5)|5] \\ &= (v_\ell + a_\ell)\frac{q^2s_{21q}\langle 24\rangle[25] + q^2s_{2q}\langle 14\rangle[15]}{\sqrt{s_{1q}s_{2q}q^2(s_{1q}s_{2q} - s_{12}q^2)}}, \end{aligned}$$

where we have used the fact that $q^\mu = p_4^\mu + p_5^\mu$.

Finally, by using the following expression for Dirac gamma matrices in order to rewrite the Levi-Civita contraction in the definition of y^μ:

$$\begin{aligned} \gamma^\mu\gamma^\nu\gamma^\rho &= g^{\mu\nu}\gamma^\rho + g^{\nu\rho}\gamma^\mu - g^{\mu\rho}\gamma^\nu - i\epsilon^{\sigma\mu\nu\rho}\gamma_\sigma\gamma^5 \\ \Rightarrow \epsilon^{\sigma\mu\nu\rho}\gamma_\sigma &= i\gamma^\mu\gamma^\nu\gamma^\rho\gamma^5 - ig^{\mu\nu}\gamma^\rho\gamma^5 - ig^{\nu\rho}\gamma^\mu\gamma^5 + ig^{\mu\rho}\gamma^\nu\gamma^5 \end{aligned}$$

we achieve:

$$\begin{aligned} \lambda_\ell > 0: \quad y^\mu [4|\gamma_\mu(v_\ell - a_\ell\gamma^5)|5\rangle &= [4|\epsilon^{\mu\nu\rho\sigma}\gamma_\mu t_\nu x_\rho z_\sigma(v_\ell - a_\ell\gamma^5)|5\rangle = i[4|\not{t}\not{x}\not{z}(v_\ell\gamma^5 - a_\ell)|5\rangle \\ &= i(v_\ell - a_\ell)\frac{s_{1q}[24]\langle 25\rangle - s_{2q}[14]\langle 15\rangle + 2\langle 25\rangle\langle 15\rangle[21][45]}{\sqrt{s_{12}}\sqrt{(s_{1q}s_{2q} - s_{12}q^2)}}. \\ \lambda_\ell < 0: \quad y^\mu \langle 4|\gamma_\mu(v_\ell - a_\ell\gamma^5)|5] &= \langle 4|\epsilon^{\mu\nu\rho\sigma}\gamma_\mu t_\nu x_\rho z_\sigma(v_\ell - a_\ell\gamma^5)|5] = i\langle 4|\not{t}\not{x}\not{z}(v_\ell\gamma^5 - a_\ell)|5] \\ &= -i(v_\ell + a_\ell)\frac{s_{1q}\langle 24\rangle[25] - s_{2q}\langle 14\rangle[15] + 2[25][15]\langle 21\rangle\langle 45\rangle}{\sqrt{s_{12}}\sqrt{(s_{1q}s_{2q} - s_{12}q^2)}}. \end{aligned}$$

Combining these projections we receive:

$$\lambda_\ell > 0: \quad \mathcal{A}_{\ell 0} = (v_\ell - a_\ell)\frac{s_{1q}[24]\langle 25\rangle - s_{2q}[14]\langle 15\rangle}{\sqrt{s_{12}s_{1q}s_{2q}}},$$

$$\mathcal{A}_{\ell +} = (v_\ell - a_\ell)\left[\frac{[24]\langle 25\rangle s_{1q}\left(\sqrt{\frac{q^2 s_{12}}{s_{1q}s_{2q}}}-1\right) + [14]\langle 15\rangle s_{2q}\left(\sqrt{\frac{q^2 s_{12}}{s_{1q}s_{2q}}}+1\right) - 2\langle 25\rangle\langle 15\rangle[21][45]}{\sqrt{2}\sqrt{s_{12}}\sqrt{(s_{1q}s_{2q}-s_{12}q^2)}}\right],$$

$$\mathcal{A}_{\ell -} = (v_\ell - a_\ell)\left[\frac{[24]\langle 25\rangle s_{2q}\left(\sqrt{\frac{q^2 s_{12}}{s_{1q}s_{2q}}}+1\right) + [14]\langle 15\rangle s_{2q}\left(\sqrt{\frac{q^2 s_{12}}{s_{1q}s_{2q}}}-1\right) + 2\langle 25\rangle\langle 15\rangle[21][45]}{\sqrt{2}\sqrt{s_{12}}\sqrt{(s_{1q}s_{2q}-s_{12}q^2)}}\right].$$

$$\lambda_\ell < 0: \quad \mathcal{A}_{\ell 0} = (v_\ell + a_\ell)\frac{s_{1q}\langle 24\rangle[25] - s_{2q}\langle 14\rangle[15]}{\sqrt{s_{12}s_{1q}s_{2q}}},$$

$$\mathcal{A}_{\ell +} = (v_\ell + a_\ell)\left[\frac{\langle 24\rangle[25] s_{1q}\left(\sqrt{\frac{q^2 s_{12}}{s_{1q}s_{2q}}}+1\right) + \langle 14\rangle[15] s_{2q}\left(\sqrt{\frac{q^2 s_{12}}{s_{1q}s_{2q}}}-1\right) + 2[25][15]\langle 21\rangle\langle 45\rangle}{\sqrt{2}\sqrt{s_{12}}\sqrt{(s_{1q}s_{2ggq}-s_{12}q^2)}}\right],$$

$$\mathcal{A}_{\ell -} = (v_\ell + a_\ell)\left[\frac{\langle 24\rangle[25] s_{1q}\left(\sqrt{\frac{q^2 s_{12}}{s_{1q}s_{2q}}}-1\right) + \langle 14\rangle[15] s_{2q}\left(\sqrt{\frac{q^2 s_{12}}{s_{1q}s_{2q}}}+1\right) - 2[25][15]\langle 21\rangle\langle 45\rangle}{\sqrt{2}\sqrt{s_{12}}\sqrt{(s_{1q}s_{2q}-s_{12}q^2)}}\right].$$

4.1.3 $\mathcal{A}_{\text{full}}$

In this subsection, we turn to the explicit expressions for the full helicity amplitude $\mathcal{A}_{\text{full}}$ on the left-hand side of the system in Eq.(4.4), which includes the decay of the intermediate vector boson into the lepton pair. Additionally, we show the rules for computing different helicity configurations of these full amplitudes. By solving the system in Eq.(4.4) for these different configurations we will get set of Z-helicity lepton-less amplitudes for various helicity values of the particles in the process.

The expressions for the leading-order (LO_1, LO_2) and next-to-leading-order (NLO_1) amplitudes are taken from ref. [65]. All results have been independently validated by comparison with calculations from ref. [52] and cross-checked against our own calculation (for LO_1 and LO_2, not at one-loop level). The expressions in ref. [65] are kept fully general, allowing application to both neutral (γ, Z) and charged ($W^\pm$) vector bosons.

The full amplitude takes the form:

$$\begin{aligned}\mathcal{A}_{\text{full}}(\dots \ell\bar{\ell}) =& e^2\Big\{\left[Q^\ell Q^q + v^\ell_{\lambda_\ell} v^q_{\lambda_q} P_Z(s_{\ell\bar{\ell}})\right]\mathcal{A}_q(\dots \ell\bar{\ell}) \\ &+ \sum_{i=1}^{n_f}\left[Q^\ell Q^q + v^\ell_{\lambda_\ell}\frac{v^i_- + v^i_+}{2} P_Z(s_{\ell\bar{\ell}})\right]\mathcal{A}_v(\dots \ell\bar{\ell})) \\ &+ \frac{v^\ell_{\lambda_\ell}}{\sin 2\theta_W} P_Z(s_{\ell\bar{\ell}})\mathcal{A}_a(\dots \ell\bar{\ell})\Big\},\end{aligned} \tag{4.11}$$

with the vector and axial couplings expressed as:

$$v_+ = \frac{g_Z}{e}\frac{v-a}{2}, v_- = \frac{g_Z}{e}\frac{v+a}{2}$$

The term proportional to $Q^\ell Q^q$ arises from the photon-mediated contribution, while the terms involving vector and axial couplings describe the Z boson contributions. $\mathcal{A}_q$ corresponds to diagrams where the γ/Z couples directly to the external quark line of flavor q; $\mathcal{A}_v$ contains diagrams where the γ/Z couples via a vector current to a closed internal quark loop, summed over n_f massless quark flavors; $\mathcal{A}_a$ involves the axial current coupling, which only receives contributions from the top-bottom isodoublet, since the axial coupling vanishes when summed over a massless isodoublet within the Standard Model. It is assumed that the mass of the top quark is massive, while all other quraks are massless.
For charged currents ($W^\pm$), analogous expressions are given by:

$$\begin{aligned}\mathcal{A}_{\text{full}}(\dots \ell^-\bar{\nu}^+) &= \frac{e^2 V_{ab}}{2\sin^2\theta_W} P_W(s_{\ell\bar{\nu}})\mathcal{A}_q(\dots \ell^-\bar{\nu}^+), \\ \mathcal{A}_{\text{full}}(\dots \nu^-\bar{\ell}^+) &= \frac{e^2 V^\dagger_{ab}}{2\sin^2\theta_W} P_W(s_{\nu\bar{\ell}})\mathcal{A}_q(\dots \nu^-\bar{\ell}^+),\end{aligned} \tag{4.12}$$

where V_{ab} is the appropriate CKM matrix element. $P_{Z,W}(s)$ denotes the ratio of the massive boson propagator to the photon propagator:

$$P_{Z,W}(s) = \frac{s}{s - m_{Z,W}^2 + i\Gamma_{Z,W} m_{Z,W}},$$

but for our purposes, since the Z and W bosons appear in the final state rather than as intermediate propagators, we set $P_Z(s) = P_W(s) = s$ throughout. Additionally, we will perform all of our calculations for the intermediate Z boson and later enforce the more general coupling in a process described in Section 3.

Each partonic process has its own color decomposition, with the full amplitude factorized into color structures and color-stripped amplitudes A_x ($x = q, v, a$), as shown in ref. [65]:

$$\begin{aligned}
V+1 \text{ jets:} \quad & \mathcal{A}_x(g_1 q_2 \bar{q}_3 \ell_4 \bar{\ell}_5) = i T^{a_1}_{\alpha_2 \bar{\alpha}_3} A_x(1; 2_q, 3_{\bar{q}}; 4_\ell, 5_{\bar{\ell}}), \\
V+2 \text{ jets:} \quad q'\bar{q}'q\bar{q}V \quad & \mathcal{A}_x(q'_1 \bar{q}'_2 q_3 \bar{q}_4 \ell_5 \bar{\ell}_6) = 2iT_F(\delta_{\alpha_1 \bar{\alpha}_4}\delta_{\alpha_3 \bar{\alpha}_2} A_x(1_{q'}, 2_{\bar{q}'}; 3_q, 4_{\bar{q}}; 5_\ell, 6_{\bar{\ell}}) \\
& \qquad + \delta_{\alpha_1 \bar{\alpha}_2}\delta_{\alpha_3 \bar{\alpha}_4} \frac{1}{N_c} B_x(1_{q'}, 2_{\bar{q}'}; 3_q, 4_{\bar{q}}; 5_\ell, 6_{\bar{\ell}})) \\
gg q\bar{q}V \quad & \mathcal{A}_x(g_1 g_2 g_3 \bar{q}_4 \ell_5 \bar{\ell}_6) = i \sum_{\sigma \in S_2} \left[T^{a_{\sigma(1)}} T^{a_{\sigma(2)}}\right]_{\alpha_3 \bar{\alpha}_4} A_x(\sigma(1), \sigma(2); 3_q, 4_{\bar{q}}; 5_\ell, 6_{\bar{\ell}}) \\
& \qquad + i \,\mathrm{tr}[T^{a_1} T^{a_2}]\, \delta_{\alpha_3 \bar{\alpha}_4} B_x(1, 2; 3_q, 4_{\bar{q}}; 5_\ell, 6_{\bar{\ell}}) \qquad .
\end{aligned} \tag{4.13}$$

The color-stripped amplitudes A_x are then expanded in α_s as:

$$\begin{aligned}
V+1 \text{ jets: } A_x &= g_s(\mu) \sum_{n=0}^{\infty} A_x^{(n)} \left(\frac{\alpha_s(\mu)}{4\pi}\right)^n; \\
V+2 \text{ jets: } A_x &= g_s^2(\mu) \sum_{n=0}^{\infty} A_x^{(n)} \left(\frac{\alpha_s(\mu)}{4\pi}\right)^n.
\end{aligned}$$

These amplitudes are written in the all-outgoing convention, which is a convenient basis for calculations and matches the convention of ref. [65]. Crossing to physical initial-state configurations is performed by helicity and momentum substitutions, along with appropriate signs from fermion crossings, discussed in detail below and in Appendix E.

For helicity amplitudes, we will present results for specific helicity configurations relevant to LO_1, NLO_1, and LO_2, with the detailed spinor structures, parity and charge conjugation relations, and their crossing into the physical channels.

$\mathbf{LO_1}$ and $\mathbf{NLO_1}$

We have the following helicity amplitudes for LO_1 and NLO_1 $0 \to gq\bar{q}\ell\bar{\ell}$ processes:

$$A_q^{(0)}(1^+; 2_q^+, 3_{\bar{q}}^-; 4_\ell^+, 5_{\bar{\ell}}^-) = -2\sqrt{2}\frac{\langle 35\rangle^2}{\langle 45\rangle\langle 12\rangle\langle 13\rangle}, \quad A_v^{(0)} = A_a^{(0)} = 0. \tag{4.14}$$

The divergent part of the one-loop helicity amplitude is given by

$$\begin{aligned}
A^{(1)}_{q,\mathrm{div}}(1^+; 2_q^+, 3_{\bar{q}}^-; 4_\ell^+, 5_{\bar{\ell}}^-) &= A_q^{(0)}(1^+; 2_q^+, 3_{\bar{q}}^-; 4_\ell^+, 5_{\bar{\ell}}^-) \\
&\times \left\{ -\frac{1}{\epsilon^2}(C_A + 2C_F) + \frac{1}{\epsilon}\left[C_A(L_{12} + L_{13} - L_{23}) + C_F(2L_{23} - 3) - \frac{\beta_0}{2}\right]\right\}.
\end{aligned} \tag{4.15}$$

The finite part of the one-loop helicity amplitude is given by

$$
\begin{aligned}
A^{(1)}_{q,\text{fin}}(1^+;2^+_q,3^-_{\bar{q}};4^+_\ell,5^-_{\bar{\ell}}) &= A^{(0)}_q(1^+,2^+_{\bar{q}},3^-_q;4^+_\ell,5^-_{\bar{\ell}}) \\
&\times \left\{ \frac{C_A}{2}\left(-L_{12}^2 - L_{13}^2 + 3L_{13} - 7 + \frac{\pi^2}{3}\right) + \left(C_F - \frac{C_A}{2}\right)\left(-L_{23}^2 + 3L_{45} - 8 + \frac{\pi^2}{6}\right) \right. \\
&+ C_A\left[-\text{Ls}_{-1}\left(\frac{s_{12}}{s_{45}},\frac{s_{13}}{s_{45}}\right) + \frac{\langle 3|24|5\rangle}{\langle 35\rangle s_{45}}\text{L}_0\left(\frac{s_{13}}{s_{45}}\right) - \frac{1}{2}\frac{\langle 3|24|5\rangle^2}{\langle 35\rangle^2 s_{45}^2}\text{L}_1\left(\frac{s_{13}}{s_{45}}\right)\right] \\
&+ (C_A - 2C_F)\left[\text{Ls}_{-1}\left(\frac{s_{12}}{s_{45}},\frac{s_{23}}{s_{45}}\right) + \left(\frac{\langle 25\rangle^2\langle 13\rangle^2}{\langle 12\rangle^2\langle 35\rangle^2} - \frac{\langle 15\rangle\langle 23\rangle + \langle 13\rangle\langle 25\rangle}{\langle 12\rangle\langle 35\rangle}\right)\text{Ls}_{-1}\left(\frac{s_{13}}{s_{45}},\frac{s_{23}}{s_{45}}\right)\right. \\
&+ \frac{2[12]\langle 25\rangle\langle 13\rangle}{\langle 35\rangle s_{45}}\text{L}_0\left(\frac{s_{13}}{s_{45}}\right) + \frac{\langle 25\rangle^2[2|1|3\rangle\,|13\rangle}{\langle 12\rangle\langle 35\rangle^2 s_{13}}\text{L}_0\left(\frac{s_{45}}{s_{13}}\right) - \frac{\langle 3|21|5\rangle\langle 25\rangle\langle 13\rangle}{\langle 12\rangle\langle 35\rangle^2 s_{23}}\text{L}_0\left(\frac{s_{45}}{s_{23}}\right) \\
&- \frac{\langle 13\rangle^2\,|1|2|5\rangle^2}{2\langle 35\rangle^2 s_{13}^2}\text{L}_1\left(\frac{s_{45}}{s_{13}}\right) - \frac{[1|2|3\rangle[4|1|5\rangle\langle 45\rangle\langle 13\rangle}{\langle 35\rangle^2 s_{23}^2}\text{L}_1\left(\frac{s_{45}}{s_{23}}\right) \\
&\left.\left. + \frac{[14]([12][34] + [13][24])\langle 13\rangle\langle 45\rangle}{2\langle 35\rangle^2[13][23][45]}\right]\right\}, \qquad (4.16)
\end{aligned}
$$

The axial current coupling term arising from the top loop contribution expanded in the powers of top mass $1/m_t^2$ is given in ref. [52] and is

$$
A^{(1)}_a(1^+;2^+_q,3^-_{\bar{q}};4^+_\ell,5^-_{\bar{\ell}}) = 4\sqrt{2}T_F[12][14][35]\left[\frac{1}{s_{45}^2}\text{L}_1\left(\frac{s_{23}}{s_{45}}\right) - \frac{1}{12 s_{45} m_t^2}\right], \quad A^{(1)}_v = 0, \qquad (4.17)
$$

where the following functions are used for shortening the length of the expressions:

$$
\text{L}_0(r) = \frac{\ln r}{1-r},\ \text{L}_1(r) = \frac{\text{L}_0(r)+1}{1-r},\ \text{Ls}_{-1}(r_1,r_2) = \text{Li}_2(1-r_1) + \text{Li}_2(1-r_2) + \ln r_1 \ln r_2 - \frac{\pi^2}{6}.
$$

To ensure analyticity and proper continuation across the physical regions, we follow the branch cut conventions of ref. [65], using the prescription: $s_{ij} \to s_{ij} + i0$ for logarithms and $\text{Im}[\text{Li}_2(1-r)] = -\ln(1-r)\text{Im}[\ln r]$ for dilogarithms, which would correspond to the following identities:

$$
\begin{aligned}
\ln r &\to \ln(-r) + i\pi \text{ for } r < 0, \\
\ln(1/r) &\to -\ln(-r) - i\pi \text{ for } r < 0, \\
\ln(-r) &\to \ln r - i\pi \text{ for } r > 0,
\end{aligned}
$$

and the dilogarithmic identities:

$$
\begin{aligned}
&\text{Li}_2(r) = -\text{Li}_2(1-r) + \frac{\pi^2}{6} - \ln r \ln(1-r) \Rightarrow \\
&\text{Li}_2(1-r) \to -\text{Li}_2(r) - \ln(1-r)(\ln(-s) + i\pi) + \frac{\pi^2}{6} \text{ for } r < 0.
\end{aligned}
$$

We consider the full set of helicity configurations for the gluon, quark, and lepton system. For the $V+1$ jet case, these can be labeled by the triplet $\lambda_g(\lambda_q,\lambda_\ell)$, where $\lambda_q,\lambda_\ell \in +1/2,-1/2$ and $\lambda_g \in +1,-1$. There are 8 such configurations:

$$
\begin{aligned}
\lambda_g(\lambda_q,\lambda_\ell): \quad &+(+,+),+(+,-), \\
&+(-,+),+(-,-), \\
&-(+,+),-(+,-), \\
&-(-,+),-(-,-).
\end{aligned}
$$

Since our final Z-helicity amplitudes are supposed to be independent of the helicity of the leptons, λ_ℓ, checking this invariance serves as a strong consistency check.

Using spinor identities and symmetry properties (charge conjugation C and parity P), it is possible to derive the transformation rules between different helicity amplitudes. These are:

$$
\begin{aligned}
A_{x,+(+;+)}(\tilde{p}_1;\tilde{p}_2,\tilde{p}_3;\tilde{p}_4,\tilde{p}_5) &= A_x(1^+;2^+_q,3^-_{\bar{q}};4^+_\ell,5^-_{\bar{\ell}}), \\
A_{x,\lambda(\lambda_q;-)}(\tilde{p}_1;\tilde{p}_2,\tilde{p}_3;\tilde{p}_4,\tilde{p}_5) &= A_{x,\lambda(\lambda_q;+)}(\tilde{p}_1;\tilde{p}_2,\tilde{p}_3;\tilde{p}_5,\tilde{p}_4), \\
A_{(q,v),\lambda(-;\lambda_\ell)}(\tilde{p}_1;\tilde{p}_2,\tilde{p}_3;\tilde{p}_4,\tilde{p}_5) &= -A_{(q,v),\lambda(+;\lambda_\ell))}(\tilde{p}_1;\tilde{p}_3,\tilde{p}_2;\tilde{p}_4,\tilde{p}_5), \\
A_{a,\lambda(-;\lambda_\ell)}(\tilde{p}_1;\tilde{p}_2,\tilde{p}_3;\tilde{p}_4,\tilde{p}_5) &= A_{a,\lambda(+;\lambda_\ell))}(\tilde{p}_1;\tilde{p}_3,\tilde{p}_2;\tilde{p}_4,\tilde{p}_5),
\end{aligned}
$$

which are derived through the action of the charge conjugation operator C on the fermion lines $4-5$ and $2-3$ respectively which exchanges the labels of the particles affected and can be interpreted as flipping the helicity sign. The extra sign for the helicity flip of the $2-3$ pair arises since the charge conjugation operator not only effects the helicity of the particles, but also flips the sign of the Z boson coupling [65]. Amplitudes with a negative-helicity gluon are obtained via parity, which flips all the helicities and conjugates all the spinors:

$$A_{(q,v),-(\lambda_q;\lambda_\ell)}(\tilde{p}_1;\tilde{p}_2,\tilde{p}_3;\tilde{p}_4,\tilde{p}_5) = A_{(q,v),+(-\lambda_q;-\lambda_\ell))}(\tilde{p}_1;\tilde{p}_2,\tilde{p}_3;\tilde{p}_4,\tilde{p}_5)\Big|_{\langle\dots\rangle\leftrightarrow[\dots]},$$
$$A_{a,-(\lambda_q;\lambda_\ell)}(\tilde{p}_1;\tilde{p}_2,\tilde{p}_3;\tilde{p}_4,\tilde{p}_5) = -A_{a,+(-\lambda_q;-\lambda_\ell))}(\tilde{p}_1;\tilde{p}_2,\tilde{p}_3;\tilde{p}_4,\tilde{p}_5)\Big|_{\langle\dots\rangle\leftrightarrow[\dots]}.$$

Overall the amplitudes that correspond to the possible helicity configurations are:

$$\begin{aligned}
\lambda : g(\lambda_q,\lambda_\ell): \quad & +(+,+) : A_{x,+(+;+)}(\tilde{p}_1;\tilde{p}_2,\tilde{p}_3;\tilde{p}_4,\tilde{p}_5),\\
& +(+,-) : A_{x,+(+;+)}(\tilde{p}_1;\tilde{p}_2,\tilde{p}_3;\tilde{p}_5,\tilde{p}_4),\\
& +(-,+) : -A_{(q,v),+(+;+)}(\tilde{p}_1;\tilde{p}_3,\tilde{p}_2;\tilde{p}_4,\tilde{p}_5),\ A_{a,+(+;+)}(\tilde{p}_1;\tilde{p}_3,\tilde{p}_2;\tilde{p}_4,\tilde{p}_5)\\
& +(-,-) : -A_{(q,v),+(+;+)}(\tilde{p}_1;\tilde{p}_3,\tilde{p}_2;\tilde{p}_5,\tilde{p}_4),\ A_{a,+(+;+)}(\tilde{p}_1;\tilde{p}_3,\tilde{p}_2;\tilde{p}_5,\tilde{p}_4)\\
& -(+,+) : -A_{(q,x),+(+;+)}(\tilde{p}_1;\tilde{p}_3,\tilde{p}_2;\tilde{p}_5,\tilde{p}_4)\Big|_{\langle\dots\rangle\leftrightarrow[\dots]}, -A_{a,+(+;+)}(\tilde{p}_1;\tilde{p}_3,\tilde{p}_2;\tilde{p}_5,\tilde{p}_4)\Big|_{\langle\dots\rangle\leftrightarrow[\dots]},\\
& -(+,-) : -A_{(q,v),+(+;+)}(\tilde{p}_1;\tilde{p}_3,\tilde{p}_2;\tilde{p}_4,\tilde{p}_5)\Big|_{\langle\dots\rangle\leftrightarrow[\dots]}, -A_{a,+(+;+)}(\tilde{p}_1;\tilde{p}_3,\tilde{p}_2;\tilde{p}_4,\tilde{p}_5)\Big|_{\langle\dots\rangle\leftrightarrow[\dots]},\\
& -(-,+) : A_{(q,v),+(+;+)}(\tilde{p}_1;\tilde{p}_2,\tilde{p}_3;\tilde{p}_5,\tilde{p}_4)\Big|_{\langle\dots\rangle\leftrightarrow[\dots]}, -A_{a,+(+;+)}(\tilde{p}_1;\tilde{p}_2,\tilde{p}_3;\tilde{p}_5,\tilde{p}_4)\Big|_{\langle\dots\rangle\leftrightarrow[\dots]},\\
& -(-,-) : A_{(q,v),+(+;+)}(\tilde{p}_1;\tilde{p}_2,\tilde{p}_3;\tilde{p}_4,\tilde{p}_5)\Big|_{\langle\dots\rangle\leftrightarrow[\dots]}, -A_{a,+(+;+)}(\tilde{p}_1;\tilde{p}_2,\tilde{p}_3;\tilde{p}_4,\tilde{p}_5)\Big|_{\langle\dots\rangle\leftrightarrow[\dots]}.
\end{aligned}$$

All amplitudes in ref. [65] are provided in the all-outgoing configuration. To relate them to physical processes with incoming particles, we apply crossing symmetry. The general rules are as follows: crossing a particle from the final to the initial state inverts its momentum ($p \to -p$), flips its helicity, and reverses its electric charge. Moreover, crossing fermions introduces an overall sign change in the amplitude.
The canonical all-outgoing helicity amplitude configuration is:

$$0 \to g_+(p_1)q_+(p_2)\bar{q}_-(p_3)\ell_+(p_4)\bar{\ell}_-(p_5) : A_{x,+(+,+)}(\tilde{p}_1;\tilde{p}_2,\tilde{p}_3;\tilde{p}_4,\tilde{p}_5) = A_x(1^+;2_q^+,3_{\bar{q}}^-;4_\ell^+,5_{\bar{\ell}}^-),$$

where $\tilde{p}_i$ denote momenta in the all-outgoing convention, and p_i correspond to physical momenta used in actual processes.
Crossing into $qg \to q\ell\bar{\ell}$ and $q\bar{q} \to g\ell\bar{\ell}$ following the rules described above is thus

$$q_+(p_1)g_-(p_2) \to q_+(p_3)\ell_+(p_4)\bar{\ell}_-(p_5) : -A_{x,+(+,+)}(-\tilde{p}_2;\tilde{p}_3,-\tilde{p}_1;\tilde{p}_4,\tilde{p}_5), \tag{4.18}$$
$$q_+(p_1)\bar{q}_-(p_2) \to g_+(p_3)\ell_+(p_4)\bar{\ell}_-(p_5) : A_{x,+(+,+)}(\tilde{p}_3;-\tilde{p}_2,-\tilde{p}_1;\tilde{p}_4,\tilde{p}_5) \tag{4.19}$$

$\mathbf{LO}_2$

We now turn to LO_2 $0 \to q'\bar{q}'q\bar{q}\ell\bar{\ell}$ amplitudes. The relevant color-stripped tree-level helicity amplitudes from ref. [65] are:

$$\begin{aligned}
A_q^{(0)}(1_{q'}^+,2_{\bar{q}'}^-;3_q^+,4_{\bar{q}}^-;5_\ell^+,6_{\bar{\ell}}^-) &= -B_q^{(0)}(1_{q'}^+,2_{\bar{q}'}^-;3_q^+,4_{\bar{q}}^-;5_\ell^+,6_{\bar{\ell}}^-)\\
&= \frac{2}{s_{12}s_{56}}\left[\frac{[13]\langle 46\rangle(\langle 12\rangle[15]-\langle 23\rangle[35])}{s_{123}} + \frac{\langle 24\rangle[35]([\langle 12\rangle\langle 26\rangle]+[14]\langle 46\rangle)}{s_{124}}\right],\\
A_q^{(0)}(1_{q'}^-,2_{\bar{q}'}^+;3_q^+,4_{\bar{q}}^-;5_\ell^+,6_{\bar{\ell}}^-) &= -B_q^{(0)}(1_{q'}^-,2_{\bar{q}'}^+;3_q^+,4_{\bar{q}}^-;5_\ell^+,6_{\bar{\ell}}^-)\\
&= \frac{2}{s_{12}s_{56}}\left[\frac{[23]\langle 46\rangle(\langle 12\rangle[25]+\langle 13\rangle[35])}{s_{123}} + \frac{\langle 14\rangle[35]([\langle 12\rangle\langle 16\rangle]-[24]\langle 46\rangle)}{s_{124}}\right],
\end{aligned}$$

All vector-loop and axial-loop contributions vanish at this order:

$$A_v^{(0)} = A_a^{(0)} = B_v^{(0)} = B_a^{(0)} = 0.$$

Loop corrections to these processes, discussed in ref. [52], begin at $\mathcal{O}(\alpha_s^3)$ and are therefore beyond the scope of this project.

For this process it is important to keep track of which out of two quarks the Z boson couples to, since, based on the Eq.(4.11), the $v^q_{\lambda_q}$ coupling depends on the flavor of the quark q, and in this channel it is possible to have diagrams with either *same flavor* and *different* incoming-outgoing quarks.

The complete set of helicity configurations for non-vanishing LO_2 amplitudes involves all combinations of fermion helicities:

$$\begin{aligned}(\lambda_{q'},\lambda_q,\lambda_\ell):\quad &(+,+,+),(+,+,-)\\ &(+,-,+),(+,-,-)\\ &(-,+,+),(-,+,-)\\ &(-,-,+),(-,-,-)\end{aligned}$$

The transformation rules among these configurations are as follows:

$$\begin{aligned}
A^{(0)}_{q,(+,+,+)}(\tilde{p}_1,\tilde{p}_2;\tilde{p}_3,\tilde{p}_4;\tilde{p}_5,\tilde{p}_6) &= A^{(0)}_q(1^+_{q'},2^-_{\bar{q}'};3^+_q,4^-_{\bar{q}};5^+_\ell,6^-_{\bar{\ell}}),\\
A^{(0)}_{q,(-,+,+)}(\tilde{p}_1,\tilde{p}_2;\tilde{p}_3,\tilde{p}_4;\tilde{p}_5,\tilde{p}_6) &= A^{(0)}_q(1^-_{q'},2^+_{\bar{q}'};3^+_q,4^-_{\bar{q}};5^+_\ell,6^-_{\bar{\ell}}) = -A^{(0)}_{q,(+,+,+)}(\tilde{p}_2,\tilde{p}_1;\tilde{p}_3,\tilde{p}_4;\tilde{p}_5,\tilde{p}_6),\\
A^{(0)}_{q,(\lambda_{q'},\lambda_q,-)}(\tilde{p}_1,\tilde{p}_2;\tilde{p}_3,\tilde{p}_4;\tilde{p}_5,\tilde{p}_6) &= A^{(0)}_{q,(\lambda_{q'},\lambda_q,+)}(\tilde{p}_1,\tilde{p}_2;\tilde{p}_3,\tilde{p}_4;\tilde{p}_6,\tilde{p}_5),\\
A^{(0)}_{q,(\lambda_{q'},-,\lambda_\ell)}(\tilde{p}_1,\tilde{p}_2;\tilde{p}_3,\tilde{p}_4;\tilde{p}_5,\tilde{p}_6) &= A^{(0)}_{q,(\lambda_{q'},+,\lambda_\ell)}(\tilde{p}_1,\tilde{p}_2;\tilde{p}_4,\tilde{p}_3;\tilde{p}_5,\tilde{p}_6),
\end{aligned}$$

where one would notice a pattern, where if the charge conjugation was applied on the fermion line that in not connected with vector boson, the amplitude not only swaps the position of the spinors but also has an extra minus sign in front of it.
Crossing from all-outgoing to physical configurations are thus:

$$\begin{aligned}
0\to q'_+(p_1)\bar{q}'_-(p_2)q_+(p_3)\bar{q}_-(p_4)\ell_+(p_5)\bar{\ell}_-(p_6):&\quad A_{x,(+,+,+)}(\tilde{p}_1,\tilde{p}_2;\tilde{p}_3,\tilde{p}_4;\tilde{p}_5,\tilde{p}_6),\\
q'_+(p_1)\bar{q}'_-(p_2)\to q_+(p_3)\bar{q}_-(p_4)\ell_+(p_5)\bar{\ell}_-(p_6):&\quad A_{x,(+,+,+)}(-\tilde{p}_2,-\tilde{p}_1;\tilde{p}_3,\tilde{p}_4;\tilde{p}_5,\tilde{p}_6), \qquad (\mathrm{SR}_{q\bar{q}\to q\bar{q}V})\\
q_+(p_1)\bar{q}_-(p_2)\to q'_+(p_3)\bar{q}'_-(p_4)\ell_+(p_5)\bar{\ell}_-(p_6):&\quad A_{x,(+,+,+)}(\tilde{p}_3,\tilde{p}_4;-\tilde{p}_2,-\tilde{p}_1;\tilde{p}_5,\tilde{p}_6), \qquad (\mathrm{SL}_{q\bar{q}\to q\bar{q}V})
\end{aligned}$$

where both expressions are corresponding to the processes with different incoming-outgoing flavor quarks. The first crossed expression ($\mathrm{SR}_{q\bar{q}\to q\bar{q}V}$) would correspond to the S-channel with vector boson coupling to the outgoing fermion leg and the second expression ($\mathrm{SL}_{q\bar{q}\to q\bar{q}V}$) would correspond to S-channel with vector boson at the incoming leg. In order to get the same flavor amplitudes one has to set all-outgoing each colored amplitudes to:

$$\mathcal{A}_x(q_1\bar{q}_2q_3\bar{q}_4\ell_5\bar{\ell}_6)=\mathcal{A}_x(q'_1\bar{q}'_2q_3\bar{q}_4\ell_5\bar{\ell}_6)-\mathcal{A}_x(q'_1\bar{q}'_4q_3\bar{q}_2\ell_5\bar{\ell}_6), \tag{4.20}$$

which corresponds, upon crossing, to the following processes:

$$\begin{aligned}
q'_+(p_1)\bar{q}_-(p_2)\to q'_+(p_3)\bar{q}_-(p_4)\ell_+(p_5)\bar{\ell}_-(p_6):&\quad -A_{x,(+,+,+)}(\tilde{p}_3,-\tilde{p}_1;-\tilde{p}_2,\tilde{p}_4;\tilde{p}_5,\tilde{p}_6), \qquad (\mathrm{TD}_{q\bar{q}\to q\bar{q}V})\\
q_+(p_1)\bar{q}'_-(p_2)\to q_+(p_3)\bar{q}'_-(p_4)\ell_+(p_5)\bar{\ell}_-(p_6):&\quad -A_{x,(+,+,+)}(-\tilde{p}_2,\tilde{p}_4;\tilde{p}_3,-\tilde{p}_1;\tilde{p}_5,\tilde{p}_6),, \qquad (\mathrm{TU}_{q\bar{q}\to q\bar{q}V})
\end{aligned}$$

where we retain the (now redundant) primed labels for clarity, to indicate which quark is being crossed to which side of the process. The first expression ($\mathrm{TD}_{q\bar{q}\to q\bar{q}V}$) corresponds to a T-channel exchange with the vector boson coupling to the lower fermion line, while the second ($\mathrm{TU}_{q\bar{q}\to q\bar{q}V}$) corresponds to a T-channel with the boson coupling to the upper line. In this setup, the q' quark resides in the upper line, carrying momentum p_1.
It is important to note that crossing also affects the color structure. Specifically, the color factor transforms as:

$$\underbrace{2T_F(\delta_{\alpha_1\bar{\alpha}_4}\delta_{\alpha_3\bar{\alpha}_2},\delta_{\alpha_1\bar{\alpha}_2}\delta_{\alpha_3\bar{\alpha}_4}\frac{1}{N_c})}_{\text{ColorFactor[1, 2, 3, 4]}}\to\underbrace{2T_F(\delta_{\alpha_2\bar{\alpha}_4}\delta_{\alpha_3\bar{\alpha}_1},\delta_{\alpha_2\bar{\alpha}_1}\delta_{\alpha_3\bar{\alpha}_4}\frac{1}{N_c})}_{\text{ColorFactor[2, 1, 3, 4]}}\ \text{for}\ \mathrm{SR}_{q\bar{q}\to q\bar{q}V},$$

ColorFactor[3, 4, 2, 1] for $\mathrm{SL}_{q\bar{q}\to q\bar{q}V}$,
ColorFactor[3, 1, 2, 4] for $\mathrm{TD}_{q\bar{q}\to q\bar{q}V}$,
ColorFactor[2, 4, 3, 1] for $\mathrm{TU}_{q\bar{q}\to q\bar{q}V}$

Since Kronecker delta indices and the delta functions themselves commute, these can be reduced to just two distinct color structures: ColorFactor[1, 2, 3, 4] for $\mathrm{SR}_{q\bar{q}\to q\bar{q}V}$ and $\mathrm{SL}_{q\bar{q}\to q\bar{q}V}$ and ColorFactor[1, 4, 3, 2]

for $\mathrm{TD}_{q\bar{q}\to q\bar{q}V}$ and $\mathrm{TU}_{q\bar{q}\to q\bar{q}V}$.
At leading order LO_2 the full amplitude takes the form:

$$\begin{aligned}
\mathcal{A}_{\text{full}}(\dots \ell\bar{\ell}) = e^2\Big\{ & \Big[Q^\ell Q^q + v^\ell_{\lambda_\ell} v^q_{\lambda_q} P_Z(s_{\ell\bar{\ell}})\Big]\,\text{ColorFactor[1, 2, 3, 4]}\,\underbrace{A_{x,(\lambda_{q'},\lambda_q,\lambda_\ell)}(-\tilde{p}_2,-\tilde{p}_1;\tilde{p}_3,\tilde{p}_4;\tilde{p}_5,\tilde{p}_6)}_{\mathrm{SR}_{q\bar{q}\to q\bar{q}V}} \\
& + \Big[Q^\ell Q^{q'} + v^\ell_{\lambda_\ell} v^{q'}_{\lambda_{q'}} P_Z(s_{\ell\bar{\ell}})\Big]\,\text{ColorFactor[1, 2, 3, 4]}\,\underbrace{A_{x,(\lambda_{q'},\lambda_q,\lambda_\ell)}(\tilde{p}_3,\tilde{p}_4;-\tilde{p}_2,-\tilde{p}_1;\tilde{p}_5,\tilde{p}_6)}_{\mathrm{SL}_{q\bar{q}\to q\bar{q}V}} \\
& - \Big[Q^\ell Q^q + v^\ell_{\lambda_\ell} v^q_{\lambda_q} P_Z(s_{\ell\bar{\ell}})\Big]\,\text{ColorFactor[1, 4, 3, 2]}\,\underbrace{A_{x,(\lambda_{q'},\lambda_q,\lambda_\ell)}(\tilde{p}_3,-\tilde{p}_1;-\tilde{p}_2,\tilde{p}_4;\tilde{p}_5,\tilde{p}_6)}_{\mathrm{TD}_{q\bar{q}\to q\bar{q}V}} \\
& - \Big[Q^\ell Q^{q'} + v^\ell_{\lambda_\ell} v^{q'}_{\lambda_{q'}} P_Z(s_{\ell\bar{\ell}})\Big]\,\text{ColorFactor[1, 4, 3, 2]}\,\underbrace{A_{x,(\lambda_{q'},\lambda_q,\lambda_\ell)}(-\tilde{p}_2,\tilde{p}_4;\tilde{p}_3,-\tilde{p}_1;\tilde{p}_5,\tilde{p}_6)}_{\mathrm{TU}_{q\bar{q}\to q\bar{q}V}}\Big\},
\end{aligned}$$

where the couplings make explicit which fermion line the vector boson is attached to, depending on the crossing.
Crossing into $qq \to qqV$ is gives:

$$\begin{aligned}
q_+(p_1)q'_+(p_2) \to q_+(p_3)q'_+(p_4)\ell_+(p_5)\bar{\ell}_-(p_6): &\quad -A_{x,(+,+,+)}(\tilde{p}_4,-\tilde{p}_2;\tilde{p}_3,-\tilde{p}_1;\tilde{p}_5,\tilde{p}_6), && (\mathrm{TU}_{qq\to qqV})\\
q_+(p_1)q'_+(p_2) \to q_+(p_3)q'_+(p_4)\ell_+(p_5)\bar{\ell}_-(p_6): &\quad -A_{x,(+,+,+)}(\tilde{p}_3,-\tilde{p}_1;\tilde{p}_4,-\tilde{p}_2;\tilde{p}_5,\tilde{p}_6), && (\mathrm{TD}_{qq\to qqV})\\
q_+(p_1)q'_+(p_2) \to q_+(p_4)q'_+(p_3)\ell_+(p_5)\bar{\ell}_-(p_6): &\quad A_{x,(+,+,+)}(\tilde{p}_3,-\tilde{p}_2;\tilde{p}_4,-\tilde{p}_1;\tilde{p}_5,\tilde{p}_6), && (\mathrm{UU}_{qq\to qqV})\\
q_+(p_1)q'_+(p_2) \to q_+(p_4)q'_+(p_3)\ell_+(p_5)\bar{\ell}_-(p_6): &\quad A_{x,(+,+,+)}(\tilde{p}_4,-\tilde{p}_1;\tilde{p}_3,-\tilde{p}_2;\tilde{p}_5,\tilde{p}_6), && (\mathrm{UD}_{qq\to qqV})
\end{aligned}$$

where the U-channel contributions ($\mathrm{UU}_{qq\to qqV}$) and ($\mathrm{UD}_{qq\to qqV}$) arise by crossing p_3 and p_4 in TU and TD cases, respectively. These could alternatively be obtained by applying Eq.(4.20) directly to the $qq \to qqV$ amplitudes.
As for color factors, $\mathrm{TU}_{qq\to qqV}$ and $\mathrm{TD}_{qq\to qqV}$ will retain ColorFactor[1,4,3,2] and $\mathrm{UU}_{qq\to qqV}$ and $\mathrm{UD}_{qq\to qqV}$ will have to be dressed with ColorFactor[1,2,3,4]. $\mathrm{TU}_{qq\to qqV}$ and $\mathrm{UU}_{qq\to qqV}$ will have coupling depending on the helicity of the q' quark ($v^{q'}_{\lambda_{q'}}$) and $\mathrm{TD}_{qq\to qqV}$ with $\mathrm{UD}_{qq\to qqV}$ will have coupling depending on the helicity of the q quark ($v^q_{\lambda_q}$).

Finally, we note an important technical point: the helicity-flip rules differ between crossings. In particular, S- and T-channels will have different fermion lines onto which conjugation operator will act. Full list of all expressions for helicity configurations for both LO_1 and LO_2 in given in Appendix E.

The LO_2 $0 \to ggq\bar{q}\ell\bar{\ell}$ color-stripped amplitudes from ref. [65] are

$$\begin{aligned}
A^{(0)}_q(1^+,2^+;3^+_q,4^-_{\bar{q}};5^+_\ell,6^-_{\bar{\ell}}) &= -4\,\frac{\langle 46\rangle^2}{\langle 12\rangle\langle 13\rangle\langle 24\rangle\langle 56\rangle},\\
A^{(0)}_q(1^+,2^-;3^+_q,4^-_{\bar{q}};5^+_\ell,6^-_{\bar{\ell}}) &= \frac{4}{s_{12}s_{56}}\Bigg[\frac{\langle 13\rangle\langle 23\rangle\langle 46\rangle\,(\langle 23\rangle[35]-\langle 12\rangle[15])}{\langle 13\rangle s_{123}} + \frac{\langle 24\rangle[35][14]\,([12]\langle 26\rangle+[14]\langle 46\rangle)}{[24]s_{124}}\\
&\quad + \frac{([12]\langle 26\rangle+[14]\langle 46\rangle)(\langle 23\rangle[35]-\langle 12\rangle[15])}{\langle 13\rangle[24]}\Bigg],\\
A^{(0)}_q(1^-,2^+;3^+_q,4^-_{\bar{q}};5^+_\ell,6^-_{\bar{\ell}}) &= \frac{4}{s_{12}s_{56}}\Bigg[\frac{[23]^2\langle 46\rangle\,(\langle 12\rangle[25]+\langle 13\rangle[35])}{[13]s_{123}} + \frac{\langle 14\rangle^2[35]\,([12]\langle 16\rangle-[24]\langle 46\rangle)}{\langle 24\rangle s_{124}}\\
&\quad + \frac{[23][14][35]\langle 46\rangle}{[13]\langle 24\rangle}\Bigg],\\
A^{(0)}_v &= A^{(0)}_a = B^{(0)}_q = B^{(0)}_v = B^{(0)}_a = 0.
\end{aligned} \tag{4.21}$$

The distinct helicity configurations of the external gluons in the $0 \to ggq\bar{q}\ell^+\ell^-$ process are explicitly stated in the structure of the amplitude defined in Eq. (4.21). This detail arises because these helicity amplitudes cannot, in general, be related to one another via simple applications of discrete symmetries such as parity or charge conjugation. This is due to the fact that gluons are vector particles and their helicities transform nontrivially under these operations. As a result, each distinct helicity combination must be treated independently in the amplitude decomposition.

Unlike the case of the 6-fermion amplitude, there is no ambiguity here regarding which fermion line the vector boson couples to, as there is only a single available quark line for the coupling.
The complete set of helicity configurations is thus:

$$\begin{aligned}\lambda_1,\lambda_2(\lambda_q;\lambda_\ell):\quad & +,+(+;+),+,+(+;-)\\ & +,+(-;+),+,+(-;-)\\ & +,-(+;+),+,-(+;-)\\ & +,-(-;+),+,-(-;-)\\ & -,+(+;+),-,+(+;-)\\ & -,+(-;+),-,+,(-;-)\\ & -,-(+;+),-,-(+;-)\\ & -,-(-;+),-,-(-;-)\end{aligned}$$

Helicity flip rules do not affect the sign of the amplitude, but change the color structure of the colorful amplitude:

$$\mathcal{A}_{x\lambda_1\lambda_2(+,+)}(\tilde{p}_1,\tilde{p}_2;\tilde{p}_3,\tilde{p}_4;\tilde{p}_5,\tilde{p}_6)=\bar{\mathbf{T}}\vec{A}_{x\lambda_1\lambda_2(+,+)}(\tilde{p}_1,\tilde{p}_2;\tilde{p}_3,\tilde{p}_4;\tilde{p}_5,\tilde{p}_6)=\bar{T}\begin{pmatrix}A_x\big(1^{\lambda_1},2^{\lambda_2};3_q^+,4_{\bar{q}}^-;5_\ell^+,6_{\bar{\ell}}^-\big)\\ A_x\big(2^{\lambda_2},1^{\lambda_1};3_q^+,4_{\bar{q}}^-;5_\ell^+,6_{\bar{\ell}}^-\big)\\ B_x\big(1^{\lambda_1},2^{\lambda_2};3_q^+,4_{\bar{q}}^-;5_\ell^+,6_{\bar{\ell}}^-\big)\end{pmatrix},$$

where we named $\bar{\mathbf{T}}$ the color basis: $\bar{\mathbf{T}}_{\alpha_3\bar{\alpha}_4}=i\,\mathrm{diag}([T^{a_1}T^{a_2}]_{\alpha_3\bar{\alpha}_4},[T^{a_2}T^{a_1}]_{\alpha_3\bar{\alpha}_4},\mathrm{tr}[T^{a_1}T^{a_2}]\delta_{\alpha_3\bar{\alpha}_4})$.

$$\begin{aligned}\vec{A}_{x\lambda_1\lambda_2(+,-)}(\tilde{p}_1,\tilde{p}_2;\tilde{p}_3,\tilde{p}_4;\tilde{p}_5,\tilde{p}_6)&=\vec{A}_{x\lambda_1\lambda_2(+,+)}(\tilde{p}_1,\tilde{p}_2;\tilde{p}_3,\tilde{p}_4;\tilde{p}_6,\tilde{p}_5),\\ \vec{A}_{q,x\lambda_1\lambda_2(-,\pm)}(\tilde{p}_1,\tilde{p}_2;\tilde{p}_3,\tilde{p}_4;\tilde{p}_5,\tilde{p}_6)&=\mathbf{V}\vec{A}_{q,x\lambda_1\lambda_2(+,\pm)}(\tilde{p}_1,\tilde{p}_2;\tilde{p}_4,\tilde{p}_3;\tilde{p}_5,\tilde{p}_6),\\ \mathcal{A}_{a\lambda_1\lambda_2(-,\pm)}(\tilde{p}_1,\tilde{p}_2;\tilde{p}_3,\tilde{p}_4;\tilde{p}_5,\tilde{p}_6)&=-\mathbf{V}\vec{A}_{a,\lambda_1\lambda_2(+,\pm)}(\tilde{p}_1,\tilde{p}_2;\tilde{p}_4,\tilde{p}_3;\tilde{p}_5,\tilde{p}_6),\\ \text{with }\mathbf{V}&=\begin{pmatrix}0&1&0\\1&0&0\\0&0&1\end{pmatrix}.\end{aligned}$$

An alternative physical interpretation of the color factor decomposition at LO_2 is that the term proportional to

$$[T^{a_2}T^{a_1}]_{\alpha_3\bar{\alpha}_4}$$

corresponds to diagrams where the two outgoing gluon legs are crossed. This structure allows for a classification of amplitudes into two distinct subsets:

(a) **Uncrossed**, where the gluon ordering is $(1^{\lambda_1},2^{\lambda_2})$:

$$A_x^{(0)}\big(1^{\lambda_1},2^{\lambda_2};3_q^+,4_{\bar{q}}^-;5_\ell^+,6_{\bar{\ell}}^-\big),$$

(b) **Crossed**, where the gluon ordering is $(2^{\lambda_2},1^{\lambda_1})$:

$$A_x^{(0)}\big(2^{\lambda_2},1^{\lambda_1};3_q^+,4_{\bar{q}}^-;5_\ell^+,6_{\bar{\ell}}^-\big).$$

While this decomposition is conceptually useful for organizing contributions with different color structures, it is not strictly necessary. The helicity flip and permutation rules apply the same to both crossed and uncrossed configurations, ensuring that the full amplitude remains consistent under the relevant symmetries, as long as the rules for exchanging the color factors are preserved.
Crossing into all the physical configurations with two gluons is straightforward:

$$\begin{aligned}0\to g_+(p_1)g_+(p_2)q_+(p_3)\bar{q}_-(p_4)\ell_+(p_5)\bar{\ell}_-(p_6):&\quad \vec{A}_{x\lambda_1\lambda_2(+,+)}(\tilde{p}_1,\tilde{p}_2;\tilde{p}_3,\tilde{p}_4;\tilde{p}_5,\tilde{p}_6),\\ g_-(p_1)g_-(p_2)\to q_+(p_3)\bar{q}_-(p_4)\ell_+(p_5)\bar{\ell}_-(p_6):&\quad \vec{A}_{x\lambda_1\lambda_2(+,+)}(-\tilde{p}_1,-\tilde{p}_2;\tilde{p}_3,\tilde{p}_4;\tilde{p}_5,\tilde{p}_6),\\ &\qquad\qquad (\mathrm{NoCr}+\mathrm{Cr}_{gg\to q\bar{q}V})\\ q_+(p_1)g_-(p_2)\to q_+(p_3)g_+(p_4)\ell_+(p_5)\bar{\ell}_-(p_6):&\quad \vec{A}_{x\lambda_1\lambda_2(+,+)}(\tilde{p}_4,-\tilde{p}_2;\tilde{p}_3,-\tilde{p}_1;\tilde{p}_5,\tilde{p}_6),\\ &\qquad\qquad (\mathrm{NoCr}+\mathrm{Cr}_{qg\to qgV})\\ q_+(p_1)\bar{q}_-(p_2)\to g_+(p_3)g_+(p_4)\ell_+(p_5)\bar{\ell}_-(p_6):&\quad \vec{A}_{x\lambda_1\lambda_2(+,+)}(\tilde{p}_4,\tilde{p}_3;-\tilde{p}_2,-\tilde{p}_1;\tilde{p}_5,\tilde{p}_6).,\\ &\qquad\qquad (\mathrm{NoCr}+\mathrm{Cr}_{q\bar{q}\to ggV})\end{aligned}$$

where the "NoCr+Cr" tag implies that the amplitude consists of all the relevant diagrams at LO_2, so both ones with uncrossed and crossed external legs. We should also note that crossing into the physical configurations does not alter the color factor and does not affect the Z boson coupling.

Full helicity flip rules for channels with two external gluons are given in Appendix E.

4.1.4 Lepton Configurations and Solving the System

To increase the number of equations in Eq. (4.4) and solve for $\mathcal{A}_\lambda$, we use Schouten identities and momentum conservation to obtain three independent solutions corresponding to different configurations of the leptons.

LO_1, NLO_1, analytic extraction

For an analytical solution, we select a subset of linear and independent Schouten identities along with momentum conservation identities for spinor products. We then solve these equations for all possible combinations of lepton-parton spinor products in terms of parton-parton spinor products. For instance, we express

$$\begin{aligned}\langle 15\rangle &= f(\langle 12\rangle, \langle 13\rangle, \langle 23\rangle),\\ \langle 14\rangle &= g(\langle 12\rangle, \langle 13\rangle, \langle 23\rangle),\\ \langle 25\rangle &= h(\langle 12\rangle, \langle 13\rangle, \langle 23\rangle),\ \text{etc.},\end{aligned}$$

where f, g, h are some functions of spinor brackets. We will see a bit further that one possible solution in the LO_1 case is to align one of the leptons with the momentum direction of p_1, p_2, or p_3.

Schouten identities used:

$$\langle 42\rangle\langle 13\rangle - \langle 41\rangle\langle 23\rangle = \langle 43\rangle\langle 12\rangle, \tag{SchoutenA}$$
$$\langle 52\rangle\langle 13\rangle - \langle 51\rangle\langle 23\rangle = \langle 53\rangle\langle 12\rangle, \tag{SchoutenB}$$

where the identification of partons and leptons in physical and all-outgoing notation follows Eq. (4.10).

Momentum conservation identities used:

$$[12]\langle 24\rangle + [13]\langle 34\rangle + [15]\langle 54\rangle = 0, \tag{Mom14}$$
$$[12]\langle 25\rangle + [13]\langle 35\rangle + [14]\langle 45\rangle = 0, \tag{Mom15}$$
$$[21]\langle 14\rangle + [23]\langle 34\rangle + [25]\langle 54\rangle = 0, \tag{Mom24}$$
$$[21]\langle 15\rangle + [23]\langle 35\rangle + [24]\langle 45\rangle = 0, \tag{Mom25}$$
$$[31]\langle 14\rangle + [32]\langle 24\rangle + [35]\langle 54\rangle = 0, \tag{Mom34}$$
$$[31]\langle 15\rangle + [32]\langle 25\rangle + [34]\langle 45\rangle = 0. \tag{Mom35}$$

where the 'external' particles are chosen as (p_1, p_4), (p_1, p_5), (p_2, p_4), (p_2, p_3), (p_3, p_4), and (p_3, p_5), respectively.

The following combinations of Schouten and momentum conservation identities give the following solutions for parton-lepton spinor products:

- Using (SchoutenA), (SchoutenB), (Mom15), along with two additional momentum conservation identities with external p_4 (e.g., (Mom24) and (Mom34)) and their conjugates, we obtain:

$$\langle 14\rangle = 0, \langle 15\rangle = \frac{(s_{12}+s_{13})\langle 35\rangle}{\langle 23\rangle[12]}, \langle 24\rangle = -\frac{\langle 45\rangle[35]}{[23]}, \langle 34\rangle = -\frac{\langle 13\rangle\langle 45\rangle[35]}{\langle 12\rangle[23]}, \langle 25\rangle = -\frac{\langle 35\rangle[13]}{[12]}. \tag{4.24}$$

- Similarly, using (SchoutenA), (SchoutenB), (Mom25), and two additional momentum conservation identities with external p_4 (e.g., (Mom24) and (Mom34)) and their conjugates, we obtain:

$$\langle 14\rangle = -\frac{\langle 45\rangle[35]}{[13]}, \langle 15\rangle = \frac{\langle 35\rangle[23]}{[12]}, \langle 24\rangle = 0, \langle 25\rangle = -\frac{(s_{12}+s_{23})\langle 35\rangle}{\langle 13\rangle[12]}, \langle 34\rangle = \frac{\langle 23\rangle\langle 45\rangle[35]}{\langle 12\rangle[13]}. \tag{4.25}$$

  This corresponds to the previous configuration with particles 1 and 2 exchanged.

$\lambda_g(\lambda_q,\lambda_\ell)/\mathcal{A}_\lambda$	$\mathcal{A}_0$	$\mathcal{A}_+$	$\mathcal{A}_-$
$+(+,\pm)$	$[g_Z(v_q-a_q)]T^{a_2}_{\alpha_1\bar{\alpha}_3}\frac{g_s}{\sqrt{2}}\frac{t(Q^2-t)}{\Delta_z}\frac{\langle 13\rangle}{\langle 23\rangle^2}$	$[g_Z(v_q-a_q)]T^{a_2}_{\alpha_1\bar{\alpha}_3}\frac{g_s}{2}\frac{t(Q^2-t)(Qs+\Delta_z)}{s\Delta_y}\frac{\langle 13\rangle}{\langle 23\rangle^2}$	$[g_Z(v_q-a_q)]T^{a_2}_{\alpha_1\bar{\alpha}_3}\frac{g_s}{2}\frac{t(Q^2-t)(Qs-\Delta_z)}{s\Delta_y}\frac{\langle 13\rangle}{\langle 23\rangle^2}$
$+(-,\pm)$	$[g_Z(v_q+a_q)]T^{a_2}_{\alpha_1\bar{\alpha}_3}\frac{g_s}{\sqrt{2}}\frac{s(Q^2+s)}{\Delta_z}\frac{\langle 13\rangle}{\langle 12\rangle^2}$	$-[g_Z(v_q+a_q)]T^{a_2}_{\alpha_1\bar{\alpha}_3}\frac{g_s}{2}\frac{\Delta_z(t+u)+Qs(t-u)}{\Delta_y}\frac{\langle 13\rangle}{\langle 12\rangle^2}$	$-[g_Z(v_q+a_q)]T^{a_2}_{\alpha_1\bar{\alpha}_3}\frac{g_s}{2}\frac{\Delta_z(t+u)-Qs(t-u)}{\Delta_y}\frac{\langle 13\rangle}{\langle 12\rangle^2}$
$-(-,\pm)$	$[g_Z(v_q+a_q)]T^{a_2}_{\alpha_1\bar{\alpha}_3}\frac{g_s}{\sqrt{2}}\frac{t(Q^2-t)}{\Delta_z}\frac{[13]}{[23]^2}$	$[g_Z(v_q+a_q)]T^{a_2}_{\alpha_1\bar{\alpha}_3}\frac{g_s}{2}\frac{t(Q^2-t)(Qs-\Delta_z)}{s\Delta_y}\frac{[13]}{[23]^2}$	$[g_Z(v_q+a_q)]T^{a_2}_{\alpha_1\bar{\alpha}_3}\frac{g_s}{2}\frac{t(Q^2-t)(Qs+\Delta_z)}{s\Delta_y}\frac{[13]}{[23]^2}$
$-(+,\pm)$	$[g_Z(v_q-a_q)]T^{a_2}_{\alpha_1\bar{\alpha}_3}\frac{g_s}{\sqrt{2}}\frac{s(Q^2+s)}{\Delta_z}\frac{[13]}{[12]^2}$	$-[g_Z(v_q-a_q)]T^{a_2}_{\alpha_1\bar{\alpha}_3}\frac{g_s}{2}\frac{\Delta_z(t+u)-Qs(t-u)}{\Delta_y}\frac{[13]}{[12]^2}$	$-[g_Z(v_q-a_q)]T^{a_2}_{\alpha_1\bar{\alpha}_3}\frac{g_s}{2}\frac{\Delta_z(t+u)+Qs(t-u)}{\Delta_y}\frac{[13]}{[12]^2}$

Table 4.1: LO$_1$ $qg\to Zq$ Z-helicity amplitudes, $\Delta_z=\sqrt{s(Q^2-u)(Q^2-t)}$, $\Delta_y=\sqrt{tu(Q^2-u)(Q^2-t)}$, expressions with the same color are the same up to a phase.

$\lambda_g(\lambda_q,\lambda_\ell)/\mathcal{A}_\lambda$	$\mathcal{A}_0$	$\mathcal{A}_+$	$\mathcal{A}_-$
$+(+,\pm)$	$[g_Z(v_q-a_q)]T^{a_3}_{\alpha_1\bar{\alpha}_2}\frac{g_s}{\sqrt{2}}\frac{t(Q^2-t)}{\Delta_z}\frac{\langle 12\rangle}{\langle 23\rangle^2}$	$[g_Z(v_q-a_q)]T^{a_3}_{\alpha_1\bar{\alpha}_2}\frac{g_s}{2}\frac{t(Q^2-t)(Qs+\Delta_z)}{s\Delta_y}\frac{\langle 12\rangle}{\langle 23\rangle^2}$	$[g_Z(v_q-a_q)]T^{a_3}_{\alpha_1\bar{\alpha}_2}\frac{g_s}{2}\frac{t(Q^2-t)(Qs-\Delta_z)}{s\Delta_y}\frac{\langle 12\rangle}{\langle 23\rangle^2}$
$+(-,\pm)$	$-[g_Z(v_q+a_q)]T^{a_3}_{\alpha_1\bar{\alpha}_2}\frac{g_s}{\sqrt{2}}\frac{u(Q^2-u)}{\Delta_z}\frac{\langle 12\rangle}{\langle 13\rangle^2}$	$[g_Z(v_q+a_q)]T^{a_3}_{\alpha_1\bar{\alpha}_2}\frac{g_s}{2}\frac{u(Q^2-u)(Qs-\Delta_z)}{s\Delta_y}\frac{\langle 12\rangle}{\langle 13\rangle^2}$	$[g_Z(v_q+a_q)]T^{a_3}_{\alpha_1\bar{\alpha}_2}\frac{g_s}{2}\frac{u(Q^2-u)(Qs+\Delta_z)}{s\Delta_y}\frac{\langle 12\rangle}{\langle 13\rangle^2}$
$-(-,\pm)$	$[g_Z(v_q+a_q)]T^{a_3}_{\alpha_1\bar{\alpha}_2}\frac{g_s}{\sqrt{2}}\frac{t(Q^2-t)}{\Delta_z}\frac{[12]}{[23]^2}$	$[g_Z(v_q+a_q)]T^{a_3}_{\alpha_1\bar{\alpha}_2}\frac{g_s}{2}\frac{t(Q^2-t)(Qs-\Delta_z)}{s\Delta_y}\frac{[12]}{[23]^2}$	$[g_Z(v_q+a_q)]T^{a_3}_{\alpha_1\bar{\alpha}_2}\frac{g_s}{2}\frac{t(Q^2-t)(Qs+\Delta_z)}{s\Delta_y}\frac{[12]}{[23]^2}$
$-(+,\pm)$	$-[g_Z(v_q-a_q)]T^{a_3}_{\alpha_1\bar{\alpha}_2}\frac{g_s}{\sqrt{2}}\frac{u(Q^2-u)}{\Delta_z}\frac{[12]}{[13]^2}$	$[g_Z(v_q-a_q)]T^{a_3}_{\alpha_1\bar{\alpha}_2}\frac{g_s}{2}\frac{u(Q^2-u)(Qs+\Delta_z)}{s\Delta_y}\frac{[12]}{[13]^2}$	$[g_Z(v_q-a_q)]T^{a_3}_{\alpha_1\bar{\alpha}_2}\frac{g_s}{2}\frac{u(Q^2-u)(Qs-\Delta_z)}{s\Delta_y}\frac{[12]}{[13]^2}$

Table 4.2: LO$_1$ $q\bar{q}\to Zg$ Z-helicity amplitudes, $\Delta_z=\sqrt{s(Q^2-u)(Q^2-t)}$, $\Delta_y=\sqrt{tu(Q^2-u)(Q^2-t)}$, expressions with the same color are the same up to a phase.

- Using (SchoutenA), (SchoutenB), (Mom35), and two additional momentum conservation identities with external p_4 (e.g., (Mom24) and (Mom34)) and their conjugates, we obtain:

$$\langle 14\rangle=\frac{\langle 13\rangle\langle 45\rangle[35]}{s_{13}+s_{23}},\langle 15\rangle=\frac{\langle 12\rangle\langle 35\rangle[23]}{s_{13}+s_{23}},\langle 24\rangle=\frac{\langle 23\rangle\langle 45\rangle[35]}{s_{13}+s_{23}},\langle 25\rangle=-\frac{\langle 12\rangle\langle 35\rangle[13]}{s_{13}+s_{23}},\langle 34\rangle=0. \tag{4.26}$$

  Here, we do not solve for $\langle 35\rangle$ and $[35]$, as eventually this dependence cancels out.

These three configurations correspond to the lepton p_4 being collinear with p_1, p_2, and p_3, respectively.

It is important to note that these are not the only possible configurations, as the solutions for $\mathcal{A}_\lambda$ are independent of lepton configurations. These specific expressions were chosen for their simplicity.

By inserting these three configurations along with projected lepton currents and expression for $\mathcal{A}_{\text{full}}$ from ref. [65] into Eq. (4.4), we effectively write out the system

$$\begin{cases}\mathcal{A}_{\text{full}}(1,2,3,1n,5)=\mathcal{A}_0(1,2,3)\mathcal{A}_{\ell 0}(1,2,3,1n,5)+\mathcal{A}_+\mathcal{A}_{\ell+}+\mathcal{A}_-\mathcal{A}_{\ell-}\Big|_{\langle 14\rangle=0,\ldots},\\ \mathcal{A}_{\text{full}}(1,2,3,2n,5)=\mathcal{A}_0(1,2,3)\mathcal{A}_{\ell 0}(1,2,3,2n,5)+\mathcal{A}_+\mathcal{A}_{\ell+}+\mathcal{A}_-\mathcal{A}_{\ell-}\Big|_{\langle 24\rangle=0,\ldots},\\ \mathcal{A}_{\text{full}}(1,2,3,3n,5)=\mathcal{A}_0(1,2,3)\mathcal{A}_{\ell 0}(1,2,3,3n,5)+\mathcal{A}_+\mathcal{A}_{\ell+}+\mathcal{A}_-\mathcal{A}_{\ell-}\Big|_{\langle 34\rangle=0,\ldots},\end{cases} \tag{4.27}$$

where we have suppressed the helicity labels $(1^{\lambda_g},2^{\lambda_q}_{\bar{q}},3^{-\lambda_q}_q,4^{\lambda_\ell}_\ell,5^{-\lambda_\ell}_{\bar{\ell}})$, where in reality of course we would have to state the helicities of the external particles explicitly and solve the system multiple type for different physical helicity configurations $(\lambda_g,\lambda_q,\lambda_\ell)$. Additionally we have avoided repeating the spinor dependence in the $\lambda=+,-$ to avoid redundancy, it is of course assumes that these terms also have the dependence on the spinors $(1^{\lambda_g},2^{\lambda_q}_{\bar{q}},3^{-\lambda_q}_q,4^{\lambda_\ell}_\ell,5^{-\lambda_\ell}_{\bar{\ell}})$. Finally, we explicitly indicated that for each line in the system one of the outgoing leptons becomes collinear to one of the partons p_1,p_2 and p_3 by writing the spinor label as $1n$, $2n$ and $3n$ respectively. It is important to note that all other spinor products are also affected by this constrain, as shown in Eq.(4.24), Eq.(4.25) and Eq.(4.26).

Discussion and the analytical results

We solve the above-written system for $\mathcal{A}_\lambda$ for various external parton helicity configurations. The full set of results, including all $\mathcal{A}_\lambda$ values and their corresponding parton helicity configurations (λ_ℓ,λ_q) in $\mathcal{A}_{\text{full}}$, is summarized in Table 4.1 for $qg\to Zq$ process and in Table 4.2 for $q\bar{q}\to Zg$ process.

Similar lepton configurations were chosen for **NLO$_1$** amplitudes. A sample of the Z-helicity amplitudes derived from the lepton-full top-loop amplitude in Eq.(4.17) is shown in Tables 4.3 and 4.4. In the

$\lambda_g(\lambda_q,\lambda_\ell)/\mathcal{A}_\lambda$	$\mathcal{A}_0$	$\mathcal{A}_+$	$\mathcal{A}_-$
$+(+,\pm)$	0	$g_Z T^{a_2}_{\alpha_1\bar{\alpha}_3} T_F g_s \frac{\alpha_s}{4\pi} \times \mathrm{L}_1\left(\frac{u}{Q^2}\right) \frac{\langle 13\rangle}{\langle 23\rangle^2} \times \Delta_x t \frac{(Q^2-t)(Q^2-u)+Q\Delta_z}{Q^3 u}$	$g_Z T^{a_2}_{\alpha_1\bar{\alpha}_3} T_F g_s \frac{\alpha_s}{4\pi} \times \mathrm{L}_1\left(\frac{u}{Q^2}\right) \frac{\langle 13\rangle}{\langle 23\rangle^2} \times \Delta_x t \frac{(Q^2-t)(Q^2-u)-Q\Delta_z}{Q^3 u}$
$+(-,\pm)$	$-g_Z T^{a_2}_{\alpha_1\bar{\alpha}_3} T_F g_s \frac{\alpha_s}{2\sqrt{2}\pi} \times \mathrm{L}_1\left(\frac{u}{Q^2}\right) \frac{\langle 13\rangle}{\langle 12\rangle^2} \times \frac{s}{Q^2}\sqrt{\frac{s(Q^2-u)}{Q^2-t}}$	$g_Z T^{a_2}_{\alpha_1\bar{\alpha}_3} T_F g_s \frac{\alpha_s}{4\pi} \times \mathrm{L}_1\left(\frac{u}{Q^2}\right) \frac{\langle 13\rangle}{\langle 12\rangle^2} \times \Delta_x s \frac{s(Q^2-u)+Q\Delta_z}{Q^3 u}$	$g_Z T^{a_2}_{\alpha_1\bar{\alpha}_3} T_F g_s \frac{\alpha_s}{4\pi} \times \mathrm{L}_1\left(\frac{u}{Q^2}\right) \frac{\langle 13\rangle}{\langle 12\rangle^2} \times \Delta_x s \frac{s(Q^2-u)-Q\Delta_z}{Q^3 u}$
$-(-,\pm)$	0	$-g_Z T^{a_2}_{\alpha_1\bar{\alpha}_3} T_F g_s \frac{\alpha_s}{4\pi} \times \mathrm{L}_1\left(\frac{u}{Q^2}\right) \frac{[13]}{[23]^2} \times \Delta_x t \frac{(Q^2-t)(Q^2-u)-Q\Delta_z}{Q^3 u}$	$-g_Z T^{a_2}_{\alpha_1\bar{\alpha}_3} T_F g_s \frac{\alpha_s}{4\pi} \times \mathrm{L}_1\left(\frac{u}{Q^2}\right) \frac{[13]}{[23]^2} \times \Delta_x t \frac{(Q^2-t)(Q^2-u)+Q\Delta_z}{Q^3 u}$
$-(+,\pm)$	$g_Z T^{a_2}_{\alpha_1\bar{\alpha}_3} T_F g_s \frac{\alpha_s}{2\sqrt{2}\pi} \times \mathrm{L}_1\left(\frac{u}{Q^2}\right) \frac{[13]}{[12]^2} \times \frac{s}{Q^2}\sqrt{\frac{s(Q^2-u)}{Q^2-t}}$	$-g_Z T^{a_2}_{\alpha_1\bar{\alpha}_3} T_F g_s \frac{\alpha_s}{4\pi} \times \mathrm{L}_1\left(\frac{u}{Q^2}\right) \frac{[13]}{[12]^2} \times \Delta_x s \frac{s(Q^2-u)-Q\Delta_z}{Q^3 u}$	$-g_Z T^{a_2}_{\alpha_1\bar{\alpha}_3} T_F g_s \frac{\alpha_s}{4\pi} \times \mathrm{L}_1\left(\frac{u}{Q^2}\right) \frac{[13]}{[12]^2} \times \Delta_x s \frac{s(Q^2-u)+Q\Delta_z}{Q^3 u}$

Table 4.3: NLO_1 top-loop $qg \to Zq$ Z-helicity amplitudes, $\Delta_z = \sqrt{s(Q^2-u)(Q^2-t)}$, $\Delta_x = \sqrt{1-\frac{Q^2 s}{(Q^2-u)(Q^2-t)}}$

top-loop diagram, the Z is emitted from a closed fermion loop and connects to the external quark line via an off-shell gluon. This setup imposes nontrivial angular momentum constraints, since any spin exchange between the parton system and the Z must be mediated by that internal gluon. To see why $\mathcal{A}_0 = 0$ for certain helicity configurations in $qg \to Vq$, consider an incoming quark in the state $\left|\frac{1}{2},\frac{1}{2}\right\rangle$, where the last component is projected along the CS axis, and an outgoing quark in either $\left|\frac{1}{2},\frac{1}{2}\right\rangle$ or $\left|\frac{1}{2},-\frac{1}{2}\right\rangle$. The intermediate gluon then carries spin $|1,1\rangle$ or $|1,0\rangle$. If the incoming gluon is also $|1,1\rangle$, combining these gives no overlap with a $|1,0\rangle$ final state - so the longitudinal Z component (i.e. $\mathcal{A}_0$) cannot be produced. On the other hand, if the incoming gluon and quark have opposite helicities, like $\left|\frac{1}{2},\frac{1}{2}\right\rangle$ and $|1,-1\rangle$, then forming a $|1,0\rangle$ state becomes possible, as the Clebsch-Gordan coefficient for this transition in non-zero, and $\mathcal{A}_0$ does not vanish. This is exactly what we find.

For the $\mathbf{LO}_2$ amplitudes, we found that using constraints involving the lepton spinor p_6, like $\langle 16\rangle = 0$, $\langle 26\rangle = 0$, or $\langle 36\rangle = 0$, gave consistent results and relatively manageable analytic expressions for extracting the $\mathcal{A}_\lambda$ amplitudes. These configurations are based on a (sub)set of momentum conservation and Schouten identities, similar to what we used for the LO_1 case.

We also tried other spinor constraints, for example, $\langle 35\rangle = 0$ *and* $\langle 46\rangle = 0$, that satisfy all the algebraic relations on paper, but turn out to *fall outside the physical region of phase space*. These kinds of configurations typically sit at the edge or just outside the physical, momentum-conserving, real-valued manifold of physical phase-space. Although some combinations of constrains do sometimes give amplitudes that seem stable or match expected values at isolated points, this agreement is likely accidental and doesn't hold more generally.

To check which constraints actually lie within the physical region, we implemented a numerical setup that randomly samples valid phase-space points and compares the extracted amplitudes to full numerical results. For constraints like $\langle 16\rangle = 0$, the comparison passed, as the analytic expressions agree with the numerics. However, even in these cases, the analytic forms are algebraically quite complicated and may have subtle issues we have not noticed yet. Although we do keep them for reference, we therefore rely primarily on the numerical results at LO_2. In the following section we explain how we achieve the numerical results.

$\mathbf{LO}_1$, $\mathbf{NLO}_1$, $\mathbf{LO}_2$, numerical extraction

To obtain numerical results, we must define the 4-momenta of all the particles. For quarks and gluons, we randomly sample momentum configurations, ensuring that, within the all-outgoing convention, the energies of physically incoming particles are negative and that momentum conservation holds by constructing the lepton momenta using Collins-Soper angles:

$$p^\mu_{1,2} = \frac{Q}{2}\left(t^\mu \pm x^\mu \sin\theta\cos\varphi \pm y^\mu \sin\theta \sin\varphi \pm z^\mu \cos\theta\right), \tag{4.28}$$

$\lambda_g(\lambda_q,\lambda_\ell)/\mathcal{A}_\lambda$	$\mathcal{A}_0$	$\mathcal{A}_+$	$\mathcal{A}_-$
$+(+,\pm)$	$g_Z T^{a_3}_{\alpha_1\bar{\alpha}_2} T_F g_s \frac{\alpha_s}{2\sqrt{2}\pi} \times \mathrm{L}_1\left(\frac{s}{Q^2}\right)\frac{\langle 12\rangle}{\langle 23\rangle^2} \times \frac{t^2}{Q^2}\sqrt{\frac{Q^2-t}{s(Q^2-u)}}$	$g_Z T^{a_3}_{\alpha_1\bar{\alpha}_2} T_F g_s \frac{\alpha_s}{4\pi} \times \mathrm{L}_1\left(\frac{s}{Q^2}\right)\frac{\langle 12\rangle}{\langle 23\rangle^2} \times \Delta_x t \frac{s(Q^2-t)+Q\Delta_z}{Q^3 s}$	$g_Z T^{a_3}_{\alpha_1\bar{\alpha}_2} T_F g_s \frac{\alpha_s}{4\pi} \times \mathrm{L}_1\left(\frac{s}{Q^2}\right)\frac{\langle 12\rangle}{\langle 23\rangle^2} \times \Delta_x t \frac{s(Q^2-t)-Q\Delta_z}{Q^3 s}$
$+(-,\pm)$	$g_Z T^{a_3}_{\alpha_1\bar{\alpha}_2} T_F g_s \frac{\alpha_s}{2\sqrt{2}\pi} \times \mathrm{L}_1\left(\frac{s}{Q^2}\right)\frac{\langle 12\rangle}{\langle 13\rangle^2} \times \frac{u^2}{Q^2}\sqrt{\frac{Q^2-u}{s(Q^2-t)}}$	$-g_Z T^{a_3}_{\alpha_1\bar{\alpha}_2} T_F g_s \frac{\alpha_s}{4\pi} \times \mathrm{L}_1\left(\frac{s}{Q^2}\right)\frac{\langle 12\rangle}{\langle 13\rangle^2} \times \Delta_x u \frac{s(Q^2-u)-Q\Delta_z}{Q^3 s}$	$-g_Z T^{a_3}_{\alpha_1\bar{\alpha}_2} T_F g_s \frac{\alpha_s}{4\pi} \times \mathrm{L}_1\left(\frac{s}{Q^2}\right)\frac{\langle 12\rangle}{\langle 13\rangle^2} \times \Delta_x u \frac{s(Q^2-u)+Q\Delta_z}{Q^3 s}$
$-(-,\pm)$	$-g_Z T^{a_3}_{\alpha_1\bar{\alpha}_2} T_F g_s \frac{\alpha_s}{2\sqrt{2}\pi} \times \mathrm{L}_1\left(\frac{s}{Q^2}\right)\frac{[12]}{[23]^2} \times \frac{t^2}{Q^2}\sqrt{\frac{Q^2-t}{s(Q^2-u)}}$	$-g_Z T^{a_3}_{\alpha_1\bar{\alpha}_2} T_F g_s \frac{\alpha_s}{4\pi} \times \mathrm{L}_1\left(\frac{s}{Q^2}\right)\frac{[12]}{[23]^2} \times \Delta_x t \frac{s(Q^2-t)-Q\Delta_z}{Q^3 s}$	$-g_Z T^{a_3}_{\alpha_1\bar{\alpha}_2} T_F g_s \frac{\alpha_s}{4\pi} \times \mathrm{L}_1\left(\frac{s}{Q^2}\right)\frac{[12]}{[23]^2} \times \Delta_x t \frac{s(Q^2-t)+Q\Delta_z}{Q^3 s}$
$-(+,\pm)$	$-g_Z T^{a_3}_{\alpha_1\bar{\alpha}_2} T_F g_s \frac{\alpha_s}{2\sqrt{2}\pi} \times \mathrm{L}_1\left(\frac{s}{Q^2}\right)\frac{[12]}{[13]^2} \times \frac{u^2}{Q^2}\sqrt{\frac{Q^2-u}{s(Q^2-t)}}$	$g_Z T^{a_3}_{\alpha_1\bar{\alpha}_2} T_F g_s \frac{\alpha_s}{4\pi} \times \mathrm{L}_1\left(\frac{s}{Q^2}\right)\frac{[12]}{[13]^2} \times \Delta_x u \frac{s(Q^2-u)+Q\Delta_z}{Q^3 s}$	$g_Z T^{a_3}_{\alpha_1\bar{\alpha}_2} T_F g_s \frac{\alpha_s}{4\pi} \times \mathrm{L}_1\left(\frac{s}{Q^2}\right)\frac{[12]}{[13]^2} \times \Delta_x u \frac{s(Q^2-u)-Q\Delta_z}{Q^3 s}$

Table 4.4: NLO$_1$ top-loop $q\bar{q} \to Zg$ Z-helicity amplitudes, $\Delta_z = \sqrt{s(Q^2-u)(Q^2-t)}$, $\Delta_x = \sqrt{1-\frac{Q^2 s}{(Q^2-u)(Q^2-t)}}$

where $\theta \equiv \theta_1$ and $\varphi \equiv \varphi_1$ are the spherical angles of the lepton p_1. Since, at leading order in QED, the vector boson decay is back-to-back in the rest frame, the angles for p_2 are given by $(\pi-\theta, \pi+\varphi)$. Finally, the vectors $t^\mu, x^\mu, y^\mu, z^\mu$ define the reference frame as discussed in Eq. (2.16a).
For certain applications, it is useful to describe the orientation of the incoming partons in terms of transverse momentum and rapidity. We already gave some basic definitions in the Section 2.6.1. In general, these variables are defined by the transformations:

$$\begin{cases} m^2 = E^2 - p_x^2 - p_y^2 - p_z^2, \\ y = \frac{1}{2}\log\left(\frac{E+p_z}{E-p_z}\right), \\ p_T = \sqrt{p_x^2+p_y^2}, \\ \phi = \arctan\left(\frac{p_y}{p_x}\right) \end{cases} \qquad \begin{cases} E = \sqrt{m^2+p_T^2}\cosh y, \\ p_x = p_T\cos\phi, \\ p_y = p_T\sin\phi, \\ p_z = \sqrt{m^2+p_T^2}\sinh y \end{cases} \tag{4.29}$$

Assuming all particles are massless, the momenta of the incoming partons are given by:

$$p_1^\mu = \xi_a E_a\,(-1,\ 0,\ 0,\ -1) = \frac{\sqrt{k_T^2}e^{y_k} + \sqrt{Q^2+q_T^2}e^{y_Z}}{2}\,(-1,\ 0,\ 0,\ -1)\,, \tag{4.30}$$

$$p_2^\mu = \xi_b E_b\,(-1,\ 0,\ 0,\ 1) = \frac{\sqrt{k_T^2}e^{-y_k} + \sqrt{Q^2+q_T^2}e^{-y_Z}}{2}\,(-1,\ 0,\ 0,\ 1)\,, \tag{4.31}$$

The replacement of ξ_a and ξ_b will be discussed in the following Section 4.5 in the context of integration over the phase space.
The total final-state transverse momentum k_T and rapidity y_k used in the expression for the initial-state partons in Eq.(4.30) are determined from the final-state momenta:

$$p_4^\mu = \left(\sqrt{k_{2T}^2}\cosh y_{k_2},\ \sqrt{k_{2T}^2}\cos\phi_{k_2},\ \sqrt{k_{2T}^2}\sin\phi_{k_2},\ \sqrt{k_{2T}^2}\sinh y_{k_2}\right), \tag{4.32}$$

$$p_3^\mu = \left(\sqrt{k_{1T}^2}\cosh y_{k_1},\ \sqrt{k_{1T}^2}\cos\phi_{k_1},\ \sqrt{k_{1T}^2}\sin\phi_{k_1},\ \sqrt{k_{1T}^2}\sinh y_{k_1}\right), \tag{4.33}$$

$$k_T = k_{1T} + k_{2T}, \qquad y_k = \frac{1}{2}\log\left(\frac{\sqrt{k_{1T}^2}e^{y_{k_1}} + \sqrt{k_{2T}^2}e^{y_{k_2}}}{\sqrt{k_{1T}^2}e^{-y_{k_1}} + \sqrt{k_{2T}^2}e^{-y_{k_2}}}\right), \tag{4.34}$$

For the leading-order configuration LO$_1$, the input variables are the invariant mass Q, the transverse momentum q_T of the lepton pair, and the rapidity y_k and azimuthal angle ϕ_k of the hadronic radiation

system k. These describe the scale, recoil, and orientation of the event. As both quickly mentined in the Section 2.6.1 and in full discussed in the integration Section 4.5, momentum conservation implies $k_T = -q_T$, since we only have one object (i.e. hadronic radiation) recoiling against the leptonic system. For LO_2, the input variables are Q, q_T, the rapidities y_{k_1}, y_{k_2}, the transverse momentum k_{1T} of one parton, and the azimuthal angles ϕ_{k_1}, ϕ_{k_2} of both.

Since at this level we have full control of the kinematics of the process, we are not bound by the Schouten and other spinor identities to get various lepton configurations – we can set θ and ϕ to randomly sampled three directions in the space and solve a similar system to Eq.(4.27), where the $\langle 14\rangle = 0, \dots$ is replaced by numerical values of the spinor products for our chosen configuration of leptons.

On the other hand, since we have *full* control over the kinematics, we are free to *choose* specific configurations for the final-state leptons. Because the polarization of the vector boson is directly linked to the lepton directions, it's possible to select configurations where one or more terms in Eq. (4.27) vanish. This allows us to further simplify – or even partially diagonalize – the system.
We observe that for an orientation of the lepton ℓ, n_ℓ, we have

$$\mathcal{A}_{\text{full}}(\lambda_\ell = +,\, n_\ell = z) = \mathcal{A}_+ c_+, \tag{4.35a}$$
$$\mathcal{A}_{\text{full}}(\lambda_\ell = -,\, n_\ell = z) = \mathcal{A}_- c_-, \tag{4.35b}$$
$$\mathcal{A}_{\text{full}}(\lambda_\ell = +,\, n_\ell = -z) = \mathcal{A}_- c'_-, \tag{4.35c}$$
$$\mathcal{A}_{\text{full}}(\lambda_\ell = -,\, n_\ell = -z) = \mathcal{A}_+ c'_+, \tag{4.35d}$$

where z is the axis in the CS frame. This leads to a more general result for Z-helicity $\lambda = \pm$:

$$\epsilon^\mu_\lambda L_{\lambda_\ell,\mu}(n_\ell = z) = c_\lambda \delta_{\lambda,\lambda_\ell}. \tag{4.36}$$

As for the $\lambda = 0$, our goal now is to find such combinations of lepton orientation n_ℓ and lepton helicities λ_ℓ that we can

$$\epsilon^\mu_\lambda \sum_{\text{configs}} (\text{some coeffs}) L_{\lambda_\ell,\mu}(n_\ell) = c_0 \delta_{\lambda 0}. \tag{4.37}$$

We use orthogonality of ε^r_λ to conclude from Eq.(4.36) that $L_{\pm\mu}(n_\ell = z) = c_+ \varepsilon^*_{\pm\mu} = c_+ \frac{1}{\sqrt{2}}(x_\mu \mp i y_\mu)$ Then, using the covariance of the result we get:

$$L_{\pm\mu}(n_\ell = x) = c_\pm \varepsilon^*_{\pm\mu}(x; y, z) = \frac{c_\pm}{\sqrt{2}}(y_\mu \mp i z_\mu),$$

where we made explicit that $\varepsilon_{\lambda\mu} = \varepsilon_{\lambda\mu}(z; x, y)$. Finally, combining the expression for the positive and negative lepton helicities we achieve

$$\frac{1}{c_+} L_{+\mu}(n_\ell = x) - \frac{1}{c_-} L_{-\mu}(n_\ell = x) = -i\sqrt{2} z_\mu = -i\sqrt{2}\varepsilon^*_{0\mu}(z)$$
$$\Rightarrow \quad -\varepsilon^*_\lambda(z)\left[\frac{1}{c_+} L_{+\mu}(n_\ell = x) - \frac{1}{c_-} L_{-\mu}(n_\ell = x)\right] = +i\sqrt{2}\varepsilon^*_\lambda(z) z_\mu = +i\sqrt{2}\delta_{\lambda 0}$$

which is the desired result.
Putting everything together, we arrive at a set of rules for extracting the Z-helicity amplitudes directly, without needing to solve the full system:

$$\mathcal{A}_\pm = \frac{1}{c_\pm}\mathcal{A}_{\text{full}}(\lambda_\ell = \pm,\, n_\ell = z), \quad c_\pm = -i\frac{g_z}{2}\epsilon^\mu_\pm L_{\lambda_\ell=\pm,\mu}(n_\ell = z) \tag{4.38}$$
$$\mathcal{A}_0 = -\frac{i}{\sqrt{2}}\left[\frac{1}{c'_+}\mathcal{A}_{\text{full}}(\lambda_\ell = +,\, n_\ell = x) - \frac{1}{c'_-}\mathcal{A}_{\text{full}}(\lambda_\ell = -,\, n_\ell = x)\right], \tag{4.39}$$
$$c'_\pm = -i\frac{g_z}{2}\frac{1}{\sqrt{2}}(y^\mu \pm i z^\mu) L_{\lambda_\ell=\pm,\mu}(n_\ell = x).$$

These configurations were used to derive the (numerical – per value of Q, q_T, y_k etc.) Z-helicity amplitudes for the LO_2 process.

4.2 Power Scaling of Helicity Amplitudes

The Z-helicity amplitudes are useful in several ways. One important application is studying how they scale in different kinematic limits. In effective field theories, like SCET, this kind of scaling analysis helps identify which momentum modes are relevant and how to organize power expansions. It can also guide the structure of factorization theorems by showing how the amplitude breaks into simpler pieces for different physical regions.

In this chapter, we analyze the leading-power behavior of LO_1 and NLO_1 helicity amplitudes in the soft limit. These limit corresponds to configurations where the transverse momentum of the final-state partons $k_T = q_T \ll Q$ becomes small, and the expansion parameter $\lambda \sim q_T/Q$ can be used to organize the amplitude in powers of λ. The soft limit corresponds to $k_T \to 0$, with the rapidity y_k staying finite, while the collinear (to the beam axis) limit, which is also present at $q_T \ll Q$, is $k_T \to 0$ with diverging rapidity. For an example of the scaling behavior of the transverse momentum for different limits see Figure. 4.1.

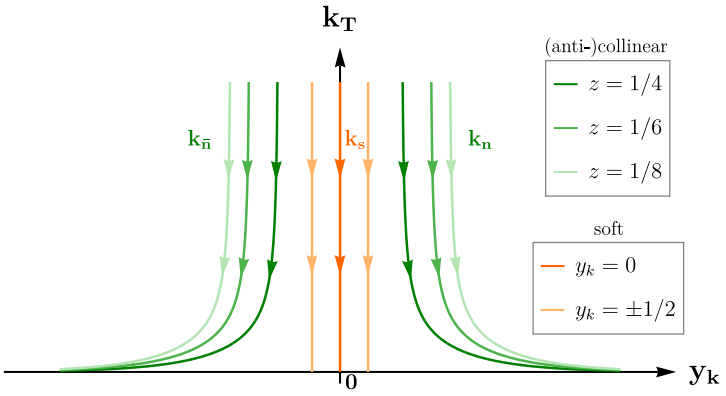


Figure 4.1: Soft and (anti-)collinear behavior of the transverse momentum of the final hadronic state k_T as a function of rapidity y_k. For soft limit the constant variable was chosen the rapidity itself, as in this limit it is finite, while for the collinear limit we have the rapidity diverging to infinity, therefore now the constant variable is the momentum fractions $z = q^-/p_a^-$ for collinear ($y_k > 0$) and $z = q^+/p_b^+$ for anticollinear ($y_k < 0$)

Our main goal in this section is to determine how individual helicity configurations scale with λ and which ones contribute at leading power in the soft limit. In our discussion we follow the treatment in ref. [61] for the structure of soft emission and use the spinor-helicity expressions presented in ref. [62].

4.2.1 Soft Scaling of Z-helicity Amplitudes in the $q_T/Q \to 0$ Limit

In the soft limit, one of the final-state partons becomes soft, with its momentum scaling as $k \to k_s \sim Q(\lambda, \lambda, \lambda)$. This regime is relevant when the vector boson recoils against low-energy radiation, such that the transverse momentum q_T of the boson is small.

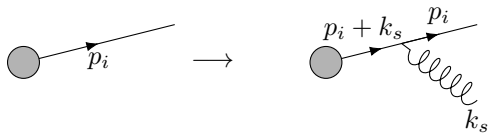
Eikonal Formula

To understand the structure of soft gluon emission from an external quark leg, consider the matrix element

$$\mathcal{M} = \bar{u}_i(p)\, \widetilde{\mathcal{M}}_i,$$

where i denotes the color index of the quark and momentum labels are left implicit. In the limit where a gluon with momentum k^μ and polarization ϵ becomes soft ($k^\mu \to 0$), the emission factorizes universally from the hard process. The soft gluon interacts eikonally with the external partons, leading to a modified amplitude of the form:

$$\underbrace{\bar{u}_i(p)\, \widetilde{\mathcal{M}}_i}_{} \quad \longrightarrow \quad \underbrace{-g_s\, \bar{u}_i(p)\, T^a_{ij} \frac{p \cdot \epsilon}{p \cdot k_s}\, \widetilde{\mathcal{M}}_j(p)}_{} \tag{4.40}$$



This is known as the **eikonal approximation**, and it captures the leading singular behavior of the amplitude in the soft limit. Importantly, the factor $\frac{p\cdot\epsilon}{p\cdot k_s}$ is independent of the spin of the emitting particle: it reflects the fact that the long-wavelength gluon cannot resolve the spin structure of the hard interaction. The eikonal factor is invariant under boosts along the emitter's direction, making it insensitive to the rapidity of the emitted gluon in the strict soft limit (i.e. at leading order only). Our already familiar color factor T^a_{ij} encodes the gluon emission in the fundamental representation of $SU(3)$, and similar expressions hold for antiquarks and gluon emitters (with appropriate group theory factors). In general, this form of the eikonal factor reflects the Feynman rules of SCET soft Wilson lines for single-gluon emission.

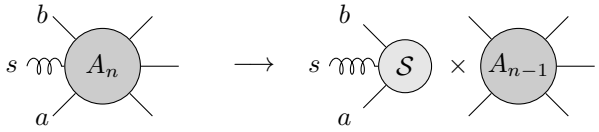
When a single soft gluon is emitted from multiple external parton legs, such that the full amplitude receives contributions from diagrams where the gluon attaches to different hard emitters, the amplitude factorizes into a sum of eikonal terms, one for each emitter, each carrying its own color generator and kinematic eikonal factor:

$$\mathcal{M}^a_{n+1}(k) = g_s \sum_{i=1}^{n} T^a_i \frac{p_i \cdot \epsilon}{p_i \cdot k_s} \mathcal{M}_n, \tag{4.41}$$

where T^a_i is the color generator for parton i, p_i is the momentum of emitter i, $\mathcal{M}_n$ is the original amplitude without the soft gluon.

Additionally, it is possible to write the soft gluon limit in terms of the spinor-helicity amplitudes. In the soft limit, where the gluon momentum $k_s \to 0$, any tree-level QCD amplitude universally factorizes into a product of a soft (eikonal) factor and a lower-point amplitude. That is,

$$A^{\text{tree}}_n(\ldots, a, s^\pm, b, \ldots) \xrightarrow{k_s \to 0} \mathcal{S}(a, s^\pm, b) \times A^{\text{tree}}_{n-1}(\ldots, a, b, \ldots), \tag{4.42}$$



where s labels the soft gluon and a, b are the two hard color-adjacent partons. The $(n-1)$-point tree-level amplitude $A^{\text{tree}}_{n-1}(\ldots, a, b, \ldots)$ is obtained by removing the soft gluon from the original n-point amplitude, leaving adjacent hard legs a and b in the color ordering. The soft factor $\mathcal{S}(a, s^\pm, b)$ captures the leading divergence and is given by: [62]

$$\mathcal{S}(a, s^+, b) = \frac{\langle a\, b\rangle}{\langle a\, s\rangle\langle s\, b\rangle}, \tag{4.43}$$

$$\mathcal{S}(a, s^-, b) = -\frac{[a\, b]}{[a\, s][s\, b]}. \tag{4.44}$$

This soft factor is universal, as it neither depends on whether a and b are quarks or gluons, nor on their helicities or the magnitude of their momenta, similar to how the eikonal factor from Eq.(4.40) does not depend on the spin structure of the interaction.
As an example consider the five-point amplitude

$$A_5(1^+_{\bar{e}}, 2^-_e, 3^+_q, 4^+_g, 5^-_{\bar{q}}) = i\, \frac{\langle 2\, 5\rangle^2}{\langle 1\, 2\rangle\langle 3\, 4\rangle\langle 4\, 5\rangle}, \tag{4.45}$$

which, in the limit $k_4 \to 0$, factorizes as

$$A_5 \xrightarrow{k_4 \to 0} \mathcal{S}(3, 4^+, 5) \times A_4(1^+, 2^-, 3^+, 5^-) = \frac{\langle 3\, 5\rangle}{\langle 3\, 4\rangle\langle 4\, 5\rangle} \times i\, \frac{\langle 2\, 5\rangle^2}{\langle 1\, 2\rangle\langle 3\, 5\rangle}. \tag{4.46}$$

Using these eikonal formulas we are able to predict how the Z-helicity amplitudes scale in leading order in $\lambda = q_T/Q$ in the soft limit.

Soft Scaling of Z-helicity amplitudes

In analyzing the helicity structure of the process in the soft limit, it is important to determine which helicity configurations contribute at leading power in the small expansion parameter λ. A necessary and

sufficient condition is that the given configuration must have a corresponding Born-level process upon removing the soft emission. Checking this ensures that the soft limit is consistent with the universal factorization properties of QCD amplitudes.

In the process $qg \to qZ$ there is no underlying Born-level configuration in the limit where the final state quark becomes soft. Since quarks carry spin and flavor charge, they cannot be removed in a gauge-invariant way. As a result, there exists no eikonal formula for soft quark emission, and amplitudes in this limit are necessarily power-suppressed. That is, such configurations enter at subleading order in λ. In contrast, the process $q\bar{q} \to Zg$ does have a Born-level counterpart, namely $q\bar{q} \to Z$. Therefore, soft gluon emission from this amplitude can contribute at leading power. However, to determine which specific helicity configurations survive in the $\lambda \to 0$ limit, one must further impose angular momentum conservation. For instance, the configurations

$$(\lambda_Z, \lambda_q, \lambda_g) = (+1, +1/2, \pm 1), (-1, -1/2, \pm 1),$$

where λ_Z, λ_q and λ_g are the helicities of the vector boson, quark and gluon in all-outgoing convention, satisfy all such constraints: they match onto the Born-level process $q\bar{q} \to Z$ and conserve spin along the beam axis. This is because for this configuration of *all-outgoing* helicities

$$0 \to g^{\pm}(p_1) q^{+}(p_2) \bar{q}^{-}(p_3) Z^{+},$$

the *crossed physical* configuration

$$\bar{q}^{-}(-p_2) q^{+}(-p_3) \to g^{\pm}(p_1) Z^{+},$$

leads to the spin states with the expectation number projected along the CS axis: $\left|\frac{1}{2}, \lambda_q\right\rangle = \left|\frac{1}{2}, \frac{1}{2}\right\rangle$ for the incoming quark $q^{+}(-p_3)$, $\left|\frac{1}{2}, \frac{1}{2}\right\rangle$ for incoming antiquark $\bar{q}^{-}(-p_2)$, which nicely combine into the $|1, 1\rangle$ state for the Z boson, which does indeed conserve the angular momentum in the system. Therefore, these helicity configurations should contribute at leading power and show the expected λ^{-1} scaling in the collinear limit, consistent with the eikonal formula (4.40), where the denominator scales as $p \cdot k_s \sim \lambda$ for a soft momentum $k_s \sim Q(\lambda, \lambda, \lambda)$.

On the other hand, configurations with $\lambda_q = -\lambda_Z$ are expected to be suppressed in the soft limit. This is because the eikonal emission from the soft gluon cannot induce a helicity flip on the quark leg and therefore cannot supply the angular momentum needed to produce such final states (e.g. $\left|\frac{1}{2}, \frac{1}{2}\right\rangle$ combined with another $\left|\frac{1}{2}, \frac{1}{2}\right\rangle$ cannot produce $|1, -1\rangle$ without insertion external angular momenta). All other helicity configurations either violate angular momentum conservation or do not have corresponding a physical Born-level diagram. They contribute only at subleading power in λ, typically starting at λ^0 or $\lambda^{1/2}$.

It is also worth noting that the leading-power scaling of the amplitude does not distinguish between helicity configurations that are related by a flip of the gluon helicity. This is the consequence of the eikonal formula.

The Tables 4.5 and 4.6 summarize the power counting behavior of different LO_1 helicity amplitudes in the soft limit ($q_T \to 0$) that we observe. Additionally, Figure 4.3 shows the magnitudes of the Z-amplitudes as functions of q_T and highlights how the function approaches its soft scaling limit as $q_T \to 0$. Finally, in Figure 4.2 we show the amplitude magnitude ratio between $|\mathcal{A}^{\mathrm{LO}_1}_{0,qg\to Zq}(\lambda_q > 0)|$ and $|\mathcal{A}^{\mathrm{LO}_1}_{+,q\bar{q}\to Zg}(\lambda_q > 0)|$, where the latter is expected to have the leading power scaling $1/\lambda$, therefore their ratio is expected to scale as $\lambda^n, n > 0$. From the Table 4.5 we can read that this scaling in the soft limit would be $\lambda^{3/2}$, which is exactly what we observe in the plot.

Soft scaling of the NLO_1 follows similar behavior as the one in LO_1, but with an addition of the $\ln\left(\frac{q_T}{Q}\right)$ terms. For example, the $|\mathcal{A}^{\mathrm{NLO}_1}_{0,qg\to Zq}(\lambda_q > 0)|$ scales as

$$\left| \frac{1}{144\sqrt{2}\pi} \sqrt{e^{y_Z - y_k}} \left(-12\left(-2y_k\left(5y_Z + 1\right) + 5y_k^2 + y_Z\left(5y_Z + 2\right) + 19\right) - 168i\pi + 61\pi^2\right) \sqrt{\frac{q_T}{Q}} \right.$$
$$\left. + \frac{1}{6\sqrt{2}\pi} \sqrt{e^{y_Z - y_k}} \left(-5y_k + 5y_Z - 1 + i\pi\right) \sqrt{\frac{q_T}{Q}} \ln\left(\frac{q_T}{Q}\right) - \frac{1}{4\sqrt{2}\pi} \sqrt{e^{y_Z - y_k}} \sqrt{\frac{q_T}{Q}} \ln\left(\frac{q_T}{Q}\right)^2 \right|,$$

where the $\lambda^{1/2}$ scaling of the LO_1 multiplies the general function

$$A(y_k, y_Z) + B(y_k, y_Z) \ln\left(\frac{q_T}{Q}\right) + C(y_k, y_Z) \ln\left(\frac{q_T}{Q}\right)^2.$$

$\lambda_g, \lambda_q, \lambda_\ell / \mathcal{A}_\lambda$	$\lvert\mathcal{A}_0\rvert$	$\lvert\mathcal{A}_+\rvert$	$\lvert\mathcal{A}_-\rvert$
LO_1 $qg \to Zq$			
$+;+,\pm$	$\mathcal{O}\left(\lambda^{1/2}\right)$	$\mathcal{O}\left(\lambda^{-1/2}\right)$	$\mathcal{O}\left(\lambda^{3/2}\right)$
$+;-,\pm$	$\mathcal{O}\left(\lambda^{1/2}\right)$	$\mathcal{O}\left(\lambda^{1/2}\right)$	$\mathcal{O}\left(\lambda^{1/2}\right)$
$-;+,\pm$	$\mathcal{O}\left(\lambda^{1/2}\right)$	$\mathcal{O}\left(\lambda^{1/2}\right)$	$\mathcal{O}\left(\lambda^{1/2}\right)$
$-;-,\pm$	$\mathcal{O}\left(\lambda^{1/2}\right)$	$\mathcal{O}\left(\lambda^{3/2}\right)$	$\mathcal{O}\left(\lambda^{-1/2}\right)$
LO_1 $q\bar{q} \to Zg$			
$+;+,\pm$	$\mathcal{O}\left(\lambda^{0}\right)$	$\mathcal{O}\left(\lambda^{-1}\right)$	$\mathcal{O}\left(\lambda\right)$
$+;-,\pm$	$\mathcal{O}\left(\lambda^{0}\right)$	$\mathcal{O}\left(\lambda\right)$	$\mathcal{O}\left(\lambda^{-1}\right)$
$-;+,\pm$	$\mathcal{O}\left(\lambda^{0}\right)$	$\mathcal{O}\left(\lambda^{-1}\right)$	$\mathcal{O}\left(\lambda\right)$
$-;-,\pm$	$\mathcal{O}\left(\lambda^{0}\right)$	$\mathcal{O}\left(\lambda\right)$	$\mathcal{O}\left(\lambda^{-1}\right)$

Table 4.5: Observed Z-helicity amplitude magnitudes scaling at soft limit. Here the scaling factor is $\lambda = q_T/Q$.

$\lambda_g, \lambda_q, \lambda_\ell / \mathcal{A}_\lambda$	$\lvert\mathcal{A}_0\rvert$	$\lvert\mathcal{A}_+\rvert$	$\lvert\mathcal{A}_-\rvert$
LO_1 $qg \to Zq$			
$+;+,\pm$	$\frac{1}{\sqrt{2}}\sqrt{\frac{q_T}{Q}}e^{(y_k-y_Z)/2}$	$\sqrt{\frac{Q}{q_T}}e^{(y_k-y_Z)/2}$	$\frac{1}{4}\sqrt{\frac{q_T^3}{Q^3}}e^{(y_k-y_Z)/2}$
$+;-,\pm$	$\sqrt{2}\sqrt{\frac{q_T}{Q}}e^{(y_k-y_Z)/2}$	$\sqrt{\frac{q_T}{Q}}e^{-(y_k-y_Z)/2}$	$\sqrt{\frac{q_T}{Q}}e^{3(y_k-y_Z)/2}$
LO_1 $q\bar{q} \to Zg$			
$+;+,\pm$	$\frac{1}{\sqrt{2}}$	$\frac{Q}{q_T}$	$\frac{1}{4}\frac{q_T}{Q}$
$+;-,\pm$	$\frac{1}{\sqrt{2}}$	$\frac{1}{4}\frac{q_T}{Q}$	$\frac{Q}{q_T}$

Table 4.6: Observed leading-order soft limit $\lambda = q_T/Q$ terms in Z-helicity amplitude magnitudes. All of these functions are given without the general prefactor $g_s^2 g_Z^2 (a_f \pm v_f)^2 C_A C_F$, with '+' for the $\lambda_q < 0$ and '−' for $\lambda_q > 0$. As expected from the eikonal formula, the leading power $q\bar{q} \to Zg$ terms do not have a y_k dependence.

Plots of the NLO_1 Z-helicity amplitude magnitudes and their leading power terms are shown in Figure 4.4.

Here we also want to comment of the choice of the polarization vectors done in Eq.(2.18). The definition of the $\epsilon_\pm^\mu$ initially used in the [13] lead to the inverted soft scaling behavior in the LO_1 Z-helicity amplitudes, which would violate the angular momentum conservation along the z axis in the corresponding Born LO_0 amplitudes. We therefore follow the convention used in [15], where the polarization vectors are defined in a frame where the incoming electrons move along the z-axis and the outgoing muons are emitted at an angle, which is exactly the setup that corresponds to the Collins-Soper frame in the Born limit. In that frame, the polarization vectors are defined as $\epsilon_\pm^\mu = \frac{1}{\sqrt{2}}(x^\mu \pm iy^\mu)$, and it is explicitly shown that this choice ensures conservation of angular momentum.

4.3 Treatment of γ_5

Defining γ^5 in D dimensions is a well-known problem in particle physics, because its usual definition only makes sense in exactly four dimensions [66, 67]. Over the years, several different schemes have been developed to deal with this issue, each suited to certain types of calculations. However, there is no single scheme that works well in all situations, so the choice often depends on the specific process being studied.

In this section we comment on the treatment of γ_5 for the virtual terms.
In our calculation of the real-virtual contributions, we work directly with the renormalized Wilson coefficients (i.e., the infrared-subtracted hard amplitudes) which are finite in $D = 4$. This setup ensures that all external partons have well-defined helicities, and in particular, for the valence[1] contributions at

[1]The valence channel refers here to the case where the flavor of the quark and antiquark matches that of the current, such as $u\bar{u} \to Vg$, where the EW current couples directly to external fermions. In contrast, the singlet contribution involves a flavor mismatch between the current and the external states (e.g., $d\bar{d} \to Vg$ via a u-loop) and arises at one loop through closed fermion-loop diagrams.

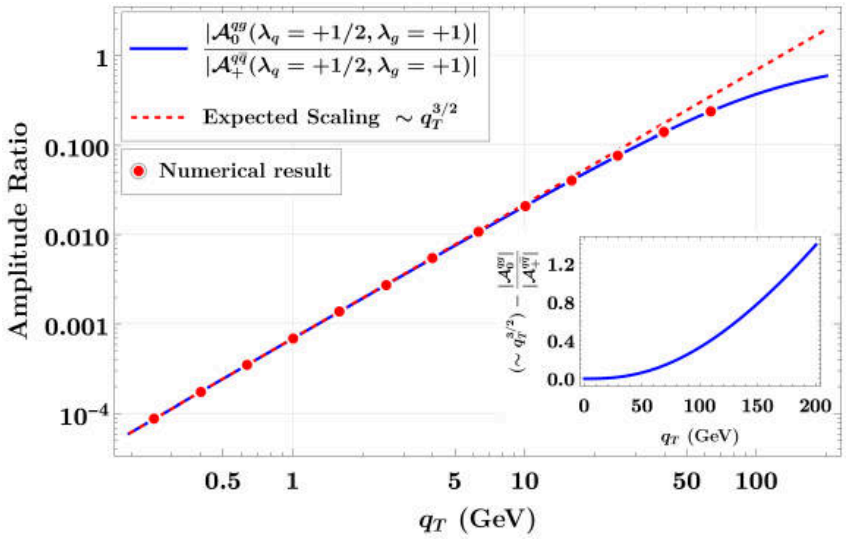


Figure 4.2: Ratio of Z-helicity amplitude magnitudes between $|\mathcal{A}^{\mathrm{LO}_1}_{0,qg\to Zq}(\lambda_q{>}0)|$ and $|\mathcal{A}^{\mathrm{NLO}_1}_{+,q\bar{q}\to Zg}(\lambda_q{>}0)|$ as a function of q_T. The blue curve represents the exact analytic expression, while the orange dashed line indicates the leading-power scaling behavior $\sim q_T^{3/2}$. Red dots denote the numerical results obtained using the prescription described in Section 4.1.4. The inset shows the deviation from the leading-power approximation, showing that the amplitude ratio asymptotically approaches the leading behavior in the small-q_T limit. Plots done for $Q = 100$ GeV, $y_Z = y_k = 0$.

NLO_1, the helicity of the external quarks uniquely fixes the relative weight of vector and axial terms at amplitude level, as seen in the e.g. $(v \pm a)$ coupling structure in Eq.(4.11). This follows from the fact that massless QCD preserves chirality, so the axial contribution does not receive any additional finite renormalization beyond tree level. The total singlet amplitude is also finite in four dimensions at NLO_1, and the way γ_5 is handled in intermediate steps does not affect the renormalized result.

More broadly, any scheme dependence associated with γ_5 is irrelevant for the hard function extracted from the SCET matching. This is because the QCD dynamics below the hard scale (as encoded in the SCET Lagrangian Eq.(2.59)) involve only the quark vector current. As a result, both the low-energy matrix elements and the renormalization of the Wilson coefficient must be independent of how γ_5 is treated in dimensional regularization. This means that the finite real-virtual contributions that enter the $\overline{\mathrm{MS}}$-renormalized hard function in $D = 4$ are *on their own* insensitive to the details of the γ_5. Therefore, we are free to adopt any (other) consistent scheme for γ_5 when computing the remaining $k^2 > 0$ contributions to the partonic cross section – in particular, for the double-real phase-space integrals and PDF counterterms discussed in Section 5.4.

4.4 Final results for LO_1 and NLO_1

Using the above mentioned spinor-helicity technique we are able to first calculate the Z-helicity amplitudes and then combine them into the components of the helicity density matrix:

$$W_{\lambda\lambda'} \sim \sum_{\text{helicities in the system}} \mathcal{A}^*_{\lambda'}\mathcal{A}_{\lambda}. \tag{4.47}$$

As an example, for LO_1 this sum would have the form:

$$\begin{aligned} W^{(1),\mathrm{R}}_{\lambda\lambda'} = \sum_X \langle |\mathcal{M}^{(1),\mathrm{R}}_{p_a p_b\to qk}|^2_{\lambda\lambda'}\rangle, \quad |\mathcal{M}^{(1),\mathrm{R}}_{p_a p_b\to qk}|^2_{\lambda\lambda'} =& \big(\mathcal{A}^{\mathrm{LO}_1}_{\lambda'}\big)^*(1^+;2^+_q,3^-_{\bar{q}})\mathcal{A}^{\mathrm{LO}_1}_{\lambda}(1^+;2^+_q,3^-_{\bar{q}}) \\ &+\big(\mathcal{A}^{\mathrm{LO}_1}_{\lambda'}\big)^*(1^+;2^-_q,3^+_{\bar{q}})\mathcal{A}^{\mathrm{LO}_1}_{\lambda}(1^+;2^-_q,3^+) \\ &+\big(\mathcal{A}^{\mathrm{LO}_1}_{\lambda'}\big)^*(1^-;2^+_q,3^-_{\bar{q}})\mathcal{A}^{\mathrm{LO}_1}_{\lambda}(1^-;2^+_q,3^-_{\bar{q}}) \\ &+\big(\mathcal{A}^{\mathrm{LO}_1}_{\lambda'}\big)^*(1^-;2^-_q,3^+_{\bar{q}})\mathcal{A}^{\mathrm{LO}_1}_{\lambda}(1^-;2^-_q,3^+_{\bar{q}}), \end{aligned} \tag{4.48}$$

where $\mathcal{A}^{\mathrm{LO}_1}_{\lambda}$ are the LO_1 Z-helicity amplitudes, derived as the solutions to Eq.(4.27) with $\mathcal{A}_{\mathrm{full}}$ from Eq.(4.14). $\langle|\mathcal{M}_{p_a p_b\to qk}|^2_{\lambda\lambda'}\rangle$ is the spin and color averaged matrix elements squared for the process

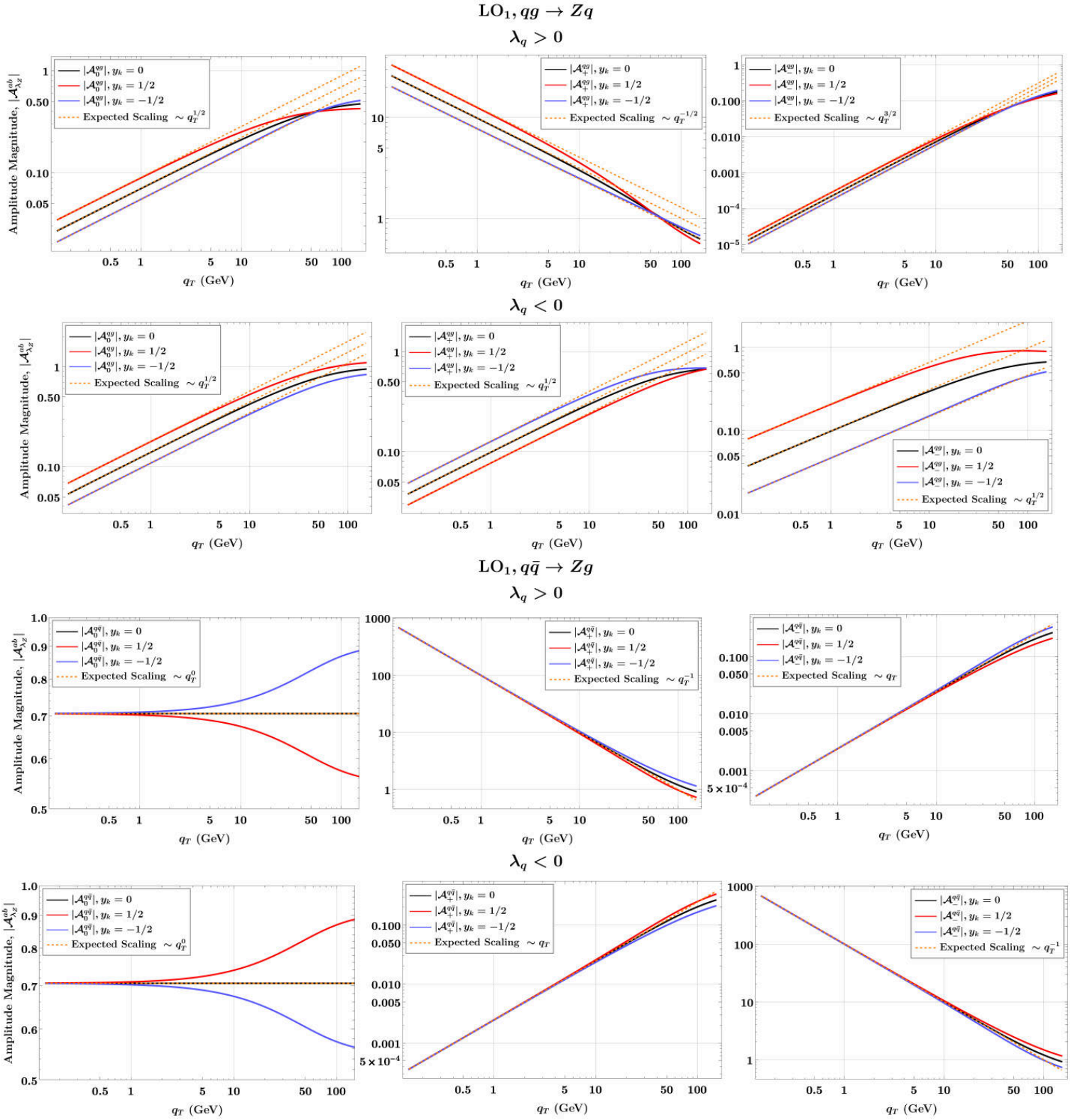


Figure 4.3: Z-helicity amplitude magnitudes at leading order (LO_1), shown as functions of the transverse momentum q_T. The structure of the figure copies the one of the Table 4.5. The top two rows correspond to the process $qg \to Zq$, and the bottom two rows to $q\bar{q} \to Zg$. Each block is split by the helicity of the quark: $\lambda_q > 0$ (top row) and $\lambda_q < 0$ (bottom row). Within each panel, amplitudes for different Z boson helicities $\lambda_Z = 0, \pm 1$ are shown. The colored curves denote the exact amplitude magnitudes for three different values of k-rapidity, $y_k = 0, \pm 1/2$, while the orange dashed lines indicate the leading small-q_T scaling behavior. Plots are stripped of all EW and color coupling and are done for $Q = 100$ GeV, $y_Z = 0$.

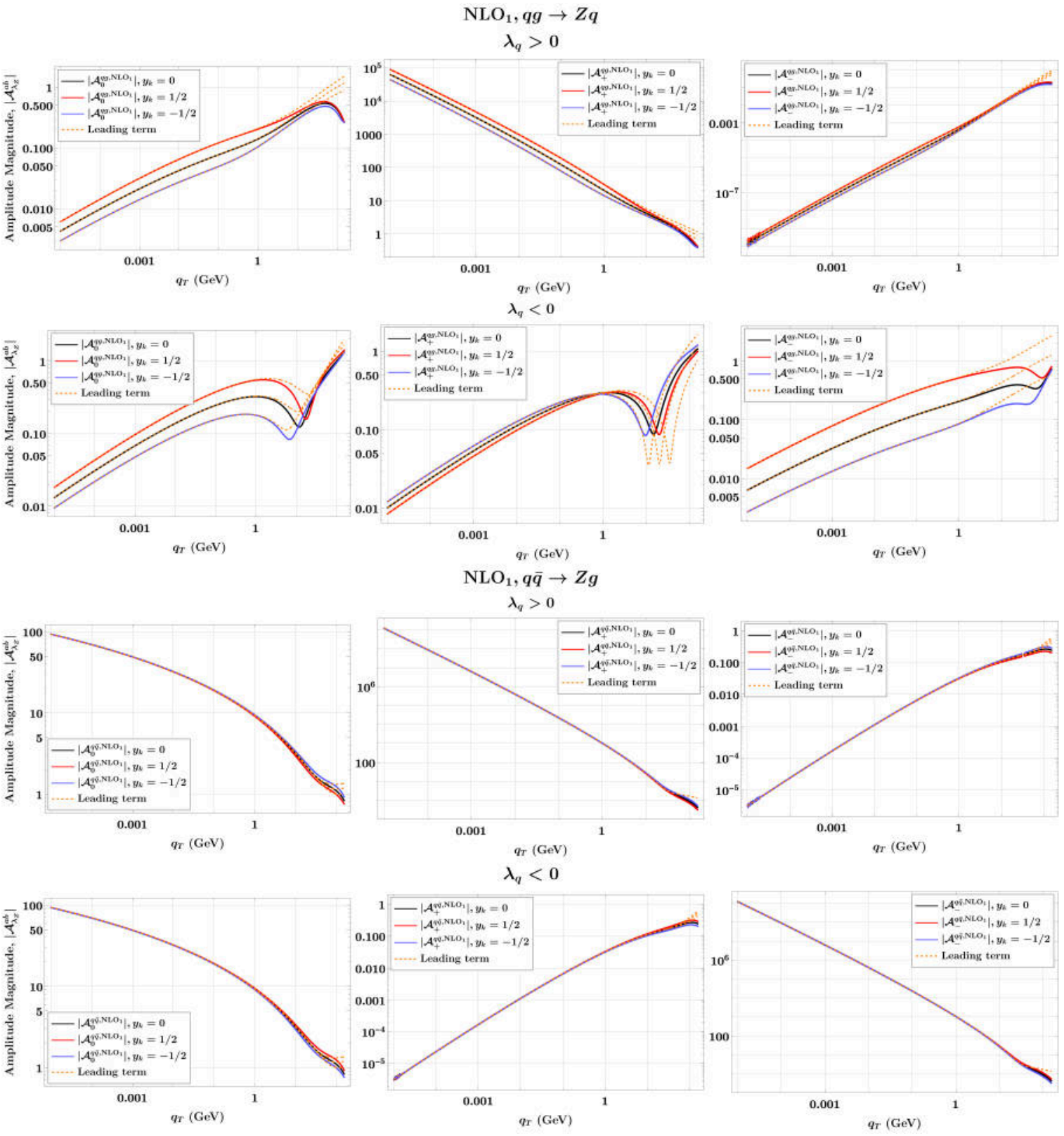


Figure 4.4: NLO_1 Z-helicity amplitude magnitudes, shown as functions of the transverse momentum q_T. The top two rows correspond to the process $qg \to Zq$, and the bottom two rows to $q\bar{q} \to Zg$. Each block is split by the helicity of the quark: $\lambda_q > 0$ (top row) and $\lambda_q < 0$ (bottom row). Within each panel, amplitudes for different Z boson helicities $\lambda_Z = 0, \pm 1$ are shown. The colored curves denote the exact amplitude magnitudes for three different values of k-rapidity, $y_k = 0, \pm 1/2$, while the orange dashed lines indicate the leading small-q_T scaling behavior. Plots are stripped of all EW and color coupling and are done for $\mu = Q = 100$ GeV, $y_Z = 0$.

$p_a p_b \to qk$, projected onto the helicity component $\lambda\lambda'$. The sup-indexes $(1), \mathrm{R}$ refer to the order of the strong coupling at which the term arises and our shorthand name (single-real, R) for these contributions. We have also omitted the sum and integral over hadronic radiation in the expression for the $W_{\lambda\lambda'}$. The integration is discussed in Section 4.5.
The components of the helicity matrix are later combined into the structure functions as defined in Eq.(2.20).

In this chapter, we present a few example matrix elements squared computed using the spinor-helicity method. We begin by reproducing the LO_1 helicity cross sections and then show some representative results for more non-trivial contributions, including the absorptive terms $W^{(2)}_{5,6,7}$, as well as the singlet contributions from fermion-loop diagrams (shown in Figures 2.3 and 2.4).

Firstly, in order to parametrize the results we use Mandelstam variables:

$$s \equiv (p_a + p_b)^2 = 2p_a \cdot p_b, \tag{4.49}$$
$$t \equiv (p_a - q)^2 = (p_b - k)^2, \tag{4.50}$$
$$u \equiv (p_b - q)^2 = (p_a - k)^2, \tag{4.51}$$
$$s_2 \equiv k^2 = s + t + u - Q^2, \tag{4.52}$$

which for the case of the massless k-particle the last line simplifies to

$$Q^2 = s + t + u. \tag{4.53}$$

Next, we note that all of the LO_1 structure functions are proportional to the following combination of constants:

$$g_{\mathrm{LO}_1} = \begin{cases} 2\,C_A C_F\, g_s^2(\mu)\, g_Z^2\, (a_f^2 + v_f^2), & i \in (-1, 0, \mathrm{incl}, 1, 2, 7), \\ 4\,C_A C_F\, g_s^2(\mu)\, g_Z^2\, a_f v_f, & i \in (3, 4, 5, 6) \end{cases} \tag{4.54}$$

where $C_A C_F$ is the color factor, g_s and g_Z are the strong and EW coupling constants.

To have a bit more intuition about the nature of the $(a_f^2 + v_f^2)$ and $a_q v_q$ coupling coefficients we have to go back at have a look at the structure of the hadronic tensor $W^{\mu\nu}$. In general, the hadronic tensor arising in vector boson production can be decomposed into parity-even and parity-odd components based on the structure of the currents in it. These currents contain both vector and axial-vector parts, and for the production of the Z-boson take the form $J^\mu = \bar{\psi}\gamma^\mu(v_f - a_f\gamma^5)\psi$, with v_f and a_f as the vector and axial-vector couplings of the gauge boson to the fermion f. When the two currents appear within the same trace, as in $W^{\mu\nu} \sim \mathrm{Tr}[\not{p}_1\gamma^\mu(v_f - a_f\gamma^5)\not{p}_2\gamma^\nu(v_f - a_f\gamma^5)]^2$, the resulting structure contains contributions proportional to v_f^2, a_f^2, and $v_f a_f$. The terms quadratic in v_f and a_f correspond to parity-even interactions: they originate from contractions of vector $\times$ vector and axial $\times$ axial currents, and produce symmetric tensors under the exchange of $\mu \leftrightarrow \nu$. On the other hand, the mixed term proportional to $v_f a_f$ arises from the interference between the vector and axial-vector parts, and gives an antisymmetric tensor. This antisymmetric component changes sign under a parity transformation and thus is parity-odd.
This is important when we are contracting the hadronic tensor with the projectors from Eq.(2.20), as some of the combinations of the projectors are parity-even ($i = -1, 0, 1, 2$) and therefore will null the parity-odd term in the hadronic tensor, only leaving the structure functions proportional to $v_f^2 + a_f^2$. Other projectors are parity-odd $(3, 4)$ and therefore they will be producing W_i that are proportional to $v_f a_f$.

The so-called T-odd[3] structure functions $i = 5, 6, 7$ will have a different scaling with $W_{5,6} \sim v_f a_f$ and $W_7 \sim (v_f^2 + a_f^2)$. This happens since these structure functions arise from the subleading ϵ poles hitting the virtual loop integrals, therefore our four-dimensional intuition for the couplings does not work here.

[2]Similar thing happens when the couplings appear in separate traces, such as in the product $W^{\mu\nu} \sim \mathrm{Tr}[\not{p}_1\gamma^\mu(v_f - a_f\gamma^5)\not{p}_2] \cdot \mathrm{Tr}[\not{p}_3\gamma^\nu(v_{f'} + a_{f'}\gamma^5)\not{p}_4]$. Each trace splits into a parity-even and parity-odd part, such that the full contraction includes contributions proportional to $v_f v_{f'}$, $a_f a_{f'}$, $v_f a_{f'}$, and $a_f v_{f'}$. The combinations $v_f v_{f'}$ and $a_f a_{f'}$ multiply parity-even structures, since they come from a product of even-even and odd-odd traces. In contrast, the mixed terms $v_f a_{f'}$ and $a_f v_{f'}$ couple even to odd, or vice versa, and produce parity-odd contributions. Thus, regardless of where the couplings sit in the hadronic tensor, in four dimension $W^{\mu\nu}$ separates into parity-even tensor structures that multiply the combinations $v_f^2 + a_f^2$ or $v_f v_{f'} + a_f a_{f'}$ and parity-odd structures proportional to $v_f a_f$ or $v_f a_{f'} + a_f v_{f'}$.

[3]In this context, T-odd refers to quantities that change sign under naive time reversal, meaning the reversal of all particle three-momenta and spins without complex conjugation or interchange of initial and final states.

Therefore, for the $qg \to Zq$ process, the LO_1 helicity projected matrix elements squared $\left|\mathcal{M}^{(1),\mathrm{R}}_{qg\to Zq}\right|^2_i$ are

$$\left|\mathcal{M}^{(1),\mathrm{R}}_{qg\to Zq}\right|^2_0(s,t,u,Q^2) = -g_{\mathrm{LO}_1} u \frac{(Q^2+s)^2+(Q^2-t)^2}{s(Q^2-u)(Q^2-t)}, \tag{4.55a}$$

$$\left|\mathcal{M}^{(1),\mathrm{R}}_{qg\to Zq}\right|^2_{\mathrm{incl}}(s,t,u,Q^2) = -g_{\mathrm{LO}_1}\left(\frac{2Q^2u}{st}+\frac{t}{s}+\frac{s}{t}\right), \tag{4.55b}$$

$$\left|\mathcal{M}^{(1),\mathrm{R}}_{qg\to Zq}\right|^2_1(s,t,u,Q^2) = -g_{\mathrm{LO}_1}\sqrt{\frac{Q^2u}{st}}\left(2\frac{Q^2-t}{Q^2-u}-\frac{Q^2-u}{Q^2-t}\right), \tag{4.55c}$$

$$\left|\mathcal{M}^{(1),\mathrm{R}}_{qg\to Zq}\right|^2_2(s,t,u,Q^2) = \left|\mathcal{M}^{(1),\mathrm{R}}_{qg\to Zq}\right|^2_0 = -g_{\mathrm{LO}_1} u \frac{(Q^2+s)^2+(Q^2-t)^2}{s(Q^2-u)(Q^2-t)}, \tag{4.55d}$$

$$\left|\mathcal{M}^{(1),\mathrm{R}}_{qg\to Zq}\right|^2_3(s,t,u,Q^2) = 2g_{\mathrm{LO}_1}\sqrt{\frac{u}{t\,(Q^2-t)\,(Q^2-u)}}\frac{\left(Q^4+2su+u^2\right)}{s}, \tag{4.55e}$$

$$\left|\mathcal{M}^{(1),\mathrm{R}}_{qg\to Zq}\right|^2_4(s,t,u,Q^2) = 2g_{\mathrm{LO}_1}\sqrt{\frac{Q^2s}{(Q^2-t)\,(Q^2-u)}}\frac{\left(Q^4-2Q^2t+u^2\right)}{st}, \tag{4.55f}$$

$$\left|\mathcal{M}^{(1),\mathrm{R}}_{qg\to Zq}\right|^2_5 = \left|\mathcal{M}^{(1),\mathrm{R}}_{qg\to Zq}\right|^2_6 = \left|\mathcal{M}^{(1),\mathrm{R}}_{qg\to Zq}\right|^2_7 = 0. \tag{4.55g}$$

For the $q\bar{q} \to Zg$ process, one has the following:

$$\left|\mathcal{M}^{(1),\mathrm{R}}_{q\bar{q}\to Zg}\right|^2_0(s,t,u,Q^2) = g_{\mathrm{LO}_1}\left(\frac{Q^2-t}{Q^2-u}+\frac{Q^2-u}{Q^2-t}\right), \tag{4.56a}$$

$$\left|\mathcal{M}^{(1),\mathrm{R}}_{q\bar{q}\to Zg}\right|^2_{\mathrm{incl}}(s,t,u,Q^2) = g_{\mathrm{LO}_1}\left(\frac{2Q^2s}{ut}+\frac{t}{u}+\frac{u}{t}\right), \tag{4.56b}$$

$$\left|\mathcal{M}^{(1),\mathrm{R}}_{q\bar{q}\to Zg}\right|^2_1(s,t,u,Q^2) = g_{\mathrm{LO}_1}\sqrt{\frac{Q^2s}{tu}}\left(\frac{Q^2-u}{Q^2-t}-\frac{Q^2-t}{Q^2-u}\right), \tag{4.56c}$$

$$\left|\mathcal{M}^{(1),\mathrm{R}}_{q\bar{q}\to Zg}\right|^2_2(s,t,u,Q^2) = \left|\mathcal{M}^{(1),\mathrm{R}}_{q\bar{q}\to Zg}\right|^2_0(s,t,u,Q^2) = g_{\mathrm{LO}_1}\left(\frac{Q^2-t}{Q^2-u}+\frac{Q^2-u}{Q^2-t}\right), \tag{4.56d}$$

$$\left|\mathcal{M}^{(1),\mathrm{R}}_{q\bar{q}\to Zg}\right|^2_3(s,t,u,Q^2) = -2g_{\mathrm{LO}_1}\sqrt{\frac{(Q^2-t)\,(Q^2-u)}{tu}}\left(\frac{Q^2-u}{Q^2-t}-\frac{Q^2-t}{Q^2-u}\right), \tag{4.56e}$$

$$\left|\mathcal{M}^{(1),\mathrm{R}}_{q\bar{q}\to Zg}\right|^2_4(s,t,u,Q^2) = -2g_{\mathrm{LO}_1}\sqrt{\frac{Q^2s}{(Q^2-t)\,(Q^2-u)}}\frac{\left(\left(Q^2-t\right)^2+\left(Q^2-u\right)^2\right)}{tu}, \tag{4.56f}$$

$$\left|\mathcal{M}^{(1),\mathrm{R}}_{q\bar{q}\to Zg}\right|^2_5 = \left|\mathcal{M}^{(1),\mathrm{R}}_{q\bar{q}\to Zg}\right|^2_6 = \left|\mathcal{M}^{(1),\mathrm{R}}_{q\bar{q}\to Zg}\right|^2_7 = 0. \tag{4.56g}$$

One can obtain the structure functions for processes with antiquark and/or reversed order by the following prescription in ref. [16]:

$W_{i,\,\bar{q}q} = W_{i,\,q\bar{q}}$	if $i \in \{-1,\,0,\,1,\,2,\,7\}$,	$W_{i,\,\bar{q}q} = -W_{i,\,q\bar{q}}$	otherwise,
$W_{i,\,gq} = W_{i,\,qg}(u \leftrightarrow t)$	if $i \in \{-1,\,0,\,2,\,3,\,6\}$,	$W_{i,\,gq} = -W_{i,\,qg}(u \leftrightarrow t)$	otherwise,
$W_{i,\,\bar{q}g} = W_{i,\,qg}$	if $i \in \{-1,\,0,\,1,\,2,\,7\}$,	$W_{i,\,\bar{q}g} = -W_{i,\,qg}$	otherwise,
$W_{i,\,g\bar{q}} = W_{i,\,qg}(u \leftrightarrow t)$	if $i \in \{-1,\,0,\,1,\,2,\,4,\,5\}$,	$W_{i,\,g\bar{q}} = -W_{i,\,qg}(u \leftrightarrow t)$	otherwise.

For the comparison with ref. [16], see Chapter 6.

At this order, one observes that $W_0 = W_2$, which reflects the well-known Lam-Tung relation [68] $A_0 = A_2$. This relation is a consequence of the spin-1/2 nature of quarks at tree level and the vector coupling of spin-1 gluons to quarks at $\mathcal{O}(\alpha_s)$. It holds up to $\mathcal{O}(\alpha_s)$ in perturbative QCD, but is violated at higher orders in the strong coupling. Moreover, the structure functions W_5, W_6, and W_7 vanish at this order, as they are related to the absorptive (imaginary) parts of the amplitude and thus receive non-zero contributions only from loop-level diagrams.

The true power of the spinor-helicity method becomes apparent when computing the NLO_1 contributions. To obtain the RV terms in the $\mathcal{O}(\alpha_s^2)$ cross section, one must contract the NLO_1 Z-helicity

amplitudes with the LO_1 amplitudes as follows:

$$\begin{aligned}
\text{e.g. } W^{(2),\mathrm{RV},\mathrm{fin}}_{\lambda\lambda'} &= \sum_X \!\!\!\!\!\!\int \langle |\mathcal{M}^{(2),\mathrm{RV},\mathrm{fin}}_{p_a p_b\to qk}|^2_{\lambda\lambda'}\rangle, \\
|\mathcal{M}^{(2),\mathrm{RV}}_{p_a p_b\to qk}|^2_{\lambda\lambda'} =& \big(\mathcal{A}^{\mathrm{NLO}_1}_{\lambda'}\big)^*(1^+;2^+_q,3^-_{\bar q})\mathcal{A}^{\mathrm{LO}_1}_{\lambda}(1^+;2^+_q,3^-_{\bar q}) + \big(\mathcal{A}^{\mathrm{LO}_1}_{\lambda'}\big)^*(1^+;2^+_q,3^-_{\bar q})\mathcal{A}^{\mathrm{NLO}_1}_{\lambda}(1^+;2^+_q,3^-_{\bar q}) \\
&+\big(\mathcal{A}^{\mathrm{NLO}_1}_{\lambda'}\big)^*(1^+;2^-_q,3^+_{\bar q})\mathcal{A}^{\mathrm{LO}_1}_{\lambda}(1^+;2^-_q,3^+) + \big(\mathcal{A}^{\mathrm{LO}_1}_{\lambda'}\big)^*(1^+;2^-_q,3^+_{\bar q})\mathcal{A}^{\mathrm{NLO}_1}_{\lambda}(1^+;2^-_q,3^+) \\
&+\big(\mathcal{A}^{\mathrm{NLO}_1}_{\lambda'}\big)^*(1^-;2^+_q,3^-_{\bar q})\mathcal{A}^{\mathrm{LO}_1}_{\lambda}(1^-;2^+_q,3^-_{\bar q}) + \big(\mathcal{A}^{\mathrm{LO}_1}_{\lambda'}\big)^*(1^-;2^+_q,3^-_{\bar q})\mathcal{A}^{\mathrm{NLO}_1}_{\lambda}(1^-;2^+_q,3^-_{\bar q}) \\
&+\big(\mathcal{A}^{\mathrm{NLO}_1}_{\lambda'}\big)^*(1^-;2^-_q,3^+_{\bar q})\mathcal{A}^{\mathrm{LO}_1}_{\lambda}(1^-;2^-_q,3^+_{\bar q}) + \big(\mathcal{A}^{\mathrm{LO}_1}_{\lambda'}\big)^*(1^-;2^-_q,3^+_{\bar q})\mathcal{A}^{\mathrm{NLO}_1}_{\lambda}(1^-;2^-_q,3^+_{\bar q}),
\end{aligned} \tag{4.57}$$

where the indexes on the element $W_{\lambda\lambda'}$ are describing:

- (2) – order in strong coupling α_s,
- RV – which out of two contributions at $\mathcal{O}(\alpha_s^2)$,
- fin – which part of the real-virtual contribution.

Here, $\mathcal{A}^{\mathrm{NLO}_1}_{\lambda}$ may refer to one of several Z-helicity NLO_1 amplitudes derived from various terms in the full amplitude $\mathcal{A}^{(1)}_{\mathrm{full}}$: the divergent part (see Eq.(4.15)), which gives the infrared poles in the RV terms – useful for comparison purposes (see Chapter 6) but not directly used in the final result; the finite remainder (Eq.(4.16)), which provides the IR-finite contribution we actually require; or the top-quark loop contribution, also part of $\mathcal{A}_{\mathrm{full}}$ (Eq.(4.17)). In general the one-loop Z-helicity amplitude is

$$\mathcal{A}^{\mathrm{NLO}_1}_{\lambda} = \mathcal{A}^{\mathrm{NLO}_1,\,\mathrm{div}}_{\lambda} + \mathcal{A}^{\mathrm{NLO}_1,\,\mathrm{fin}}_{\lambda} + \mathcal{A}^{\mathrm{NLO}_1,\,\text{top-loop}}_{\lambda},$$

where each term is coming from various terms in the full amplitude.

Since the resulting expressions are rather lengthy, we will present only representative examples. We begin by showing the derived T-odd helicity matrix elements squared constructing $W_5^{(2),\mathrm{RV},\mathrm{fin}}$, $W_6^{(2),\mathrm{RV},\mathrm{fin}}$ and $W_7^{(2),\mathrm{RV},\mathrm{fin}}$. These have the contributions only from the finite terms $\mathcal{A}^{\mathrm{NLO}_1,\,\mathrm{fin}}_{\lambda}$, and possibly the top-loop ones $\mathcal{A}^{\mathrm{NLO}_1,\,\text{top-loop}}_{\lambda}$.
The finite terms in the helicity cross sections have similar general coupling structure, where the only addition is the extra power of the strong coupling α_s:

$$g^{\mathrm{fin}}_{\mathrm{RV}} = \begin{cases} 2\alpha_s\, C_A C_F\, g_s^2(\mu)\, g_Z^2\, (a_f^2+v_f^2), & i\in(-1,0,\mathrm{incl},1,2,7), \\ 4\alpha_s\, C_A C_F\, g_s^2(\mu)\, g_Z^2\, a_f v_f, & i\in(3,4,5,6). \end{cases} \tag{4.58}$$

The fifth, sixth and seventh second order helicity matrix elements squared for the $qg\to Zq$ process are

thus

$$|\mathcal{M}^{(2),\mathrm{RV},\mathrm{fin}}_{qg\to Zq}|^2_5 = g^{\mathrm{fin}}_{\mathrm{RV}}\frac{u}{s}\sqrt{\frac{Q^2 s}{(Q^2-t)(Q^2-u)}}\left[\frac{C_F}{2}\cdot\frac{2Q^2+s}{Q^2-t}\right.$$
$$\left.-\left(C_F-\frac{C_A}{2}\right)\cdot\left[\frac{Q^2}{Q^2-u}+\frac{Q^2-t}{t}\left(1-\frac{Q^2-u}{t}\ln\left(\frac{Q^2-u}{s}\right)\right)+\frac{Q^2-u}{s}\ln\left(\frac{(Q^2-t)(Q^2-u)}{tu}\right)\right]\right], \tag{4.59a}$$

$$|\mathcal{M}^{(2),\mathrm{RV},\mathrm{fin}}_{qg\to Zq}|^2_6 = g^{\mathrm{fin}}_{\mathrm{RV}}\frac{Q^2 u}{\sqrt{(Q^2-u)(Q^2-t)ut}}\left[\frac{C_F}{2}\cdot\frac{t-2u}{Q^2-t}\right.$$
$$\left.-\left(C_F-\frac{C_A}{2}\right)\cdot\left[\frac{u}{Q^2-u}+\frac{Q^2}{s^2}-\frac{(Q^2-u)u}{s^2}\ln\left(\frac{(Q^2-u)(Q^2-t)}{ut}\right)\right]\right], \tag{4.59b}$$

$$|\mathcal{M}^{(2),\mathrm{RV},\mathrm{fin}}_{qg\to Zq}|^2_7 = -2g^{\mathrm{fin}}_{\mathrm{RV}}\frac{u}{s}\sqrt{\frac{Q^2 s}{ut}}\left[\frac{-C_F}{2}\cdot\frac{2Q^2u+st}{(Q^2-t)^2}\right.$$
$$\left.-\left(C_F-\frac{C_A}{2}\right)\cdot\left[\frac{2Q^2 s}{(Q^2-u)^2}-\frac{Q^4-ut}{(Q^2-u)(Q^2-t)}+\frac{u}{t}\ln\left(\frac{Q^2-u}{s}\right)-\frac{u}{s}\ln\left(\frac{(Q^2-u)(Q^2-t)}{ut}\right)\right]\right]. \tag{4.59c}$$

Similar structure functions are achieved for the $q\bar{q}\to Zg$ process:

$$|\mathcal{M}^{(2),\mathrm{RV},\mathrm{fin}}_{q\bar{q}\to Zg}|^2_5 = g^{\mathrm{fin}}_{\mathrm{RV}}\sqrt{\frac{Q^2 s}{(Q^2-u)(Q^2-t)}}\left[\frac{-C_F}{2}\cdot\left(\frac{Q^2-t}{Q^2-u}+\frac{Q^2-u}{Q^2-t}\right)\right.$$
$$\left.+\left(C_F-\frac{C_A}{2}\right)\cdot\left[\frac{Q^2-t}{t}\left(1-\frac{s}{t}\ln\left(\frac{Q^2-u}{s}\right)\right)+\frac{Q^2-u}{u}\left(1-\frac{s}{u}\ln\left(\frac{Q^2-t}{s}\right)\right)\right]\right], \tag{4.60a}$$

$$|\mathcal{M}^{(2),\mathrm{RV},\mathrm{fin}}_{q\bar{q}\to Zg}|^2_6 = g^{\mathrm{fin}}_{\mathrm{RV}}\frac{Q^2 s}{\sqrt{(Q^2-u)(Q^2-t)ut}}\left[C_F\cdot\left(\frac{Q^2-t}{Q^2-u}-\frac{Q^2-u}{Q^2-t}\right)\right.$$
$$\left.+\left(C_F-\frac{C_A}{2}\right)\cdot\left[\frac{Q^2-u}{u}\ln\left(\frac{Q^2-t}{s}\right)-\frac{Q^2-t}{t}\ln\left(\frac{Q^2-u}{s}\right)\right]\right], \tag{4.60b}$$

$$|\mathcal{M}^{(2),\mathrm{RV},\mathrm{fin}}_{q\bar{q}\to Zg}|^2_7 = -2g^{\mathrm{fin}}_{\mathrm{RV}}\sqrt{\frac{Q^2 s}{ut}}\left[C_F\cdot\left(1-\frac{ut}{2(Q^2-t)(Q^2-u)}\right)\left(\frac{Q^2-t}{Q^2-u}-\frac{Q^2-u}{Q^2-t}\right)\right.$$
$$\left.+\left(C_F-\frac{C_A}{2}\right)\cdot\left[\frac{Q^2}{Q^2-t}-\frac{Q^2}{Q^2-u}-\frac{s}{t}\ln\left(\frac{Q^2-u}{s}\right)+\frac{s}{u}\ln\left(\frac{Q^2-t}{s}\right)\right]\cdot\right] \tag{4.60c}$$

These structure functions have been derived in the literature [16, 27] and we discuss their comparison with the known results in the Chapter 6.
We show these structure functions for illustration purposes, although our results include the full set of NLO_1 structure functions for $i=-1,\ldots,7$, which to our knowledge have not been presented in the literature.
Additionally, the helicity structure functions associated with the top-loop contributions also do not have an explicit derivation available in existing references. Here, we also provide the complete set of these results for both NLO_1 subprocesses. These top-loop contributions involve a slightly modified coupling structure, as they result from the interference between the LO_1 and the top-loop-induced NLO_1 amplitudes. The coupling prefactor takes the form:

$$g^{\mathrm{top}}_{\mathrm{RV}} = \begin{cases} 8\frac{\alpha_s}{4\pi}\,C_A C_F T_F\,g_S^2(\mu)\,g_Z^2\,a_f a_t, & i\in(-1,0,\mathrm{incl},1,2,7),\\ 16\frac{\alpha_s}{4\pi}\,C_A C_F T_F\,g_S^2(\mu)\,g_Z^2\,v_f v_t, & i\in(3,4,5,6),\end{cases} \tag{4.61}$$

where v_t and a_t denote the vector and axial-vector couplings of the top quark, respectively. We work in the heavy-top limit $1/m_t \to 0$, assuming that the top quark mass is large compared to the relevant external scales.
Thus the helicity matrix elements squared for a top-loop contribution of the NLO_1 $qg \to Zq$ process are

$$|\mathcal{M}^{(2),\mathrm{RV},\mathrm{top}}_{qg\to Zq}|^2_{\mathrm{incl}} = g^{\mathrm{top}}_{\mathrm{RV}} \left(\frac{Q^2+u}{Q^2-u}\right) \left(1-\frac{Q^2}{u-Q^2}\ln\left(-\frac{u}{Q^2}\right)\right), \tag{4.62a}$$

$$|\mathcal{M}^{(2),\mathrm{RV},\mathrm{top}}_{qg\to Zq}|^2_{0} = g^{\mathrm{top}}_{\mathrm{RV}} u \left(\frac{1}{Q^2-t}+\frac{1}{Q^2-u}\right) \left(1-\frac{Q^2}{u-Q^2}\ln\left(-\frac{u}{Q^2}\right)\right), \tag{4.62b}$$

$$|\mathcal{M}^{(2),\mathrm{RV},\mathrm{top}}_{qg\to Zq}|^2_{1} = g^{\mathrm{top}}_{\mathrm{RV}} \sqrt{\frac{Q^2 u}{ts}} \frac{u^2-2st+su}{2(Q^2-t)Q^2} \left(1-\frac{Q^2}{u-Q^2}\ln\left(-\frac{u}{Q^2}\right)\right), \tag{4.62c}$$

$$|\mathcal{M}^{(2),\mathrm{RV},\mathrm{top}}_{qg\to Zq}|^2_{2} = |\mathcal{M}^{(2),\mathrm{RV},\mathrm{top}}_{qg\to Zq}|^2_{0} = g^{\mathrm{top}}_{\mathrm{RV}} u \left(\frac{1}{Q^2-t}+\frac{1}{Q^2-u}\right) \left(1-\frac{Q^2}{u-Q^2}\ln\left(-\frac{u}{Q^2}\right)\right), \tag{4.62d}$$

$$|\mathcal{M}^{(2),\mathrm{RV},\mathrm{top}}_{qg\to Zq}|^2_{3} = g^{\mathrm{top}}_{\mathrm{RV}} \sqrt{\frac{ut}{(Q^2-u)(Q^2-t)}} \left(1+\frac{u}{2t}+\frac{Q^2-t}{Q^2-u}\right) \left(1-\frac{Q^2}{u-Q^2}\ln\left(-\frac{u}{Q^2}\right)\right), \tag{4.62e}$$

$$|\mathcal{M}^{(2),\mathrm{RV},\mathrm{top}}_{qg\to Zq}|^2_{4} = g^{\mathrm{top}}_{\mathrm{RV}} t \sqrt{\frac{s}{Q^2(Q^2-u)(Q^2-t)}} \left(1-\frac{u^2}{2st}-\frac{Q^2(Q^2-t)}{t(Q^2-u)}\right) \left(1-\frac{Q^2}{u-Q^2}\ln\left(-\frac{u}{Q^2}\right)\right), \tag{4.62f}$$

$$|\mathcal{M}^{(2),\mathrm{RV},\mathrm{top}}_{qg\to Zq}|^2_{5} = g^{\mathrm{top}}_{\mathrm{RV}} \frac{\pi}{4} u \sqrt{\frac{Q^2}{s(Q^2-t)(Q^2-u)}} \frac{u(t-s)-2s^2}{(Q^2-u)^2}, \tag{4.62g}$$

$$|\mathcal{M}^{(2),\mathrm{RV},\mathrm{top}}_{qg\to Zq}|^2_{6} = g^{\mathrm{top}}_{\mathrm{RV}} \frac{\pi}{4} Q^2 \sqrt{\frac{u}{t(Q^2-t)(Q^2-u)}} (u(t-s)+2st)(Q^2-u)^2, \tag{4.62h}$$

$$|\mathcal{M}^{(2),\mathrm{RV},\mathrm{top}}_{qg\to Zq}|^2_{7} = -g^{\mathrm{top}}_{\mathrm{RV}} \pi \sqrt{\frac{Q^2 u}{ts}} \frac{u(t-s)}{(Q^2-u)^2} \tag{4.62i}$$

Similarly, the contributions for the $q\bar{q} \to Zg$ process are

$$|\mathcal{M}^{(2),\mathrm{RV},\mathrm{top}}_{q\bar{q}\to Zg}|^2_{\mathrm{incl}} = -g^{\mathrm{top}}_{\mathrm{RV}} \left(\frac{Q^2+s}{Q^2-s}\right) \left(1-\frac{Q^2}{s-Q^2}\ln\left(\frac{s}{Q^2}\right)\right), \tag{4.63a}$$

$$|\mathcal{M}^{(2),\mathrm{RV},\mathrm{top}}_{q\bar{q}\to Zg}|^2_{0} = -g^{\mathrm{top}}_{\mathrm{RV}} \left(1-\frac{s(t-u)^2}{(Q^2-u)(Q^2-t)(Q^2-s)}\right) \left(1-\frac{Q^2}{s-Q^2}\ln\left(\frac{s}{Q^2}\right)\right), \tag{4.63b}$$

$$|\mathcal{M}^{(2),\mathrm{RV},\mathrm{top}}_{q\bar{q}\to Zg}|^2_{1} = g^{\mathrm{top}}_{\mathrm{RV}} \frac{1}{2} \sqrt{\frac{s}{Q^2 tu}} \frac{(t-u)\left(Q^2\left(s^2-2tu\right)-stu\right)}{(Q^2-s)(Q^2-t)(Q^2-u)} \left(1-\frac{Q^2}{s-Q^2}\ln\left(\frac{s}{Q^2}\right)\right), \tag{4.63c}$$

$$|\mathcal{M}^{(2),\mathrm{RV},\mathrm{top}}_{q\bar{q}\to Zg}|^2_{2} = |\mathcal{M}^{(2),\mathrm{RV},\mathrm{top}}_{0,q\bar{q}\to Zg}|^2 = -g^{\mathrm{top}}_{\mathrm{RV}} \left(1-\frac{s(t-u)^2}{(Q^2-u)(Q^2-t)(Q^2-s)}\right) \left(1-\frac{Q^2}{s-Q^2}\ln\left(\frac{s}{Q^2}\right)\right), \tag{4.63d}$$

$$|\mathcal{M}^{(2),\mathrm{RV},\mathrm{top}}_{q\bar{q}\to Zg}|^2_{3} = g^{\mathrm{top}}_{\mathrm{RV}} \frac{1}{2} \frac{(t-u)\left(2tu-s^2\right)}{(t+u)\sqrt{tu\,(Q^2-t)\,(Q^2-u)}} \left(1-\frac{Q^2}{s-Q^2}\ln\left(\frac{s}{Q^2}\right)\right), \tag{4.63e}$$

$$|\mathcal{M}^{(2),\mathrm{RV},\mathrm{top}}_{q\bar{q}\to Zg}|^2_{4} = g^{\mathrm{top}}_{\mathrm{RV}} \frac{\sqrt{s}}{2} \frac{2\left(\left(Q^2-s\right)^2-tu\right)+5s\left(Q^2-s\right)+4s^2}{\sqrt{Q^2}\,(Q^2-s)\,\sqrt{(Q^2-t)\,(Q^2-u)}} \left(1-\frac{Q^2}{s-Q^2}\ln\left(\frac{s}{Q^2}\right)\right), \tag{4.63f}$$

$$|\mathcal{M}^{(2),\mathrm{RV},\mathrm{top}}_{q\bar{q}\to Zg}|^2_{5} = |\mathcal{M}^{(2),\mathrm{RV},\mathrm{top}}_{q\bar{q}\to Zg}|^2_{6} = |\mathcal{M}^{(2),\mathrm{RV},\mathrm{top}}_{q\bar{q}\to Zg}|^2_{7} = 0. \tag{4.63g}$$

Finally, for the $D = 4$ comparison with the RR results, derivation of which will be discussed in the next chapter, we square the LO_2 Z-helicity amplitudes:

$$W^{(2),\mathrm{RR}}_{\lambda\lambda'} = \sum\!\!\!\!\!\!\int_X \langle |\mathcal{M}^{(2),\mathrm{RR}}_{p_a p_b\to q k_1 k_2}|^2_{\lambda\lambda'}\rangle,$$
$$|\mathcal{M}^{(2),\mathrm{RR}}_{p_a p_b\to qk}|^2_{\lambda\lambda'} = \sum_{\text{helicities of the system}} \left(\mathcal{A}^{\mathrm{LO}_2}_{\lambda'}\right)^*(1,2,3,4)\mathcal{A}^{\mathrm{LO}_2}_{\lambda}(1,2,3,4), \tag{4.64}$$

where the sets of possible helicities depend on the process at hand and they are discussed in full in Section 4.1.3 and in Appendix E. We can compare these results at the level of amplitudes squared, before the integrating over the final-state hadronic radiation.

4.5 Rewriting $2 \to 2$ phase space

In this section we derive the $2 \to 2$ decay phase space $\mathrm{d}\phi_{(p_a p_b \to qk)}$ required for producing the R and RV structure functions from the matrix elements squared $\left|\mathcal{M}_{p_a p_b \to qk}\right|_i^2$. We perform the derivation in fully general D dimensions, as it will turn out to be useful for the integration of the double-real terms. Of course, for the RV terms, specifically for the hard function, it is enough to have the expressions only in 4 dimensions.

For the convenience, we absorb the momentum fractions measure from the PDF convolution integral (2.29) into our $2 \to 2$ decay phase space:

$$d\phi_{(p_a p_b \to qk)} = \frac{d\xi_a}{\xi_a}\frac{d\xi_b}{\xi_b}\left[\frac{d^{4-2\epsilon}q}{(2\pi)^{4-2\epsilon}}(2\pi)\delta(q^2-m_q^2)\theta(q^0)\right]\left[\frac{d^{4-2\epsilon}k}{(2\pi)^{4-2\epsilon}}(2\pi)\delta(k^2-m_k^2)\theta(k^0)\right]\frac{dm_k^2}{2\pi}\frac{dm_q^2}{2\pi} \times (2\pi)^{4-2\epsilon}\delta^{(4-2\epsilon)}(\xi_a P_a + \xi_b P_b - k - q), \quad (4.65)$$

where the integrals go over the final states q, k with their masses m_q, m_k.

For further simplification of the phase space we will go to the lightcone coordinates as defined in Eq.(2.38a) and Eq.(2.38b). The integration measure then reads:

$$d^4k = \frac{1}{2}dk^- dk^+ dk_x dk_y = \frac{1}{4}dk^- dk^+ dk_T^2 d\phi, \quad (4.66a)$$

$$d^{4-2\epsilon}k = \frac{1}{2}dk^- dk^+ d^{2-2\epsilon}k_T = \frac{(p_T^2)^{-\epsilon}}{4}dk^- dk^+ dk_T^2 d\Omega^{(2-2\epsilon)}. \quad (4.66b)$$

Delta-functions in lightcone coordinates are thus:

$$\delta^4(k) = 2\delta(k^-)\delta(k^+)\delta(k_x)\delta(k_y), \quad (4.67a)$$

$$\delta^{4-2\epsilon}(k) = 2\delta(k^-)\delta(k^+)\delta^{(2-2\epsilon)}(k_T), \quad (4.67b)$$

$$\delta(k^2-m^2)\theta(E) = \delta(k^-k^+ - k_T^2 - m^2)\theta(k^-)\theta(k^+). \quad (4.67c)$$

Using this parametrization together with the D-dimensional definition of the momenta of the incoming particles in lab frame $P_a = E_a(1,0,\ldots,0,1)$ and $P_b = E_b(1,0,\ldots,0,-1)$ we are able to simplify phase space further and rewrite:

$$d^{4-2\epsilon}q = \frac{(q_T^2)^{-\epsilon}}{4}dq^- dq^+ dq_+^2 d\Omega^{(2-2\epsilon)},$$
$$\delta(q^2-m_q^2)\theta(q^0) = \delta(q^-q^+ - q_T^2 - m_q^2)\theta(q^-)\theta(q^+),$$
$$\delta^{(4-2\epsilon)}(\xi_a P_a + \xi_b P_b - k - q) = 2\delta(2\xi_a E_a - k^- - q^-)\delta(2\xi_b E_b - k^+ - q^+)\delta^{(2-2\epsilon)}(k_T + q_T).$$

Substituting this into 4.65 we then achieve:

$$d\phi_{(p_a p_b \to qk)} = (2\pi)^2\frac{d\xi_a}{\xi_a}\frac{d\xi_b}{\xi_b}\left[\frac{(q_T^2)^{-\epsilon}}{4}\frac{dq^- dq^+ dq_T^2 d\Omega_a^{(2-2\epsilon)}}{(2\pi)^{4-2\epsilon}}\delta(q^2-m_q^2)\theta(q^-)\theta(q^+)\right] \times \left[\frac{dk^- dk^+ d^{2-2\epsilon}k_T}{2(2\pi)^{4-2\epsilon}}\delta(k^2-m_k^2)\theta(k^-)\theta(k^+)\right]\frac{dm_k^2}{2\pi}\frac{dm_q^2}{2\pi} \times (2\pi)^{4-2\epsilon}2\delta(2\xi_a E_a - k^- - q^-)\delta(2\xi_b E_b - k^+ - q^+)\delta^{(2-2\epsilon)}(k_T + q_T). \quad (4.68)$$

Following this we now integrate $(4 + (2-2\epsilon))$ delta functions over k_T, m_k^2, m_q^2, ξ_a, ξ_b. We obtain that after integration all functions depending on these variables change according to:

$$k_T \to -q_T,\ m_k^2 \to k^2,\ m_q^2 \to q^2,$$
$$\xi_a \to \frac{k^- + q^-}{2E_a}, \quad \xi_b \to \frac{k^+ + q^+}{2E_b}. \quad (4.69)$$

Also note that since ξ_a and ξ_b are the momentum fractions their values have to be $0 \le \xi_a \le 1$ and $0 \le \xi_b \le 1$, which causes an additional pair of theta functions $\theta(2E_a - k^- - q^-)\theta(2E_b - k^+ - q^+)$ to appear in the expression:

$$d\phi_{(p_a p_b \to qk)} = \frac{1}{k^- + q^-}\frac{1}{k^+ + q^+}dk^- dk^+ \frac{(q_T^2)^{-\epsilon}}{4}\frac{dq^- dq^+ dq_T^2 d\Omega_q^{(2-2\epsilon)}}{(2\pi)^{4-2\epsilon}} \times \theta(q^-)\theta(q^+)\theta(k^-)\theta(k^+)\theta(2E_a - k^- - q^-)\theta(2E_b - k^+ - q^+). \quad (4.70)$$

Finally, from the formula

$$\Omega^{(D)} = \frac{2\pi^{D/2}}{\Gamma(D/2)}, \tag{4.71}$$

where the $\Gamma(x)$ is the Euler's Gamma function, we get the following integrated solid angles:

$$\Omega_q^{(2-2\epsilon)} = \frac{2\pi^{1-\epsilon}}{\Gamma(1-\epsilon)}, \quad \Omega_q^{(1-2\epsilon)} = 2(4\pi)^{-\epsilon}\frac{\Gamma(1-\epsilon)}{\Gamma(1-2\epsilon)}. \tag{4.72}$$

Integrating over $\Omega_q^{(2-2\epsilon)}$ we obtain:

$$\begin{aligned} d\phi_{(p_a p_b \to qk)} = &\frac{(4\pi)^\epsilon}{(4\pi)^2}\frac{1}{2\pi}\frac{(q_T^2)^{-\epsilon}}{\Gamma(1-\epsilon)}\frac{dk^- dk^+ dq^- dq^+ dq_T^2}{(k^-+q^-)(k^++q^+)} \\ &\times \theta(q^-)\theta(q^+)\theta(k^-)\theta(k^+)\theta(2E_a - k^- - q^-)\theta(2E_b - k^+ - q^+). \end{aligned} \tag{4.73}$$

Combining with spin, color averaging, symmetry factor, leptonic factors, flux $E_{\rm cm}$ and summing over the hadronic radiation X the we arrive at the $\mathrm{N}^{n-1}\mathrm{LO}_1$ partonic helicity cross section:

$$\begin{aligned} d\hat{\sigma}^{(n)}_{i,VV',ab} &= L_{(\pm)i,VV'}\sum_{k\in X}\int \mathrm{d}\phi_{p_a p_b\to qk}\frac{\left|\mathcal{M}^{(n)}_{p_a p_b\to qk,VV'}\right|_i^2}{2E_{\rm cm}^2}\frac{1}{n_a n_b N_a N_b} \times \text{sym.} \\ &= L_{(\pm)i,VV'}\sum_{k\in X}\int \frac{(4\pi)^\epsilon}{(4\pi)^2\Gamma(1-\epsilon)}\frac{(q_T^2)^{-\epsilon}}{2E_{\rm cm}^2}\frac{\mathrm{d}k^-\mathrm{d}k^+\mathrm{d}q^-\mathrm{d}q^+\mathrm{d}q_T^2}{(k^-+q^-)(k^++q^+)}\frac{1}{n_a n_b N_a N_b}\delta(k^2)\left|\mathcal{M}^{(n)}_{p_a p_b\to qk,VV'}\right|_i^2 \times \text{sym.} \\ &\quad \times \theta(q^-)\theta(q^+)\theta(k^-)\theta(k^+)\theta(2E_a - k^- - q^-)\theta(2E_b - k^+ - q^+), \end{aligned} \tag{4.74}$$

where n_a, n_b and N_a, N_b are the spins and color factors of the incoming particles respectively. $\left|\mathcal{M}_{p_a p_b\to qk}\right|_i^2$ are the matrix elements squared, projected onto a i helicity state. Leptonic factors $L_{(\pm)i}$ are defined in Eq.(2.26). As for previous variable change momentum fractions ξ_a and ξ_b are equal to $(k^-+q^-)/2E_a$ and $(k^++q^+)/2E_b$ respectively.

Since the R and RV processes for a set a and b incoming particles can have only one type of the particle in the hadronic radiation, the sum over $k \in X$ drops out. As we drop the leptonic factors and the flux, we arrive to the formula for first and second order helicity-projected hard function, which could already be used in Eq.(2.77) and Eq.(2.86) accounting for the fact that we have absorbed the measure from Eq.(2.66) into the partonic cross section:

$$\begin{aligned} H^{(1)}_{i\,ab} = &\int \frac{1}{(4\pi)^2}\frac{\mathrm{d}k^-\mathrm{d}k^+\mathrm{d}q^-\mathrm{d}q^+\mathrm{d}q_T^2}{(k^-+q^-)(k^++q^+)}\frac{1}{n_a n_b N_a N_b}\delta(k^2)\left|\mathcal{M}^{(1),R}_{p_a p_b\to qk}\right|_i^2 \times \text{sym.} \\ &\times \theta(q^-)\theta(q^+)\theta(k^-)\theta(k^+)\theta(2E_a - k^- - q^-)\theta(2E_b - k^+ - q^+), \end{aligned} \tag{4.75}$$

$$\begin{aligned} H^{(2)}_{i,\,ab} = &\int \frac{1}{(4\pi)^2 1}\frac{\mathrm{d}k^-\mathrm{d}k^+\mathrm{d}q^-\mathrm{d}q^+\mathrm{d}q_T^2}{(k^-+q^-)(k^++q^+)}\frac{1}{n_a n_b N_a N_b}\delta(k^2)\left|\mathcal{M}^{(2),RV}_{p_a p_b\to qk}\right|_i^2\Big|_{\text{finite+top}} \times \text{sym.} \\ &\times \theta(q^-)\theta(q^+)\theta(k^-)\theta(k^+)\theta(2E_a - k^- - q^-)\theta(2E_b - k^+ - q^+). \end{aligned} \tag{4.76}$$

Chapter 5

Computation of double-real remainder terms

Now we turn to the non-singular part of the full cross section, as defined in Eq.(2.87). For this part, we compute the double-real (RR) contributions from scratch, without using the spinor-helicity method. Instead, we work directly with standard Feynman rules and later *integrate* (not just multiply with the phase space element, as we did for the R and RV) over the full hadronic decay phase space. This is necessary because the phase space for a $2 \to 3$ process involves a nontrivial integration over the final-state parton momenta k_1 and k_2. Once the amplitude and phase space integration are done, we perform the renormalization of the remaining infrared divergences via PDF counterterms.

5.1 Calculating and squaring matrix elements

As discussed in Section 2.6.3, we expect the RR contribution to contain IR poles that need to be removed by PDF renormalization. The ultraviolet poles have already been accounted for via the $V+$jet threshold factorization in the singular part of the cross section. What remains are the finite $k^2 > 0$ terms, which can still contain initial-final IR divergences. Since these contributions require working in dimensional regularization, we cannot use the spinor-helicity formalism to compute the helicity amplitudes, as it is strictly defined only in four dimensions.

Instead we compute the structure functions, and more specifically matrix elements squared, directly using Feynman rules. The required rules for this calculation are summarized in Appendix A. We follow the framework described in Section 2.2 and first obtain the hadronic tensor, onto which we later apply the projection operators defined in Eq.(2.20). We perform this process for all five RR channels.

To simplify the computation and avoid the overhead from symbolically handling large tensor expressions, we used Feynman gauge for summing over the polarizations of external gluons. In this gauge, the polarization sum is $\sum_s \epsilon_s^\mu \epsilon_s^{*\nu} = -g^{\mu\nu}$, which sums over *all* of the polarizations of the spin-1 particle. Since our external gluons are on-shell, only transverse polarizations should contribute, therefore the correct approach would be to include a projection onto the physical polarizations using an auxiliary lightlike vector r, which leads to:

$$\sum_s \epsilon_s^\mu \epsilon_s^{*\nu} = -g^{\mu\nu} + \frac{r^\mu p^\nu + p^\mu r^\nu}{r \cdot p}, \text{ and similarly for the internal propagators.}$$

However, inserting this expression into the hadronic tensor introduces a large number of additional terms and makes the calculation significantly more time consuming. To avoid this, we kept the simple $-g^{\mu\nu}$ sum and instead included ghost diagrams, which cancel the contributions from the unphysical polarization states. This correction is only needed for diagrams with external gluons. For six-fermion processes, such as $q\bar{q} \to q\bar{q}V$ or $qq \to qqV$, this issue does not arise. In fact, the problem only appears in diagrams involving three-gluon vertices, since in diagrams where gluons attach to fermion lines, the quark-gluon vertex, combined with the Dirac equation, effectively forces the gluons to be transversely polarized. Interference between such diagrams and three-gluon diagrams also only involves physical polarizations, because the fermion-gluon vertex side enforces the sum to run over only transverse polarization. The only truly problematic terms are those where both sides of the interference come from three-gluon diagrams. For those, we include the ghost diagrams, shown in Fig. 5.1, in order to cancel the unphysical terms.

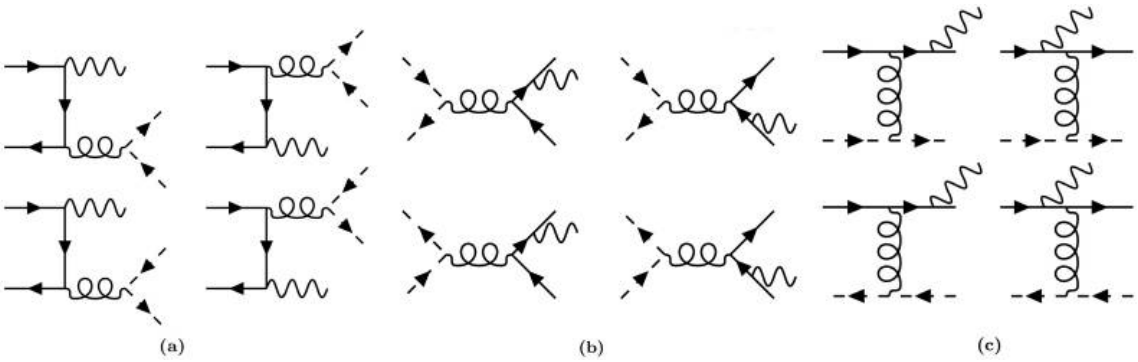


Figure 5.1: Feynman diagrams with ghosts (denoted with dashed lines), included to cancel unphysical polarizations that arise when using Feynman gauge for the sum over external gluon polarization vectors. Ghost diagrams are shown for the (a) $q\bar{q} \to Vgg$ channel, (b) $gg \to Vq\bar{q}$ channel, (c) $qg \to Vqg$ channel.

Although, for the full confidence in the $\mathcal{O}(\epsilon)$ terms, it would be valuable to repeat this calculation in the axial gauge for both the external polarization sum and the gluon propagators, avoiding ghosts entirely.

Finally, we used our numerical results for the LO_2 Z-helicity amplitudes, obtained via the extended spinor-helicity method, to cross-check the matrix elements squared computed from Feynman rules against those derived using the spinor-helicity approach, all in order to have self-consistency within our pipeline.

5.2 Integrating over k-particle phase space

Our next step in achieving the RR terms in to derive the phase space and integrate over the hadronic radiation. This process is more complicated than the one presented in the Section 4.5, since in this case the number of final state particles is higher and the phase space has to be factorized to account for it.

5.2.1 Phase space of decay into N particles

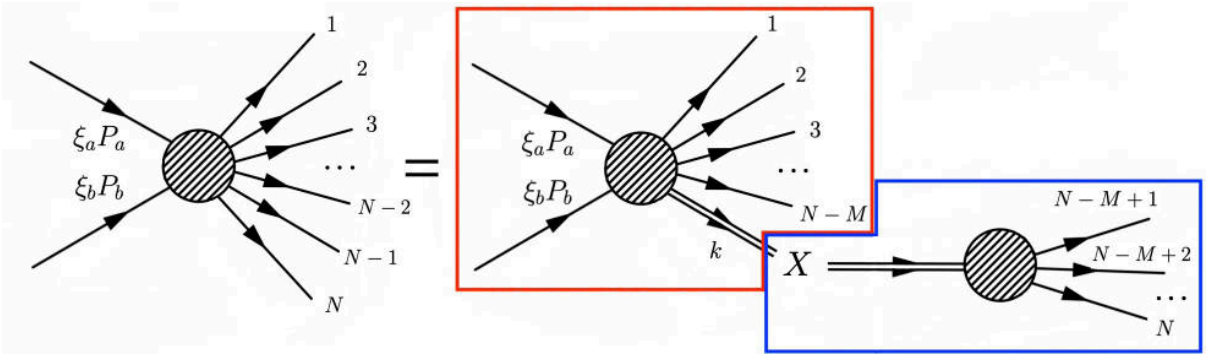


Figure 5.2: An illustration of the factorization of the phase space of the decay into N particles

Here we will derive our expressions for the phase space, starting from the most general case of the decay into N particles: $(\xi_a P_a)\ (\xi_a P_a) \to \{p_i\}_{i=1}^N$ and show how it applies for our calculations.
The phase space for the decay into N particles can be described in terms of a product of two decay spaces: one into M particles and other into $N-M$ particles. Formally we can write full decay space as follows:

$$d\phi_N = \frac{d\xi_a}{\xi_a}\frac{d\xi_b}{\xi_b}\prod_{i=1}^{N}\left[\frac{d^{4-2\epsilon}p_i}{(2\pi)^{4-2\epsilon}}(2\pi)\delta(p_i^2 - m_i^2)\theta(p_i^0)\right](2\pi)^{4-2\epsilon}\delta^{(4-2\epsilon)}\left(\xi_a P_a + \xi_b P_b - \sum_{i=1}^{N} p_i\right), \tag{5.1}$$

where p_i, $i = 1, \ldots, N$ are the momenta of outgoing particles and m_i are their corresponding masses. We have also included the $d\xi_i/\xi_i$, $i = a, b$ factors from the expression of the collinear factorization of the

differential cross section in Eq.(2.29).
Substituting identity in the form of

$$\frac{d^{4-2\epsilon}k}{(2\pi)^{4-2\epsilon}}(2\pi)\delta(k^2-m^2)\theta(k^0)\delta^{(4-2\epsilon)}\Big(k-\sum_{i=1}^{M}p_i\Big)(2\pi)^{4-2\epsilon}\frac{dm^2}{2\pi}=1, \tag{5.2}$$

yields the following expression of Eq. 5.1 as a product of two decay spaces:

$$\begin{aligned} d\phi_N = &\frac{d\xi_a}{\xi_a}\frac{d\xi_b}{\xi_b}\prod_{i=1}^{N-M}\left[\frac{d^{4-2\epsilon}p_i}{(2\pi)^{4-2\epsilon}}(2\pi)\delta(p_i^2-m_i^2)\theta(p_i^0)\right] \\ &\times\frac{d^{4-2\epsilon}k}{(2\pi)^{4-2\epsilon}}(2\pi)\delta(k^2-m^2)\theta(k^0)(2\pi)^{4-2\epsilon}\delta^{(4-2\epsilon)}\Big(\xi_aP_a+\xi_bP_b-\sum_{i=1}^{N-M}p_i-k\Big) \\ \times&\prod_{i=N-M+1}^{N}\left[\frac{d^{4-2\epsilon}p_i}{(2\pi)^{4-2\epsilon}}(2\pi)\delta(p_i^2-m_i^2)\theta(p_i^0)\right](2\pi)^{4-2\epsilon}\delta^{(4-2\epsilon)}\Big(k-\sum_{i=N-M+1}^{N}p_i\Big)\frac{dm^2}{2\pi}, \end{aligned} \tag{5.3}$$

where k momentum is taken as a sum of the momenta of M particles, which decay separately in the second phase space, described in the last line of Eq.(5.3).
Additionally, refer to Fig.5.2 for a schematic representation of the phase space factorization. The formulas in the red and blue boxes correspond to the phase spaces associated with the diagrams shown in these respective boxes.

Phase space of the decay into 4 particles

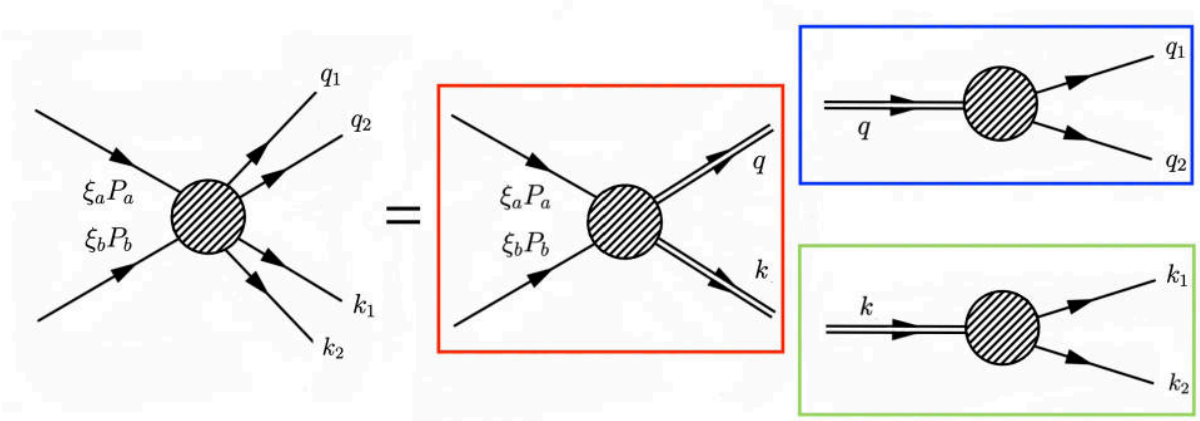


Figure 5.3: An illustration of the factorization of the phase space of the decay into 4 particles

In our case, we focus on the decay into four particles ($p_ap_b \to Vk_1k_2 \to q_1q_2k_1k_2$, where q_1q_2 correspond to the momenta of the final leptons and k_1k_2 correspond to the momenta of two particles that are left after the production of the vector boson, that is two quarks, two gluons or a quark and a gluon), which we decompose as a product of two decay spaces, each into two particles:

$$d\phi_4=\frac{d\xi_a}{\xi_a}\frac{d\xi_b}{\xi_b}\prod_{i=1}^{4}\left[\frac{d^{4-2\epsilon}p_i}{(2\pi)^{4-2\epsilon}}(2\pi)\delta(p_i^2-m_i^2)\theta(p_i^0)\right](2\pi)^{4-2\epsilon}\delta^{(4-2\epsilon)}\Big(\xi_aP_a+\xi_bP_b-\sum_{i=1}^{4}p_i\Big), \tag{5.4}$$

where we now substitute two resolutions of the identity:

$$1=\frac{d^{4-2\epsilon}k}{(2\pi)^{4-2\epsilon}}(2\pi)\delta(k^2-m_k^2)\theta(k^0)\delta^{(4-2\epsilon)}(k-k_1-k_2)(2\pi)^{4-2\epsilon}\frac{dm_k^2}{2\pi}, \tag{5.5}$$

$$1=\frac{d^{4-2\epsilon}q}{(2\pi)^{4-2\epsilon}}(2\pi)\delta(q^2-m_q^2)\theta(q^0)\delta^{(4-2\epsilon)}(q-q_1-q_2)(2\pi)^{4-2\epsilon}\frac{dm_q^2}{2\pi}. \tag{5.6}$$

So that the decomposition is:

$$d\phi_4 = \frac{d\xi_a}{\xi_a}\frac{d\xi_b}{\xi_b}\left[\frac{d^{4-2\epsilon}q}{(2\pi)^{4-2\epsilon}}(2\pi)\delta(q^2-m_q^2)\theta(q^0)\right]\left[\frac{d^{4-2\epsilon}k}{(2\pi)^{4-2\epsilon}}(2\pi)\delta(k^2-m_k^2)\theta(k^0)\right]\frac{dm_k^2}{2\pi}\frac{dm_q^2}{2\pi}$$
$$\times(2\pi)^{4-2\epsilon}\delta^{(4-2\epsilon)}(\xi_a P_a+\xi_b P_b-k-q)$$
$$\times\frac{d^{4-2\epsilon}q_1}{(2\pi)^{4-2\epsilon}}\frac{d^{4-2\epsilon}q_2}{(2\pi)^{4-2\epsilon}}(2\pi)^2\delta(q_1^2-m_{q_1}^2)\delta(q_2^2-m_{q_2}^2)\theta(q_1^0)\theta(q_2^0)(2\pi)^{4-2\epsilon}\delta^{(4-2\epsilon)}(q-q_1-q_2)$$
$$\times\frac{d^{4-2\epsilon}k_1}{(2\pi)^{4-2\epsilon}}\frac{d^{4-2\epsilon}k_2}{(2\pi)^{4-2\epsilon}}(2\pi)^2\delta(k_1^2-m_{k_1}^2)\delta(k_2^2-m_{k_2}^2)\theta(k_1^0)\theta(k_2^0)(2\pi)^{4-2\epsilon}\delta^{(4-2\epsilon)}(k-k_1-k_2). \quad (5.7)$$

Refer to Fig.5.3 for an illustration of the phase space factorization. The formulas inside the colored boxes in Eq.(5.7) correspond to the phase spaces depicted in the diagrams in the figure.

Thus we can write:

$$d\phi_4 = d\phi_{(p_a p_b\to qk)}\,d\phi_{(q\to q_1 q_2)}\,d\phi_{(k\to k_1 k_2)}, \quad (5.8)$$

where $d\phi_{(p_a p_b\to qk)}$ is already derived the phase space of the decay $2\to 2$ particles (see Eq.(4.73)), $d\phi_{(k\to k_1 k_2)}$ is the $1\to 2$ decay space of the hadronic radiation, and $d\phi_{(q\to q_1 q_2)}\equiv d\phi_L$ leptonic decay phase space. The last one is left untouched, as it will be absorbed into the leptonic factor in Eq.(2.26).

Rewriting $1\to 2$ phase space

Phase space of the $1\to 2$ decay from Eq.(5.7) is:

$$d\phi_{(k\to k_1 k_2)} = \frac{d^{4-2\epsilon}k_1}{(2\pi)^{4-2\epsilon}}\frac{d^{4-2\epsilon}k_2}{(2\pi)^{4-2\epsilon}}(2\pi)^2\delta(k_1^2-m_{k_1}^2)\delta(k_2^2-m_{k_2}^2)\theta(k_1^0)\theta(k_2^0)$$
$$\times(2\pi)^{4-2\epsilon}\delta^{(4-2\epsilon)}(k-k_1-k_2). \quad (5.9)$$

Integrating over k_2 and assuming that the masses of the final states are zero, i.e. that $m_{k_1}=m_{k_2}=0$, we get:

$$d\phi_{(k\to k_1 k_2)} = \frac{d^{4-2\epsilon}k_1}{(2\pi)^{2-2\epsilon}}\delta(k_1^2)\delta((k-k_1)^2)\theta(k_1^0)\theta(k^0-k_1^0)$$
$$= \frac{dk_1^0 d|\vec{k_1}||\vec{k_1}|^{2-2\epsilon}d\Omega^{(3-2\epsilon)}}{(2\pi)^{2-2\epsilon}}\delta((k_1^0)^2-|\vec{k_1}|^2)\delta((k^0)^2-2k^0k_1^0-2\vec{k}\cdot\vec{k_1}+k_1^2)\theta(k_1^0)\theta(k^0-k_1^0) \quad (5.10)$$

where we can now use that $dk_1^0=\frac{d(k_1^0)^2}{2k_1^0}$ and integrate the delta function over $(k_1^0)^2$, which together with the $\theta(k_1^0)$ substitutes $k_1^0\to|\vec{k_1}|$, to obtain:

$$d\phi_{(k\to k_1 k_2)} = \frac{d|\vec{k_1}||\vec{k_1}|^{2-2\epsilon}}{2|\vec{k_1}|}\frac{d\Omega^{(3-2\epsilon)}}{(2\pi)^{2-2\epsilon}}\delta((k^0)^2-2k^0|\vec{k_1}|-2\vec{k}\cdot\vec{k_1})\theta(k^0-|\vec{k_1}|) \quad (5.11)$$

All the three phase factors are Lorentz invariant, so we can work with each in its own reference frame. Therefore, going to the k rest frame, we have:

$$k = E(1,0,0,\dots 0)$$
$$k_1 = \frac{E}{2}(1,\dots,\sin\theta_1\sin\theta_2\cos\theta_3,\sin\theta_1\cos\theta_2,\cos\theta_1)$$
$$k_2 = \frac{E}{2}(1,\dots,-\sin\theta_1\sin\theta_2\cos\theta_3,-\sin\theta_1\cos\theta_2,-\cos\theta_1).$$

We finally obtain:

$$d\phi_{(k\to k_1 k_2)} = \frac{1}{2E}(E/2)^{1-2\epsilon}\frac{d\Omega^{(3-2\epsilon)}}{2(2\pi)^{2-2\epsilon}} = \frac{d\Omega^{(3-2\epsilon)}}{(2\pi)^{2-2\epsilon}}2^{2\epsilon-3}(k^2)^{-\epsilon}, \quad (5.12)$$

where the differential $d\Omega^{(3-2\epsilon)}$ represents integration over $D-2=2-2\epsilon$ angles $\theta_1,\theta_2,\theta_3,\dots$ and one arbitrary azimuthal angle ϕ.

5.2.2 Final cross section

As the final cross section, collecting all the expressions above, integrating and multiplying by a flux factor, we then receive:

$$d\hat{\sigma}^{(n)}_{i,VV',ab} = L_{(\pm)i,VV'} \sum_{k\in X} \int \mathrm{d}\phi_{p_a p_b \to qk} \int d\phi_{k\to k_1 k_2} \frac{|\mathcal{M}^{(n)}_{p_a p_b \to q k_1 k_2, VV'}|^2_i}{2E^2_{cm}} \frac{1}{n_a n_b N_a N_b} \times \text{sym.}$$

$$= L_{(\pm)i,VV'} \sum_{k\in X} \int \frac{(4\pi)^\epsilon}{(4\pi)^2\Gamma(1-\epsilon)} \frac{(q_T^2)^{-\epsilon}}{2E^2_{cm}} \frac{\mathrm{d}k^-\mathrm{d}k^+\mathrm{d}q^-\mathrm{d}q^+\mathrm{d}q_T^2}{(k^-+q^-)(k^++q^+)} \frac{1}{n_a n_b N_a N_b} \int \frac{d\phi_{k\to k_1 k_2}}{2\pi} |\mathcal{M}^{(n)}_{p_a p_b \to q k_1 k_2, VV'}|^2_i \times \text{sym.}$$
$$\times \theta(q^-)\theta(q^+)\theta(k^-)\theta(k^+)\theta(2E_a - k^- - q^-)\theta(2E_b - k^+ - q^+), \tag{5.13}$$

where n_a, n_b and N_a, N_b are the spins and color factors of the incoming particles respectively. sym is the symmetry factor. $|\mathcal{M}_{(p_a p_b \to q k_1 k_2)}|^2_i$ is the helicity matrix element squared, which in our case is equal to contracting the hadronic tensor with relevant projectors.

5.2.3 Master integrals

In this subsection, we focus on integrating the squared matrix element over the variables $k_1^-, k_1^+, k_2^-, k_2^+$. We will express these variables in terms of angular parameters defined in the rest frame of $k = k_1 + k_2$. We will also present the relevant master integrals, which will be used to perform the integration over the angles.

Angular dependencies in propagators

We proceed by expressing the variables $k_1^-, k_1^+, k_2^-, k_2^+$ in terms of angles within the k rest frame frame.

$$k_1^\mu = \frac{\sqrt{k^-k^+ - q_T^2}}{2}(1, \ldots, \cos\theta_3 \sin\theta_2 \sin\theta_1, \cos\theta_2 \sin\theta_1, \cos\theta_1), \tag{5.14a}$$

$$k_2^\mu = \frac{\sqrt{k^-k^+ - q_T^2}}{2}(1, \ldots, -\cos\theta_3 \sin\theta_2 \sin\theta_1, -\cos\theta_2 \sin\theta_1, -\cos\theta_1). \tag{5.14b}$$

Plus (minus) components of these momenta can be achieved by taking a product of k_1 or k_2 with $n = (1, 0, \ldots, 0, 1)(\overline{n} = (1, 0, \ldots, 0, -1)$, which must be boosted from the lab frame to the k center of mass frame.
Transformation from lab frame to the rest frame of k can be written in two steps:

1. Longitudinal boost along k rapidity y_k in z-axis into the gluon frame.

$$\begin{cases} t' = t\cosh y_k - z\sinh y_k, \\ x_1' = x_1, \\ \ldots, \\ x'_{D-3} = x_{D-3}, \\ y' = y, \\ z' = -t\cosh y_k + z\sinh y_k, \end{cases}$$

where in lightcone coordinates $\cosh y_k = \dfrac{k^- + k^+}{2\sqrt{k^-k^+}}$ and $\sinh y_k = \dfrac{k^- - k^+}{2\sqrt{k^-k^+}}$.

2. Transverse boost along $\vec{k}_T$ in y-axis into the rest frame of k.

$$\begin{cases} t'' = \gamma t' - \beta y' \\ x_1'' = x_1', \\ \ldots, \\ x''_{D-3} = x'_{D-3}, \\ y'' = -\beta t' + \gamma y' \\ z'' = z', \end{cases}$$

where $\beta\gamma = \dfrac{k_T}{\sqrt{k^2}} = -\dfrac{q_T}{\sqrt{k^-k^+ - q_T^2}}$ and $\gamma = \dfrac{\sqrt{k^2 + k_T^2}}{\sqrt{k^2}} = \sqrt{\dfrac{k^-k^+}{k^-k^+ - q_T^2}}$.

Therefore, n and $\overline{n}$ boosted to the k rest frame read:

$$n_{\text{boosted}} = \left(\sqrt{\frac{k^-k^+}{k^-k^+ - q_T^2}}\sqrt{\frac{k^+}{k^-}}, 0, \ldots, 0, -\frac{q_T}{\sqrt{k^-k^+ - q_T^2}}\sqrt{\frac{k^+}{k^-}}, \sqrt{\frac{k^+}{k^-}}\right), \tag{5.15a}$$

$$\overline{n}_{\text{boosted}} = \left(\sqrt{\frac{k^-k^+}{k^-k^+ - q_T^2}}\sqrt{\frac{k^+}{k^-}}, 0, \ldots, 0, -\frac{q_T}{\sqrt{k^-k^+ - q_T^2}}\sqrt{\frac{k^+}{k^-}}, -\sqrt{\frac{k^+}{k^-}}\right). \tag{5.15b}$$

Therefore, minus and plus components are as follows:

$$\begin{aligned}
k_1^- &= k_1 \cdot n_{\text{boosted}} = \frac{k^-}{2}\left(1 - \frac{q_T}{\sqrt{k^-k^+}}\cos\theta_2\sin\theta_1 - \sqrt{1 - \frac{q_T^2}{k^-k^+}}\cos\theta_1\right)\\
k_1^+ &= k_1 \cdot \overline{n}_{\text{boosted}} = \frac{k^+}{2}\left(1 - \frac{q_T}{\sqrt{k^-k^+}}\cos\theta_2\sin\theta_1 + \sqrt{1 - \frac{q_T^2}{k^-k^+}}\cos\theta_1\right)\\
k_2^- &= k_2 \cdot n_{\text{boosted}} = \frac{k^-}{2}\left(1 + \frac{q_T}{\sqrt{k^-k^+}}\cos\theta_2\sin\theta_1 + \sqrt{1 - \frac{q_T^2}{k^-k^+}}\cos\theta_1\right)\\
k_2^+ &= k_2 \cdot \overline{n}_{\text{boosted}} = \frac{k^+}{2}\left(1 + \frac{q_T}{\sqrt{k^-k^+}}\cos\theta_2\sin\theta_1 - \sqrt{1 - \frac{q_T^2}{k^-k^+}}\cos\theta_1\right),
\end{aligned}$$

where one could notice that the lightcone components of k_1 and k_2 depend only on two angles θ_1 and θ_2.

Using previous expressions and our definition for $p_a = \xi_a E_a(1, 0, \ldots, 0, 1)$ and $p_b = \xi_b E_b(1, 0, \ldots, 0, -1)$ we can achieve the following expressions for propagators[1] written in terms of k^-, k^+, q_T, as well as their angles in k rest frame

$$(p_a - k_1)^2 = -2\xi_a E_a k_1^+ = -\frac{(k^- + q^-)}{2}k^+\left(1 - \frac{q_T}{\sqrt{k^-k^+}}\cos\theta_2\sin\theta_1 + \sqrt{1 - \frac{q_T^2}{k^-k^+}}\cos\theta_1\right), \tag{5.16a}$$

$$(p_a - k_2)^2 = -2\xi_a E_a k_2^+ = -\frac{(k^- + q^-)}{2}k^+\left(1 + \frac{q_T}{\sqrt{k^-k^+}}\cos\theta_2\sin\theta_1 - \sqrt{1 - \frac{q_T^2}{k^-k^+}}\cos\theta_1\right), \tag{5.16b}$$

$$(p_b - k_1)^2 = -2\xi_b E_b k_1^- = -\frac{(k^+ + q^+)}{2}k^-\left(1 - \frac{q_T}{\sqrt{k^-k^+}}\cos\theta_2\sin\theta_1 - \sqrt{1 - \frac{q_T^2}{k^-k^+}}\cos\theta_1\right), \tag{5.16c}$$

$$(p_b - k_2)^2 = -2\xi_b E_b k_2^- = -\frac{(k^+ + q^+)}{2}k^-\left(1 + \frac{q_T}{\sqrt{k^-k^+}}\cos\theta_2\sin\theta_1 + \sqrt{1 - \frac{q_T^2}{k^-k^+}}\cos\theta_1\right), \tag{5.16d}$$

$$\begin{aligned}
(q + k_1)^2 = 4\xi_a E_a \xi_b E_b - 2\xi_a E_a k_2^+ - 2\xi_b E_b k_2^- = \\
\frac{1}{2}(2q^-q^+ + k^-q^+ + k^+q^-)\left(1 - \frac{q_T}{\sqrt{k^-k^+}}\frac{2k^-k^+ + k^-q^+ + k^+q^-}{2q^-q^+ + k^-q^+ + k^+q^-}\cos\theta_2\sin\theta_1\right.\\
\left. + \sqrt{1 - \frac{q_T^2}{k^-k^+}}\frac{k^+q^- - k^-q^+}{2q^-q^+ + k^-q^+ + k^+q^-}\cos\theta_1\right),
\end{aligned} \tag{5.16e}$$

$$\begin{aligned}
(q + k_2)^2 = 4\xi_a E_a \xi_b E_b - 2\xi_a E_a k_1^+ - 2\xi_b E_b k_1^- = \\
\frac{1}{2}(2q^-q^+ + k^-q^+ + k^+q^-)\left(1 + \frac{q_T}{\sqrt{k^-k^+}}\frac{2k^-k^+ + k^-q^+ + k^+q^-}{2q^-q^+ + k^-q^+ + k^+q^-}\cos\theta_2\sin\theta_1\right.\\
\left. - \sqrt{1 - \frac{q_T^2}{k^-k^+}}\frac{k^+q^- - k^-q^+}{2q^-q^+ + k^-q^+ + k^+q^-}\cos\theta_1\right),
\end{aligned} \tag{5.16f}$$

[1] In this and following sections we use 'propagator' to call the combination of the two momenta $[(p_i \pm k_j)^2]^n$, $i = a, b$ or q, $j = 1, 2$, no matter if the power n is positive or negative, since either way we will have to integrate over this structure. We also use 'propagator' and 'denominator' interchangeably, assuming that the power of the denominator in the squared matrix element can be negative (which corresponds to propagator power being positive)

	$(p_a-k_1)^2$	$(p_a-k_2)^2$	$(p_b-k_1)^2$	$(p_b-k_2)^2$	$(q+k_1)^2$	$(q+k_2)^2$
$(p_a-k_1)^2$	One den, massless (5.18)	Separable	Two den's, both massless (5.22a)	Two den's, both massless (5.22b)	Two den's, one massive (5.23a)	Two den's, one massive (5.23b)
$(p_a-k_2)^2$	Separable	One den, massless (5.18)	Two den's, both massless (5.22b)	Two den's, both massless (5.22a)	Two den's, one massive (5.23b)	Two den's, one massive (5.23a)
$(p_b-k_1)^2$	Two den's, both massless (5.22a)	Two den's, both massless (5.22b)	One den, massless (5.19)	Separable	Two den's, one massive (5.23c)	Two den's, one massive (5.23d)
$(p_b-k_2)^2$	Two den's, both massless (5.22b)	Two den's, both massless (5.22a)	Separable	One den, massless (5.19)	Two den's, one massive (5.23d)	Two den's, one massive (5.23c)
$(q+k_1)^2$	Two den's, one massive (5.23a)	Two den's, one massive (5.23b)	Two den's, one massive (5.23c)	Two den's, one massive (5.23d)	One den, massive (5.20)	Separable
$(q+k_2)^2$	Two den's, one massive (5.23b)	Two den's, one massive (5.23a)	Two den's, one massive (5.23d)	Two den's, one massive (5.23c)	Separable	One den, massive (5.20)

Table 5.1: Possible combinations of propagators, number of unique denominators (den's), their type and corresponding master integrals.

where we have used that ξ_a and ξ_b are put to $\dfrac{k^- + q^-}{2E_a}$ and $\dfrac{k^+ + q^+}{2E_b}$ respectively by the delta function in Eq.(4.69).

Propagators, such as $(p_a + p_b)^2$, are not included in this list, since they do not have an explicit dependence on k_1, k_2 and therefore on the angles. These propagators are not of interest in this subsection. However, certain propagators, such as $(p_a - k_1)^2$, present specific challenges that will be addressed in subsequent sections.

Possible functions of propagators and their integrals

In certain Feynman diagrams, the matrix element squared can involve up to four distinct propagators, each appearing with different powers in both the numerator and denominator. This subsection outlines the method for handling up to two distinct types of denominators. The procedure for reducing the four denominators to two through partial fraction decomposition is described in detail in the following subsection.

The primary challenge arises when dealing with two denominator propagators. Specifically, integrals of the form $(1-\beta_1\cos\phi\sin\theta-\beta_2\cos\theta)^{-j_1}(1+\beta_1\cos\phi\sin\theta-\beta_2\cos\theta)^{-j_2}$ for non-zero positive j_1 and j_2 are non-trivial to evaluate. To address this, we use the general solution for such integrals, as presented in ref. [69]. All subsequent expressions for phase space **master integrals** in this work are drawn from that paper and modified for our propagators.

Table 5.1 provides an overview of the combinations of six types of propagators, along with references to the corresponding integrals and/or the methods for evaluating them.

No denominators

Terms with no dependence on the propagators would be integrated over the $k \to k_1 k_2$ phase space in the following way:

$$C\int \frac{d\phi_{k\to k_1k_2}}{2\pi} = C\frac{2^{2\epsilon-3}}{(2\pi)^{2-2\epsilon}}\frac{1}{2\pi}(k^+k^- - q_T^2)^{-\epsilon}\Omega^{(3-2\epsilon)} = C\frac{(4\pi)^\epsilon}{(k^+k^- - q_T^2)^\epsilon}\frac{1}{(4\pi)^2}\frac{\Gamma(1-\epsilon)}{\Gamma(2-2\epsilon)}, \tag{5.17}$$

where C is some function of p_a, p_b and q, but not of k_1 or k_2.

One denominator, massless

Label 'massless' refers to the square of the p_n, p_m vectors, which are derived from the combination

$$\int \frac{d\phi_{k\to k_1k_2}}{2\pi} \frac{1}{(\text{den } 1)^{j_1}(\text{den } 2)^{j_2}\dots(\text{den N})^{j_N}} = \int \frac{d\phi_{k\to k_1k_2}}{2\pi} \frac{1}{(p_1\cdot q)^{j_1}(p_2\cdot q)^{j_2}\dots(p_N\cdot q)^{j_N}},$$

where $q^\mu = (1,\dots,\cos\phi\sin\theta,\cos\theta)$ and $p_1^\mu \dots p_N^\mu$ are fixed vectors in D dimensional space as introduced in ref. [69]:

$$\begin{aligned}
&p_1^\mu = (1, 0_{D-2}, \beta_1),\\
&p_2^\mu = (1, 0_{D-3}, \beta_2\sin\chi_2^{(1)}, \beta_2\cos\chi_2^{(1)}),\\
&p_3^\mu = (1, 0_{D-4}, \beta_3\sin\chi_3^{(2)}\sin\chi_3^{(1)}, \beta_3\cos\chi_3^{(2)}\sin\chi_3^{(1)}, \beta_3\cos\chi_3^{(1)}),\\
&\vdots\\
&p_N^\mu = (1, 0_{D-1-N}, \beta_N\prod_{k=0}^{N-1}\sin\chi_N^{(k)}, \beta_N\cos\chi_N^{(N-1)}\prod_{k=0}^{N-2}\sin\chi_N^{(k)}, \dots, \beta_N\cos\chi_N^{(2)}\sin\chi_N^{(1)}, \beta_N\cos\chi_N^{(1)}).
\end{aligned}$$

As an illustrative example, see

$$\int \frac{d\phi_{k\to k_1k_2}}{2\pi} \frac{1}{[(p_a-k_1)^2]^{j_1}[(p_b-k_1)^2]^{j_2}},$$

here

$$\begin{aligned}
\left[(p_a-k_1)^2\right]^{j_1} &= -\left[\frac{(k^-+q^-)}{2}k^+\left(1-\frac{q_T}{\sqrt{k^-k^+}}\cos\phi\sin\theta+\sqrt{1-\frac{q_T^2}{k^-k^+}}\cos\theta\right)\right]^{j_1}\\
&= \left[\frac{(k^-+q^-)}{2}k^+\right]^{j_1}(p_2\cdot q)^{j_1},
\end{aligned}$$

where $p_2^\mu = \left(1,0,\dots,0,\frac{q_T}{\sqrt{k^-k^+}},\sqrt{1-\frac{q_T^2}{k^-k^+}}\right)$. Finally, a simple calculation shows that $p_2^2 = 0$. Similar conclusions can be made for $\left[(p_b-k_1)^2\right]^{j_2}$.

'Massless' propagators include: (p_a-k_1), (p_a-k_2), (p_b-k_1) and (p_b-k_2):

$$\begin{aligned}
&\int \frac{d\phi_{k\to k_1k_2}}{2\pi}\frac{1}{[(p_a-k_1)^2]^j} = \int \frac{d\phi_{k\to k_1k_2}}{2\pi}\frac{1}{[(p_a-k_2)^2]^j} =\\
&\quad (-1)^j\frac{(4\pi)^\epsilon}{(k^+k^- - q_T^2)^\epsilon}\left[k^+(k^-+q^-)\right]^{-j}\frac{1}{(4\pi)^2}\frac{\Gamma(1-j-\epsilon)}{\Gamma(2-j-2\epsilon)}.
\end{aligned} \tag{5.18}$$

$$\begin{aligned}
&\int \frac{d\phi_{k\to k_1k_2}}{2\pi}\frac{1}{[(p_b-k_1)^2]^j} = \int \frac{d\phi_{k\to k_1k_2}}{2\pi}\frac{1}{[(p_b-k_2)^2]^j} =\\
&\quad (-1)^j\frac{(4\pi)^\epsilon}{(k^+k^- - q_T^2)^\epsilon}\left[k^-(k^++q^+)\right]^{-j}\frac{1}{(4\pi)^2}\frac{\Gamma(1-j-\epsilon)}{\Gamma(2-j-2\epsilon)}.
\end{aligned} \tag{5.19}$$

One denominator, massive

Similar to the massless case, 'massive' denominators are defined as ones in which vector p_n^μ has a non-zero square. These propagators are: $(q+k_1)^2$ and $(q+k_2)^2$:

$$\begin{aligned}
&\int \frac{d\phi_{k\to k_1k_2}}{2\pi}\frac{1}{[(q+k_1)^2]^j} = \int \frac{d\phi_{k\to k_1k_2}}{2\pi}\frac{1}{[(q+k_2)^2]^j} =\\
&\quad (-1)^j\frac{(4\pi)^\epsilon}{(k^+k^- - q_T^2)^\epsilon}\left[\frac{(k^++q^+)q_T^2}{k^+} - q^+(k^-+q^-)\right]^{-j}\frac{1}{(4\pi)^2}\frac{\Gamma(1-\epsilon)}{\Gamma(2-2\epsilon)}\\
&\qquad\qquad \times {}_2F_1\left(\frac{j}{2},\frac{j+1}{2};\frac{3}{2}-\epsilon;1-\frac{(k^-+q^-)(k^++q^+)\left(q^-q^+-q_T^2\right)}{\left(k^-q^+ + q^-(k^++2q^+)\right)^2}\right),
\end{aligned} \tag{5.20}$$

where ${}_2F_1\left(a,b;c;z\right)$ is an ordinary hypergeometric function, which is defined as power series for $|z|<1$:

$$ {}_2F_1\left(a,b;c;z\right)=\sum_{n=0}^{\infty}\frac{(a)_n(b)_n}{(c)_n}\frac{z^n}{n!}, $$

where $(a)_n$ is a Pochhammer symbol, also known as a rising factorial:

$$ (a)_n=\begin{cases}1, & n=0\\ a(a+1)(a+2)\dots(a+n-1), & n>0.\end{cases} $$

Separable

Cases labeled 'separable' can be separated into terms with one denominator. For example, for $j_1=1,j_2=1$:

$$ \frac{1}{(p_a-k_1)^2(p_a-k_2)^2}=\frac{1}{(p_a-k)^2}\left(\frac{1}{(p_a-k_1)^2}+\frac{1}{(p_a-k_2)^2}\right). \tag{5.21} $$

It is possible to reach similar conclusion for $j_1,j_2>1$ by applying separation procedure recursively. For example:

$$ \begin{aligned}\frac{1}{(p_a-k_1)^2\left[(p_b-k_2)^2\right]^2}&=\frac{1}{(p_a-k)^2}\left(\frac{1}{(p_a-k_1)^2}+\frac{1}{(p_a-k_2)^2}\right)\frac{1}{(p_b-k_2)^2}\\ &=\frac{1}{\left[(p_a-k)^2\right]^2}\left(\frac{1}{(p_a-k_1)^2}+\frac{1}{(p_a-k_2)^2}\right)+\frac{1}{(p_a-k)^2}\frac{1}{\left[(p_a-k_2)^2\right]^2}.\end{aligned} $$

Two denominators, both massless

Full master integrals for two 'massless' denominators are thus:

$$ \begin{aligned}\int\frac{d\phi_{k\to k_1k_2}}{2\pi}\frac{1}{\left[(p_a-k_1)^2\right]^{j_1}\left[(p_b-k_1)^2\right]^{j_2}}&=\int\frac{d\phi_{k\to k_1k_2}}{2\pi}\frac{1}{\left[(p_a-k_2)^2\right]^{j_1}\left[(p_b-k_2)^2\right]^{j_2}}=\\ &(-1)^{j_1+j_2}\frac{(4\pi)^\epsilon}{(k^+k^--q_T^2)^\epsilon}\left[k^+(k^-+q^-)\right]^{-j_1}\left[k^-(k^++q^+)\right]^{-j_2}\\ &\times\frac{1}{(4\pi)^2}\frac{\Gamma(1-j_1-\epsilon)\Gamma(1-j_2-\epsilon)}{\Gamma(1-\epsilon)\Gamma(2-j_1-j_2-2\epsilon)}{}_2F_1\left(j_1,j_2;1-\epsilon;\frac{q_T^2}{k^-k^+}\right).\end{aligned} \tag{5.22a} $$

$$ \begin{aligned}\int\frac{d\phi_{k\to k_1k_2}}{2\pi}\frac{1}{\left[(p_a-k_1)^2\right]^{j_1}\left[(p_b-k_2)^2\right]^{j_2}}&=\int\frac{d\phi_{k\to k_1k_2}}{2\pi}\frac{1}{\left[(p_a-k_2)^2\right]^{j_1}\left[(p_b-k_1)^2\right]^{j_2}}=\\ &(-1)^{j_1+j_2}\frac{(4\pi)^\epsilon}{(k^+k^--q_T^2)^\epsilon}\left[k^+(k^-+q^-)\right]^{-j_1}\left[k^-(k^++q^+)\right]^{-j_2}\\ &\times\frac{1}{(4\pi)^2}\frac{\Gamma(1-j_1-\epsilon)\Gamma(1-j_2-\epsilon)}{\Gamma(1-\epsilon)\Gamma(2-j_1-j_2-2\epsilon)}{}_2F_1\left(j_1,j_2;1-\epsilon;1-\frac{q_T^2}{k^-k^+}\right),\end{aligned} \tag{5.22b} $$

where j_1 and j_2 can be any integer number, both positive and negative.

Two denominators, one massive:

The master integrals for massive cases include Appell functions of the first kind $F_1(a,b_1,b_2;c;z_1,z_2)$. These function are defined for $|x|<1,|y|<1$:

$$ F_1(a,b_1,b_2;c;z_1,z_2)=\sum_{m,n=0}^{\infty}\frac{(a)_{m+n}(b_1)_m(b_2)_n}{(c)_{m+n}m!n!}z_1^mz_2^n. $$

Relevant master integrals are thus:

$$\int \frac{d\phi_{k\to k_1k_2}}{2\pi} \frac{1}{[(q+k_1)^2]^{j_1}\,[(p_a-k_1)^2]^{j_2}} = \int \frac{d\phi_{k\to k_1k_2}}{2\pi} \frac{1}{[(q+k_2)^2]^{j_1}\,[(p_a-k_2)^2]^{j_2}} =$$
$$(-1)^{j_1+j_2} \frac{(4\pi)^\epsilon}{(k^+k^- - q_T^2)^\epsilon} \left[\frac{(k^++q^+)q_T^2}{k^+} - q^+(k^-+q^-)\right]^{-j_1} \left[k^+(k^-+q^-)\right]^{-j_2} \frac{1}{(4\pi)^2} \frac{\Gamma(1-j_2-\epsilon)}{\Gamma(2-j_2-2\epsilon)}$$
$$\times F_1\Bigg(j_1, 1-j_2-\epsilon, 1-j_2-\epsilon, 2-j_2-2\epsilon,$$
$$1 - \frac{k^+\left(\sqrt{4\,(k^-+q^-)\,(k^++q^+)\,q_T^2 + (k^+q^- - k^-q^+)^{\,2}} + k^-q^+ + q^-\,(k^+ + 2q^+)\right)}{2k^+q^+\,(k^-+q^-) - 2\,(k^++q^+)\,q_T^2}$$
$$1 - \frac{k^+\left(-\sqrt{4\,(k^-+q^-)\,(k^++q^+)\,q_T^2 + (k^+q^- - k^-q^+)^{\,2}} + k^-q^+ + q^-\,(k^+ + 2q^+)\right)}{2k^+q^+\,(k^-+q^-) - 2\,(k^++q^+)\,q_T^2}\Bigg). \tag{5.23a}$$

$$\int \frac{d\phi_{k\to k_1k_2}}{2\pi} \frac{1}{[(q+k_1)^2]^{j_1}\,[(p_a-k_2)^2]^{j_2}} = \int \frac{d\phi_{k\to k_1k_2}}{2\pi} \frac{1}{[(q+k_2)^2]^{j_1}\,[(p_a-k_1)^2]^{j_2}} =$$
$$(-1)^{j_1+j_2} \frac{(4\pi)^\epsilon}{(k^+k^- - q_T^2)^\epsilon} \left[-\frac{(k^++q^+)(k^+q^- + q_T^2)}{k^+}\right]^{-j_1} \left[k^+(k^-+q^-)\right]^{-j_2} \frac{1}{(4\pi)^2} \frac{\Gamma(1-j_2-\epsilon)}{\Gamma(2-j_2-2\epsilon)}$$
$$\times F_1\Bigg(j_1, 1-j_2-\epsilon, 1-j_2-\epsilon, 2-j_2-2\epsilon,$$
$$1 - \frac{k^+\left(\sqrt{4\,(k^-+q^-)\,(k^++q^+)\,q_T^2 + (k^+q^- - k^-q^+)^{\,2}} + k^-q^+ + q^-\,(k^+ + 2q^+)\right)}{2\,(k^++q^+)\,(k^+q^- + q_T^2)}$$
$$1 - \frac{k^+\left(-\sqrt{4\,(k^-+q^-)\,(k^++q^+)\,q_T^2 + (k^+q^- - k^-q^+)^{\,2}} + k^-q^+ + q^-\,(k^+ + 2q^+)\right)}{2\,(k^++q^+)\,(k^+q^- + q_T^2)}\Bigg). \tag{5.23b}$$

$$\int \frac{d\phi_{k\to k_1k_2}}{2\pi} \frac{1}{[(q+k_1)^2]^{j_1}\,[(p_b-k_1)^2]^{j_2}} = \int \frac{d\phi_{k\to k_1k_2}}{2\pi} \frac{1}{[(q+k_2)^2]^{j_1}\,[(p_b-k_2)^2]^{j_2}} =$$
$$(-1)^{j_1+j_2} \frac{(4\pi)^\epsilon}{(k^+k^- - q_T^2)^\epsilon} \left[\frac{(k^-+q^-)q_T^2}{k^-} - q^-(k^++q^+)\right]^{-j_1} \left[k^-(k^++q^+)\right]^{-j_2} \frac{1}{(4\pi)^2} \frac{\Gamma(1-j_2-\epsilon)}{\Gamma(2-j_2-2\epsilon)}$$
$$\times F_1\Bigg(j_1, 1-j_2-\epsilon, 1-j_2-\epsilon, 2-j_2-2\epsilon,$$
$$1 - \frac{k^-\left(\sqrt{4\,(k^-+q^-)\,(k^++q^+)\,q_T^2 + (k^+q^- - k^-q^+)^{\,2}} + k^-q^+ + q^-\,(k^+ + 2q^+)\right)}{2k^-q^-\,(k^++q^+) - 2\,(k^-+q^-)\,q_T^2}$$
$$1 - \frac{k^-\left(-\sqrt{4\,(k^-+q^-)\,(k^++q^+)\,q_T^2 + (k^+q^- - k^-q^+)^{\,2}} + k^-q^+ + q^-\,(k^+ + 2q^+)\right)}{2k^-q^-\,(k^++q^+) - 2\,(k^-+q^-)\,q_T^2}\Bigg). \tag{5.23c}$$

$$\int \frac{d\phi_{k\to k_1k_2}}{2\pi} \frac{1}{[(q+k_1)^2]^{j_1}\,[(p_b-k_2)^2]^{j_2}} = \int \frac{d\phi_{k\to k_1k_2}}{2\pi} \frac{1}{[(q+k_2)^2]^{j_1}\,[(p_b-k_1)^2]^{j_2}} =$$

$$(-1)^{j_1+j_2} \frac{(4\pi)^\epsilon}{(k^+k^- - q_T^2)^\epsilon} \left[-\frac{(k^-+q^-)(k^-q^+ + q_T^2)}{k^-}\right]^{-j_1} \left[k^-(k^+ + q^+)\right]^{-j_2} \frac{1}{(4\pi)^2} \frac{\Gamma(1-j_2-\epsilon)}{\Gamma(2-j_2-2\epsilon)}$$

$$\times F_1\Bigg(j_1, 1-j_2-\epsilon, 1-j_2-\epsilon, 2-j_2-2\epsilon,$$

$$1 - \frac{k^-\left(\sqrt{4\,(k^-+q^-)\,(k^++q^+)\,q_T^2 + (k^+q^- - k^-q^+)^{\,2}} + k^-q^+ + q^-\,(k^+ + 2q^+)\right)}{2\,(k^-+q^-)\,(k^-q^+ + q_T^2)}$$

$$1 - \frac{k^-\left(-\sqrt{4\,(k^-+q^-)\,(k^++q^+)\,q_T^2 + (k^+q^- - k^-q^+)^{\,2}} + k^-q^+ + q^-\,(k^+ + 2q^+)\right)}{2\,(k^-+q^-)\,(k^-q^+ + q_T^2)}\Bigg). \tag{5.23d}$$

Levi-Civita terms

Some of the integrants have terms proportional to $\epsilon^{\mu\nu\alpha\beta}k_{1\mu}k_{2\nu}p_{a\alpha}p_{b\beta} \equiv \epsilon^{k_1k_2p_ap_b}$, which create some trouble during angular integration.
In this subsection we will explain how we deal with these terms and why they do not play a role in our computation.

Physical reasoning:

As discussed in the previous subsection, in the k rest frame, the momenta k_1^μ and k_2^μ depend on $D-2$ angular variables: $\theta_1, \theta_2, \ldots, \theta_{D-2}$ (see Eqs. (5.14a) and (5.14b)). The momenta p_a^μ and p_b^μ can be boosted into the k rest frame, taking the same form as n_{boosted} in Eq.(5.15a) and $\overline{n}_{\text{boosted}}$ in Eq.(5.15b), respectively.

As shown in Eqs. (5.15a) and (5.15b), both vectors have at most two non-zero spatial components. As a result, their contractions with k_1 and k_2 lead to a final expression that depends only on two angles: θ_1 and θ_2. This is the case that we see in the propagators in Eq.(5.16a)-(5.16f).

However, the Levi-Civita tensor $\epsilon^{\mu\nu\rho\sigma}p_{a\nu}p_{b\rho}k_{1\sigma}$ resides in the space orthogonal to both p_a and p_b. As a result, it must include a non-zero third component, which, when contracted with $k_{2\mu}$, introduces a new angular variable, denoted as θ_3 in the $\cos\theta_3$.

Although θ_3 appears in the system, its contribution vanishes upon integration over this angle:

$$\int\int f(\theta_1,\theta_2)\int_0^\pi d\theta_3 \cos\theta_3 \sin^{-1-2\epsilon}\theta_3 = 0. \tag{5.24}$$

This means that the contribution from the angle θ_3 does not affect the final result. Since the only object where the dependence on θ_3 can appear in is the Levi-Civita tensor, its contribution would lead to zero result.

Computation for four dimensions:

The contraction of the Levi-Civita symbol with four-momenta can be expressed as the determinant of the momenta components:

$$\epsilon^{\mu\nu\alpha\beta}k_{1\mu}k_{2\nu}p_{a\alpha}p_{b\beta} = \det\begin{pmatrix} k_1^{(0)} & k_1^{(1)} & k_1^{(2)} & k_1^{(3)} \\ k_2^{(0)} & k_2^{(1)} & k_2^{(2)} & k_2^{(3)} \\ p_a^{(0)} & p_a^{(1)} & p_a^{(2)} & p_a^{(3)} \\ p_b^{(0)} & p_b^{(1)} & p_b^{(2)} & p_b^{(3)} \end{pmatrix} = \frac{1}{2}(k^-+q^-)(k^++q^+)(k_1^{(2)}k_2^{(1)} - k_1^{(1)}k_2^{(2)}), \tag{5.25}$$

where the last step uses the definitions of the 0th and 3rd components of k_1, k_2, p_a, and p_b provided earlier.

The 1st and 2nd components of k_1 and k_2 can be obtained by boosting k_1 and k_2 in the rest frame of k along the directions corresponding to the vectors $(0,1,0,0)$ and $(0,0,1,0)$, respectively.

Using the transformations defined in subsection 5.2.3, the boosted vectors take the following form:

$$(0,1,0,0)_{\text{boosted}} = (0,1,0,0),$$
$$(0,0,1,0)_{\text{boosted}} = \left(\frac{q_T}{\sqrt{k^-k^+ - q_T^2}}, 0, \sqrt{\frac{k^-k^+}{k^-k^+ - q_T^2}}, 0\right).$$

Thus, the 1st and 2nd components of k_1 and k_2 are:

$$\begin{aligned}
k_1^{(1)} &= \frac{\sqrt{k^-k^+ - q_T^2}}{2}\sin\phi\sin\theta, \\
k_1^{(2)} &= \frac{1}{2}\left(q_T + \cos\phi\sin\theta\sqrt{k^-k^+}\right), \\
k_2^{(1)} &= \frac{\sqrt{k^-k^+ - q_T^2}}{2}(-\sin\phi\sin\theta), \\
k_2^{(2)} &= \frac{1}{2}\left(q_T - \cos\phi\sin\theta\sqrt{k^-k^+}\right).
\end{aligned}$$

Thus, the contraction of the Levi-Civita tensor becomes:

$$\epsilon^{k_1k_2p_ap_b} = \frac{1}{2}q_T\sqrt{k^-k^+ - q_T^2}\sin\phi\sin\theta.$$

Since $\sin\phi$ only appears in the Levi-Civita contraction and is an odd function, its integration over the angular range results in zero:

$$\int_0^\pi d\theta \int_0^{2\pi} d\phi \sin\phi f(\sin\theta, \cos\phi, \cos\theta) = 0.$$

As a consequence, any contributions from terms proportional to $\epsilon^{k_1k_2p_ap_b}$ vanish after integration, leading these terms to not appear in the final expression.

5.2.4 Partial fraction decomposition

From the Feynman rules, we observe that the matrix element squared can contain up to four unique denominators. We have previously described the method for performing angular integration in cases with up to two denominators. Here, we will briefly outline the process of simplifying the initial expression, reducing it to terms that contain no more than two unique denominators.

In general, a fraction that has m variables $\{x_i\}, x_1 = 1$ and is factorised into a product of n terms (denominators) can be partial fraction decomposed in the following way:

$$\frac{1}{\prod_{k=1}^{n}\left(\sum_{i=1}^{m} M_{ki}x_i\right)} = \sum_{j=1}^{n} \frac{c_j}{\prod_{\substack{k=1\\k\neq j}}^{n}\left(\sum_{i=1}^{m} M_{ki}x_i\right)}, \tag{5.26}$$

where $\sum_{j=1}^{n}\sum_{i=1}^{m} c_jM_{ji}x_i = 1$. Using the fact that all variables $\{x_i\}$ are independent with respect to each other, it is possible to find values for the coefficients: $\sum_{j=1}^{n} c_jM_{ji} = \delta_{mi}$.

The system of equations for this would look like:

$$\begin{cases}
c_1M_{11} + c_2M_{21} + \cdots + c_nM_{n1} = 0, \\
c_1M_{12} + c_2M_{22} + \cdots + c_nM_{n2} = 0, \\
\vdots \\
c_1M_{1m} + c_2M_{2m} + \cdots + c_nM_{nn} = 1.
\end{cases} \tag{5.27}$$

Returning to propagators, it is useful to parameterize our angular dependence in the propagators

using independent variables x and y:

$$(p_a - k_1)^2 = -\frac{(k^- + q^-)}{2} k^+ (1 - x)\,, \tag{5.28a}$$

$$(p_a - k_2)^2 = -\frac{(k^- + q^-)}{2} k^+ (1 + x)\,, \tag{5.28b}$$

$$(p_b - k_1)^2 = -\frac{(k^+ + q^+)}{2} k^- (1 - y)\,, \tag{5.28c}$$

$$(p_b - k_2)^2 = -\frac{(k^+ + q^+)}{2} k^- (1 + y)\,, \tag{5.28d}$$

$$(q + k_1)^2 = \frac{1}{2}\left(k^+ q^- + k^- q^+ + 2q^- q^+ - k^+ x(k^- + q^-) - k^- y(k^+ + q^+)\right), \tag{5.28e}$$

$$(q + k_2)^2 = \frac{1}{2}\left(k^+ q^- + k^- q^+ + 2q^- q^+ + k^+ x(k^- + q^-) + k^- y(k^+ + q^+)\right), \tag{5.28f}$$

where we have written

$$x = \frac{q_T}{\sqrt{k^- k^+}} \cos\theta_2 \sin\theta_1 - \sqrt{1 - \frac{q_T^2}{k^- k^+}} \cos\theta_1,$$

$$y = \frac{q_T}{\sqrt{k^- k^+}} \cos\theta_2 \sin\theta_1 + \sqrt{1 - \frac{q_T^2}{k^- k^+}} \cos\theta_1.$$

We can now apply Eq.(5.26) to perform partial fraction decomposition on the combination of four denominators, reducing it to a sum of four terms, each with three denominators. By repeating this procedure, we obtain 12 terms, each with two denominators, which can then be integrated using master integrals.

5.3 PDF renormalization for double-real term

After computing the matrix elements squared, integrating them using master integrals and finally multiplying the results by the appropriate phase space measure given in Eq. (5.13), we get the integrated contribution from the double-real processes at NNLO. However, these terms contain leftover infrared divergences, which must be canceled in order to obtain a finite physical cross section.

To cancel these IR poles, we apply the PDF renormalization procedure according to the general prescription given by the master formula in Eq. (2.40). Here, the bare NNLO cross section $\sigma^{\text{bare }(2)}_{i,\,ab}$ corresponds to our integrated and phase-space-weighted RR result for a helicity configuration i and incoming partons a and b, while the bare NLO cross section $\sigma^{\text{bare }(1)}_{i,\,ab}$ represents the single-real contribution that enters the convolution with the DGLAP splitting functions P_{ij}. Specifically, the relevant single-real helicity cross sections are obtained by integrating the NLO matrix elements over the $2 \to 2$ final-state phase space, as defined in Eq. (4.74). The not yet integrated structure functions for the $qg \to Vq$ and $q\bar{q} \to Vg$ channels are given in Eqs. (4.55a) and (4.56a), respectively. The necessary splitting functions used for PDF renormalization appear in Appendix D.

As an illustration of the PDF renormalization procedure, we focus on the $qq \to Vqq$ channel. This case is particularly simple in the context of PDF counterterms, as it involves the fewest single-real subtraction terms.

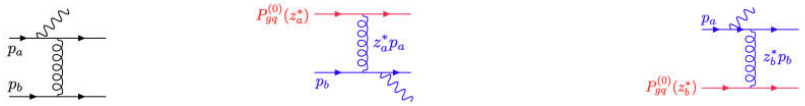
The renormalized second-order partonic cross section for this channel is given by:

$$\begin{aligned}\hat{\sigma}^{(2)}_{i,qq}(p_a,p_b,q) = \hat{\sigma}^{\text{bare }(2)}_{i,qq}(p_a,p_b,q) &+ \frac{1}{\epsilon}\frac{P^{(0)}_{gq}(z^*_a)}{\Delta^*_a}\bar{\sigma}^{\text{bare }(1)}_{i,gq}(z^*_a p_a,p_b,q) + \frac{1}{\epsilon}\frac{P^{(0)}_{qq}(z^*_a)}{\Delta^*_a}\bar{\sigma}^{\text{bare }(1)}_{i,qq}(z^*_a p_a,p_b,q) \\ &+ \frac{1}{\epsilon}\frac{P^{(0)}_{gq}(z^*_b)}{\Delta^*_b}\bar{\sigma}^{\text{bare }(1)}_{i,gq}(p_a,z^*_b p_b,q) + \frac{1}{\epsilon}\frac{P^{(0)}_{qq}(z^*_b)}{\Delta^*_b}\bar{\sigma}^{\text{bare }(1)}_{i,qq}(p_a,z^*_b p_b,q),\end{aligned} \tag{5.29}$$

where the functions $P^{(0)}_{ij}(z)$ are the leading-order DGLAP splitting kernels, and $\Delta^*_{a,b}$ are the corresponding Jacobians from the collinear phase space mappings.

In this particular channel, the counterterms involving $\bar{\sigma}^{\text{bare }(1)}_{i,qq}$ vanish, since there is no single-real process with two incoming quarks that produces a final state with only one additional parton. Therefore, only the qg and gq channels contribute nontrivially to the subtraction.

With the vanishing $\bar{\sigma}^{(1)}_{i,qq}$ terms removed, the renormalized $qq \to Vqq$ cross section simplifies to



$$\hat{\sigma}^{(2)}_{i,qq}(p_a,p_b,q) = \hat{\sigma}^{\text{bare }(2)}_{i,qq}(p_a,p_b,q) + \frac{1}{\epsilon}\frac{P^{(0)}_{gq}(z^*_a)}{\Delta^*_a}\bar{\sigma}^{\text{bare }(1)}_{i,gq}(z^*_a p_a,p_b,q) + \frac{1}{\epsilon}\frac{P^{(0)}_{gq}(z^*_b)}{\Delta^*_b}\bar{\sigma}^{\text{bare }(1)}_{i,qg}(p_a,z^*_b p_b,q), \tag{5.30}$$

where to help visualize the structure of these terms, we use colors to separate the two main components of each counterterm both in the Eq. (5.30) and in the figure above Eq. (5.30):

- In red we show the splitting function factors $P^{(0)}_{gq}(z)$, which arise from PDF renormalization and represent the collinear emission probabilities for partons inside the proton.
- In blue we highlight the single-real matrix elements, $\bar{\sigma}^{(1)}_{i,gq}$ and $\bar{\sigma}^{(1)}_{i,qg}$, evaluated with rescaled momenta due to initial-state parton momentum fraction shifts $z^*_{a,b}$.

So each term in the subtraction corresponds to the convolution of a splitting function with a lower-order partonic cross section, capturing the collinear structure that must be absorbed into the PDFs to ensure that the physical cross section is IR finite.

As a specific example, consider the helicity channel $i = 0$. The terms entering the counterterms are:

$$\frac{1}{\epsilon}\frac{P_{gq}^{(0)}(z_a^*)}{\Delta_a^*}\frac{1}{2E_{cm}^2}\underbrace{L_+(q^2)\left(\mathrm{d}\phi_{gq\to Vq}\langle|\mathcal{M}_{gq\to Zq}^{(1),R}|_0^2\rangle(z_a^* p_a, p_b, q)\right)}_{\bar{\sigma}_{i,gq}^{(1)}},$$

$$\frac{1}{\epsilon}\frac{P_{gq}^{(0)}(z_b^*)}{\Delta_b^*}\frac{1}{2E_{cm}^2}\underbrace{L_+(q^2)\left(\mathrm{d}\phi_{qg\to Vq}\langle|\mathcal{M}_{qg\to Zq}^{(1),R}|_0^2\rangle(p_a, z_b^* p_b, q)\right)}_{\bar{\sigma}_{i,qg}^{(1)}}.$$

The corresponding helicity matrix elements squared for the single-real processes in $D = 4$ dimensions[2] are given below. These expressions are rescaled by the momentum fractions z_a^* and z_b^*, and the kinematics is expressed in terms of massive Mandelstam variables as defined in Chapter 4.4:

$$\begin{aligned}|\mathcal{M}_{gq\to Zq}^{(1),R}|_0^2(z_a^* p_a, p_b, q) &\overset{D=4}{=} C_A C_F g_s^2 g_Z^2 (a_f^2 + v_f^2)\\ &\times \frac{-z_a^*(Q^2-u)\left(t(3s+2u)+(2s+u)^2\right)+s{z_a^*}^2(Q^2+s)^2-2t(Q^2-u)^2}{z_a^* s(Q^2-u)(Q^2-t)}\end{aligned} \tag{5.31}$$

$$\begin{aligned}|\mathcal{M}_{qg\to Zq}^{(1),R}|_0^2(p_a, z_b^* p_b, q) &\overset{D=4}{=} C_A C_F g_s^2 g_Z^2 (a_f^2 + v_f^2))\\ &\times \frac{-z_b^*(Q^2-t)\left(u(3s+2t)+(2s+t)^2\right)+s{z_b^*}^2(Q^2+s)^2-2u(Q^2-t)^2}{s z_b^*(Q^2-u)(Q^2-t)}\end{aligned} \tag{5.32}$$

The relevant phase space factor, which here includes the averaging over the spins and color, is taken from Eq. (4.73)[3]:

$$\begin{aligned}\mathrm{d}\phi_{qg\to Vq} = \mathrm{d}\phi_{gq\to Vq} =& \frac{\mathrm{d}k^-\mathrm{d}k^+\mathrm{d}q^-\mathrm{d}q^+\mathrm{d}q_T^2}{(4\pi)^2 s z_a^*}\frac{1}{4C_A\left(C_A^2-1\right)}\\ &\times\theta(q^-)\theta(q^+)\theta(k^-)\theta(k^+)\theta(2E_a-k^--q^-)\theta(2E_b-k^+-q^+),\end{aligned} \tag{5.33}$$

where z_a^* should be replaced by z_b^* for the corresponding counterterm.
The leading-order splitting function entering the PDF renormalization is:

$$P_{gq}^{(0)}(z_a) = \frac{2C_F\left((1-z_a)^2+1\right)}{z_a}. \tag{5.34}$$

Finally, the momentum fractions and their corresponding Jacobians in terms of massive Mandelstam variables are:

$$z_a^* = \frac{s_2+u}{u}, \quad z_a^* = \frac{s_2+t}{t}, \tag{5.35}$$

$$\Delta_a^* = -u, \qquad \Delta_b^* = -t. \tag{5.36}$$

Taken together, these components form the full set of counterterms, which precisely cancel the infrared poles in the $i = 0$ component of the RR $qq \to Vqq$ cross section. The same cancellation mechanism holds for all other helicities and all the RR channels as well, ensuring the infrared finiteness of the renormalized result, as can be seen in Figure 5.4.

[2]For the cancellation of IR poles it is sufficient to evaluate the NLO structure functions at $D = 4$. However, to ensure full consistency, including effects from the γ_5 prescription, the $\mathcal{O}(\epsilon)$ terms should be retained in the complete calculation.

[3]Note that the counterterm here corresponds to not only the partonic cross section $\hat{\sigma}$, due to the inclusion of the PDF convolution measure in the phase space. However, the difference is only in normalization, so either form can be used as long as consistency is maintained – and we have used the same phase space expression for all the R, RV and RR, so that it is consistent.

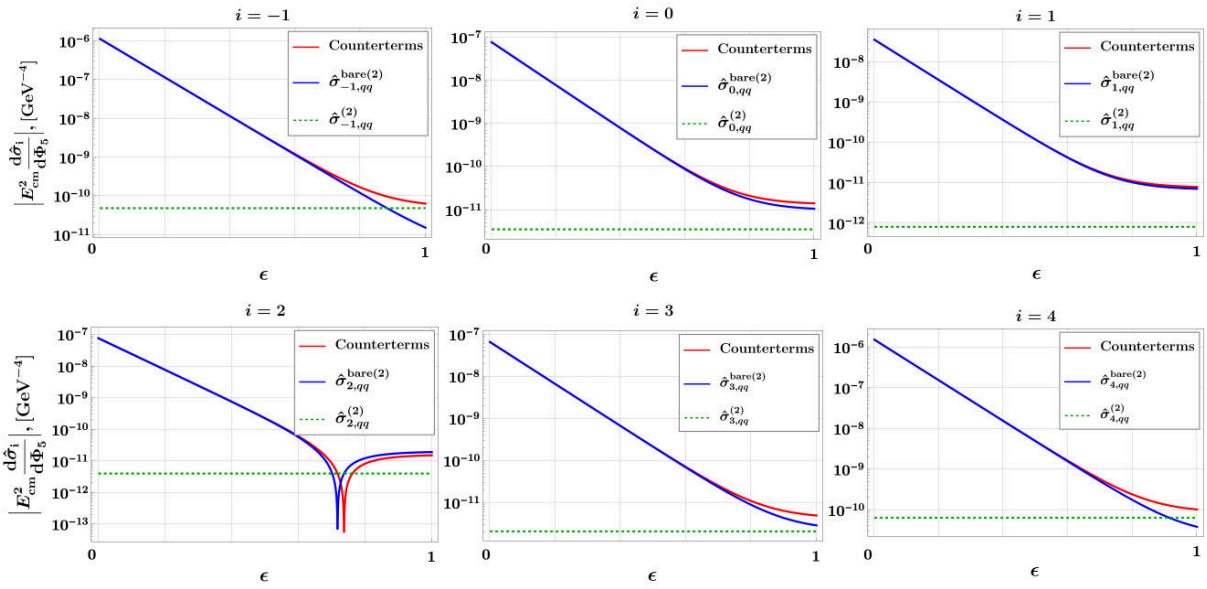


Figure 5.4: Cancellation of infrared poles in the double-real contribution across helicity channels $i = -1, 0, 1, 2, 3, 4$ for $qq \to Vqq$ channel. The blue curve shows the bare RR cross section $\hat{\sigma}_i^{\text{bare}\,(2)}$ as a function of the dimensional regulator ϵ, while the red curve represents the corresponding counterterm contribution from PDF renormalization. The green dashed line indicates the finite renormalized result $\hat{\sigma}_i^{(2)}$, obtained after subtraction. The rapid drop of the red and blue curves and their near-perfect overlap confirm that the counterterms cancel the IR poles precisely, leaving a finite remainder in the $\epsilon \to 0$ limit. Plots done for $\mu = Q = m_Z, q_T = 10$ GeV, $y_Z = 0, y_k = 2, k^2 = 100$ GeV, $\mathrm{d}\Phi_5 = \mathrm{d}k^+\mathrm{d}k^-\mathrm{d}q^+\mathrm{d}q^-\mathrm{d}q_T^2$ and without leptonic prefactors.

5.4 γ_5 scheme for double-real terms

Since we work with dimensional regularization for the RR terms, we also need to specify the γ^5 scheme used in the calculation.

Choosing a consistent and well-defined scheme is important, since certain structure functions – particularly those proportional to $v_f a_f$, such as W_3 and W_4 – are directly affected by the definition of γ^5 starting at order $\mathcal{O}(\alpha_s^2)$. These structure functions are among the main new results of this work, as they had not been computed analytically before, therefore having a consistent treatment of γ^5 is as crucial as it can get.

In general, any self-consistent γ^5 scheme can introduce scheme-dependent counterterms into the bare cross sections, both at LO_2:

$$\hat{\sigma}^{\text{bare},(2)}_{i,\mathrm{X}}(p_a,p_b,q) = \begin{cases} \frac{1}{\epsilon}\Big[c_1(p_a,p_b,q)\cdot(v_f^2+a_f^2)\Big] + c_2(p_a,p_b,q)\cdot(v_f^2+a_f^2) + c_{\mathrm{X}}(p_a,p_b,q)\cdot a_f^2, & i\in\{-1,0,1,2\}, \\ \frac{1}{\epsilon}[d_1(p_a,p_b,q)\cdot a_f v_f] + d_2(p_a,p_b,q)\cdot a_f v_f + d_{\mathrm{X}}(p_a,p_b,q)\cdot a_f v_f, & i\in\{3,4\}, \end{cases} \tag{5.37}$$

and at LO_1:

$$\hat{\sigma}^{(1)}_{i,\mathrm{X}}(p_a,p_b,q) = \begin{cases} c_1'(p_a,p_b,q)\cdot(v_f^2+a_f^2) + \epsilon\, c_{\mathrm{X}}'(p_a,p_b,q)\cdot a_f^2, & i\in\{-1,0,1,2\}, \\ d_1'(p_a,p_b,q)\cdot a_f v_f + \epsilon\, d_{\mathrm{X}}'(p_a,p_b,q)\cdot a_f v_f, & i\in\{3,4\}. \end{cases} \tag{5.38}$$

Here, $\hat{\sigma}_{i,\mathrm{X}}$ denotes the partonic helicity cross section computed in some specific γ^5 scheme "X". The coefficients c_1, c_2, d_1, d_2, etc., are general functions of the external momenta. The scheme dependence enters at subleading order in ϵ, affecting the finite part of the RR cross section through additional c_{X} and d_{X} contributions and the $\mathcal{O}(\epsilon)$ R cross section through c'_{X} and d'_{X} terms.

Note that these counterterms are different than the ones we introduced through PDF renormalization. These ones are inherent to the γ^5 scheme and are related to the modifications of the axial current in it. In general, the counterterms c_{X} and d_{X} should be included in the explicit computation of the bare cross section. However, as could be seen below, for the RR terms, their precise form is irrelevant, as these

axial-current-related terms cancel between the RR and R contributions during PDF renormalization, therefore only a consistent γ^5 scheme is required. The only place where they could have a physical effect is in the RV terms. But since we use spinor-helicity results from the literature, which have to already include these counterterms implicitly, we do not need to track them explicitly.

In this project, we examined several different γ^5 schemes for the RR contributions, each with its own set of advantages and limitations.
Our first approach was to use the **naive anticommutation (NAC)** scheme:

1. We assume that γ^5 anticommutes with all other gamma matrices. Consequently, all Dirac traces containing an even number of γ^5 factors can be rewritten as traces involving only standard gamma matrices:

$$\mathrm{Tr}[\gamma^{\mu_1}\gamma^{\mu_2}\gamma^5\gamma^{\mu_3}\dots\gamma^{\mu_{2n}}\gamma^5] \to \mathrm{Tr}[\gamma^{\mu_1}\gamma^{\mu_2}\gamma^{\mu_3}\dots\gamma^{\mu_{2n}}].$$

2. The traces with a single γ^5 and odd number of other gamma matrices are set to zero.

3. The problematic cases are traces with a single γ^5 and an even number of other gamma matrices. Using the anticommutation relation, such traces can always be rewritten as a string of gamma matrices with a single γ^5 at the end of the trace. Finally, we replace the γ^5 using the Levi-Civita definition:

$$\gamma^5 = -\frac{i}{4!}\epsilon^{abcd}\gamma_a\gamma_b\gamma_c\gamma_d. \tag{5.39}$$

In processes where the hadronic tensor contains only a single fermion trace involving γ^5 – such as in $q\bar{q} \to Zq\bar{q}$ S-channel or T-channel diagrams with Q_u^2 – this scheme preserves the expected coupling structure, since the vector boson couples to only one fermion line. However, complications arise in processes with two separate fermion lines contributing γ^5 traces, such as the T-channel $q\bar{q} \to Zq\bar{q}$ diagrams with Q_uQ_d couplings. In such cases, it is not immediately clear why this scheme should still reproduce the correct coupling structure proportional to $v_uv_d + a_ua_d$. Here we refer to the discussion in ref. [23], which treats RR processes including the T-channel interference. There it is argued that for certain *fully finite* RR diagrams (i.e. the ones that do not require PDF renormalization, so the T-channel interference), the final result is independent of the γ^5 prescription, as long as the result preserves the coupling structure. We observe that the NAC scheme preserves this structure. This implies that

$$c_{\mathrm{NAC}}(p_a, p_b, q) = c'_{\mathrm{NAC}}(p_a, p_b, q) = 0.$$

While simple, this scheme is ultimately problematic, as it ignores subtle issues with the (anti)commutation of γ^5 under dimensional regularization. For example, in the computation of RR structure functions W_5 and W_6 ($\sim v_fa_f$) – which should vanish after phase space integration, we found that the squared matrix elements contain explicit ϵ-dependent terms. In diagrams like the T-channel $q\bar{q} \to Zq\bar{q}$ with Q_u^2 couplings, these ϵ terms can combine with $1/\epsilon$ poles from master integrals, resulting in spurious finite contributions, which are not canceled even after the PDF renormalization, since NAC scheme produces $d'_{\mathrm{NAC}} = 0$ in single-real cross section. Therefore and moreover, this scheme lacks a principled way to predict the scheme-dependent terms d_{NAC} that appear in the v_fa_f-type structure functions. As such, its use in there structure functions beyond leading-order in ϵ is not well-justified.

Next, we turn to the **Larin** γ^5 scheme [70], which we adopt in our current analysis. In this scheme, γ^5 does *not* anticommute with the other Dirac matrices. Instead, any occurrences of $\gamma_\mu\gamma^5$ in the axial-vector currents, before they even appear in traces, are replaced by

$$\gamma_\mu\gamma^5 = \frac{i}{6}\epsilon_{\mu\nu\rho\sigma}\gamma^\nu\gamma^\rho\gamma^\sigma. \tag{5.40}$$

Note that this scheme computationally is much more time consuming, as it increases the amount Dirac gamma matrices in the traces.

Importantly, this scheme leads to explicit non-zero values for the scheme-dependent terms $c_{\mathrm{L}}, c'_{\mathrm{L}}$, and potentially also for $d_{\mathrm{L}}, d'_{\mathrm{L}}$. However, both sets of terms in RR and R originate from the same the modified treatment of axial currents and as a result, they cancel once inserted into the PDF renormalization master

formula:

$$\begin{aligned}
\hat{\sigma}^{(2)}_{i,\mathrm{L}}(p_a,p_b,q) &= \hat{\sigma}^{\text{bare, }(2)}_{i,\mathrm{L}}(p_a,p_b,q) + \frac{1}{\epsilon}P\otimes\hat{\sigma}^{(1)}_{i,\mathrm{L}}(p_a,p_b,q),\\
\hat{\sigma}^{(2)}_{i,\mathrm{L}}(p_a,p_b,q) &= \left[\frac{1}{\epsilon}\left(c_1(p_a,p_b,q)\cdot(v_f^2+a_f^2)\right) + c_2(p_a,p_b,q)(v_f^2+a_f^2) + c_{\mathrm{L}}(p_a,p_b,q)\cdot a_f^2\right]\\
&\qquad - \left[\frac{1}{\epsilon}P\otimes\left(\left(c_1'(p_a,p_b,q)\cdot(v_f^2+a_f^2)\right) + \epsilon c_{\mathrm{L}}'(p_a,p_b,q)\cdot a_f^2\right)\right],\\
&\Rightarrow \frac{1}{\epsilon}c_1(p_a,p_b,q) - \frac{1}{\epsilon}P\otimes c_1'(p_a,p_b,q) = 0\\
&\Rightarrow c_{\mathrm{L}}(p_a,p_b,q) - \frac{1}{\epsilon}P\otimes\epsilon c_{\mathrm{L}}'(p_a,p_b,q) = 0,
\end{aligned}$$

Since the combinations of c_{L} and c_{L}' cancel, this scheme reproduces the same results as the naive anti-commutation scheme for the structure functions proportional to $v_f^2+a_f^2$. In the NAC, the correctness of these terms is ensured axiomatically by construction, so this agreement provides a strong consistency check for the Larin.
As an example of the LO_1 $\left|\mathcal{M}^{(1),\mathrm{R}}_{qg\to Zq}\right|^2_0$ contributions in D dimensions computed throught the Larin scheme see the following expression:

$$\begin{aligned}
\left|\mathcal{M}^{(1),\mathrm{R}}_{qg\to Zq}\right|^2_0(s,t,u,Q^2) &= -g_{\mathrm{LO}_1,D}(v_f^2+a_f^2)u\frac{(Q^2+s)^2+(Q^2-t)^2}{s(Q^2-u)(Q^2-t)} +\\
+\epsilon\cdot g_{\mathrm{LO}_1,D}\Bigg[a_f^2&\frac{\left(u-Q^2\right)\left(u\left(6s^2-7st-t^2\right)+2s\left(s^2-4st+t^2\right)+4u^2(2s+t)+4u^3\right)}{3st\left(Q^2-t\right)\left(Q^2-u\right)}\\
&+ a_f^2\frac{3u\left(\left(Q^2+s\right)^2+\left(Q^2-t\right)^2\right)}{s\left(Q^2-t\right)\left(Q^2-u\right)} + v_f^2\frac{u(Q^2-u)}{s(Q^2-t)}\Bigg] + \mathcal{O}(\alpha_s^2),
\end{aligned} \tag{5.41}$$

where $g_{\mathrm{LO}_1,D} = 2\,C_A C_F\,g_s^2(\mu)\,g_Z^2$. Of course since we have only singular poles in the PDF renomalization master formula, we do not require to know the ϵ^2,ϵ^3, and ϵ^4 terms in the D-dimensional LO_1.

Moreover, the Larin scheme correctly produces vanishing results for the W_5 and W_6 structure functions, implying that $d_{\mathrm{L}} - d_{\mathrm{L}}' = 0$ for $i = 5,6$. However, we currently lack a full cross-check for the remaining helicity cross sections. In particular, there is no axiomatic argument to confirm that the combination $d_{\mathrm{L}} - d_{\mathrm{L}}'$ produced for the $v_f a_f$ terms is correct in *all* the cases. Still, the fact that the Larin scheme agrees with NAC in the cases where the latter is expected to hold – i.e. in reproducing the $v_f^2+a_f^2$ structure functions after including PDF renormalization counterterms – provides a meaningful partial check.

If we had access to an additional, independent scheme X that produced both

$$d_{\mathrm{L}} - d_{\mathrm{L}}' = d_{\mathrm{X}} - d_{\mathrm{X}}' \quad\text{and}\quad c_{\mathrm{L}} - c_{\mathrm{L}}' = c_{\mathrm{X}} - c_{\mathrm{X}}',$$

we would then have stronger evidence that the Larin scheme gives the correct finite contributions and can be used for all structure functions.

Finally, we briefly outline another (not yet implemented) γ^5 scheme based on local, process-defined reference vectors. The idea is motivated by the fact that Lorentz invariance is explicitly broken in fully differential helicity cross sections by fixing external momenta p_a, p_b, and q. This allows us to define

$$\gamma^5 = i\gamma^0\gamma^1\gamma^2\gamma^3 = i\not{t}\not{x}\not{y}\not{z},$$

where $\{t,x,y,z\}$ form a local orthonormal frame constructed from external momenta. A natural choice is the Collins–Soper basis already used in our projector definitions. In this setup, axial currents reduce to products of three gamma matrices, e.g., $x\cdot J_a \sim i\not{t}\not{y}\not{z}$.
This definition can be applied consistently at both LO_1 and LO_2, as it depends only on external kinematics. Compared to the Larin scheme, it avoids explicit $\epsilon_{\mu\nu\rho\sigma}$ tensors and simplifies the Dirac algebra, at the cost of introducing explicit dependence on the CS basis throughout the calculation.
If this prescription can be implemented through the LO_2 master integrals and shown to produce finite, PDF-renormalized results matching those of Larin, it would provide a strong check of scheme-independence.

5.5 Obtaining the non-singular remainder terms

In the previous Chapter 4, we described the derivation of the second-order hard function using the massless spinor-helicity formalism, which provides all the ingredients needed to compute the singular part of the full Drell-Yan helicity cross sections. In the following Chapter 5, we covered the computation of the fully renormalized set of real-real helicity cross sections. The final step in assembling the full cross section is to extract the non-singular contribution from the RR results.

In this section, we describe the expected behavior of the full RR cross sections in the $k^2 \to 0$ limit and explain how the non-singular part is isolated using the subtraction defined in Eq.(2.87):

$$\hat{\sigma}^{\text{non-sing}}_{i,ab}(p_a, p_b, q, k^2, \mu) = \hat{\sigma}^{\text{full, }RR}_{i,ab}(p_a, p_b, q, k^2, \mu) - \hat{\sigma}^{\text{sing}}_{i\,ab}(\tilde{p}_a, \tilde{p}_b, q, k^2, \mu)\Big|_{k^2>0}. \tag{5.42}$$

The expected behavior of the RR cross section in the $k^2 \to 0$ limit is given by the singular factorization formula in Eq.(2.86), evaluated at finite $k^2 > 0$, as discussed in Section 2.6.4:

$$\hat{\sigma}^{\text{sing}}_{i\,ab}(\tilde{p}_a, \tilde{p}_b, q, \mu)\Big|_{k^2>0} = \frac{1}{2\tilde{p}_a^- \tilde{p}_b^+} \sum_{VV'} L_{(\pm)i,VV'} \Big(\frac{\alpha_s(\mu)}{4\pi} H^{(1)}_{i\,VV'\,ab}(\tilde{p}_a, \tilde{p}_b, q) \big(S^{(1)}_{ab}(k^2, y_k) + J^{(1)}_{j(ab)}(k^2) \big) \Big)\Big|_{k^2>0}. \tag{5.43}$$

In this expression the soft and jet functions at finite k^2 could be obtained from Eq. (2.81), (2.82),(2.83) and (2.84) by implementing the following rules:

$$\delta(k^2)\Big|_{k^2>0} \to 0, \quad \text{and} \quad \mathcal{L}_n(k^2 > 0) = \frac{\ln^n k^2}{k^2}. \tag{5.44}$$

We now go through the different partonic channels and write down their expected singular limits based on SCET V + jet factorization.

We start with the channels that do *not* have a singular $1/k^2$ contribution in the $k^2 \to 0$ expansion, namely, those without a corresponding single-real process in that limit. These are the $gg \to Zq\bar{q}$ and $qq \to Zqq$ channels. In our results, we indeed find that these channels are free of $1/k^2$-type divergences, meaning their full RR contribution is already non-singular:

$$\sigma^{\text{non-sing}}_{i,\,gg/qq} = \sigma^{\text{full, RR}}_{i,\,gg/qq}.$$

Next, we consider channels that *do* contain a singular piece, specifically, those with single-real counterparts at $k^2 \to 0$. For the $ab = q\bar{q}$ case, which includes both $q\bar{q} \to Zgg$ and $q\bar{q} \to Zq\bar{q}$, the expected small-k^2 scaling is:

$$\frac{1}{2E_{\text{cm}}^2} L_{(\pm)i} \frac{\alpha_s(\mu)}{4\pi} H^{(1)}_{i\,q\bar{q}}(\tilde{p}_a, \tilde{p}_b, q) \Big(S^{(1)}_{q\bar{q}}(k^2, y_k) + J^{(1)}_{g(q\bar{q})}(k^2) \Big)\Big|_{k^2>0},$$

where $H^{(1)}_{i,\,q\bar{q}}$ is the first order hard function defined in Eq.(4.75), for which the squared matrix elements are given in Eq.(4.56a). Soft and jet functions can be obtained from Eq.(2.82) and (2.84) by applying the rules in Eq.(5.44).
For the inclusive helicity cross section in light-cone coordinates, the explicit form of this limit becomes:

$$\begin{aligned} & g_Z^2 \left(a_f^2 + v_f^2\right) \frac{1}{2E_{\text{cm}}^2} \frac{\alpha_s(\mu)^2}{4\pi^2} \frac{C_F}{C_A} \frac{1}{k^2} \frac{(q^+)^2 (k^- + q^-)^2 + (q^-)^2 (k^+ + q^+)^2}{24 k^- k^+ (k^- + q^-)^2 (k^+ + q^+)^2} \\ & \quad \times \left(-12(C_A - 4C_F) \log\left(k^2\right) + 12(C_A - 2C_F) \log\left(k^- k^+\right) - 11 C_A - 48 C_F \log(\mu) + 4 n_f T_F\right) \end{aligned} \tag{5.45}$$

where we omit the leptonic prefactor, the phase space integration measure $\mathrm{d}k^+\,\mathrm{d}k^-\,\mathrm{d}q^+\,\mathrm{d}q^-\,\mathrm{d}q_T^2$, and the relevant theta functions for simplicity. Term proportional to n_f will be corresponding to the $k^2 \to 0$ scaling of the $q\bar{q} \to Zq\bar{q}$ channel, while everything else comes from $q\bar{q} \to Zgg$ singular terms.
A similar analysis applies to the $qg \to Zqg$ channel:

$$\frac{1}{2E_{\text{cm}}^2} L_{(\pm)i} \frac{\alpha_s(\mu)}{4\pi} H^{(1)}_{i\,qg}(\tilde{p}_a, \tilde{p}_b, q) \Big(S^{(1)}_{qg}(k^2, y_k) + J^{(1)}_{q(qg)}(k^2) \Big)\Big|_{k^2>0},$$

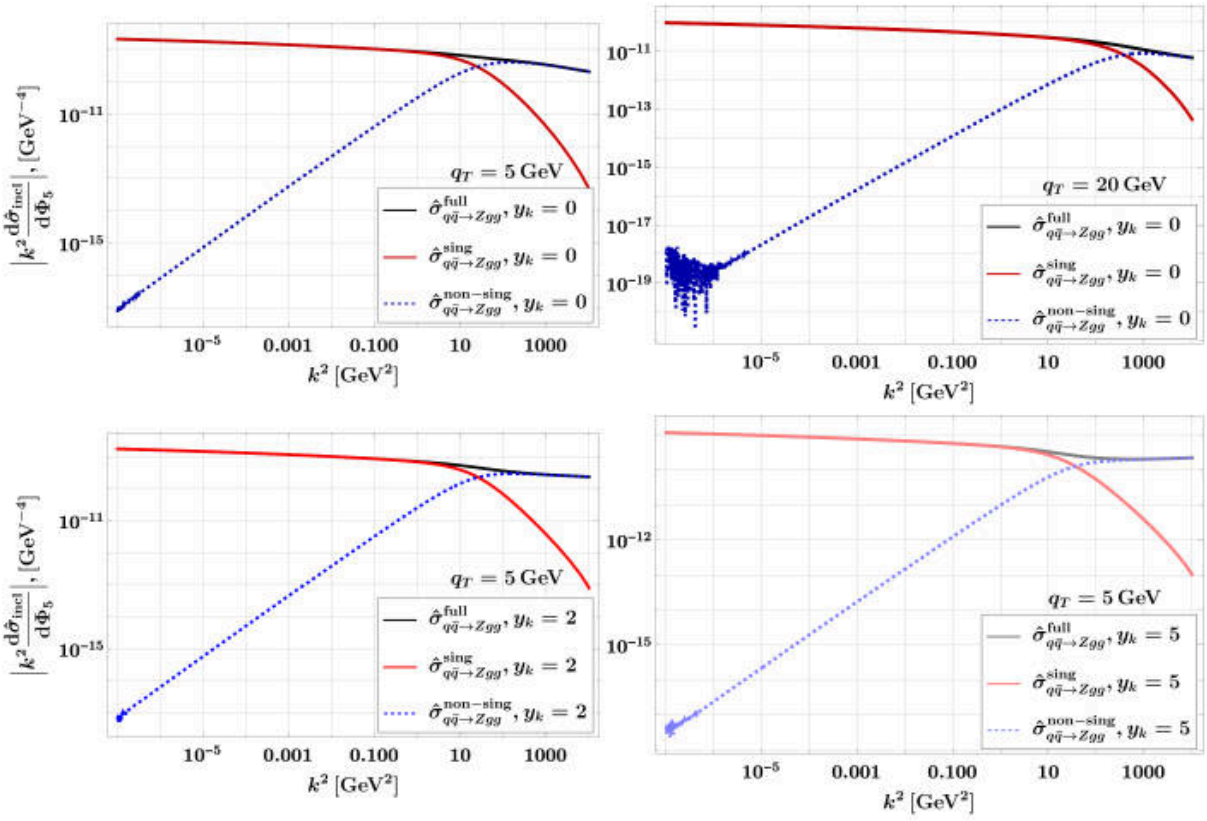


Figure 5.5: Singular-non-singular comparison for the $q\bar{q} \to Zgg$ process, showing how the prediction from the singular part of the RR helicity cross section approaches the full result in the $k^2 \to 0$ limit. The difference between the full and singular contributions defines the non-singular term, which scales as $\mathcal{O}(1)$. Each panel corresponds to a different rapidity cut $y_k = 0, 2, 5$, with transverse momentum $q_T = 5$ GeV and $q_T = 20$ GeV. Plots done for $\mu = Q = m_Z, q_T = 10$ GeV, $y_Z = 0$, $\mathrm{d}\Phi_5 = \mathrm{d}k^+\mathrm{d}k^-\mathrm{d}q^+\mathrm{d}q^-\mathrm{d}q_T^2$ and without leptonic prefactors.

where $H^{(1)}_{i,\,qg}$ is also defined in Eq.(4.75), and the corresponding squared matrix elements are given in Eq.(4.55a).
Explicitly this expressions is:

$$g_Z^2\left(a_f^2+v_f^2\right)\frac{1}{2E_{\text{cm}}^2}\frac{\alpha_s(\mu)^2}{4\pi^2}\frac{C_F}{C_A^2-1}\frac{1}{k^2}\frac{(q^+)^2\left(k^-+q^-\right)^2+\left(k^+\left(k^-+q^-\right)+k^-\left(k^++q^+\right)\right)^2}{8k^-\left(k^-+q^-\right)^2\left(k^++q^+\right)^3}$$
$$\times\left(4(2C_A+C_F)\log\left(k^2\right)-8(C_A+C_F)\log(\mu)-4C_A\log\left(k^-k^+\right)-3C_F\right). \tag{5.46}$$

The comparison between the full RR helicity cross sections and their expected small-k^2 behavior predicted from SCET is shown in Figure 5.5. As seen in the plots, the full cross section smoothly approaches the singular prediction in the $k^2 \to 0$ limit, and the difference between them defines the non-singular term, which scales as $\mathcal{O}(1)$ in k^2.
The plots exhibit numerical instability at small values of k^2 (around 10^{-5} GeV^2). At this scale, the difference between the full and singular contributions begins to misbehave due to numerical cancellations, essentially, we're subtracting two large, nearly equal numbers, which leads to a loss of precision.
Since the singular behaviour is known analytically, the sensible approach is to define the nonsingular remainder by subtracting the SCET-predicted singular limit from the full renormalized cross section, and to impose a lower cutoff at $k^2 = 10^{-5}$ GeV^2 when performing numerical integration.
To estimate the numerical error introduced by this cutoff, we can compare the nonsingular and full contributions to the partonic cross section at $k^2 = 10^{-5}$ GeV^2. This gives a relative error estimate of order 10^{-7} for $\sigma^{\text{non-sing}}/\sigma^{\text{full}}$, before convolution with PDFs. An alternative approach is to analytically expand the full cross section in powers of k^2, subtracting only the $1/k^2$ singular piece (which we verified matches the SCET prediction).

Chapter 6

Comparison with previous results in the literature

In the previous chapters we have shown how we derive both the singular and non-singular pieces of the full partonic cross section. Here we will discuss the main comparisons with literature that we did.

6.1 Cross-checks and Comparing with literature

To make sure our results are reliable, we carried out a number of internal consistency checks throughout the calculation: these are checks within our own framework, comparing different methods for computing the same quantity. Later in this chapter we also compare our results against known expressions in the literature.

Internal cross-checks

- **Spinor-Helicity vs. Feynman Rules for Single-Real Structure Functions**

  We independently computed the single-real structure functions using both spinor-helicity methods and conventional Feynman rules in four dimensions. For each channel and all non-zero structure functions, the results agree exactly.

- **(numerical) Spinor-Helicity vs. Feynman Rules for Double-Real Structure Functions**

  For the double-real contribution, we performed a numerical comparison between the spinor-helicity and conventional Feynman methods by evaluating squared matrix elements at selected phase space points. This was done for all five partonic subprocesses. We checked not only the total squared amplitude (summed over all diagrams in a given process), but also decomposed contributions from individual kinematic channels – specifically T-channel, S-channel, and interference terms. In all cases, the results from both methods fully agree numerically.

  As an additional check, we directly constructed *the full differential cross section* at fixed phase space points. On the Feynman side, we computed the squared hadronic matrix elements, combined them with the known leptonic prefactors and spherical harmonics, as in (2.27), obtained the full result and evaluated it numerically. On the spinor-helicity side, we did not decompose into Z-helicity amplitudes, instead, we squared the full lepton-full amplitude $\mathcal{A}_{\text{full}}$ directly and summed over all helicities. The two results agree numerically *up to an overall sign in the $a_f v_f$ terms.*

- **Born-Level Comparison**

  Although not included in the main text, we also repeated the Born-level computation using both spinor-helicity and Feynman rules. The $(1 + \cos^2\theta)$ term (from W_0) matches exactly between the two, while the parity-odd $\cos\theta$ term (from W_4) shows the same *sign flip.*

- **Counterterm and Renormalization Checks**

  We confirmed that the PDF counterterms from Eq. (2.40) correctly cancel all ϵ-poles in the RR structure functions for every channel. At the same time, we checked that there's no leftover γ_E or $\ln 4\pi$ dependence in the cross section after renormalization, as these are properly removed by using the correct form of the $\overline{\text{MS}}$ coupling in Eq. (2.7). Finally, we checked that the W_5, W_6 and W_7 from RR results are zero after integration and renormalization.

- **Collinear and Soft Limit Checks**

  To test the behaviour of our result in singular limits, we first looked at the collinear limit of the inclusive structure function before phase space integration. We compared it to the analytic expression in Eq. (2.8) and Appendix B of ref. [71], which helped us identify and fix missing ghost contributions early on. After the inclusion of the ghost contributions our results for all channels agreed with the limit. We also verified the soft limit ($k^2 \to 0$) of the integrated, renormalized cross section, comparing it to the SCET prediction from Eq. (2.73). The result matches, as shown in Fig. 5.5 and discussed in the previous section.

Comparing with literature
We performed several comparisons with existing results in the literature to validate different parts of our calculation.

- **Single Real Emission**

  We compared our conventional-Feynman-calculated single-real structure functions against the expressions in [16], as well as the inclusive results in [23] and [48]. For the process $qg \to Zq$, our helicity matrices squared $|\mathcal{M}^{(1),R}_{qg\to Zq}|_i$ (shown in Eq. (4.55a) for $i = 0, \text{incl}, 1, 2, 3$) agree with the expressions on page 12 of ref.[16], up to an overall factor of $4\, g_s^2\, g_Z^2\, C_A C_F$, assuming $a_f = v_f = 1$. This factor reflects couplings on the [16] side that were not included in our comparison. For $i = 4$, the agreement holds up to a sign flip: the factor becomes $-4\, g_s^2\, g_Z^2\, C_A C_F$.

  Similarly, for $q\bar{q} \to Zg$, our results $|\mathcal{M}^{(1),R}_{q\bar{q}\to Zg}|_i$ (Eq. (4.56a)) match the expressions in [16] for $i = 0, \text{incl}, 1, 2$, again up to the same factor. The $i = 3, 4$ components agree up to the same factor with an extra minus sign.

- **Absorptive Part of the NNLO Cross Section**

  We compared our absorptive RV structure functions (calculated using spinor-helicity and shown in Eqs. (4.59a)-(4.59c)) with results in [16] and [27].

  For $qg \to Zq$ (with $a_f = v_f = 1$), the agreement with Appendix B of [16] (page 34) is as follows:

  - $i = 5$: up to $32\sqrt{2}\pi\ \alpha_s\, g_Z^2\, C_A C_F$
  - $i = 6$: up to $16\pi\ \alpha_s g_Z^2\, C_A C_F$
  - $i = 7$: up to $4\sqrt{2}\pi\ \alpha_s g_Z^2\, C_A C_F$

  For $q\bar{q} \to Zg$ (with $a_f = v_f = 1$), the comparison is:

  - $i = 5$: up to $32\sqrt{2}\pi\ \alpha_s\, g_Z^2\, C_A C_F$
  - $i = 6$: up to $-16\pi\ \alpha_s\, g_Z^2\, C_A C_F$
  - $i = 7$: up to $-4\sqrt{2}\pi\ \alpha_s\, g_Z^2\, C_A C_F$

  In contrast, the comparison with Eqs.(21-26) in [27] gave more consistent results. For both $qg \to Zq$ and $q\bar{q} \to Zg$, we find:

  - $i = 5, 6$: agree up to $8\, a_f v_f\, \alpha_s\, g_s^2\, g_Z^2\, C_A C_F$ (without coupling normalization), or 16 (with coupling factor $g_{qg;i}$, $g_{q\bar{q};i}$ from [27] included).
  - $i = 7$: agrees up to $4\,(a_f^2 + v_f^2)\, \alpha_s\, g_s^2\, g_Z^2\, C_A C_F$ (or 8 with coupling $g_{qg;i}$, $g_{q\bar{q};i}$).

  The slight mismatch in overall normalization may be due to a different but equivalent parametrization of the lepton angular distribution in [27], which could introduce an additional positive factor.

- $\boldsymbol{H^{(2)}_{\text{incl, ab}}}$ **(IR-Finite Terms in RV Structure functions) Comparison**
  We also compared our inclusive IR-finite RV terms, computed via spinor-helicity, with the hard functions in ref. [48]. These matched exactly, up to a universal overall positive factor common to both the $q\bar{q}$ and qg channels.

- **Inclusive IR Real-Virtual Pole Structure**

  Although we do not rely on explicit pole structures in our RV calculation, we extracted the inclusive Z-helicityamplitudes for the IR-divergent part of the full RV amplitude $\mathcal{A}^{(1)}_{q,\text{div}}$ in Eq.(4.15), combined tham into the inclusive cross section and compared it with the divergent terms in RV contribution from ref. [23] (Eqs. A4, A5 for $qg \to Zq$, and A7, A8 for $q\bar{q} \to Zg$). The results agree exactly, including the normalization.

- **Inclusive Top-Loop Contributions**

  We also verified that our results reproduce the inclusive top-loop contributions (Eqs. A6 and A9 in [23]) in the limit $1/m_t \to 0$ for both channels, *up to an overall sign.*

- **$\hat{\sigma}^{\text{sing}}_{\text{incl, ab}}$ without leptonic prefactors**

  We also compared our fully assembled inclusive singular cross section $\hat{\sigma}^{\text{sing}}_{\text{incl, ab}}$ (excluding leptonic prefactors) with the IR-finite singular in $s_2 = k^2 \to 0$ terms in Eq. (2.12) of [23] for both qg and $q\bar{q}$ channels. We first compared the terms involving plus distributions, which in [23] arise from the real-real singular contribution. These matched exactly with the corresponding plus-distribution-dependent part of the second line in our simplified SCET expression (Eq. (2.86)). We then compared the $\delta(k^2)$ contributions, which had initially some differences with the expressions in ref. [23].

  In reviewing Eq. (2.12) of [23], which gives the expressions for the $qg \to Zq$ channel, we identified several typos: the second line of Eq. (2.12) appears to be missing the C_3^{qG} term, which should appear without any $\delta(s_2)$ factor. Moreover, both C_1^{qG} and C_2^{qG} should multiply $\delta(s_2)$. Additionally, the coefficient C_2^{qG} is missing a factor of n_f, the number of active quark flavors. This is inconsistent with how B_2^{qG} is written and leads to incorrect cancellation of the single poles. The corrected structure should read:

  $$\delta(s_2)\big(B_1 + B_2\, n_f + C_1 + C_2\, n_f\big),$$

  and the term in the third line originally labeled C_2^{qG} should be relabeled as C_3^{qG}, appearing without a delta function.

  There is also a mismatch in the mass dimensions on both sides of the equation. The denominator $(2\pi\mu^2)^{2\omega}$ should in fact be $(2\pi\mu)^{2\omega}$. As for the term-by-term check:

  - B_2^{qG} and B_3^{qG} are correct and were checked independently: both using the spinor-helicity methods described in this thesis and by our collaborator using Feynman rules.
  - B_1^{qG}, however, contains a sign error. Specifically, the last four lines of Eq. (A4) – the terms not proportional to A^{qG} – appear to have the wrong overall sign.

  With the corrected signs and structure, we find complete agreement.

Chapter 7

Conclusions

In this thesis, we analytically computed all partonic helicity cross sections $\hat{\sigma}_{i\,ab}(p_a, p_b, q)$ for both charged and neutral-current Drell-Yan production in unpolarized proton-proton collisions at finite transverse momentum ($q_T > 0$). From these results, it is possible to construct the angular coefficients A_i, defined as normalized helicity cross sections, which capture the angular distribution of the final-state leptons and serve as precise probes of electroweak structure and QCD dynamics.

To handle the infrared divergences in the soft and collinear limits, we used a subtraction method based on the SCET V + jet threshold factorization theorem. This allowed us to cleanly separate the singular part of the cross section $\hat{\sigma}^{\text{sing}}_{i,ab}$ from the finite non-singular remainder $\hat{\sigma}^{\text{non-sing}}_{i,ab}$.

The singular piece includes contributions from both real-virtual and part of the real-real terms, its factorized expression at $\mathcal{O}(\alpha_s^2)$ is shown in Eq.(2.86). The only missing input from the literature was the second-order helicity-projected hard function $H^{(2)}_{i,ab}$, which we calculated in this work using a method based on spinor-helicity amplitudes. This approach uses known massless NLO_1 spinor-helicity amplitudes with vector boson decay into leptons to extract the Z-helicity dependence directly, isolating the purely partonic part of the process into the Z-helicity amplitudes. These amplitudes are later combined into the helicity-projected matrix elements squared, as shown in Section 4.4, which when integrated over the hadronic radiation give the structure functions which IR-finite terms have a one-to-one correspondence with the hard function.

The nonsingular part, which contains only double-real contributions, was computed from scratch using conventional Feynman rules. We used helicity projectors to extract the relevant structure functions and performed a fully analytic integration over the hadronic phase space using a set of derived master integrals. The RR infrared poles were removed using a master formula Eq.(2.40) derived in this thesis. The nonsingular cross section was then obtained by subtracting the predicted singular part from the full renormalized RR result at $k^2 > 0$ as described in Section 5.5.

Finally, we organized the electroweak coupling factors using the diagrammatic method with Pysanka diagrams (see Chapter 3), which provides a clear and succinct way to structure the couplings at all orders in strong coupling for a set number of incoming partons. This framework allowed us to consistently assemble the full helicity cross sections.

Therefore, **this work constitutes the first complete set of all nine partonic helicity cross sections at $\mathcal{O}(\alpha_s^2)$, including both tree-level and loop contributions, fully differential at $q_T > 0$.**

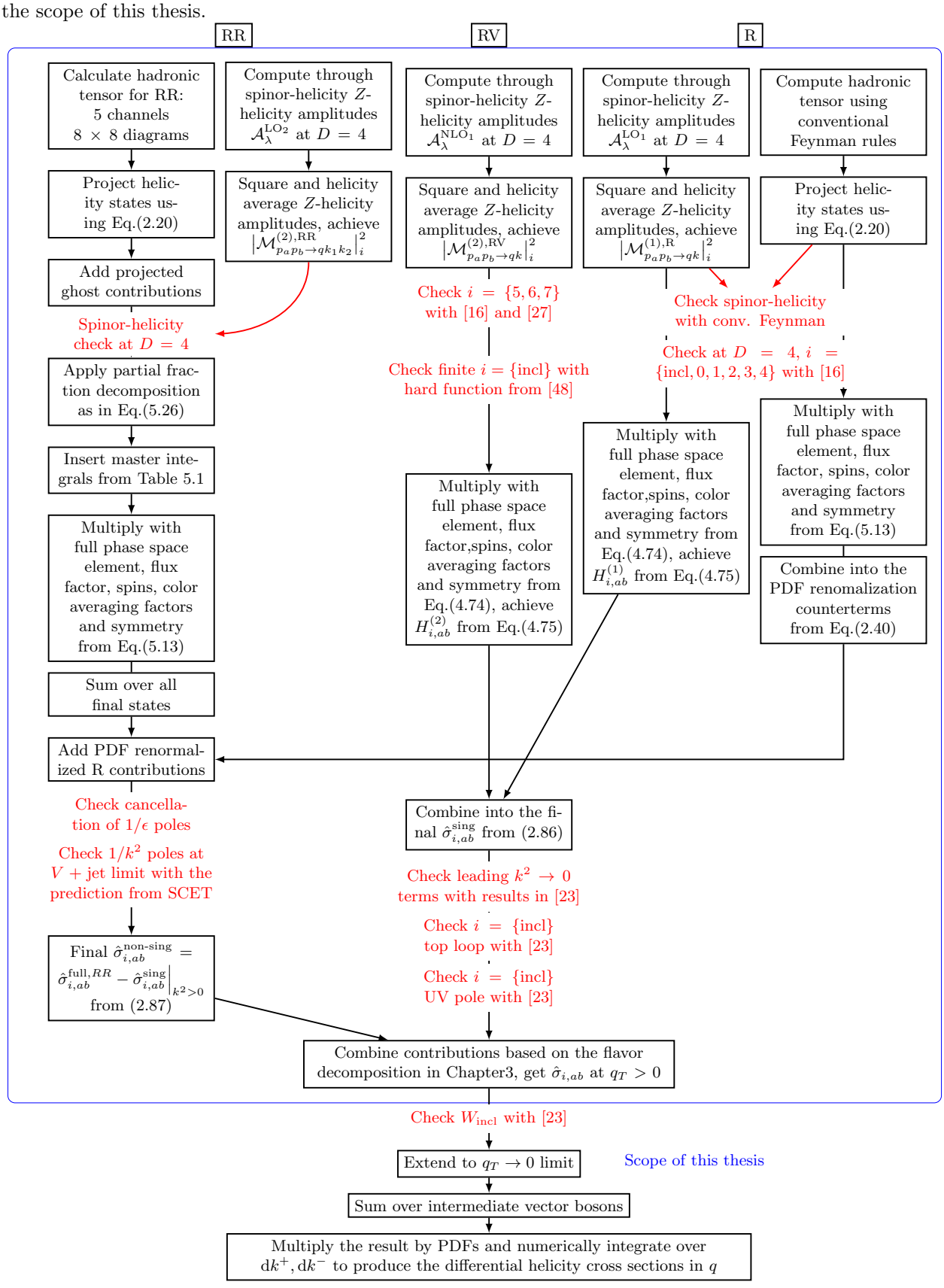
During the calculation we performed a wide range of cross-checks to ensure consistency: spinor-helicity vs Feynman diagram comparisons, comparisons in known (soft and collinear) limits, and detailed comparisons with the available results from the literature.

There are several directions this work can be extended to. First and foremost, we have not yet cross-checked the full inclusive cross sections for the combined singular+non-singular terms. This should be done to ensure the full consistency with the available results and their EW couplings in, for example, [23]. Next, since our entire computation has been carried out in the $q_T > 0$ region, we need to extend the result to the $q_T \to 0$ limit. The procedure for doing this closely parallels the approach used in the $k^2 \to 0$ limit. For all structure functions W_i with $i \neq \text{incl}, 4$, which start at $\mathcal{O}(\alpha_s)$ are power suppressed at small q_T when matched onto leading-twist PDFs [68], this constitutes the complete $\mathcal{O}(\alpha_s^2)$ result. The total NNLO result for W_{incl} and W_4, which start at $\mathcal{O}(\alpha_s^0)$ and are leading and singular at small q_T, can easily be assembled by performing a differential q_T subtraction [24, 25] using their leading-power factorization at small q_T, which contains the $\mathcal{O}(\alpha_s^0)$ Born and all purely virtual corrections. Finally, combining the full result with PDFs and performing the numerical integration over q_T would then give the fully differential over q cross section $\mathrm{d}\sigma_i/\mathrm{d}^4 q$.

Additionally, some of our intermediate results might have uses beyond this specific project: The Z-helicity amplitudes we obtained allow us to study different scaling behaviors in various limits. In this thesis, we focused on the soft limit, but it's also possible to extract the (anti-)collinear behavior from the same amplitudes. On more practical note, the master integrals we derived for the hadronic phase space integration are quite general and can be reused in other processes with similar propagator structures.

Main pipeline

Additionally, we provide a flowchart illustrating the step-by-step process of the project as well as the intermediate checks. In black are the main calculations, in red are the checks and the blue box outlines the scope of this thesis.

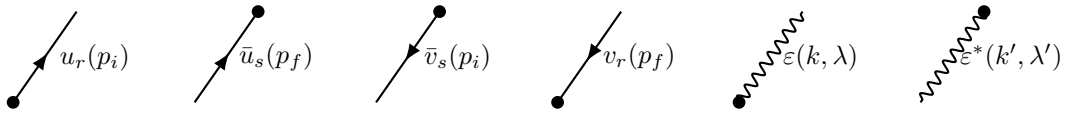


Appendix A

Feynman Rules

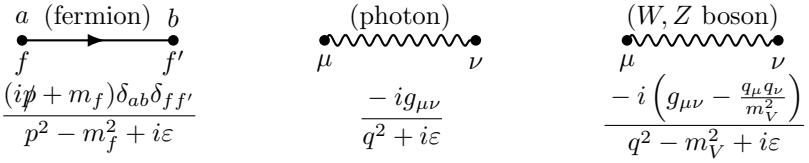
Here we present the Feynman rules which were used throughout this project. They are based on the rules presented in ref.[61, 72] and implemented using `Feyncalc` [67] and `FeynArts` [73].

External Lines

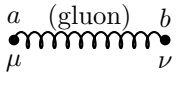


where $u_r(p)$, $\bar{u}_s(p)$, $v_r(p)$, and $\bar{v}_s(p)$ are spinors for incoming/outgoing fermions and antifermions, and $\varepsilon^\mu(k,\lambda)$ is the polarization vector for an incoming gauge boson.

Propagators



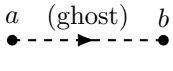
where $\not{p} = \gamma^\mu p_\mu$, m_f is the fermion mass, and $m_V \in \{m_W, m_Z\}$ are vector boson masses.



$$\frac{-i\delta_{ab}\left(g_{\mu\nu}+(\xi-1)\frac{q_\mu q_\nu}{m_V^2}\right)}{k^2+i\varepsilon}$$
covariant gauge

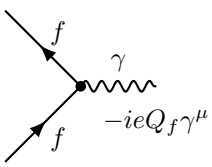
$$\frac{-i\delta_{ab}}{k^2+i\epsilon}\left(g^{\mu\nu}-\frac{k^\mu n^\nu+k^\nu n^\mu}{k\cdot n}\right)$$
lightcone gauge $n^2=0$

ξ is the gauge parameter ($\xi = 1$ gives Feynman gauge). In the lightcone gauge, n^μ is a fixed gauge vector. In covariant gauges (e.g., Feynman or Landau gauge), the gauge-fixing procedure introduces unphysical degrees of freedom, and it is therefore necessary to include Faddeev-Popov ghost fields to preserve unitarity and correctly cancel the contributions of longitudinal and scalar gluon modes:

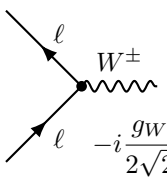


$$\frac{i\delta_{ab}}{k^2+i\varepsilon}$$

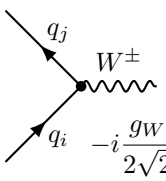
Vertices



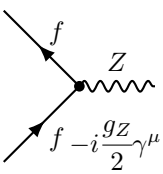
$$-ieQ_f\gamma^\mu$$



$$-i\frac{g_W}{2\sqrt{2}}\gamma^\mu(1-\gamma^5)$$



$$-i\frac{g_W}{2\sqrt{2}}\gamma^\mu(1-\gamma^5)V_{ji}$$

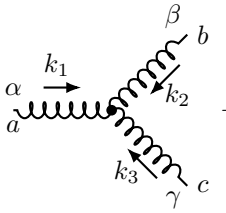


$$-i\frac{g_Z}{2}\gamma^\mu\big[\epsilon_L(f)(1-\gamma^5)+\epsilon_R(f)(1+\gamma^5)\big]$$
$$=-i\frac{g_Z}{2}\gamma^\mu(v_f-a_f\gamma^5)$$

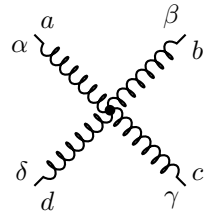
The QED vertex involves the electromagnetic coupling e and the fermion's electric charge Q_f.
The charged current interaction via the W boson couples only to left-handed fermions and involves the weak coupling $g_W = e/\sin\theta_W$, where θ_W is Weinberg angle. For quark transitions, the CKM matrix element V_{ji} appears.
The Z boson vertex is expressed using vector and axial-vector couplings:

$$\epsilon_L(f) = I_{3f} - Q_f \sin^2\theta_W, \quad \epsilon_R(f) = -Q_f \sin^2\theta_W$$
$$v_f = I_{3f} - 2Q_f \sin^2\theta_W, \quad a_f = I_{3f}, \quad g_Z = \frac{e}{\sin\theta_W \cos\theta_W},$$

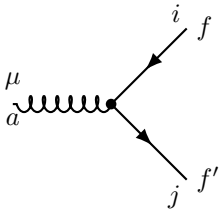
where I_{3f} is the third component of weak isospin, Q_f is the electric charge, g_Z is the coupling of the Z-boson to fermions, e is the electromagnetic coupling, and θ_W is the Weinberg angle.



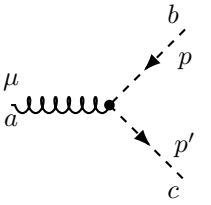
$$-g_s f^{abc}\Big[g^{\alpha\beta}(k_1-k_2)^\gamma + g^{\beta\gamma}(k_2-k_3)^\alpha + g^{\gamma\alpha}(k_3-k_1)^\beta\Big]$$



$$-ig_s^2\Big[f^{abe}f^{cde}(g^{\alpha\gamma}g^{\beta\delta} - g^{\alpha\delta}g^{\beta\gamma}) + f^{ace}f^{bde}(g^{\alpha\beta}g^{\gamma\delta} - g^{\alpha\delta}g^{\gamma\beta}) + f^{ade}f^{bce}(g^{\alpha\beta}g^{\delta\gamma} - g^{\alpha\gamma}g^{\delta\beta})\Big]$$



$$-ig_s(T^a)^j_i\gamma^\mu\delta_{ff'}$$



$$g_s f^{abc} p'^\mu$$

The 3- and 4-gluon vertices arise from the non-Abelian SU(3) structure of QCD, with f^{abc} the structure constants.
The quark-gluon vertex involves the SU(3) generator T^a, and the ghost-gluon vertex is a result of the Faddeev-Popov procedure in covariant gauges.

Appendix B

Spinor Identities

In the Dirac representation γ^μ, $\mu = \{0,1,2,3\}$ and γ^5 are

$$\gamma^0 = \begin{pmatrix} 1 & 0 \\ 0 & -1 \end{pmatrix}, \quad \gamma^i = \begin{pmatrix} 0 & \sigma^i \\ -\sigma^i & 0 \end{pmatrix}, \quad \gamma^5 = \begin{pmatrix} 0 & 1 \\ 1 & 0 \end{pmatrix}$$

Taking $n_i^\mu = (1,0,0,1)$, from the Dirac equation $\not{p}u(p) = 0$, $p^2 = 0$ we have standard solutions $|p\pm\rangle = \frac{1 \pm \gamma^5}{2} u(p)$:

$$|p+\rangle = \frac{1}{\sqrt{2}} \begin{pmatrix} \sqrt{p^-} \\ \sqrt{p^+} e^{i\phi_p} \\ \sqrt{p^-} \\ \sqrt{p^+} e^{i\phi_p} \end{pmatrix}, \quad |p-\rangle = \frac{1}{\sqrt{2}} \begin{pmatrix} \sqrt{p^+} e^{-i\phi_p} \\ -\sqrt{p^-} \\ -\sqrt{p^+} e^{-i\phi_p} \\ \sqrt{p^-} \end{pmatrix}$$

where

$$p^\pm = p^0 \mp p^3, \quad e^{\pm i\phi_p} = \frac{p^1 \pm ip^2}{\sqrt{p^+ p^-}} \tag{B.1}$$

For negative p^0 and $p^\pm$:

$$|(-p)\pm\rangle = i|p\pm\rangle \tag{B.2}$$

The conjugate spinors are:

$$\langle p\pm| = \mathrm{sgn}(p^0)\bar{u}(p)\frac{1 \mp \gamma^5}{2} = \mathrm{sgn}(p^0)\overline{|p\pm\rangle}. \tag{B.3}$$

The additional minus sign for negative p^0 is included to use the same branch of the square root for both types of spinors, i.e., for $p^0 > 0$:

$$\langle(-p)\pm| = -\overline{|(-p)\pm\rangle} = i\langle p\pm| \tag{B.4}$$

Spinor products are defined as:

$$\langle pq\rangle = \langle p-|q+\rangle, \quad [pq] = \langle p+|q-\rangle \tag{B.5}$$

Extra signs for conjugation of the spinor products:

$$\langle p-|q+\rangle^* = \mathrm{sgn}(p^0 q^0)\langle q+|p-\rangle \tag{B.6}$$

If there are several momenta p_i, it is common to abbreviate

$$|p_i\pm\rangle = |i\pm\rangle\,, \langle p_i p_j\rangle = \langle ij\rangle, [p_i p_j] = [ij].$$

A few identities coming directly from the definition of the spinor product:

$$\langle pq\rangle = -\langle qp\rangle, [pq] = -[qp], \langle pp\rangle = [pp] = 0$$
$$[p|\gamma^\mu|p\rangle = \langle p|\gamma^\mu|p] = 2p^\mu$$

Completeness relations and a few results coming from it:

$$|p\pm\rangle\langle p\pm| = \frac{1 \pm \gamma^5}{2}\not{p} \tag{B.7}$$

$$\not{p} = |p]\langle p| + |p\rangle[p| \tag{B.8}$$

More importantly we get the following relations for the s_{ij} variables:

$$\langle pq\rangle[qp] = \frac{1}{2}\mathrm{Tr}\left[(1-\gamma^5)\not{p}\not{q}\right] = 2p\cdot q = s_{pq},$$
$$|\langle pq\rangle| = |[pq]| = \sqrt{|s_{pq}|}.$$

Charge conjugation invariance of the current, the Fierz identity and the Schouten identity are

$$[p|\gamma^\mu|q\rangle = \langle q|\gamma^\mu|p] \tag{B.9}$$

$$[p|\gamma^\mu|q\rangle[k|\gamma_\mu|l\rangle = 2[pk]\langle lq\rangle \tag{B.10}$$

$$\langle pq\rangle\langle kl\rangle = \langle pk\rangle\langle ql\rangle + \langle pl\rangle\langle kq\rangle \tag{B.11}$$

Momentum conservation

$$\sum_{i=1}^{n} p_i = 0,$$

which implies

$$\sum_{i=1}^{n} [ji]\langle ik\rangle = 0.$$

The following Feynman rules can be used for translating the physical spinors to the braket notation.

	$m \neq 0$	$h = +1/2$	$h = -1/2$
particle incoming	$u(p)$	$\|p\rangle$	$\|p]$
anti-particle incoming	$\bar{v}(p)$	$\langle p\|$	$[p\|$
particle outgoing	$\bar{u}(p)$	$[p\|$	$\langle p\|$
anti-particle outgoing	$v(p)$	$\|p]$	$\|p\rangle$

The polarization vectors of an outgoing gluon with momentum p_i are given in the helicity formalism by a combination of two massless spinors:

$$\epsilon^+_\mu(p,r) = \frac{[r|\gamma_\mu|p\rangle}{\sqrt{2}\langle rp\rangle}, \quad (\epsilon^-)_\mu = \epsilon^-_\mu(p_i,r) = -\frac{\langle r|\gamma_\mu|i]}{\sqrt{2}[rp]}, \tag{B.12}$$

where the r^μ is the reference momentum - an arbitrary massless spinor which must not be aligned with p^μ. For each of the external states p_i^μ it is allowed to choose different reference vector. Right choice of the reference vector can greatly simplify the calculation, canceling many diagrams.
Another form of the polarization vectors, already contracted with the γ^μ is as follows:

$$\not{\epsilon}^+(p,r) = \sqrt{2}\frac{r\rangle[p}{\langle rp\rangle}, \quad \not{\epsilon}^-(p,r) = \sqrt{2}\frac{p\rangle[r}{[pr]}. \tag{B.13}$$

Appendix C

Functions and Distributions

C.1 Plus Distribution

In perturbative QCD, partonic cross sections often develop divergences in the soft and collinear limits. Plus distributions (also called "plus prescriptions") provide a systematic way to regulate these singularities, ensuring meaningful convolution with smooth functions. This chapter summarizes their definition, properties, and applications.

A plus distribution is defined for a function $f(x)$ which is less singular than $1/x^2$ at $x \to 0$ as:

$$[f(x)]_+^{[x,x_0]} = \lim_{\epsilon\to 0}\left[f(x)\theta(x-\epsilon) + \delta(x-\epsilon)\int_{x_0}^{x} dy\, f(y)\right], \tag{C.1}$$

where x_0 is the boundary of the plus distribution. For distributions supported on $[0,1]$, it is standard to take $x_0 = 1$. Therefore if it is not stated explicitly, we will assume the boundary to be $x_0 = 1$.

The action of a plus distribution on a test function $g(x)$ is:

$$\int_0^1 dx\,[f(x)]_+\, g(x) = \int_0^1 dx\, f(x)[g(x) - g(0)]. \tag{C.2}$$

Several important plus distributions that appear in practice are:

$$\left[\frac{1}{1-x}\right]_+ = \lim_{\epsilon\to 0}\left(\frac{1}{1-x}\theta(1-x-\epsilon) + \delta(1-x)\ln\epsilon\right),$$
$$\left[\frac{\ln(1-x)}{1-x}\right]_+, \quad \left[\frac{\ln^n(1-x)}{1-x}\right]_+ \quad (n \geq 0),$$

In the next expressions, following the notation in [74], we denote dimensionless plus distributions as:

$$\mathcal{L}_n(x) \equiv \left[\frac{\theta(x)\ln^n x}{x}\right]_+ = \lim_{\epsilon\to 0}\left[\frac{\theta(x-\epsilon)\ln^n x}{x} + \delta(x-\epsilon)\frac{\ln^{n+1}\epsilon}{n+1}\right], \text{ with } n \geq 0, \tag{C.3}$$

$$\mathcal{L}^a(x) \equiv \left[\frac{\theta(x)}{x^{1-a}}\right]_+ = \lim_{\epsilon\to 0}\left[\frac{\theta(x-\epsilon)}{x^{1-a}} + \delta(x-\epsilon)\frac{x^a-1}{a}\right], \text{ with } a > -1. \tag{C.4}$$

Shorthands for the distributions with dimensionfull arguments in one spacial dimension:

$$\mathcal{L}_n(k,\mu) \equiv \frac{1}{\mu}\mathcal{L}_n\left(\frac{k}{\mu}\right), \qquad \mathcal{L}_n(t,\mu^2) \equiv \frac{1}{\mu^2}\mathcal{L}_n\left(\frac{t}{\mu^2}\right),$$
$$\mathcal{L}^a(k,\mu) \equiv \frac{1}{\mu}\mathcal{L}^a\left(\frac{k}{\mu}\right), \qquad \mathcal{L}^a(t,\mu^2) \equiv \frac{1}{\mu^2}\mathcal{L}^a\left(\frac{t}{\mu^2}\right).$$

Key properties of the plus distributions are:

- **Linearity:** The plus operation is linear: $[af(x) + bg(x)]_+ = a[f(x)]_+ + b[g(x)]_+$,
- **Integral Identity:**

$$\int_0^1 dx\,[f(x)]_+ = 0,$$

- **Definiteness on Positive Domain:**

$$\mathcal{L}_n(x>0)=\frac{\ln^n x}{x},\quad \mathcal{L}^a(x>0)=\frac{1}{x^{1-a}}.$$

In QCD, plus distributions appear in partonic cross sections, splitting functions, and matching conditions in effective theories. For example, the DGLAP (Dokshitzer-, Gribov-, Lipatov-, Altarelli- and Parisi) splitting functions [30, 31, 32] involve terms like:

$$P_{qq}(x)=C_F\left[\frac{1+x^2}{(1-x)}\right]_+. \tag{C.5}$$

These singular terms regulate the divergence as $x\to 1$.

Plus distributions help regularize divergent expressions in dimensional regularization. For instance, in $d=4-2\epsilon$ dimensions:

$$(1-x)^{-1-\epsilon}=-\frac{1}{\epsilon}\delta(1-x)+\left[\frac{1}{1-x}\right]_+ +\mathcal{O}(\epsilon). \tag{C.6}$$

This decomposition separates poles and finite contributions cleanly.

C.2 Distributional expansion

Some of the RR processes (i.e. S-channel $q\bar{q}\to Zq\bar{q}$ with Z coupling to the outgoing fermion line) introduce a collinear pole in the cross section due to the propagator $k^2=(k_1+k_2)^2$ diverging when the sum of momenta k_1 and k_2 becomes small.

To extract the pole, it is possible to use the following distributional expansion for small ϵ in dimensional regularization:

$$\frac{1}{x^{1+\epsilon}}=-\frac{\delta(x)}{\epsilon}+\sum_{n=0}^{\infty}(-1)^n\mathcal{L}_n(x)\frac{\epsilon^n}{n!}, \tag{C.7}$$

where $\mathcal{L}_n(x)$ represents a generalized logarithmic distribution.

Appendix D

PDF Renormalization

Similar to the renormalization group equation for the strong coupling, we can write the anomalous dimension of the Parton Distribution Function (PDF) as given by the DGLAP (Dokshitzer-Gribov-Lipatov-Altarelli-Parisi) [30, 31, 32] evolution equation:

$$\mu\frac{\partial}{\partial\mu}f_k^{[h]}(\xi,\mu)=\sum_{n=0}^{\infty}\left(\frac{\alpha_s(\mu)}{4\pi}\right)^{n+1}\int_\xi^1\frac{dz}{z}\sum_{j=1}^{2n_f+1}f_j^{[h]}\left(\frac{\xi}{z},\mu\right)P_{kj}^{(n)}(z), \quad \text{(D.1)}$$

where the splitting functions $P_{kj}^{(n)}(z)$ encode the probability density for parton j to emit or absorb another parton, transforming into parton k with a fraction z of the momentum.

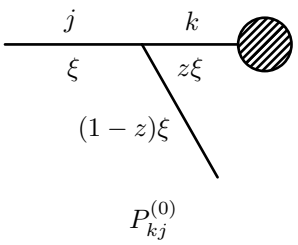


Figure D.1: LO splitting $j \to k$ with momentum fractions $\xi \to (z\xi, (1-z)\xi)$, described by $P_{kj}^{(0)}(z)$.

The splitting functions for different parton combinations depend on the type of interaction and the order of perturbation theory. For example, $P_{qq}^{(0)}(z)$ describes quark-to-quark splitting at leading order, while $P_{gq}^{(0)}(z)$ represents gluon emission from a quark. Expressions for these factors are: They are given by:

$$P_{qq}^{(0)}(z)=2C_F\theta(z)P_{qq}(z),\quad P_{qq}(z)=\left(2\mathcal{L}_0(1-z)-\theta(1-z)(1+z)+\frac{3}{2}\delta(1-z)\right)=\left[\theta(1-z)\frac{1+z^2}{1-z}\right]_+,$$

$$P_{gq}^{(0)}(z)=2C_F\theta(z)P_{gq}(z),\quad P_{gq}(z)=\theta(1-z)\frac{1+(1-z)^2}{z},$$

$$P_{qg}^{(0)}(z)=2T_F\theta(z)P_{qg}(z),\quad P_{qg}(z)=\theta(1-z)[1-2z(1-z)],$$

$$P_{gg}^{(0)}(z)=2C_A\theta(z)P_{gg}(z)+\beta_0\delta(1-z),\quad P_{gg}(z)=2\mathcal{L}_0(1-z)+\theta(1-z)\Big[2z(1-z)+\frac{2(1-z)}{z}-2\Big],$$

where $\beta_0=\frac{11}{3}C_A-\frac{4}{3}T_Fn_f$ is the leading-order QCD beta function coefficient.

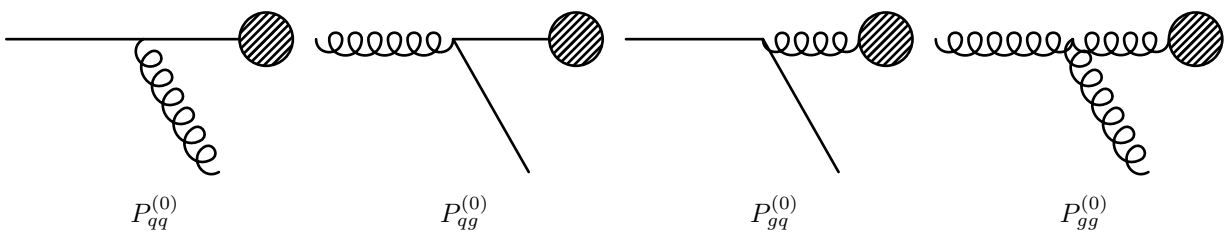


Figure D.2: Leading-order parton splitting processes contributing to DGLAP evolution: $P_{qq}^{(0)}$ (quark emitting a gluon), $P_{qg}^{(0)}$ (gluon splitting into a quark-antiquark pair), $P_{gq}^{(0)}$ (quark radiating a gluon with the gluon entering the hard interaction), and $P_{gg}^{(0)}$ (gluon splitting into two gluons). Shaded blobs represent the hard scattering process.

Higher-order corrections $P_{kj}^{(n)}(z), n \geq 1$ refine these probabilities, contribute to higher-order α_s terms.

For compactness, we write the convolution notation:

$$f(\mu)\otimes P^{(n)}=\int_\xi^1\frac{dz}{z}\sum_{j=1}^{2n_f+1}f_j^{[h]}\left(\frac{\xi}{z},\mu\right)P_{kj}^{(n)}(z). \tag{D.2}$$

Using this notation, Eq.(D.1) can be rewritten as:

$$\mu\frac{\partial}{\partial\mu}f_k^{[h]}(\xi,\mu)=\frac{\alpha_s(\mu)}{4\pi}f(\mu)\otimes P^{(0)}+\left(\frac{\alpha_s(\mu)}{4\pi}\right)^2 f(\mu)\otimes P^{(1)}+\mathcal{O}(\alpha_s^3). \tag{D.3}$$

Analogous to coupling renormalization, our goal is to derive the bare PDFs. The bare PDF is expressed as a combination of the renormalized PDF and higher-order corrections:

$$\begin{aligned}f_k^{[h],\text{ bare}}(\xi)=&f_k^{[h]}(\xi,\mu)+\sum_{n=0}^{\infty}\left(\frac{\alpha_s(\mu)}{4\pi}\right)^{n+1}\int_\xi^1\frac{dz}{z}\sum_{j=1}^{2n_f+1}f_j^{[h]}\left(\frac{\xi}{z},\mu\right)P_{kj}^{(n),\text{ bare}}(z)\\ =&f_k^{[h]}(\xi,\mu)+\frac{\alpha_s(\mu)}{4\pi}f(\mu)\otimes P^{(0),\text{ bare}}\\ &+\left(\frac{\alpha_s(\mu)}{4\pi}\right)^2 f(\mu)\otimes P^{(1),\text{ bare}}+\mathcal{O}(\alpha_s^3).\end{aligned} \tag{D.4}$$

Since the bare PDF is independent of the renormalization scale, taking the derivative $\mu\partial/\partial\mu$ on both sides and substituting the renormalization group equation for α_s gives:

$$\begin{aligned}0=&\mu\frac{\partial}{\partial\mu}f_k^{[h]}(\xi,\mu)\\ &+\frac{\alpha_s(\mu)}{4\pi}\left[-\epsilon f(\mu)\otimes P^{(0),\text{ bare}}+\mu\frac{\partial}{\partial\mu}f(\mu)\otimes P^{(0),\text{ bare}}\right]\\ &+\left(\frac{\alpha_s(\mu)}{4\pi}\right)^2\left[-\beta_0 f(\mu)\otimes P^{(0),\text{ bare}}-2\epsilon f(\mu)\otimes P^{(1),\text{ bare}}+\mu\frac{\partial}{\partial\mu}f(\mu)\otimes P^{(1),\text{ bare}}\right]\\ &+\mathcal{O}(\alpha_s^3).\end{aligned} \tag{D.5}$$

Solving recursively yields the derivative of the PDF:

$$\begin{aligned}\mu\frac{\partial}{\partial\mu}f_k^{[h]}(\xi,\mu)=&\frac{\alpha_s(\mu)}{4\pi}f(\mu)\otimes(\epsilon P^{(0),\text{ bare}})\\ &+\left(\frac{\alpha_s(\mu)}{4\pi}\right)^2 f(\mu)\otimes\left[2\epsilon P^{(1),\text{ bare}}-\epsilon P^{(0),\text{ bare}}\otimes P^{(0),\text{ bare}}+\beta_0 P^{(0),\text{ bare}}\right]\\ &+\mathcal{O}(\alpha_s^3).\end{aligned}$$

Comparing this with Eq.(D.3), we find expressions for the first two bare splitting functions:

$$\begin{aligned}P^{(0),\text{ bare}}&=\frac{1}{\epsilon}P^{(0)},\\ P^{(1),\text{ bare}}&=\frac{1}{2\epsilon}P^{(1)}+\frac{1}{2\epsilon^2}P^{(0)}\otimes P^{(0)}-\frac{\beta_0}{2\epsilon^2}P^{(0)}.\end{aligned}$$

Finally, the bare PDF is:

$$\begin{aligned}f_k^{[h],\text{ bare}}(\xi)=&f_k^{[h]}(\xi,\mu)+\frac{\alpha_s(\mu)}{4\pi}\frac{1}{\epsilon}f(\mu)\otimes P^{(0)}\\ &+\left(\frac{\alpha_s(\mu)}{4\pi}\right)^2 f(\mu)\otimes\left[\frac{1}{2\epsilon}P^{(1)}+\frac{1}{2\epsilon^2}P^{(0)}\otimes P^{(0)}-\frac{\beta_0}{2\epsilon^2}P^{(0)}\right]+\mathcal{O}(\alpha_s^3).\end{aligned} \tag{D.6}$$

This can be rewritten as:

$$\begin{aligned}&f_k^{[h],\text{ bare}}(\xi)=\int_\xi^1\frac{dz}{z}\sum_{j=1}^{2n_f+1}\Gamma_{ij}(z)f_j^{[h]}\left(\frac{\xi}{z},\mu\right),\text{ where}\\ &\Gamma_{ij}(z)=\delta_{ij}\delta(1-z)+\frac{\alpha_s(\mu)}{4\pi}\frac{P_{ij}^{(0)}(z)}{\epsilon}\\ &\qquad+\left(\frac{\alpha_s(\mu)}{4\pi}\right)^2\left[\frac{1}{2\epsilon}P_{ij}^{(1)}+\frac{1}{2\epsilon^2}(P^{(0)}\otimes P^{(0)})_{ij}-\frac{\beta_0}{2\epsilon^2}P_{ij}^{(0)}\right]+\mathcal{O}(\alpha_s^3)\end{aligned} \tag{D.7}$$

Appendix E

Helicity Configurations

In this Appendix we give explicit rules for the helicity flip rules for physical processes in LO_1 adn LO_2.

E.1 F.1 LO_1 (and NLO_1)

The following color-stripped tree amplitude corresponding to the crossed $q_+(p_1)g(p_2) \to q_+(p3)\ell_+(p_4)\bar{\ell}_-(p_5)$ process is achieved from applying the rules in Eq.(4.18) on Eq.(4.14):

$$A_q^{(0),qg\to qV}(1_q^+;2^+;3_{\bar{q}}^-;4_\ell^+,5_{\bar{\ell}}^-) = 2\sqrt{2}\frac{\langle 15\rangle^2}{\langle 45\rangle\langle 23\rangle\langle 21\rangle},$$

similar expression for $qg \to q\ell\bar{\ell}$ at all orders can be achieved from performing swaps $p_1 \to p_2, p_2 \to p_3, p_3 \to p_1$ to the original all-outgoing amplitude NLO_1 in Eq.(4.15), (4.16) and (4.17).

All possible helicity configurations which give us unique results are thus:

$$\begin{aligned}
\lambda(\lambda_q,\lambda_\ell): \quad & +(+,+): A^{qg\to qV}_{x,+(+;+)}(\tilde{p}_1;\tilde{p}_2;\tilde{p}_3;\tilde{p}_4,\tilde{p}_5) = A_x(1_q^+;2^+,3_{\bar{q}}^-;4_\ell^+,5_{\bar{\ell}}^-),\\
& +(-,+): -A^{qg\to qV}_{(q,v),+(+;+)}(\tilde{p}_3;\tilde{p}_2;\tilde{p}_1;\tilde{p}_4,\tilde{p}_5),\ A^{qg\to qV}_{a,+(+;+)}(\tilde{p}_3;\tilde{p}_2;\tilde{p}_1;\tilde{p}_4,\tilde{p}_5)\\
& -(+,+): -A^{qg\to qV}_{(q,x),+(+;+)}(\tilde{p}_3;\tilde{p}_2;\tilde{p}_1;\tilde{p}_5,\tilde{p}_4)\Big|_{\langle\dots\rangle\leftrightarrow[\dots]}, -A^{qg\to qV}_{a,+(+;+)}(\tilde{p}_3;\tilde{p}_2;\tilde{p}_1;\tilde{p}_5,\tilde{p}_4)\Big|_{\langle\dots\rangle\leftrightarrow[\dots]},\\
& -(-,+): A^{qg\to qV}_{(q,v),+(+;+)}(\tilde{p}_1;\tilde{p}_2;\tilde{p}_3;\tilde{p}_5,\tilde{p}_4)\Big|_{\langle\dots\rangle\leftrightarrow[\dots]}, -A^{qg\to qV}_{a,+(+;+)}(\tilde{p}_1;\tilde{p}_2;\tilde{p}_3;\tilde{p}_5,\tilde{p}_4)\Big|_{\langle\dots\rangle\leftrightarrow[\dots]}.
\end{aligned}$$

Similarly for $q_+(p_1)\bar{q}_-(p_2) \to g_+(p_3)\ell_+(p_4)\bar{\ell}_-(p_5)$ the tree-level LO_1 amplitude follows from Eq.(4.19):

$$A_q^{(0),q\bar{q}\to gV}(1_q^+;2_{\bar{q}}^-;3^+;4_\ell^+,5_{\bar{\ell}}^-) = -2\sqrt{2}\frac{\langle 15\rangle^2}{\langle 45\rangle\langle 32\rangle\langle 31\rangle},$$

and the NLO_1 amplitudes similarly follow from $p_1 \leftrightarrow p_3$. All possible helicity amplitudes are thus:

$$\begin{aligned}
\lambda(\lambda_q,\lambda_\ell): \quad & +(+,+): A^{q\bar{q}\to gV}_{x,+(+;+)}(\tilde{p}_1,\tilde{p}_2;\tilde{p}_3;\tilde{p}_4,\tilde{p}_5) = A_x(1_q^+,2_{\bar{q}}^-;3^+;4_\ell^+,5_{\bar{\ell}}^-),\\
& +(-,+): -A^{q\bar{q}\to gV}_{(q,v),+(+;+)}(\tilde{p}_2,\tilde{p}_1;\tilde{p}_3;\tilde{p}_4,\tilde{p}_5),\ A^{q\bar{q}\to gV}_{a,+(+;+)}(\tilde{p}_2,\tilde{p}_1;\tilde{p}_3;\tilde{p}_4,\tilde{p}_5)\\
& -(+,+): -A^{q\bar{q}\to gV}_{(q,x),+(+;+)}(\tilde{p}_2,\tilde{p}_1;\tilde{p}_3;\tilde{p}_5,\tilde{p}_4)\Big|_{\langle\dots\rangle\leftrightarrow[\dots]}, -A^{q\bar{q}\to gV}_{a,+(+;+)}(\tilde{p}_2,\tilde{p}_1;\tilde{p}_3;\tilde{p}_5,\tilde{p}_4)\Big|_{\langle\dots\rangle\leftrightarrow[\dots]},\\
& -(-,+): A^{q\bar{q}\to gV}_{(q,v),+(+;+)}(\tilde{p}_1,\tilde{p}_2;\tilde{p}_3;\tilde{p}_5,\tilde{p}_4)\Big|_{\langle\dots\rangle\leftrightarrow[\dots]}, -A^{q\bar{q}\to gV}_{a,+(+;+)}(\tilde{p}_1,\tilde{p}_2;\tilde{p}_3;\tilde{p}_5,\tilde{p}_4)\Big|_{\langle\dots\rangle\leftrightarrow[\dots]}.
\end{aligned}$$

E.2 F.2 LO_2

E.2.1 $q\bar{q} \to q\bar{q}\ell\bar{\ell}$

Following the crossing rules in Eq.($\mathrm{SR}_{q\bar{q}\to q\bar{q}V}$), ($\mathrm{SL}_{q\bar{q}\to q\bar{q}V}$), ($\mathrm{TD}_{q\bar{q}\to q\bar{q}V}$) and ($\mathrm{TU}_{q\bar{q}\to q\bar{q}V}$):

$$
\begin{aligned}
A^{\mathrm{SR}_{q\bar{q}\to q\bar{q}V}}_{x,(+,+,+)}(\tilde{p}_1,\tilde{p}_2;\tilde{p}_3,\tilde{p}_4;\tilde{p}_5,\tilde{p}_6) &= A_{x,(+,+,+)}(-\tilde{p}_2,-\tilde{p}_1;\tilde{p}_3,\tilde{p}_4;\tilde{p}_5,\tilde{p}_6),\\
A^{\mathrm{SL}_{q\bar{q}\to q\bar{q}V}}_{x,(+,+,+)}(\tilde{p}_1,\tilde{p}_2;\tilde{p}_3,\tilde{p}_4;\tilde{p}_5,\tilde{p}_6) &= A_{x,(+,+,+)}(\tilde{p}_3,\tilde{p}_4;-\tilde{p}_2,-\tilde{p}_1;\tilde{p}_5,\tilde{p}_6),\\
A^{\mathrm{TD}_{q\bar{q}\to q\bar{q}V}}_{x,(+,+,+)}(\tilde{p}_1;\tilde{p}_2;\tilde{p}_3;\tilde{p}_4;\tilde{p}_5,\tilde{p}_6) &= -A_{x,(+,+,+)}(\tilde{p}_3,-\tilde{p}_1;-\tilde{p}_2,\tilde{p}_4;\tilde{p}_5,\tilde{p}_6),\\
A^{\mathrm{TU}_{q\bar{q}\to q\bar{q}V}}_{x,(+,+,+)}(\tilde{p}_1;\tilde{p}_2;\tilde{p}_3;\tilde{p}_4;\tilde{p}_5,\tilde{p}_6) &= -A_{x,(+,+,+)}(-\tilde{p}_2,\tilde{p}_4;\tilde{p}_3,-\tilde{p}_1;\tilde{p}_5,\tilde{p}_6)
\end{aligned}
$$

Possible unique helicity combinations are thus[1]:

$$
\begin{aligned}
(\lambda_{q'},\lambda_q,\lambda_\ell):\quad
&(+,+,+): A^{\mathrm{SR}_{q\bar{q}\to q\bar{q}V}}_{q,(+,+,+)}(\tilde{p}_1,\tilde{p}_2;\tilde{p}_3,\tilde{p}_4;\tilde{p}_5,\tilde{p}_6), \quad A^{\mathrm{SL}_{q\bar{q}\to q\bar{q}V}}_{q,(+,+,+)}(\tilde{p}_1,\tilde{p}_2;\tilde{p}_3,\tilde{p}_4;\tilde{p}_5,\tilde{p}_6),\\
&(-,+,+): -A^{\mathrm{SR}_{q\bar{q}\to q\bar{q}V}}_{q,(+,+,+)}(\tilde{p}_2,\tilde{p}_1;\tilde{p}_3,\tilde{p}_4;\tilde{p}_5,\tilde{p}_6), \quad A^{\mathrm{SL}_{q\bar{q}\to q\bar{q}V}}_{q,(+,+,+)}(\tilde{p}_2,\tilde{p}_1;\tilde{p}_3,\tilde{p}_4;\tilde{p}_5,\tilde{p}_6),\\
&(+,-,+): A^{\mathrm{SR}_{q\bar{q}\to q\bar{q}V}}_{q,(+,+,+)}(\tilde{p}_1,\tilde{p}_2;\tilde{p}_4,\tilde{p}_3;\tilde{p}_5,\tilde{p}_6), \quad -A^{\mathrm{SL}_{q\bar{q}\to q\bar{q}V}}_{q,(+,+,+)}(\tilde{p}_1,\tilde{p}_2;\tilde{p}_4,\tilde{p}_3;\tilde{p}_5,\tilde{p}_6),\\
&(-,-,+): -A^{\mathrm{SR}_{q\bar{q}\to q\bar{q}V}}_{q,(+,+,+)}(\tilde{p}_2,\tilde{p}_1;\tilde{p}_4,\tilde{p}_3;\tilde{p}_5,\tilde{p}_6), -A^{\mathrm{SL}_{q\bar{q}\to q\bar{q}V}}_{q,(+,+,+)}(\tilde{p}_2,\tilde{p}_1;\tilde{p}_4,\tilde{p}_3;\tilde{p}_5,\tilde{p}_6).
\end{aligned}
$$

$$
\begin{aligned}
(\lambda_{q'},\lambda_q,\lambda_\ell):\quad
&(+,+,+): A^{\mathrm{TD}_{q\bar{q}\to q\bar{q}V}}_{q,(+,+,+)}(\tilde{p}_1;\tilde{p}_2;\tilde{p}_3;\tilde{p}_4;\tilde{p}_5,\tilde{p}_6), \quad A^{\mathrm{TU}_{q\bar{q}\to q\bar{q}V}}_{q,(+,+,+)}(\tilde{p}_1;\tilde{p}_2;\tilde{p}_3;\tilde{p}_4;\tilde{p}_5,\tilde{p}_6),\\
&(-,+,+): -A^{\mathrm{TD}_{q\bar{q}\to q\bar{q}V}}_{q,(+,+,+)}(\tilde{p}_3;\tilde{p}_2;\tilde{p}_1;\tilde{p}_4;\tilde{p}_5,\tilde{p}_6), \quad A^{\mathrm{TU}_{q\bar{q}\to q\bar{q}V}}_{q,(+,+,+)}(\tilde{p}_3;\tilde{p}_2;\tilde{p}_1;\tilde{p}_4;\tilde{p}_5,\tilde{p}_6),\\
&(+,-,+): A^{\mathrm{TD}_{q\bar{q}\to q\bar{q}V}}_{q,(+,+,+)}(\tilde{p}_1;\tilde{p}_4;\tilde{p}_3;\tilde{p}_2;\tilde{p}_5,\tilde{p}_6), \quad -A^{\mathrm{TU}_{q\bar{q}\to q\bar{q}V}}_{q,(+,+,+)}(\tilde{p}_1;\tilde{p}_4;\tilde{p}_3;\tilde{p}_2;\tilde{p}_5,\tilde{p}_6),\\
&(-,-,+): -A^{\mathrm{TD}_{q\bar{q}\to q\bar{q}V}}_{q,(+,+,+)}(\tilde{p}_3;\tilde{p}_4;\tilde{p}_1;\tilde{p}_2;\tilde{p}_5,\tilde{p}_6), -A^{\mathrm{TU}_{q\bar{q}\to q\bar{q}V}}_{q,(+,+,+)}(\tilde{p}_3;\tilde{p}_4;\tilde{p}_1;\tilde{p}_2;\tilde{p}_5,\tilde{p}_6).
\end{aligned}
$$

E.2.2 $qq \to qq\ell\bar{\ell}$

From the crossing rules in Eq.($\mathrm{UU}_{qq\to qqV}$), ($\mathrm{UD}_{qq\to qqV}$), ($\mathrm{TD}_{qq\to qqV}$), ($\mathrm{TU}_{qq\to qqV}$):

$$
\begin{aligned}
A^{\mathrm{UU}_{qq\to qqV}}_{x,(+,+,+)}(\tilde{p}_1;\tilde{p}_2;\tilde{p}_3;\tilde{p}_4;\tilde{p}_5,\tilde{p}_6) &= A_{x,(+,+,+)}(\tilde{p}_3,-\tilde{p}_2;\tilde{p}_4,-\tilde{p}_1;\tilde{p}_5,\tilde{p}_6),\\
A^{\mathrm{UD}_{qq\to qqV}}_{x,(+,+,+)}(\tilde{p}_1;\tilde{p}_2;\tilde{p}_3;\tilde{p}_4;\tilde{p}_5,\tilde{p}_6) &= A_{x,(+,+,+)}(\tilde{p}_4,-\tilde{p}_1;\tilde{p}_3,-\tilde{p}_2;\tilde{p}_5,\tilde{p}_6),\\
A^{\mathrm{TD}_{qq\to qqV}}_{x,(+,+,+)}(\tilde{p}_1;\tilde{p}_2;\tilde{p}_3;\tilde{p}_4;\tilde{p}_5,\tilde{p}_6) &= -A_{x,(+,+,+)}(\tilde{p}_3,-\tilde{p}_1;\tilde{p}_4,-\tilde{p}_2;\tilde{p}_5,\tilde{p}_6),\\
A^{\mathrm{TU}_{qq\to qqV}}_{x,(+,+,+)}(\tilde{p}_1;\tilde{p}_2;\tilde{p}_3;\tilde{p}_4;\tilde{p}_5,\tilde{p}_6) &= -A_{x,(+,+,+)}(\tilde{p}_4,-\tilde{p}_2;\tilde{p}_3,-\tilde{p}_1;\tilde{p}_5,\tilde{p}_6).
\end{aligned}
$$

Possible helicity flips are as following:

$$
\begin{aligned}
(\lambda_{q'},\lambda_q,\lambda_\ell):\quad
&(+,+,+): A^{\mathrm{UU}_{qq\to qqV}}_{q,(+,+,+)}(\tilde{p}_1;\tilde{p}_2;\tilde{p}_3;\tilde{p}_4;\tilde{p}_5,\tilde{p}_6), \quad A^{\mathrm{UD}_{qq\to qqV}}_{q,(+,+,+)}(\tilde{p}_1;\tilde{p}_2;\tilde{p}_3;\tilde{p}_4;\tilde{p}_5,\tilde{p}_6),\\
&(-,+,+): A^{\mathrm{UU}_{qq\to qqV}}_{q,(+,+,+)}(\tilde{p}_4;\tilde{p}_2;\tilde{p}_3;\tilde{p}_1;\tilde{p}_5,\tilde{p}_6), \quad -A^{\mathrm{UD}}_{q,(+,+,+)}(\tilde{p}_4;\tilde{p}_2;\tilde{p}_3;\tilde{p}_1;\tilde{p}_5,\tilde{p}_6),\\
&(+,-,+): -A^{\mathrm{UU}_{qq\to qqV}}_{q,(+,+,+)}(\tilde{p}_1;\tilde{p}_3;\tilde{p}_2;\tilde{p}_4;\tilde{p}_5,\tilde{p}_6), \quad A^{\mathrm{UD}}_{q,(+,+,+)}(\tilde{p}_1;\tilde{p}_3;\tilde{p}_2;\tilde{p}_4;\tilde{p}_5,\tilde{p}_6),\\
&(-,-,+): -A^{\mathrm{UU}_{qq\to qqV}}_{q,(+,+,+)}(\tilde{p}_4;\tilde{p}_3;\tilde{p}_2;\tilde{p}_1;\tilde{p}_5,\tilde{p}_6), -A^{\mathrm{UD}}_{q,(+,+,+)}(\tilde{p}_4;\tilde{p}_3;\tilde{p}_2;\tilde{p}_1;\tilde{p}_5,\tilde{p}_6).
\end{aligned}
$$

$$
\begin{aligned}
(\lambda_{q'},\lambda_q,\lambda_\ell):\quad
&(+,+,+): A^{\mathrm{TD}_{qq\to qqV}}_{q,(+,+,+)}(\tilde{p}_1;\tilde{p}_2;\tilde{p}_3;\tilde{p}_4;\tilde{p}_5,\tilde{p}_6), \quad A^{\mathrm{TU}_{qq\to qqV}}_{q,(+,+,+)}(\tilde{p}_1;\tilde{p}_2;\tilde{p}_3;\tilde{p}_4;\tilde{p}_5,\tilde{p}_6),\\
&(-,+,+): -A^{\mathrm{TD}_{qq\to qqV}}_{q,(+,+,+)}(\tilde{p}_3;\tilde{p}_2;\tilde{p}_1;\tilde{p}_4;\tilde{p}_5,\tilde{p}_6), \quad A^{\mathrm{TU}_{qq\to qqV}}_{q,(+,+,+)}(\tilde{p}_3;\tilde{p}_2;\tilde{p}_1;\tilde{p}_4;\tilde{p}_5,\tilde{p}_6),\\
&(+,-,+): A^{\mathrm{TD}_{qq\to qqV}}_{q,(+,+,+)}(\tilde{p}_1;\tilde{p}_4;\tilde{p}_3;\tilde{p}_2;\tilde{p}_5,\tilde{p}_6), \quad -A^{\mathrm{TU}_{qq\to qqV}}_{q,(+,+,+)}(\tilde{p}_1;\tilde{p}_4;\tilde{p}_3;\tilde{p}_2;\tilde{p}_5,\tilde{p}_6),\\
&(-,-,+): -A^{\mathrm{TD}_{qq\to qqV}}_{q,(+,+,+)}(\tilde{p}_3;\tilde{p}_4;\tilde{p}_1;\tilde{p}_2;\tilde{p}_5,\tilde{p}_6), -A^{\mathrm{TU}_{qq\to qqV}}_{q,(+,+,+)}(\tilde{p}_3;\tilde{p}_4;\tilde{p}_1;\tilde{p}_2;\tilde{p}_5,\tilde{p}_6).
\end{aligned}
$$

[1] Important to note that due to different available helicities in S- and T-channel it is not allowed to interfere amplitudes $A^{\mathrm{S}}_{(\pm,\mp,\pm)}$ and $A^{\mathrm{T}}_{(\pm,\mp,\pm)}$, as these helicity numberings correspond to different actual helicities for p_2 and p_4

E.2.3 $gg \to q\bar{q}\ell\bar{\ell}$

Following the crossing rules from Eq.(NoCr+Cr$_{gg\to q\bar{q}V}$):

$$\vec{A}^{gg\to q\bar{q}V}_{x\lambda_1\lambda_2(+,+)}(\tilde{p}_1,\tilde{p}_2;\tilde{p}_3,\tilde{p}_4;\tilde{p}_5,\tilde{p}_6) = \vec{A}_{x\lambda_1\lambda_2(+,+)}(-\tilde{p}_1,-\tilde{p}_2;\tilde{p}_3,\tilde{p}_4;\tilde{p}_5,\tilde{p}_6).$$

This means that the helicity configurations are:

$$\begin{aligned}
\lambda_1,\lambda_2(\lambda_q,\lambda_\ell): \quad \lambda_1,\lambda_2(+,+): &\quad \vec{A}^{gg\to q\bar{q}V}_{x\lambda_1\lambda_2(+,+)}(\tilde{p}_1,\tilde{p}_2;\tilde{p}_3,\tilde{p}_4;\tilde{p}_5,\tilde{p}_6),\\
\lambda_1,\lambda_2(-,+): &\quad \mathbf{V}\vec{A}^{gg\to q\bar{q}V}_{q,x\lambda_1\lambda_2(-,+)}(\tilde{p}_1,\tilde{p}_2;\tilde{p}_4,\tilde{p}_3;\tilde{p}_5,\tilde{p}_6), \quad -\mathbf{V}\vec{A}^{gg\to q\bar{q}V}_{a\lambda_1\lambda_2(-,+)}(\tilde{p}_1,\tilde{p}_2;\tilde{p}_4,\tilde{p}_3;\tilde{p}_5,\tilde{p}_6),\\
&\text{where } \mathbf{V} = \begin{pmatrix} 0 & 1 & 0\\ 1 & 0 & 0\\ 0 & 0 & 1\end{pmatrix}.
\end{aligned}$$

The different helicities of the external gluons are reflected in the definition of the amplitude in Eq.(4.21).

E.2.4 $qg \to qg\ell\bar{\ell}$

From the crossing rules in Eq.(NoCr+Cr$_{qg\to qgV}$)

$$\vec{A}^{qg\to qgV}_{x\lambda_1\lambda_2(+,+)}(\tilde{p}_1,\tilde{p}_2;\tilde{p}_3,\tilde{p}_4;\tilde{p}_5,\tilde{p}_6) = \vec{A}_{x\lambda_1\lambda_2(+,+)}(\tilde{p}_4,-\tilde{p}_2;\tilde{p}_3,-\tilde{p}_1;\tilde{p}_5,\tilde{p}_6).$$

The helicity configurations are thus:

$$\begin{aligned}
\lambda_1,\lambda_2(\lambda_q,\lambda_\ell): \quad \lambda_1,\lambda_2(+,+): &\quad \vec{A}^{qg\to qgV}_{x\lambda_1\lambda_2(+,+)}(\tilde{p}_1,\tilde{p}_2;\tilde{p}_3,\tilde{p}_4;\tilde{p}_5,\tilde{p}_6),\\
\lambda_1,\lambda_2(-,+): &\quad \mathbf{V}\vec{A}^{qg\to qgV}_{q,x\lambda_1\lambda_2(+,+)}(\tilde{p}_3,\tilde{p}_2;\tilde{p}_1,\tilde{p}_4;\tilde{p}_5,\tilde{p}_6), \quad -\mathbf{V}\vec{A}^{qg\to qgV}_{a\lambda_1\lambda_2(+,+)}(\tilde{p}_3,\tilde{p}_2;\tilde{p}_1,\tilde{p}_4;\tilde{p}_5,\tilde{p}_6).
\end{aligned}$$

E.2.5 $q\bar{q} \to gg\ell\bar{\ell}$

From the crossing rules in Eq.(NoCr+Cr$_{q\bar{q}\to ggV}$)

$$\vec{A}^{q\bar{q}\to ggV}_{x\lambda_1\lambda_2(+,+)}(\tilde{p}_1,\tilde{p}_2;\tilde{p}_3,\tilde{p}_4;\tilde{p}_5,\tilde{p}_6) = \vec{A}_{x\lambda_1\lambda_2(+,+)}(\tilde{p}_4,\tilde{p}_3,-\tilde{p}_2,-\tilde{p}_1;\tilde{p}_5,\tilde{p}_6).$$

The helicity configurations are thus:

$$\begin{aligned}
\lambda_1,\lambda_2(\lambda_q,\lambda_\ell): \quad \lambda_1,\lambda_2(+,+): &\quad \vec{A}^{q\bar{q}\to ggV}_{x\lambda_1\lambda_2(+,+)}(\tilde{p}_1,\tilde{p}_2;\tilde{p}_3,\tilde{p}_4;\tilde{p}_5,\tilde{p}_6),\\
\lambda_1,\lambda_2(-,+): &\quad \mathbf{V}\vec{A}^{q\bar{q}\to ggV}_{x\lambda_1\lambda_2(+,+)}(\tilde{p}_2,\tilde{p}_1;\tilde{p}_3,\tilde{p}_4;\tilde{p}_5,\tilde{p}_6).
\end{aligned}$$

Bibliography

[1] ATLAS Collaboration, *Observation of a new particle in the search for the standard model higgs boson with the atlas detector at the lhc*, *Physics Letters B* **716** (2012) 1–29 [1207.7214].

[2] CMS Collaboration, *Observation of a new boson at a mass of 125 gev with the cms experiment at the lhc*, *Physics Letters B* **716** (2012) 30–61 [1207.7235].

[3] ATLAS Collaboration, *Precise measurements of w- and z-boson transverse momentum spectra with the atlas detector using pp collisions at* $\sqrt{s} = 5.02$ *tev and 13 tev*, *The European Physical Journal C* **84** (2024) [2404.06204].

[4] CMS Collaboration, *High-precision measurement of the w boson mass with the cms experiment at the lhc*, 2412.13872.

[5] S. Camarda, G. Ferrera and M. Schott, *Determination of the strong-coupling constant from the z-boson transverse-momentum distribution*, *The European Physical Journal C* **84** (2024) [2203.05394].

[6] ATLAS Collaboration, *A precise determination of the strong-coupling constant from the recoil of z bosons with the atlas experiment at* $\sqrt{s} = 8$ *tev*, 2309.12986.

[7] S. Camarda, M. Boonekamp, G. Bozzi, S. Catani, L. Cieri, J. Cuth et al., *Dyturbo: fast predictions for drell–yan processes*, *The European Physical Journal C* **80** (2020) [1910.07049].

[8] R. Gavin, Y. Li, F. Petriello and S. Quackenbush, *Fewz 2.0: A code for hadronic z production at next-to-next-to-leading order*, *Computer Physics Communications* **182** (2011) 2388–2403 [1011.3540].

[9] L. Faddeev and V. Popov, *Feynman diagrams for the yang-mills field*, *Physics Letters B* **25** (1967) 29.

[10] D. J. Gross and F. Wilczek, *Ultraviolet behavior of non-abelian gauge theories*, *Phys. Rev. Lett.* **30** (1973) 1343.

[11] H. D. Politzer, *Reliable perturbative results for strong interactions?*, *Phys. Rev. Lett.* **30** (1973) 1346.

[12] S. D. Drell and T.-M. Yan, *Massive lepton-pair production in hadron-hadron collisions at high energies*, *Phys. Rev. Lett.* **25** (1970) 316.

[13] M. A. Ebert, J. K. L. Michel, I. W. Stewart and F. J. Tackmann, *Drell-Yan* q_t *resummation of fiducial power corrections at N3LL*, *Journal of High Energy Physics* **2021** (2021) [2006.11382].

[14] J. Cleymans and M. Kuroda, *Angular distribution of dileptons in hadronic collisions*, *Nuclear Physics B* **155** (1979) 480.

[15] M. E. Peskin and D. V. Schroeder, *An Introduction to Quantum Field Theory*. Westview Press, 1995.

[16] E. Mirkes, *Angular decay distribution of leptons from w-bosons at nlo in hadronic collisions*, *Nuclear Physics B* **387** (1992) 3.

[17] FNAL E866/NuSea Collaboration collaboration, L. Y. Zhu, J. C. Peng, P. E. Reimer, T. C. Awes, M. L. Brooks, C. N. Brown et al., *Measurement of angular distributions of drell-yan dimuons in* $p + d$ *interactions at* 800 GeV/c, *Phys. Rev. Lett.* **99** (2007) 082301 [hep-ex/0609005].

[18] CDF Collaboration collaboration, T. Aaltonen, B. Álvarez González, S. Amerio, D. Amidei, A. Anastassov, A. Annovi et al., *First measurement of the angular coefficients of drell-yan e^+e^- pairs in the z mass region from $p\bar{p}$ collisions at $\sqrt{s} = 1.96$ TeV*, *Phys. Rev. Lett.* **106** (2011) 241801 [1103.5699].

[19] CMS Collaboration, *Angular coefficients of z bosons produced in pp collisions at s=8 tev and decaying to + as a function of transverse momentum and rapidity*, *Physics Letters B* **750** (2015) 154 [1504.03512].

[20] G. Aad, B. Abbott, J. Abdallah, O. Abdinov, B. Abeloos, R. Aben et al., *Measurement of the angular coefficients in z-boson events using electron and muon pairs from data taken at $\sqrt{s} = 8$ tev with the atlas detector*, *Journal of High Energy Physics* **2016** (2016) [1606.00689].

[21] LHCb collaboration, R. Aaij et al., *First Measurement of the Z→μ+μ- Angular Coefficients in the Forward Region of pp Collisions at s=13 TeV*, *Phys. Rev. Lett.* **129** (2022) 091801 [2203.01602].

[22] P. B. Arnold and M. H. Reno, *The Complete Computation of High p_T W and Z Production in 2nd Order QCD*, *Nucl. Phys. B* **319** (1989) 37 [hep-ph/9708239].

[23] R. J. Gonsalves, J. Pawłowski and C.-F. Wai, *Qcd radiative corrections to electroweak-boson production at large transverse momentum in hadron collisions*, *Phys. Rev. D* **40** (1989) 2245.

[24] S. Catani and M. Grazzini, *An NNLO subtraction formalism in hadron collisions and its application to Higgs boson production at the LHC*, *Phys. Rev. Lett.* **98** (2007) 222002 [hep-ph/0703012].

[25] J. Gaunt, M. Stahlhofen, F. J. Tackmann and J. R. Walsh, *N-jettiness Subtractions for NNLO QCD Calculations*, *JHEP* **09** (2015) 058 [1505.04794].

[26] K. Hagiwara, K.-i. Hikasa and N. Kai, *Parity Odd Asymmetries in W Jet Events at Hadron Colliders*, *Phys. Rev. Lett.* **52** (1984) 1076.

[27] V. E. Lyubovitskij, W. Vogelsang, F. Wunder and A. S. Zhevlakov, *Perturbative t-odd asymmetries in the drell-yan process revisited*, *Physical Review D* **109** (2024) [2403.18741].

[28] T. Kinoshita, *Mass singularities of Feynman amplitudes*, *J. Math. Phys.* **3** (1962) 650.

[29] T. D. Lee and M. Nauenberg, *Degenerate systems and mass singularities*, *Phys. Rev.* **133** (1964) B1549.

[30] Y. L. Dokshitzer, *Calculation of the Structure Functions for Deep Inelastic Scattering and e+ e- Annihilation by Perturbation Theory in Quantum Chromodynamics.*, *Sov. Phys. JETP* **46** (1977) 641.

[31] V. N. Gribov and L. N. Lipatov, *e+ e- pair annihilation and deep inelastic e p scattering in perturbation theory*, *Sov. J. Nucl. Phys.* **15** (1972) 675.

[32] G. Altarelli and G. Parisi, *Asymptotic freedom in parton language*, *Nuclear Physics B* **126** (1977) 298.

[33] C. W. Bauer, S. Fleming and M. Luke, *Summing sudakov logarithms in $\vec{B} \, X_s\gamma$ in effective field theory*, *Phys. Rev. D* **63** (2000) 014006 [hep-ph/0005275].

[34] C. W. Bauer, S. Fleming, D. Pirjol and I. W. Stewart, *An effective field theory for collinear and soft gluons: Heavy to light decays*, *Physical Review D* **63** (2001) [hep-ph/0011336].

[35] C. W. Bauer and I. W. Stewart, *Invariant operators in collinear effective theory*, *Physics Letters B* **516** (2001) 134–142 [hep-ph/0107001].

[36] C. W. Bauer, D. Pirjol and I. W. Stewart, *Soft-collinear factorization in effective field theory*, *Phys. Rev. D* **65** (2002) 054022 [hep-ph/0109045].

[37] M. Beneke, A. Chapovsky, M. Diehl and T. Feldmann, *Soft-collinear effective theory and heavy-to-light currents beyond leading power*, *Nuclear Physics B* **643** (2002) 431–476 [hep-ph/0206152].

[38] E. Fermi, *An attempt of a theory of beta radiation. 1.*, *Z. Phys.* **88** (1934) 161.

[39] F. L. Wilson, *Fermi's Theory of Beta Decay*, *Am. J. Phys.* **36** (1968) 1150.

[40] T. Becher, A. Broggio and A. Ferroglia, *Introduction to Soft-Collinear Effective Theory*. Springer International Publishing, 2015, 10.1007/978-3-319-14848-9, [1410.1892].

[41] I. W. Stewart, *Lectures on the soft-collinear effective theory*, 2013.

[42] I. Z. Rothstein and I. W. Stewart, *An effective field theory for forward scattering and factorization violation*, *Journal of High Energy Physics* **2016** (2016) [1601.04695].

[43] T. Becher and M. D. Schwartz, *Direct photon production with effective field theory*, *JHEP* **02** (2010) 040 [0911.0681].

[44] T. Becher, C. Lorentzen and M. D. Schwartz, *Resummation for W and Z production at large pT*, *Phys. Rev. Lett.* **108** (2012) 012001 [1106.4310].

[45] T. Becher, C. Lorentzen and M. D. Schwartz, *Precision Direct Photon and W-Boson Spectra at High p_T and Comparison to LHC Data*, *Phys. Rev. D* **86** (2012) 054026 [1206.6115].

[46] T. Becher, G. Bell and S. Marti, *Nnlo soft function for electroweak boson production at large transverse momentum*, *Journal of High Energy Physics* **2012** (2012) [1201.5572].

[47] Z. L. Liu and M. Stahlhofen, *Three-loop soft function for energetic electroweak boson production at hadron colliders*, *JHEP* **02** (2021) 128 [2010.05861].

[48] T. Becher, C. Lorentzen and M. D. Schwartz, *Precision direct photon and w-boson spectra at high p_t and comparison to lhc data*, *Physical Review D* **86** (2012) [1206.6115].

[49] L. D. Landau, *On the angular momentum of a system of two photons*, *Dokl. Akad. Nauk SSSR* **60** (1948) 207.

[50] C. N. Yang, *Selection rules for the dematerialization of a particle into two photons*, *Phys. Rev.* **77** (1950) 242.

[51] W. T. Giele and E. W. N. Glover, *Higher-order corrections to jet cross sections in e^+e^- annihilation*, *Phys. Rev. D* **46** (1992) 1980.

[52] Z. Bern, L. Dixon and D. A. Kosower, *One-loop amplitudes for e^+e^- to four partons*, *Nuclear Physics B* **513** (1998) 3–86 [hep-ph/9708239].

[53] J. G. Korner and P. Sieben, *Use of helicity methods in evaluating loop integrals: A QCD example*, *Nucl. Phys. B* **363** (1991) 65.

[54] L. Garland, T. Gehrmann, E. Glover, A. Koukoutsakis and E. Remiddi, *Two-loop qcd helicity amplitudes for e+e→3jets*, *Nuclear Physics B* **642** (2002) 227–262 [hep-ph/0206067].

[55] L. Garland, T. Gehrmann, E. Glover, A. Koukoutsakis and E. Remiddi, *The two-loop qcd matrix element for e+e→3 jets*, *Nuclear Physics B* **627** (2002) 107–188 [hep-ph/0112081].

[56] P. D. Causmaecker, R. Gastmans, W. Troost and T. T. Wu, *Multiple bremsstrahlung in gauge theories at high-energies. 1. general formalism for quantum electrodynamics*, *Nucl. Phys. B* **206** (1982) 53.

[57] F. A. Berends, R. Kleiss, P. D. Causmaecker, R. Gastmans, W. Troost and T. T. Wu, *Multiple bremsstrahlung in gauge theories at high-energies. 2. single bremsstrahlung*, *Nucl. Phys. B* **206** (1982) 61.

[58] J. F. Gunion and Z. Kunszt, *Improved analytic techniques for tree graph calculations and the g g q anti-q lepton anti-lepton subprocess*, *Phys. Lett. B* **161** (1985) 333.

[59] Z. Xu, D. H. Zhang and L. Chang, *Helicity amplitudes for multiple bremsstrahlung in massless nonabelian gauge theories*, *Nucl. Phys. B* **291** (1987) 392.

[60] Z. Bern, L. J. Dixon and D. A. Kosower, *Progress in one-loop qcd computations*, *Ann. Rev. Nucl. Part. Sci.* **46** (1996) 109.

[61] M. D. Schwartz, *Quantum Field Theory and the Standard Model*. Cambridge University Press, 2014.

[62] L. J. Dixon, *A brief introduction to modern amplitude methods*, *arXiv preprint arXiv:1310.5353* (2013) [1310.5353].

[63] H. Elvang and Y. tin Huang, *Scattering Amplitudes in Gauge Theory and Gravity*. Cambridge University Press, 2015, [1308.1697].

[64] N. Arkani-Hamed, T.-C. Huang and Y. tin Huang, *Scattering amplitudes for all masses and spins*, *JHEP* **11** (2021) 70 [1709.04891].

[65] I. Moult, I. W. Stewart, F. J. Tackmann and W. J. Waalewijn, *Employing helicity amplitudes for resummation*, *Physical Review D* **93** (2016) [1508.02397].

[66] S. Moch, J. A. M. Vermaseren and A. Vogt, *On* $gamma_5 in higher - order qcd calculations and the nnlo evolution of the polarized valence distribution$, 2015.

[67] V. Shtabovenko, R. Mertig and F. Orellana, *Feyncalc 10: Do multiloop integrals dream of computer codes?*, *Computer Physics Communications* **306** (2025) 109357 [2312.14089].

[68] C. S. Lam and W.-K. Tung, *Systematic approach to inclusive lepton pair production in hadronic collisions*, *Phys. Rev. D* **18** (1978) 2447.

[69] G. Somogyi, *Angular integrals in d dimensions*, *Journal of Mathematical Physics* **52** (2011) [1101.3557].

[70] S. Larin, *The renormalization of the axial anomaly in dimensional regularization*, *Physics Letters B* **303** (1993) 113–118.

[71] S. Alioli, P. Nason, C. Oleari and E. Re, *A general framework for implementing NLO calculations in shower Monte Carlo programs: the POWHEG BOX*, *JHEP* **06** (2010) 043 [1002.2581].

[72] Y. Nagashima, *Elementary Particle Physics: Foundations of the Standard Model V2*, no. v. 2. Wiley, 2013.

[73] T. Hahn, *Generating feynman diagrams and amplitudes with feynarts 3*, *Computer Physics Communications* **140** (2001) 418–431 [hep-ph/0012260].

[74] Z. Ligeti, I. W. Stewart and F. J. Tackmann, *Treating the b quark distribution function with reliable uncertainties*, *Physical Review D* **78** (2008) [0807.1926].